Universitat de Girona

NEW MANGANESE COMPLEXES WITH NITROGEN DONOR LIGANDS. CATALYSTS FOR OXIDATION REACTIONS

Jordi RICH MASALLERA

Dipòsit legal: GI. 1382-2012
http://hdl.handle.net/10803/84056

Universitat de Girona

Doctoral dissertation

NEW MANGANESE COMPLEXES WITH NITROGEN DONOR LIGANDS.
CATALYSTS FOR OXIDATION REACTIONS.

Presented by: **Jordi Rich Masallera**

In candidancy for the degree of
Doctor per la Universitat de Girona

Girona, March 2012

Universitat de Girona

Departament de Química

Àrea de Química Inorgànica

La Dra. M.Isabel Romero García, professora titular del Departament de Química de la Universitat de Girona, i la Dra. Montserrat Rodríguez Pizarro, professora agregada del Departament de Química de la Universitat de Girona,

CERTIFIQUEM:

Que aquest treball, titulat "New manganese complexes with nitrogen donor ligands. Catalysts for oxidation reactions", que presenta Jordi Rich Masallera per a l'obtenció del títol de doctor, ha estat realitzat sota la nostra direcció i que compleix els requeriments per poder optar a Menció Europea.

Dra. M.Isabel Romero García   Dra. Montserrat Rodríguez Pizarro

Girona, 16 de març de 2012.

A la meva família

i a l'Íngrid

Agraïments

Sembla mentida que, després d'escriure més de 250 pàgines en anglès, costi tant enfrontar-se a un full en blanc on pots expressar-te en el teu propi idioma. I és que no és fàcil plasmar en una pàgina l'agraïment a tota la gent que ha fet possible acabar aquest treball i amb qui he pogut compartir aquesta experiència que va començar ja fa quasi 5 anys.

Per començar vull donar les gràcies a les dues persones més importants perquè aquesta tesi hagi estat possible, les meves directores de tesi: Dra. Marisa Romero i Dra. Montse Rodríguez. Us vull agrair que em donéssiu l'oportunitat de realitzar una tesi doctoral dins el vostre grup. A vegades encara em pregunto què n'hauria estat de la meva vida si la Marisa no m'hagués proposat fer un treball experimental. Però ara puc ben dir que ha valgut molt la pena. Sempre m'heu aportat bones idees i confiança, però sobretot al vostre costat he après molt, tant científicament com personalment. Fora de la Universitat també hem passat bones estones, especialment amb tu Montse, que espero que continuïn i estic segur que així serà.

També vull fer extensiu el meu agraïment a tots els col·laboradors que han fet possible aquest treball. Al Prof. Piet van Leeuwen i al Prof. Antoni Llobet, de l'ICIQ, pels treballs que hem realitzat, pels consells i bones idees que sempre han aportat. Al Dr. Xavi Sala, de la UAB, per la col·laboració, pels consells i l'ajuda que sempre m'ha donat. Al Dr. Albert Poater pels càlculs fets (i els "bitxos" que encara estan corrent). Als Serveis Tècnics de Recerca: la Dra. Lluïsa Matas pels espectres de RMN, l'Anna Costa pels anàlisis elementals i masses i en Xavier Fontrodona per les estructures de Raigs X. I també a la Marta Serrano, de l'ICIQ, per les mesures de rotació òptica i els MALDI.

A special acknowledgement to Dra. Marie-Noëlle Collomb, from Grenoble, who hosted me in her lab during my stay of 4 months in France. Thanks for your dedication, for everything you taught me and for the collaboration together with Dra. Carole Duboc.

Al llarg d'aquests 5 anys també he conegut a molta gent a la qual vull donar les gràcies perquè han aconseguit que sigui una etapa molt important de la meva vida, que mai oblidaré pels bons moments que hem passat tant dins com fora de la Facultat.

Començaré pels companys del grup, amb els quals he compartit més temps. I no puc començar per una altra que no sigui la Isabel, la millor companya de grup que es pot tenir. Si em deixessin escollir sempre et triaria a tu perquè estàs sempre disposada a ajudar, no tens mai un no per resposta i perquè em vas ensenyar molt. També per les sempre interessants converses esportives (tot i tenir diferents preferències) i pels sopars i festes que espero que continuïn.

Els antics companys, Quim i Mohamed, i les futures doctores, Mònica i Íngrid, gràcies pels bons moments viscuts. Mònica, espero que acabi d'anar bé aquesta estada a Alemanya i que et vagi tot genial en el futur.

També vull donar les gràcies a tots els companys de despatx (Arnau, Anna, Laura, Alícia, Irene, Plani i Pep Anton) pels bons moments viscuts tant al despatx com al bar, sempre amb converses ben animades i esbojarrades. En aquest punt també hi han tingut un paper important tant en Pep Duran com la Mª Ángeles.

Gràcies també a la resta de becaris amb qui he compartit grans moments, en especial a les "cats" (A.Dachs, Sandra, Lídia, Magda i M.Raduán) i a en Rafael (pels infinits sopars i festes, i per les excursions a Grenoble i Tarragona, mai oblidaré el "Fonru vols peixicu?"). També als companys de Grenoble, especialment en Marcello (le justicier) i en Fabien, un gran amic que em va acollir a casa seva durant un temps, espero que et vagi molt bé el postdoc per Salt Lake City.

Als amics (Xevi, Barret, Miki, Lardo, Palma i Marc) per ser-hi sempre i fer-me gaudir de la vida (perquè no tot ha de ser química). I a l'Isaac, un bon amic i un bon company. Després de molts anys ha arribat el dia en què hem agafat camins diferents i espero que et vagi molt bé aquesta nova etapa.

Si he arribat fins aquí és gràcies a la meva família. Pare, mare, Nuri i Litus, vosaltres sou les persones més importants de la meva vida, sempre m'heu ajudat, m'heu donat suport i tot el que fes falta per arribar on estic i per ser qui sóc. Us estaré eternament agraït a vosaltres i també a l'avi i l'àvia, el tiet Barranc, l'Eugènia, en Franc, la Sandra i els petits de casa: Clara, Sergi, Carla, Nonna i Cesc.

I ja per acabar, Íngrid, si no he entrat en detall sobre tu quan parlava dels companys és perquè et reservava un apartat especial. Només per l'oportunitat de conèixe't ja ha valgut la pena fer aquest doctorat. M'has ajudat molt en aquesta recta final i em fas molt feliç. Gràcies per ser-hi.

List of publications

- *Mn(II) complexes containing the polypyridylic chiral ligand (–)-pinene[5,6]bipyridine. Catalysts for oxidation reactions.*
  Rich, J.; Rodríguez, M.; Romero, I.; Vaquer, L.; Sala, X.; Llobet, A.; Corbella, M.; Collomb, M.-N. *Dalton Trans.* **2009**, 8117-8126.

- *Investigation of the Zero-Field Splitting in six- and seven-coordinate mononuclear Mn^{II} complexes with N/O-based ligands by combining EPR spectroscopy and quantum chemistry.*
  Rich J.; Castillo, C.E.; Romero, I.; Rodríguez, M.; Duboc, C.; Collomb, M.-N. *Eur. J. Inorg. Chem.* **2010**, 3658-3665.

- *Multireversible redox processes in pentanuclear bis(triple-helical) manganese complexes featuring an oxo-centered triangular $\{Mn^{II}_2Mn^{III}(\mu_3\text{-}O)\}^{5+}$ or $\{Mn^{II}Mn^{III}_2(\mu_3\text{-}O)\}^{6+}$ core wrapped by two $\{Mn^{II}_2(bpp)_3\}^{-}$.*
  Romain, S.; Rich, J.; Sens, C.; Stoll, T.; Benet-Buchholz, J.; Llobet, A.; Rodríguez, M.; Romero, I.; Clérac, R.; Mathonière, C.; Duboc, C.; Deronzier, A; Collomb, M.-N. *Inorg. Chem.* **2011**, *50*, 8427-8436.

- *Reusable Catalytic Systems for Alkene Epoxidation with Manganese (II) Complexes. Evidence of high-valent oxo-bridged binuclear $Mn_2(IV,IV)$ and mixed-valent $Mn_2(III,IV)$ active oxidant species.*
  Rich, J.; Rodríguez, M.; Romero, I.; Molton, F.; Duboc, C.; Collomb, M.-N. *submitted for publication.*

Abbreviations

Bpy	2,2'-bibyridine
Hbpp	3,5-bis(pyridin-2-yl)-pyrazole
ESI-MS	Electrospray Ionization Mass Spectrometry
MALDI	Matrix assisted laser desorption/ionization
m/z	mass-to-charge ratio
UV-vis	Ultraviolet-visible spectroscopy
λ	wavelength
IR	Infra Red
ν	frequency
Anal. found (calcd.)	Analysis found (analysis calculated)
CV	Cyclic Voltammetry
E	Potential
$E_{1/2}$	Half wave potential
E_{pa}	Anodic peak potential
E_{pc}	Cathodic peak potential
E_{app}	Applied potential
TBAH	Tetra(n-butyl)ammonium hexafluorophosphate
$[(nBu)_4N]PF_6$	Tetra(n-butyl)ammonium hexafluorophosphate
SSCE	Sodium Saturated Calomel Electrode
LMCT	Ligand to Metal Charge Transfer
EPR	Electron Paramagnetic Resonance
ZFS	Zero Field Splitting
DFT	Density Functional Theory
SOC	Spin-Orbit Coupling
SSC	Spin-Spin Coupling
J	Coupling constant
GC	Gas Chromatography
Conv.	Conversion
Select.	Selectivity
ee	Enantiomeric excess
eq	Equivalents
T	Temperature
RT	Room Temperature

IL	Ionic Liquid
RTIL	Room Temperature Ionic Liquid
TON	Turnover Number
NMR	Nuclear Magnetic Resonance
NOESY	Nuclear Overhauser Effect Spectroscopy
HSQC	Heteronuclear Single-Quantum Correlation spectroscopy
s	singlet
d	doublet
t	triplet
m	multiplet
ppm	parts per million
vs	versus

Electronic supporting information

The material listed below can be found in the attached CD:

- pdf file of the PhD dissertation
- pdf files of the publications
- cif files for each crystal structure presented within this thesis

Chapter	Crystal Structure	Code
Chapter 3	[{Mn((−)-**L**)Cl}$_2$(μ-Cl)$_2$]	720648
	[{Mn((−)-**L**)}$_2$(μ-OAc)$_3$](PF$_6$)	720646
	[Mn((−)-**L**)Cl$_2$(H$_2$O)]	720650
	[Mn((−)-**L**)$_2$Cl$_2$]	720645
	[Mn((−)-**L**)$_2$(CF$_3$SO$_3$)$_2$]	720649
	[Mn((−)-**L**)$_2$)(NO$_3$)(H$_2$O)](NO$_3$)	720647
Chapter 5	[Mn(SPANrac)Cl$_2$]	C1
	[Mn(SPANrac)(CF$_3$SO$_3$)$_2$]	C2
	[Mn(SPAN(+)-pinene[4,5])(NO$_3$)$_2$]	C6
	[Mn(SPANrac-pinene[5,6])(CF$_3$SO$_3$)$_2$]	C8
	[Mn(SPAN(-)-pinene[5,6])(CF$_3$SO$_3$)$_2$]	C14
Chapter 6	[{Mn^{II}(μ-bpp)$_3$}$_2$Mn^{II}$_2$Mn^{III}(μ$_3$-O)](ClO$_4$)$_3$	818591
	[{Mn^{II}(μ-bpp)$_3$}$_2$Mn^{II}Mn^{III}$_2$(μ$_3$-O)](ClO$_4$)$_4$	818592

Graphical abstracts

CHAPTER 1. General Introduction (pages 1-46)

CHAPTER 2. General objectives (pages 47-50)

CHAPTER 3. Mn(II) complexes containing the polypyridylic chiral ligand (–)-pinene[5,6]bipyridine. Investigation of the Zero-Field Splitting by combining EPR Spectroscopy and Quantum Chemistry. (pages 51-100)

A series of mononuclear and dinuclear chiral manganese (II) complexes containing the neutral bidentate chiral nitrogen-donor ligand (–)-pinene[5,6]bipyridine, (–)-**L**, were prepared from different manganese salts. These complexes have been characterized through structural, analytical, spectroscopic and electrochemical techniques. The magnetic properties of the two binuclear complexes have been studied and display a weak antiferromagnetic coupling. The electronic properties of the six-coordinate mononuclear complexes, together with other six- and seven-coordinate mononuclear complexes synthesized previously, have been investigated by X- and Q-band EPR spectroscopy. The zero-field splitting (ZFS) parameters have been predicted by density functional theory (DFT) calculations using two types of functionals, BP86 and B3LYP.

CHAPTER 4. Catalytic activity of Mn(II) complexes containing the polypyridylic chiral ligand (–)-pinene[5,6]bipyridine: reusable catalytic systems for alkene epoxidation. Evidence of high-valent oxo-bridged binuclear Mn$_2$(IV,IV) and mixed-valent Mn$_2$(III,IV) active oxidant species. (pages 101-136)

The reactivity of the new complexes synthesized in the previous chapter has been tested with regard to the epoxidation of aromatic and aliphatic alkenes with peracetic acid as oxygen donor. The catalytic performance of the chloro complexes is enhanced by the use of additives (NaHCO$_3$ and imidazole) and also when a [bmim]:acetonitrile mixture (bmim = 1-butyl-3-methyl-imidazolium) is used as reaction media. The latter conditions allow for the recyclability of the catalytic system keeping good selectivity and conversion values. The nature of the intermediate catalytic species for three of the catalysts has been investigated through EPR, ESI-MS and UV-vis techniques. The results obtained point in all cases to the formation of binuclear [Mn(μ-O)$_2$Mn]$^{n+}$ species but displaying different oxidation states as a function of the starting Mn(II) complex ((IV,IV) for the chloro complexes; (III,IV) for the triflate complex), thus evidencing a significant role of the Cl or triflate ligands in the formation of the intermediate species.

CHAPTER 5. New N-tetradentate SPANamine type of ligands and their Mn(II) complexes as catalysts for epoxidation of alkenes. (pages 137-202)

Five new tetradentate N-donor ligands with the spirobi(chroman) skeleton (either chiral or racemic) have been synthesized and fully characterized by NMR, ESI-MS and optical polarimetry. These ligands have been coordinated to a series of manganese salts affording a family of new chiral and racemic Mn (II) complexes, which have also been characterized through analytical and spectroscopic techniques. The crystallographic structure of five of them has been obtained by X-Ray diffraction, all showing distorted octahedral geometry with the ligand adopting a *cis*-α conformation over the Mn ion. All the complexes have been tested in the catalytic epoxidation of styrene and the conversion and selectivity values increase in presence of additives in the catalytic media. Experimental results and computational calculations demonstrate the stereospecificity for the *cis* epoxide in the epoxidation of *cis*-β-methylstyrene mediated by one of the complexes synthesized.

CHAPTER 6. Multi-reversible redox processes in pentanuclear bis(triple-helical) manganese complexes featuring an oxo-centered triangular {Mn$^{II}_2$Mn^{III}(μ_3-O)}$^{5+}$ or {Mn^{II}Mn$^{III}_2$(μ_3-O)}$^{6+}$ core wrapped by two {Mn$^{II}_2$(bpp)$_3$}$^-$. Evaluation of the catalytic activity in oxidation reactions. (pages 203-240)
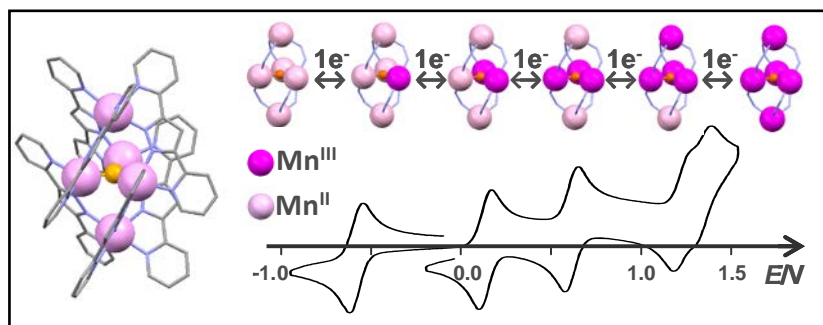
A new pentanuclear bis(triple-helical) manganese complex has been isolated and characterized by X-ray diffraction in two oxidation states. The structure consists of a central {Mn$_3$(μ_3-O)} core of Mn$^{II}_2$Mn^{III} (**1**$^{3+}$) or Mn^{II}Mn$^{III}_2$ (**1**$^{4+}$) ions connected to two apical Mn^{II} ions through six bpp$^-$ ligands. This complex exhibits a very rich redox behavior with five distinct and reversible one-electron processes and displays an unexpected and excellent stability of the pentanuclear structure in the following four oxidation states: Mn$^{II}_5$, Mn$^{II}_4$Mn^{III}, Mn$^{II}_3$Mn$^{III}_2$ and Mn$^{II}_2$Mn$^{III}_3$. The spectroscopic characteristics in solution of these four species as well as the solid state magnetic properties of Mn$^{II}_4$Mn^{III} (**1**$^{3+}$) and Mn$^{II}_3$Mn$^{III}_2$ (**1**$^{4+}$) have been investigated. Furthermore, Mn$^{II}_4$Mn^{III} has been tested as catalyst in epoxidation reactions.

CHAPTER 7. General conclusions (pages 241-247)

Table of contents

CHAPTER 3. Mn(II) complexes containing the polypyridylic chiral ligand (–)-pinene[5,6]bipyridine. Investigation of the Zero-Field Splitting by combining EPR Spectroscopy and Quantum Chemistry. (pages 51-100)

CHAPTER 4. Catalytic activity of Mn(II) complexes containing the polypyridylic chiral ligand (–)-pinene[5,6]bipyridine: reusable catalytic systems for alkene epoxidation. Evidence of high-valent oxo-bridged binuclear $Mn_2(IV,IV)$ and mixed-valent $Mn_2(III,IV)$ active oxidant species. (pages 101-136)

CHAPTER 5. New N-tetradentate SPANamine type of ligands and their Mn(II) complexes as catalysts for epoxidation of alkenes. (pages 137-202)

CHAPTER 6. Multi-reversible redox processes in pentanuclear bis(triple-helical) manganese complexes featuring an oxo-centered triangular $\{Mn^{II}_2Mn^{III}(\mu_3\text{-}O)\}^{5+}$ or $\{Mn^{II}Mn^{III}_2(\mu_3\text{-}O)\}^{6+}$ core wrapped by two $\{Mn^{II}_2(bpp)_3\}^-$. Evaluation of the catalytic activity in oxidation reactions. (pages 203-240)

CHAPTER 7. General conclusions (pages 241-247)

Summary

Based on the experience of the group in the synthesis of complexes containing N-pyridyl ligands and their subsequent application in catalysis, in this thesis we have synthesized different types of ligands (some of them chiral) with the idea of studying their coordination to different manganese salts, as well as the performance of the complexes synthesized in epoxidation reactions.

The first ligand synthesized was a bipyridine with a pinene moiety fused at the 5 and 6 positions of one of the pyridine rings. In chapter 3 we describe the coordination of this ligand to manganese (II) affording a series of mono- and dinuclear complexes which have been fully characterized. We pay special attention to the magnetic behaviour of the dinuclear complexes and the zero-field splitting of the mononuclear complexes, studied by means of EPR and computational calculations. In chapter 4 we describe the catalytic activity of the complexes synthesized with regard to the epoxidation of aromatic and aliphatic alkenes, using peracetic acid as oxidant. We also study the influence of additives present in the catalytic media and the effect of the use of ionic liquids as co-solvents, a system that allows reusing the catalysts. Moreover, we have investigated the nature of the active catalytic species at low temperature combining EPR, ESI-MS and UV-vis techniques. The results obtained point in all cases to the formation of binuclear $[Mn(\mu\text{-}O)_2Mn]^{n+}$ species but displaying different oxidation states as a function of the starting Mn(II) complex ((IV,IV) for the chloro complexes studied; (III,IV) for the triflate complex), thus evidencing a significant role of the Cl or triflate ligands in the formation of the intermediate species and consequently in the catalytic performance.

The second family of ligands synthesized is based on tetradentate N-donor ligands containing a flexible spiro backbone (SPAN) and pinene-pyridine building blocks. In chapter 5 we describe the synthesis of five new ligands which can contain a racemic or chiral spiro backbone and pyridyl arms with or without pinene fused rings. The ligands have been coordinated to different manganese (II) salts and the resulting complexes have been fully characterized and tested as epoxidation catalysts, unfortunately with low enantiomeric excesses. Their stereospecificity is also studied experimentally with the aid of computational calculations.

Finally, in chapter 6 we describe the synthesis and complete characterization of a pentanuclear complex with a bridging tetra-N-dentate ligand. A thorough study performed by means of electrochemical techniques evidences the excellent stability in solution of this pentanuclear complex in four different oxidation states. This particular compound also presents a good performance in catalytic epoxidation reactions.

Resum

Basats en l'experiència del grup en la síntesi de complexos que contenen lligands de tipus N-piridílic i la seva posterior aplicació en catàlisi, en aquesta tesi hem sintetitzat diferents tipus de lligands (alguns d'ells quirals) amb la idea d'estudiar la seva coordinació a diferents sals de manganès, així com l'activitat dels complexos sintetitzats en reaccions d'epoxidació.

El primer lligand sintetitzat va ser una bipiridina amb un grup pinè fusionat a les posicions 5 i 6 d'un dels anells piridina. En el capítol 3 descrivim la coordinació d'aquest lligand a manganès (II), generant una sèrie de complexos mono- i dinuclears que s'han caracteritzar completament. Incidim de manera especial en l'estudi del comportament magnètic dels complexos dinuclears i del desdoblament a camp nul dels complexos mononuclears, aquests últims estudiats a partir d'EPR i de càlculs computacionals. En el capítol 4 descrivim l'activitat catalítica dels complexos sintetitzats en l'epoxidació d'alquens aromàtics i alifàtics, utilitzant àcid peracètic com a oxidant. També s'avalua l'efecte que té la presència d'additius en el medi catalític i l'efecte de l'ús de líquids iònics com a co-disolvents, que van permetre el disseny d'un sistema catalític reutilitzable. A més, també hem investigat en la natura de l'espècie catalíticament activa combinant les tècniques d'EPR, ESI-MS i UV-vis a baixa temperatura. Els resultats obtinguts apunten cap a la formació d'una espècie dinuclear $[Mn(\mu\text{-}O)_2Mn]^{n+}$ en tots els casos, però amb un estat d'oxidació diferent en funció del complex de partida (estat d'oxidació (IV,IV) pels cloro complexos i (III,IV) pels complexos amb triflat). Aquest resultat evidencia que els lligands Cl i triflat tenen un paper important en la formació d'intermedis i conseqüentment en l'activitat catalítica.

La segona família de lligands sintetitzats està basada en lligands tetradentats N-donors que contenen un esquelet "spiro" flexible (SPAN) i grups piridil. En el capítol 5 descrivim la síntesi de cinc nous lligands que poden contenir un esquelet "spiro" quiral o racèmic i substituents derivats de la piridina amb o sense grups pinè fusionats. Aquests lligands s'han coordinat a diferents sals de manganès (II) i els complexos obtinguts s'han caracteritzat completament i se n'ha avaluat l'activitat catalítica en reaccions d'epoxidació, tot i que malauradament es van obtenir excessos enantiomèrics baixos. També s'ha estudiat la seva estereospecificitat tant experimentalment com amb mètodes computacionals.

Finalment, en el capítol 6 es descriu la síntesi i caracterització d'un complex pentanuclear amb un lligand pont de tipus tetra-N-dentat. Un estudi electroquímic exhaustiu posa de manifest l'excel·lent estabilitat d'aquest complex en solució per a quatre estats d'oxidació diferents. A més, aquest compost s'ha mostrat molt eficaç en reaccions d'epoxidació catalítiques.

Chapter 1

General Introduction
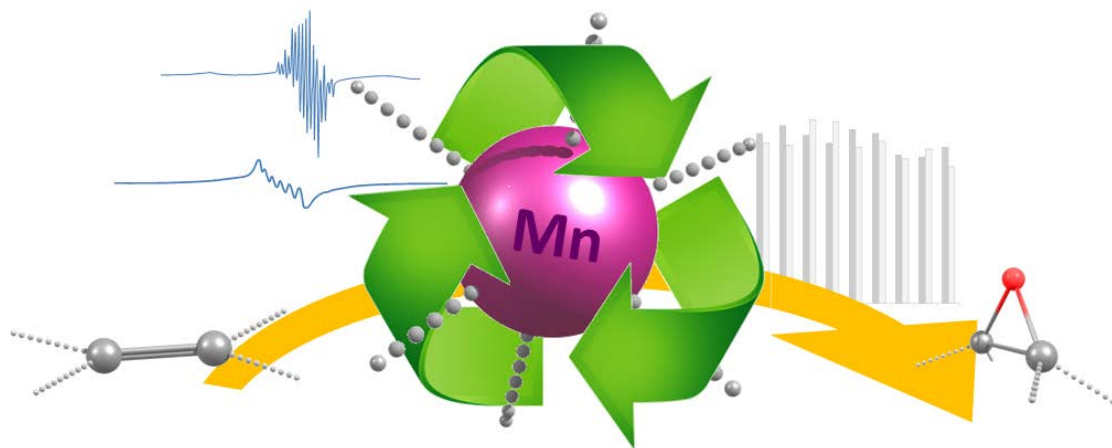
TABLE OF CONTENTS

CHAPTER 1. General introduction

1.1. Generalities of manganese

1.1.1. Properties of manganese

Manganese is a relatively abundant metal, constituting about 0.1% of the earth's crust (1000 ppm), making it the 12th most abundant element and the third most abundant transition element (exceeded only by iron and titanium). It is found in over 300 different and widely distributed minerals of which about twelve are commercially important. As a class-A metal it occurs in primary deposits as the silicate. Of more commercial importance are the secondary deposits of oxides and carbonates such as pyrolusite (MnO_2), hausmannite (Mn_3O_4), and rhodochrosite ($MnCO_3$). Millions of tons of manganese are used annually, and its most common mineral, pyrolusite, has been used in glassmaking since the time of the Pharaohs. The metal is produced by reduction of its oxides with sodium, magnesium, and aluminum, or by electrolysis. Nearly all manganese produced commercially is used in the steel industry as ferromanganese.

Manganese is similar to iron in its physical and chemical properties but is harder and more brittle, though less refractory (mp 1247 ºC). At room temperature, manganese metal is not particularly reactive to air, despite it being quite electropositive; however it frequently reacts vigorously when heated. Thus it burns in O_2 to form the manganese oxide Mn_3O_4, in N_2 to yield the nitride Mn_3N_2, and in Cl_2 to form $MnCl_2$, and reacts with Br_2, I_2, or F_2 to form $MnBr_2$, MnI_2 and both MnF_2 and MnF_3, respectively. It dissolves readily in dilute nonoxidizing acids to form manganese (II) salts ($[Mn(H_2O)_6]^{2+}$) liberating H_2 gas.[1-3]

The most common oxidation states of manganese are +2, +3, +4, +6 and +7, though oxidation states from −3 to +7 are observed. Figure 1 summarizes the relative stabilities of different oxidation states in aqueous solution. The most obvious feature is the relative position of the +2 oxidation state, which is much the most stable, with the +3, +4, +5 and +6 states becoming increasingly less stable. Manganese compounds where manganese is in oxidation state +7, which are restricted to the unstable oxide Mn_2O_7 and compounds of the intensely purple permanganate anion MnO_4^-, are powerful oxidizing agents. Compounds with oxidation states +5 (blue) and +6 (green) are strong oxidizing agents and are vulnerable to disproportionation.

a)

b)
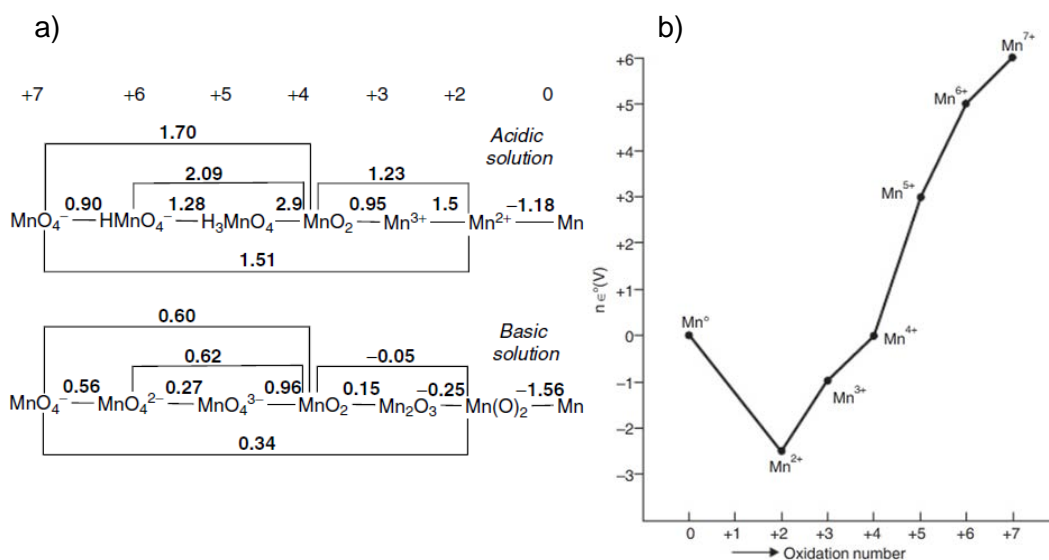
Figure 1. a) Latimer diagrams with standard reduction potentials (E⁰/V) for acidic and basic solution. b) Frost diagram plotting volt-equivalent versus oxidation state in acidic solution.

Table 1 lists representative examples of manganese compounds in various oxidation states.

Table 1. Oxidation state and geometry of some manganese compounds.

Oxidation state	Coord. number	Geometry[a]	Examples
Mn^{II}, d^5	2	Linear	$Mn[C(SiMe_3)_3]_2$
	3	Trig. Planar	$[Mn\{N(SiMe_3)_2\}_3]^-$
	4	Tet	$[MnCl_4]^{2-}$
	4	Square	$[Mn(H_2O)_4]SO_4{\cdot}H_2O$
	5	Tbp	$[Mn(trenMe_6)Br]Br$
	5	Dist. Tbp	$[Mn(ntb)Cl]Cl$
	6	Oct	$[Mn(H_2O)_6]^{2+}$
	6	Dist. Oct	$[Mn(bipy)_3]^{2+}$
	7	Pbp	$MnX_2(N_5macrocycle)$
	7	Dist. Pbp	$[Mn(dmu)_2(NO_3)_2]$
	8	Dod	$[Mn(NO_3)_2(N_4Schiff\ base)]]$
Mn^{III}, d^4	3	Trig. Planar	$Mn[N(SiMe_3)_2]_3$
	4	Square	$[Mn(S_2C_6H_3Me)_2]^-$
	5	Sqpy	$[bipyH_2]MnCl_5$
	5	Tbp	$MnI_3(PMe)_2$
	6	Oct	$Mn(acac)_3$
	6	Dist. Oct	MnF_3, $Mn(terpy)F_3$
	7	Pbp	$[Mn(NO_3)_3(bipy)]$
Mn^{IV}, d^3	4	Tet	$Mn(1\text{-norbornyl})_4$
	6	Oct	MnO_2, $MnCl_6^{2-}$
Mn^{V}, d^2	4	Tet	MnO_4^{3-}, $[Mn(NBu^t)_2\}(\mu\text{-}NBu^t)]_2^{2-}$
Mn^{VI}, d^1	4	Tet	MnO_4^{2-}, $[Mn(NBu^t)_2\}(\mu\text{-}NBu^t)]_2$
Mn^{VII}, d^0	3	Planar	MnO_3^+
	4	Tet	MnO_4^-, $MnO3F$, $MnCl(NBu^t)_2$

[a] Oct: octahedral; Sqpy: square pyramidal; Tbp: trigonal bipyramidal; Tet: tetrahedral; Pbp: pentagonal bipyramidal; Dod: dodecahedral; Dist: distorted.

6

1.1.2. Manganese (II) compounds

This is the dominant oxidation state and the most stable. Manganese (II) is a hard acid and this is manifested, for example, in the preference for O-donor rather than N-donor ligands. Few compounds are also known with P, As, and S-donor ligands.[4] Manganese (II) compounds are generally quite labile. The spin state of the majority of Mn^{II} complexes is high-spin d^5, because of their stable half-filled d electron shell; few low-spin compounds have been isolated,[5,6] for example, $[Mn(CN)_6]^{4-}$. The coordination number and geometries are quite variable because of the lack of ligand-field stabilization energy for the high-spin configuration and appear to depend largely on ligand steric and electronic effects, being coordination geometry six the most common. Lower coordination numbers (three, four and five) are fairly rare, while higher coordination numbers (seven and eight) are more common than for other first-row (+2) transition elements, a reflection of the larger size of Mn^{II}.[4]

In octahedral fields, the high-spin configuration involves, in electronic transitions, the pairing of some electrons and therefore spin-forbidden as well as parity-forbidden character, thus accounting for the extremely pale color of such compounds. In tetrahedral environments, the transitions are still spin-forbidden but no longer parity-forbidden; these transitions are therefore ~ 100 times stronger and the compounds have a noticeable green-yellow color. In low-spin configuration, compounds are strongly colored since a spin-allowed absorption band is expected in the visible region.[1,2]

Magnetic susceptibilities are easily recorded and the high-spin configuration gives an essentially spin-only, temperature independent magnetic moment of $5.92\mu_B$.[1] The strong paramagnetic behaviour unfortunately renders NMR useless, giving broad signals. Single-crystal X-ray diffraction still provides the only unequivocal form of characterization and is now used routinely. The studies in solution remain a major difficulty with these labile systems, and assumptions about the nature of the compounds in solution are often necessary.

Conventional X- and Q-band EPR spectra are generally complex and often difficult to interpret. The recent use of high-field and high-frequency EPR spectroscopy (HF-EPR) has led to simplified spectra with remarkable resolution and provides an accurate determination of the electronic parameters of the studied compounds. Therefore, with

this technique, structural information can be afforded both on solid state and in solution.[7]

Many compounds, generally high-spin, with a variety of open-chain polydentate nitrogen ligands (bidentate to heptadentate) have been isolated with or without additional anion ligands, for example, halides or carboxylates. For example, the tripodal tetradentate ligand ntb (tris(2-benzimidazolylmethyl)amine) with chloride, acetate, or nitrate anions, forms the five to seven-coordinate mononuclear complexes [Mn(ntb)X]Cl (X = Cl, O_2CMe) and [Mn(ntb)$(NO_2)_2$], having trigonal bipyramidal or distorted octahedral geometries.[8] 8N and 7N coordination are found respectively in [Mn($L^1)_2$]$^{2+}$ (Figure 2, **1**),[9] and [MnL^2]$^{2+}$ (Figure 2, **2**);[10] this latter complex has been investigated as superoxide dismutase mimic. The new structure of a rare low-spin, six-coordinate complex [Mn($L^3)_2$] (Figure 2, **3**) has been obtained.[6]

[Mn($L^1)_2$]$^{2+}$
(**1**)

[MnL^2]$^{2+}$
(**2**)

[Mn($L^3)_2$]
(**3**)
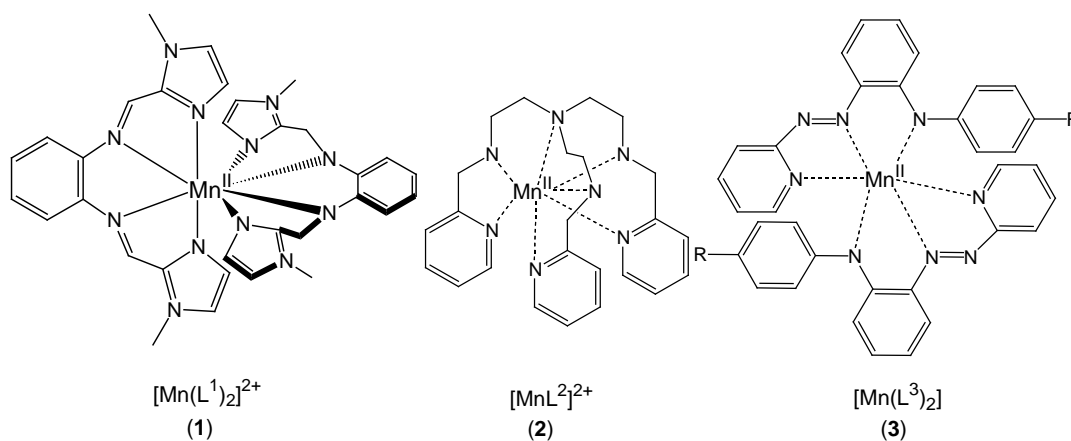
Figure 2. Examples of Mn^{II} coordinated by N-donor ligands.

1.1.3. Manganese compounds in higher oxidation state

The aqua ion of manganese (III) can be obtained by electrolytic or peroxo sulphate oxidation of Mn^{2+} solutions, or by reduction of MnO_4^-.[2] This ion is often subject to disproportionation into manganese (IV) and manganese (II). The chemistry of manganese (III) is dominated by dinuclear, trinuclear and tetranuclear complexes with oxo, alkoxo and carboxylate bridges. The propensity of these complexes to be in mixed-valence states such as manganese (II,III) or manganese (III,IV) requires the confirmation of their structures by spectroscopic and X-ray structural methods. Mononuclear compounds can be stabilized by Schiff-base ligands, nitrogen-base

ligands and macrocyclic ligands. The most commonly observed coordination numbers of manganese (III) are 5[11] and 6.[12] The electronic configuration of manganese (III) is d^4, and therefore, the high-spin configuration (S = 2) in an octahedral field is subject to Jahn-Teller distortion.[13]

Much of the manganese (IV) chemistry involves O-donor ligands.[14,15] The compounds are generally high-spin d^3 (S = 3/2) species and many of them are octahedral. Many porphyrins have Mn=O bonds and have been largely studied as oxygen transfer agents, for example in the epoxidation of C=C bonds.[16] Complexes with oxo bridges are very characteristic of manganese (IV) chemistry (see below).

Most of the high oxidation state compounds (manganese V, VI and VII) also involve oxo compounds; however some other compounds in these oxidation states have been synthesized and characterized, especially those based on nitrido and imido ligands.

1.1.4. Manganese compounds in mixed oxidation state (II to IV)

Small clusters, comprising two to four metal ions, are relevant to biological systems such as manganese catalases and the oxygen-evolving complex of Photosystem II.[17] Apart from these, a large interest has been invested in larger clusters, not only for their biological relevance, but also for their interesting magnetic properties. Those with carboxylate ligands are the most common, although other ligands employed are pyridine, polypyridyl, pyrazolylborates, triazacyclononanes and Schiff bases of various sorts. These have been obtained in oxidation states II-IV with both unitary and mixed valences. The majority of the mixed valence complexes form crystallographically valence-trapped species with distinct sites for each oxidation level. The electronic, magnetic and electrochemical properties of these compounds have been largely investigated. HF-EPR technique has been proposed as a useful tool for the structural investigation of these complexes, especially when incorporating a Mn(III) ion.

The majority of the dinuclear complexes Mn_2(III,IV) and Mn_2(IV,IV) have bis-μ-oxo or bis-μ-oxo mono-μ-carboxylato cores,[18-22] and one example of bis-μ-oxo bis-μ-carboxylato Mn_2(III,IV) is also known.[23] For Mn_2(III,III) complexes, mono-μ-oxo bis-μ-carboxylato and bis-μ-alkoxo mono-μ-carboxylato cores are the most common.[24] Few examples of tris-μ-oxo, di-μ-oxo mono-$\mu_{1,2}$-peroxo, and mono-μ-oxo bridged dinuclear complexes are known.[25,26]

Several Mn_2(II,II) complexes exist with different bridging patterns including solely carboxylates, or those associated with aqua, hydroxo, alkoxo, phenoxo or, more rarely, chloro bridges.[27,28] Conversely, mixed-valent Mn_2(II,III) derivatives have received much less attention.[29]

Higher nuclearity clusters have been reported combining different oxidation states. Some examples are: $[Mn_2^{III}Mn_4^{IV}]$,[23] $[Mn_2^{III}Mn_6^{IV}]$,[30] $[Mn_2^{II}Mn_4^{III}Mn_3^{IV}]$,[31] $[Mn_4^{II}Mn_6^{III}]$,[32] $[Mn_8^{III}Mn_4^{IV}]$,[33] $[Mn_2^{II}Mn_{10}^{III}Mn_4^{IV}]$,[34] $[Mn_{12}^{III}Mn_9^{IV}]$[35] and $[Mn_{18}^{II}Mn_{10}^{III}Mn_4^{IV}]$.[36]

1.2. Manganese in catalysis

1.2.1. Biomimetic oxidations

Nowadays a lot of studies are focused to mimic natural systems that carry out chemical transformations with excellent effectiveness in terms of selectivity and energy consumption. Concretely, the oxidation of organic substrates has received a special interest.[37-41]

Selective oxidation of raw materials is an important area for the chemical industry, due to the necessity to produce oxygen-containing chemicals from fossil hydrocarbons avoiding the complete conversion to carbon dioxide. Selective oxidation is often a difficulty during the preparation of fine chemicals, since it is still challenging to cleanly introduce an alcohol function at the desired position of a drug precursor in the same manner as enzymes.

Many enzymes are present in nature acting as "biological catalysts" capable of catalyzing oxidation reactions in living organisms.[42] Metals in enzymes participate in complex biochemical reactions and highly specialized biological functions thanks to their ability to exist in multiple oxidation states and different geometries. Manganese compounds are used as biomimetic catalysts due to its biological role. Manganese is an essential trace nutrient in all forms of life. Traces of manganese are found in many plants and bacteria, and a healthy human adult contains about 10-20 mg of Mn. The classes of enzymes that have manganese cofactors are very broad, and include oxidoreductases, transferases, hydrolases, lyases, isomerases, ligases, lectins and integrins. The reverse transcriptases of many retroviruses contain manganese. The

best-known manganese-containing polypeptides may be arginase, the diphtheria toxin, and Mn-containing superoxide dismutase (Mn-SOD).

These enzymes are frequently studied by using model complexes which provide information on the nature and reactivity of the active site and also about possible reaction mechanisms. Several factors modulate the reactivity of the active center, such as the nature of the metal and the ligand or the coordination geometry of the metal center. Based on the manganese or iron containing enzymes and on the related model complexes various oxidation catalysts have been studied.

Superoxide (O_2^-), a harmful radical for living organisms, is the product of single electron reduction of oxygen. Due to its high toxicity it needs to be converted to less reactive species. Superoxide dismutases (SOD) are metalloenzymes which catalyze the dismutation of the superoxide (O_2^-) to oxygen (O_2) and hydrogen peroxide (H_2O_2).[43] This latter product can be degraded by catalase enzymes to water and oxygen. The active site of manganese SOD contains a mononuclear five-coordinate Mn^{III} ion bound to three histidines, one aspartate residue and one water or hydroxide ligand.[44]

Manganese is also important in photosynthetic oxygen evolution in chloroplasts in plants. The oxygen-evolving complex (OEC) is a part of photosystem II contained in the thylakoid membranes of chloroplasts. It is responsible for the terminal photooxidation of two water molecules to dioxygen during the light reactions of photosynthesis. Based on many spectroscopic measurements it has been recognized that a tetranuclear Mn-cluster is the active catalyst for the oxygen evolution,[45] which has been confirmed by the crystal structure of PSII.[46,47] However, the exact mechanism of the water oxidation has not been elucidated so far.

Catalases decompose hydrogen peroxide to water and oxygen[48] and some of these manganese enzymes have been isolated from different bacteria.[49,50] X-ray crystallographic structure analysis elucidated that these catalases contain a dinuclear manganese center.[51,52] During the catalytic process the dinuclear manganese active sites cycle between the Mn^{II}_2- and Mn^{III}_2-oxidation states (Scheme 1).[53]

Many compounds containing a dinuclear manganese core encompassed by a variety of ligand types have been employed as catalase mimic complexes.[27,54 -60]
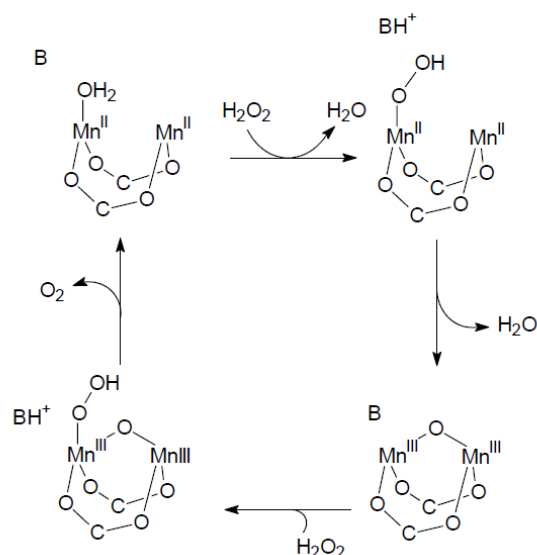
Scheme 1. Proposed mechanism for manganese catalases.

The development of artificial models of cytochrome P450 in oxidation reactions of organic substrates has also received special attention.[38,61] Although iron models have received much more attention, synthetic manganese porphyrins have been extensively used as P450 models, and both Mn(IV)-oxo and Mn(V)-oxo porphyrin complexes have been characterized.[62,63]

Nature is able to efficiently perform monooxygenation reactions by introducing one oxygen atom of molecular oxygen into a defined substrate, while the second oxygen atom of O_2 is eliminated as a water molecule with the associated consumption of two electrons provided by NAD(P)H:

$$R\text{—}H + O_2 + 2e^- + 2H^+ \xrightarrow[\text{(e.g. Cytochrome P450)}]{\text{Monooxygenase}} R\text{—}OH + H_2O$$
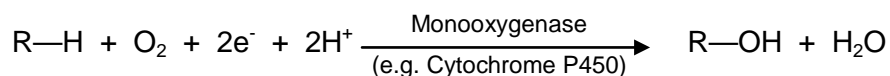
Although many artificial systems based on molecular oxygen together with an electron source have been reported to catalyze hydroxylation and epoxidation reactions, it has been observed the formation of water as the main product instead the expected alcohol or epoxide, via the $2e^-$ reduction of the intermediate metal-oxo species.[64] An alternative way to avoid this difficulty is to use peroxides or single oxygen atom donors such as hydrogen peroxide (H_2O_2), alkylperoxides (ROOH), iodosylbenzene (PhIO), hypochlorite (NaOCl), monopersulfate ($KHSO_5$) or peracids. The use of oxygen atom donors to generate the oxidized species is known as the "peroxide shunt" (Scheme 2).[65-67] In particular hydrogen peroxide is the suitable "green" oxidant since the only

side product after an oxidation reaction is water. However, peroxides have a weak and rather symmetrical O-O bond. The low dissociation energy leads to spontaneous homolytic cleavage and the formation of hydroxyl radicals HO•. Alkylhydroperoxides ROOH can be easily cleaved by transition metal complexes and the resulting alkoxyl radicals RO• are able to efficiently abstract hydrogen atoms from alkanes leading to a mixture of alcohols and ketones as in autoxidation reactions.[68]
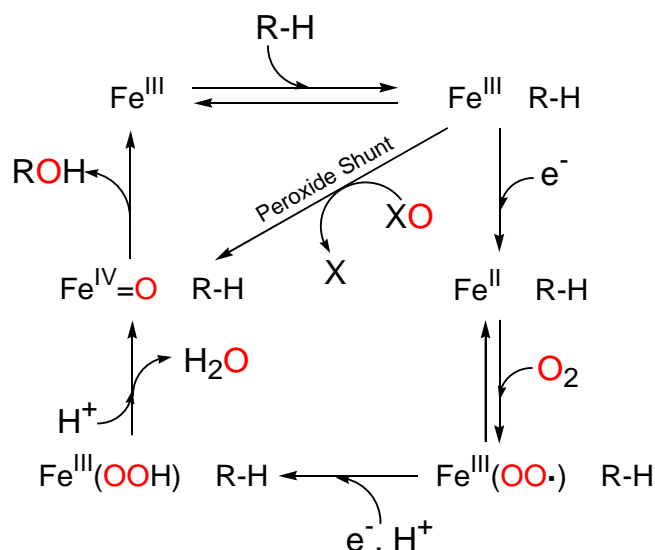
Scheme 2. Catalytic cycle for oxygen activation and transfer by cytochrome P450.

Effective monooxygenase models are able to perform both hydroxylation of alkanes and epoxidation of olefins, since the active species is an electrophilic high-valent metal-oxo entity like in the corresponding metalloenzymes. The metal center is able to activate the oxidant and then to control the oxygen atom transfer from the metal-oxo species to the substrate (the oxygen rebound mechanism involves an organic radical intermediate controlled by the metal center, without formation of free radicals). All the different studies on the modeling of oxygenases clearly confirm that the coordination of olefins to the metal-oxo center is not necessary to produce epoxides.

All the biomimetic oxidations have largely contributed to the development of methods for the characterization of high-valent metal-oxo species[69-71] and to the understanding of their chemical reactivity with respect to organic substrates,[72-75] although new studies are required to deepen in the processes and mechanisms.

1.2.2. Asymmetric epoxidation of alkenes

The increasing demand for enantiomerically pure materials leads to a constant development of new methods of asymmetric oxidations allowing the preparation of highly useful synthons from low cost starting materials, such as olefins, ketones, etc. Among all the different asymmetric reactions leading to the incorporation of one or two oxygen atom(s) within a substrate, the most desirable and the most challenging is the catalytic asymmetric oxidation.[38,76,77]

Although great advances in oxidation technologies have been developed over the last century, an important remaining challenge is to achieve more efficient and selective incorporation of oxidized functionalities into organic frameworks using inexpensive and environmentally friendly conditions. Most oxidants have the disadvantage that, in addition to the oxidized products, stoichiometric amounts of waste products are generated. Thus, there is special interest on the use of environmentally friendly "green" oxidants to minimize the amount of waste.[38] Among the environmentally benign oxidants, the most efficient are peroxides, in particular hydrogen peroxide since the only side product after the oxidation reaction is water and it is relatively cheap. However, hydrogen peroxide also presents some disadvantages such as the easy generation of highly reactive hydroxyl radicals (•OH), giving rise to non-selective oxidation reactions, and often self-disproportionation in the presence of transition metals.[78]

Olefin epoxidation has received considerable interest from both academics and industry. Concretely enantiomerically pure epoxides constitute an important and versatile class of intermediates and building blocks in organic synthesis to obtain more elaborated chemical products both in organic synthesis itself and in industrial production of bulk and fine chemicals.[39,79,80] The epoxides can be transformed into a variety of functionalized products. For example their reduction, rearrangements or ring-opening reactions with various nucleophiles can lead to the formation of diols, aminoalcohols, allylic alcohols, ketones, etc. (Scheme 3).[81-84]

Although numerous procedures have been developed, the need to understand the mechanisms of metal-mediated oxygen processes demands the synthesis of new stable and available catalysts. For this reason, the selective epoxidation of olefins is an important field of research in industry and academia.
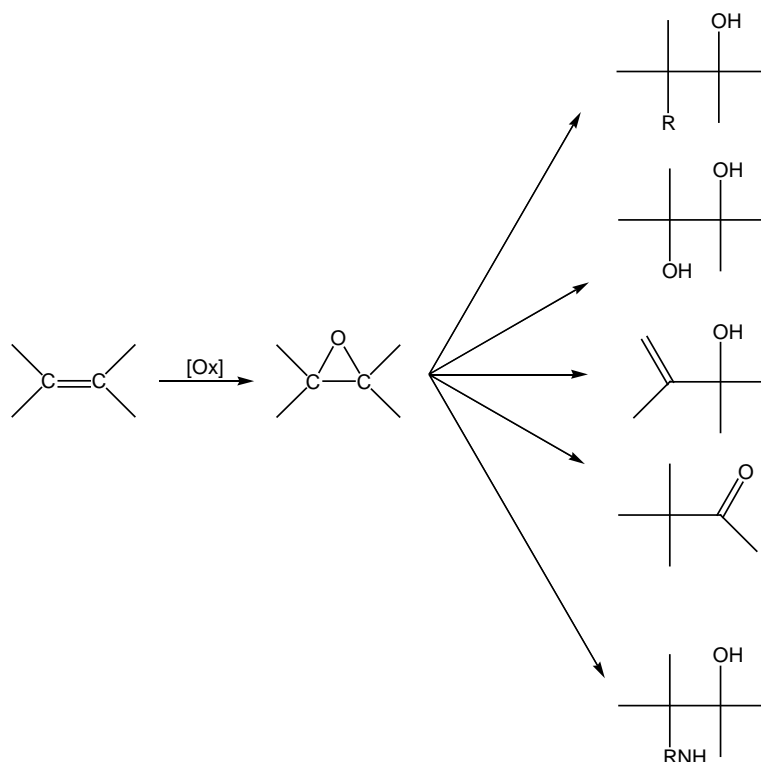
Scheme 3. Epoxide formation and possible further conversions.

The field of catalytic asymmetric oxidation was introduced in 1980 by Sharpless and Katsuki on the asymmetric epoxidation of allylic alcohols by combining Ti(iOPr)$_4$, an optical active tartrate ester and t-butyl hydroperoxide.[85] This reaction has been successfully developed at the industrial scale for the preparation of many different allylic epoxides. Furthermore, this catalytic system has been adapted to the asymmetric oxidation of sulfides to chiral sulfoxides with high enantiomeric purity.[77,86] These optically active sulfoxides are useful chiral auxiliaries in asymmetric organic synthesis.

The field of biomimetic asymmetric oxidations started initially with chiral metallo-porphyrins, but it was found to be applicable in organic synthesis when chiral Schiff base complexes were developed independently by Jacobsen[77,87] and Katsuki.[88-90]

1.2.2.1. Asymmetric oxidations catalyzed by chiral metalloporphyrins

Cytochrome P450 enzymes are able to perform asymmetric oxygenation reactions (epoxidation and hydroxylation) because of the chiral environment created by the amino acids of the active site. In the late 1970s no chemical catalysts were able to

perform such reactions. However, the discovery of metalloporphyrins (Figure 3) as biomimetic catalysts able to epoxidize olefins and hydroxylate alkanes without free radical intermediates, triggered in 1983-1988 the initial reports on asymmetric epoxidations of non-activated olefins catalyzed by chiral metalloporphyrins.
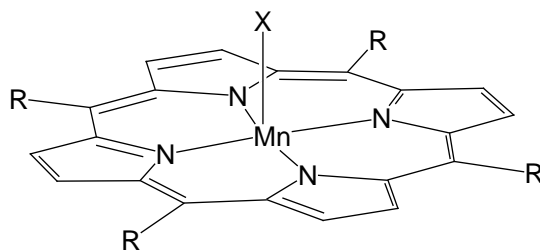
Figure 3. Structure of metalloporphyrin Mn catalysts used in asymmetric epoxidations.

Different oxidants have been used in these metalloporphyrin-catalyzed asymmetric epoxidations: iodosylbenzene (PhIO), sodium hypochlorite, meta-chloroperbenzoic acid (m-CPBA), alkylhyroperoxides, peracids and H_2O_2, being iodosylbenzene and hypochlorite the most studied.[68,91-97] With this latter oxidant and chiral manganese porphyrins, Kodadek *et al.* reported high turnover numbers with styrene-type olefins, ranging from 950 to 18700 cycles, and high *ee* values ranging from 40% to 70%.[98] With aliphatic olefins they obtained 15000 cycles with a remarkable 85% *ee* value. The first attempts of epoxidation of olefins with H_2O_2 as oxidant were unsuccessful due to the dismutation of H_2O_2. Mansuy *et al.* demonstrated that the catalytic system could be greatly improved by performing the oxidation reaction in the presence of large amounts of imidazole, giving epoxide yields up to 99%.[99] It was found that the employment of co-catalysts such as pyridines, imidazoles and quaternary ammonium salts results in a significant change of catalytic activity of metalloporphyrins, in particular manganese (III) porphyrin catalysts.[100,101]

Concerning the design of chiral metalloporphyrin catalysts, Collman *et al.* reported that the D_4 symmetry seems to provide the most efficient metalloporphyrin catalysts in asymmetric epoxidations.[102]

In 1990 Groves and Viski reported the first asymmetric hydroxylations with a vaulted manganese porphyrin catalyst with *ee* values ranging from 40% to 72%, with iodosylbenzene as oxidant.[103] Stereoselective hydroxylation at single inactivated carbon atoms of chiral substrates was also performed with a manganese porphyrin

carrying four β-cyclodextrin substituents.[104] It must be noted that the rate of this sophisticated hydroxylation reaction is close to that observed for cytochrome P450.

1.2.2.2. Asymmetric oxidations catalyzed by chiral Schiff base complexes

In 1980, it was reported that catalytic amounts of manganese Schiff bases associated with sodium hypochlorite as oxygen atom donor were able to epoxidize styrene (8% epoxide yield after 3 hours).[92,93] Some years later, Kochi *et al.* used chromium[105] and manganese[106] Schiff base complexes as catalysts for olefin epoxidation in the presence of iodosylbenzene. Although the obtained yields were moderate with these non-chiral catalysts, these preliminary works evidenced that Schiff base complexes were able to mimic the monooxygenase activity of heme proteins, in a similar way as synthetic metalloporphyrins. A few years after the discovery of Kochi, the groups of Katsuki[88] and Jacobsen[87] independently described a breakthrough in this olefin epoxidation by the introduction of a chiral diamine functionality in the salen ligand.

Thus, enantioselective oxidations catalyzed by chiral manganese complexes with Schiff base ligands were first described by Katsuki *et al.*[88,107-109] These manganese complexes, bearing four chiral centers (Figure 4), have been used for the epoxidation of non-functionalized olefins, with iodosylbenzene as oxidant. For the epoxidation of *cis*-olefins, *ee* values up to 96% were obtained, whereas lower *ee* values were observed for *trans*-olefins.
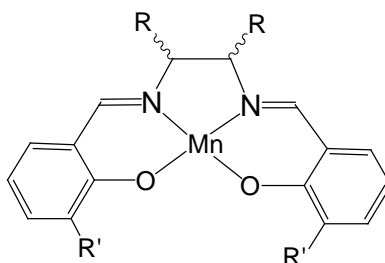
Figure 4. General structure of a manganese Schiff base complex.

During the same period, Jacobsen *et al.* developed a series of manganese Schiff base complexes bearing only two asymmetric centers on the diamine moiety and *tert*-butyl

substituents in *ortho* position to the phenol function.[87] With iodosylmesitylene as the oxidant, the epoxidation of 1,2-dihydronaphtalene was obtained with 72% yield and 78% *ee*.

Then, Jacobsen *et al.* described the synthesis and use of about one hundred metal complexes based on C_2 symmetric salen chiral ligands.[77,110,111] The presence of bulky substituents is important for two reasons: they enforce the prochiral olefin approach near the dissymmetric diimine bridge and they create a cage effect around the generated manganese-oxo species.

In some cases, the presence of bases as axial ligands increases both catalytic activity and enantioselectivity.[112] The presence of electron-donating groups on the catalyst provides higher enantioselectivities in epoxidation reactions.[113]

The best Jacobsen's catalyst (Figure 5) can be prepared on a large scale[114] and is now commercially available. When associated with the simple and cheap oxidant NaOCl, this catalyst was found to be efficient and has been widely developed for the asymmetric epoxidation of a variety of interesting and important substrates. Especially remarkable is the epoxidation of 2,2-dimethyl-3-chromene derivatives (*ee* = 98%).[115] The enantioselective epoxidation of 6-cyano-2,2-dimethyl-3-chromene was a key step for the synthesis of the antihypertensive agent chromakalim. The epoxidation of *cis*-ethyl cinnamate ester (*ee* = 95-97%) was applied to the synthesis of the Taxol C-13 side chain.[112] This method of direct epoxidation of an α,β-unsaturated ester via an oxo transfer was also used in the asymmetric synthesis of the antihypertensive diltiazem.[116]
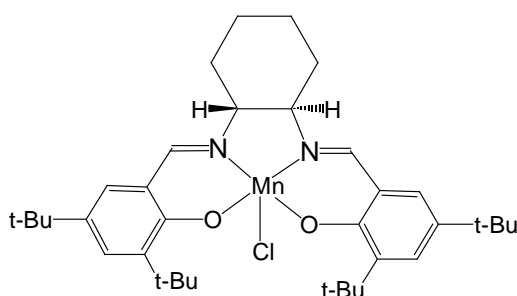
Figure 5. Structure of the best Jacobsen's catalyst.

The facts that *cis*-olefins are generally more reactive in the Mn(III)salen-catalyzed epoxidation, and that the epoxidation of conjugated *cis*-olefins gives *trans*-epoxide as the major product,[117] suggest a strategy for the regio- and enantioselective synthesis of

trans,trans-diene monoepoxides by epoxidation of *cis,trans*-conjugated dienes. This strategy was successfully applied to the synthesis of a variety of optically active vinyl epoxides.[118]

Manganese-salen complexes were also used for the epoxidation of one of the chemical industry's most important prochiral olefins, styrene, with ee up to 83% using the Jacobsen's catalyst displayed in Figure 5, m-CPBA as oxidant and N-methylmorpholine N-oxide as co-catalyst.[119]

The same Schiff base ligands coordinated to chromium(III) were used for the enantioselective ring-opening of epoxides with trimethylsilyl azide, providing optically pure α-azido trimethylsiloxy intermediates (Figure 6).[120] This asymmetric ring-opening of meso and racemic epoxides by TMSN$_3$ displayed a particularly high enantioselectivity for the opening of epoxides fused to five-membered rings.[121,122] This method has been applied for the synthesis of carbocyclic nucleoside analogues used as potential anti-HIV agents.[123]
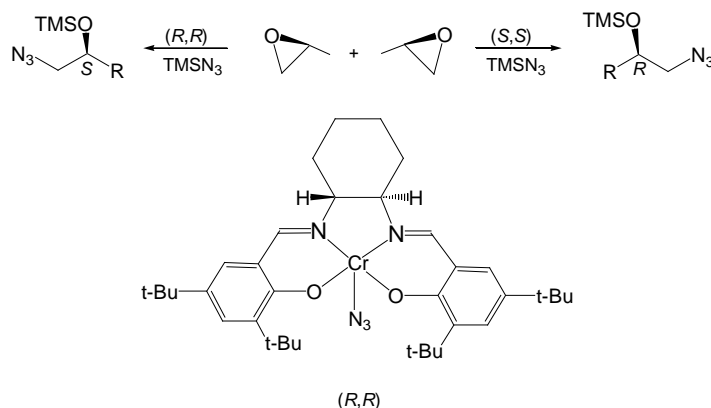
Figure 6. Asymmetric ring opening of epoxides by trimethylsilyl azide.

In order to improve the activity and selectivity, and to broaden the scope of substrates of chiral manganese Schiff base complexes (especially in the epoxidation of terminal olefins), a new series of ligands and metal complexes based on the optically active binaphthyl moiety was developed (Figure 7).[124,125] In order to enlarge the availability of these chiral ligands, they were coordinated to Mn, Fe, Co, Ni, Cu and Zn with different results.[125]

X = H, Cl, Br, *t*-Bu or NO$_2$

M = Mn, Ni, Fe, Co, Zn, Cu
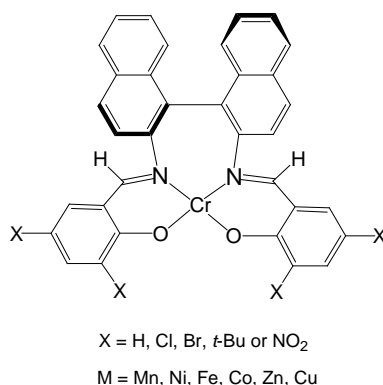
Figure 7. Complexes with binaphthyl moiety.

In spite of a chiral environment, the manganese complexes displayed poor catalytic activity and enantioselectivity probably due to extensive degradation of the manganese binaphthyl-based complexes under the oxidation reaction conditions (sodium hypochlorite, hydrogen peroxide or m-chloroperbenzoic acid/N-methylmorpholine N-oxide as oxidant). This instability could be due to the highly distorted geometry of the complexes, more compatible with tetrahedral rather than octahedral or square-pyramidal coordination.

Compared with chiral manganese porphyrin complexes, the use of Mn-salen catalysts generally results in higher *ee*'s and yields. However, the main limitations of Mn-salen complexes are the relatively limited substrate scope, relatively high catalyst loading requirement (5-10%) and easy catalyst degradation, leaving many opportunities for improvement.

1.2.2.3. Other ligands for asymmetric oxidation catalysis

In 2004 Stack *et al*. presented a new tetradentate N-donor system (Figure 8) that, when coordinated to manganese, is able to catalyze epoxidation of terminal olefins with peracetic acid, with 400-1000 TON in only 5 minutes.[126] A comparison between the performances obtained using commercial peracetic acid (pH ~ 1) or peracetic acid prepared with acidic resins (pH ~ 4) determined that some manganese complexes with neutral polyamines show dependence on the acidic conditions, with better reactivity in less acidic conditions.[127]
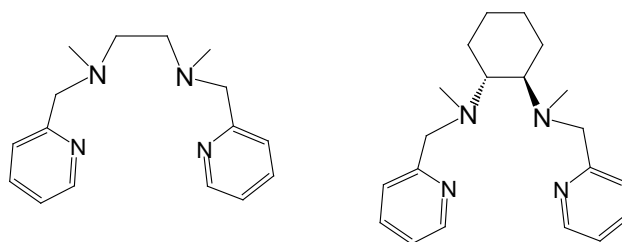
Figure 8. Structure of some ligands used by Stack.

Stack also presented a simple complex prepared "in situ", $[Mn(bpy)_2]^{2+}$, with a conversion of 99% and yield of 95% (> 1000 TON/min) for the epoxidation of 1-octene with peracetic acid previously prepared from acidic resins.[127]

Feringa *et al.* developed a series of dinuclear manganese complexes prepared "in situ" from $Mn(OAc)_3 \cdot 2H_2O$ and polidentate ligands (Figure 9). These complexes oxidize selectively primary and secondary alcohols to aldehydes and ketones with H_2O_2 as oxidant (TON up to 900).[128]
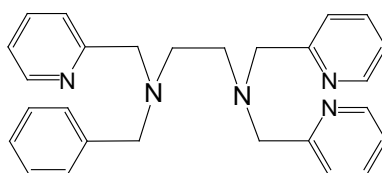
Figure 9. Structure of one of the ligands used by Feringa.

More recently, Pfaltz *et al.* reported a system based on N4 diamino-bisoxazoline manganese complexes (Figure 10). Modest stereoselectivity (up to 21%) was observed using peracetic acid as oxidant.[129]
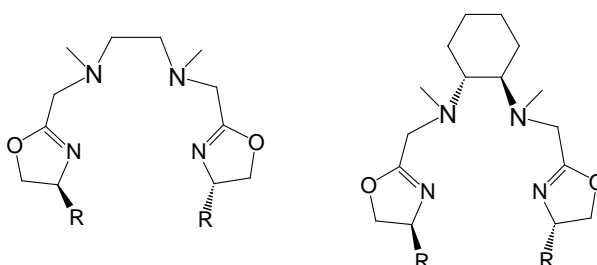
Figure 10. Structure of the ligands reported by Pfaltz.

1.2.3. Oxidations in ionic liquids

As the introduction of cleaner technologies has become a major concern throughout both industry and academia, the search for alternatives to the most damaging solvents has become a high priority.[130] The chemical industry is under considerable pressure to replace many of the volatile organic compounds (VOCs) that are currently used as solvents in organic synthesis. The toxic and/or dangerous properties of many solvents, notably chlorinated hydrocarbons, combined with serious environmental issues, such as atmospheric emissions and contamination of aqueous effluents are making their use prohibitive. This is an important driving force in the quest for novel reaction media.

The current emphasis on novel reaction media is also motivated by the need for efficient methods for recycling homogeneous catalysts. The key to waste minimization in chemicals manufacture is the general substitution of classical "stoichiometric" syntheses by atom efficient, catalytic alternatives.[131]

In this sense, the use of ionic liquids as novel reaction media may offer a convenient solution to both the solvent toxicity and the catalyst recycling problems.[132-142]

Over the last decade, growing attention has been devoted to the use of ionic liquids (ILs) as solvents for organic synthesis. The strong interest in ILs for catalyzed reactions is due to the expected immobilization of the catalyst in the IL that would allow the recycling of the tandem catalyst/solvent.[143] Furthermore, ILs have a rate acceleration effect on some catalytic reactions, and they are often considered as green alternatives to volatile organic solvents although their toxicity and biodegradability are yet to be fully determined.[144-148]

Ionic liquids are in general defined as liquid electrolytes composed entirely of ions. More recently, the melting point criterion has been proposed to distinguish between molten salt (high melting, highly viscous, and very corrosive medium) and ionic liquids (liquid below 100ºC and relatively low viscosity).[134] Generally, ionic liquids include liquid compounds which involve organic compounds and organominerals. Those ionic liquids based on quaternary ammonium or phosphonium salts, usually named room temperature ionic liquids (RTILs), exhibit interesting physicochemical properties:[147,149,150]

-they have a relatively wide electrochemically stable window and good electrical conductivity

-they have essentially no vapor pressure. Ionic liquids are nonvolatile, hence they may be used in high-vacuum systems and eliminate many containment problems

-they generally have reasonable thermal and chemical stabilities

-they are non-flammable

-they are able to dissolve a wide range of organic, inorganic and organometallic compounds

-the solubility of gases into ILs is generally good, which makes them attractive solvents for catalytic hydrogenations, carbonylations, hydroformylations and aerobic oxidations

-they are immiscible with a number of organic solvents

-polarity and hydrophilicity/lipophilicity can be readily adjusted by a suitable choice of cations and anions, thus ionic liquids have been referred to as "designer solvents"

-they are often composed of weakly coordinating anions and, hence, have the potential to be highly polar yet non-coordinating solvents

These properties make them a good candidate to comply with contemporary environmental standards and economical requirements. Additionally, properties such as temperature-depending miscibility with water make them attractive alternatives to organic solvents. Organometallic complexes which are immiscible with hydrocarbons are often soluble in ILs. Therefore they provide a non-aqueous polar alternative for two-phase catalysis, in which the catalyst is immobilized in the ionic liquid phase and can easily be separated from the product.

Then, ionic liquids are possible solvents for reactions with homogeneous catalysts. However, depending on the coordinative properties of the anion, the IL can be regarded as an "innocent" solvent or as a cocatalyst. When the IL is considered an inert solvent, its role is solely to provide a polar, weakly coordinating medium for the transition metal catalyst that additionally offers special solubility for feedstock and products. The use of ILs often allows a combination of solvent properties which cannot be reached with water or common organic solvents.

As mentioned earlier, room temperature ionic liquids are generally salts of organic cations. The most common salts in use are those with alkylammonium, alkylphosphonium, N-alkypyridinium and N,N'-dialkylimidazolium cations (Figure 11). In order to be liquid at room temperature, the cation should preferably be unsymmetrical.

Typically, the anions are inorganic and include $[PF_6]^-$, $[BF_4]^-$, $[CF_3SO_3]^-$ and $[(CF_3SO_2)_2N]^-$.

cations:

anions: BF_4^-, PF_6^-, SbF_6^-, NO_3^-, $CF_3SO_3^-$, $(CF_3SO_3)_2N^-$, $ArSO_3^-$, $CF_3CO_2^-$, $CH_3CO_2^-$, $Al_2Cl_7^-$
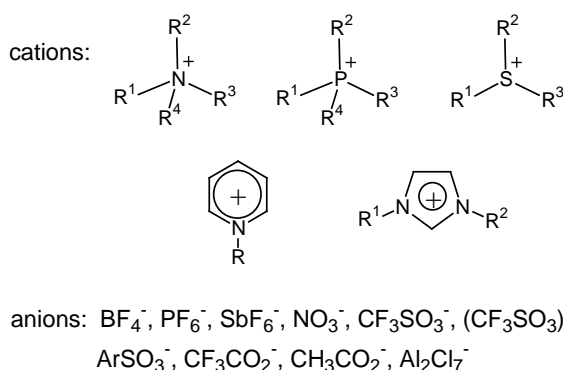
Figure 11. Structures of common components in ionic liquids.

Ionic liquids represent a new class of solvents with nonmolecular ionic character. Even though the first representative has been known since 1914, ionic liquids have only been investigated as solvents for transition metal catalysis in the past twenty years, and this has led to a greater than exponential growth in the number of papers published. Publications to date show that replacing an organic solvent by an ionic liquid can lead to remarkable improvements in well-known processes.[151,152] There are also indications that switching from a normal organic solvent to an ionic liquid can lead to novel and unusual chemical reactivity. This opens up a wide field for future investigations into this new class of solvents in catalytic applications.

In 2000, Song *et al.* reported the first example of a transition metal catalyzed oxidation reaction in an ionic liquid. They disclosed a procedure to recycle achiral Jacobsen-type (salen)Mn(III) epoxidation catalyst (Scheme 4).[153] The asymmetric epoxidations were carried out at 0ºC in [bmim][PF_6], with NaOCl as the oxidant, and a co-solvent (CH_2Cl_2, 1:4 v/v) since the IL solidifies at the reaction temperature. The authors described a clear enhancement of the catalyst activity by the addition of the ionic liquid to the organic solvent. In the presence of the ionic liquid an 86% conversion of 2,2-dimethylchromene was observed after 2h. Without the ionic liquid the same conversion was obtained only after 6h. In both cases the enantiomeric excess was as high as 96%. Moreover, the use of the ionic liquid solvent allowed an easy catalyst recycling without the need of any catalyst modification. After five recycles the conversion dropped from 83% to 53% under identical reaction conditions. The authors explain this loss in activity by a slow degradation of the [Mn^III(salen)] complex.
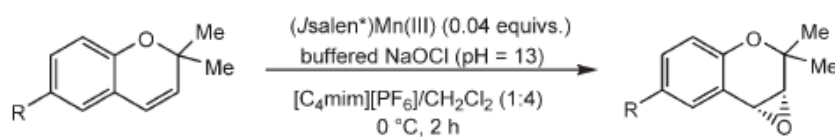
R = H: 86% yield, 96% ee (5th use: 53% yield, 86% ee)
R = CN: 72% yield, 94% ee

Scheme 4. Epoxidation with Jacobsen-type catalyst in IL.

Smith *et al*. used a chiral Katsuki-type (salen)Mn(III) catalyst for the epoxidation at 0°C of 1,2-dihydronaphthalene with NaOCl, in a mixture of [bmim][X] (X = PF$_6$ or BF$_4$) and an organic solvent (CH$_2$Cl$_2$ or EtOAc), and in the presence of 4-phenylpyridine-*N*-oxide (Scheme 5). A higher reactivity and similar *ee*'s were achieved when compared to those obtained in chlorinated solvents. Under identical experimental conditions, (*K*salen*)Mn(III) provided higher yield and enantioselectivity than (*J*salen*)Mn(III) but required a longer reaction time. Up to 100% *ee* was obtained under some specific conditions.[154]
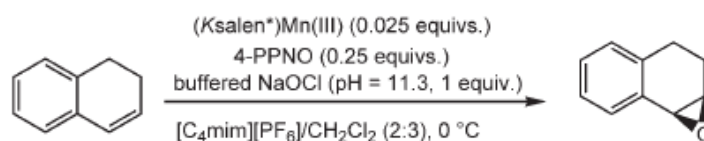
1st use, 1 h: 81% yield, 93% ee
5th use, 2.5 h: 63% yield, 90% ee
9th use, 5 h: 50% yield, 79% ee

Scheme 5. Epoxidation with Katsuki-type catalyst in IL.

Manganese porphyrins in a mixture of [bmim][PF$_6$] and CH$_2$Cl$_2$ were used, at ambient temperature, by Xia *et al*. for the efficient catalytic epoxidation of various alkenes with iodosylbenzene diacetate, this latter being more efficient than PhIO (Scheme 6). Effective recycling of the catalytic system was obtained.[155-157]

R^1 = n-pentyl, R^2 = H: 74%, 6th cycle: 86%
R^1-R^2 = C$_4$H$_8$: 74%, 6th cycle: 56%

MnTPPCl: 90%; MnTMOPPCl: 92%
MnTFPPCl: 99%, 10th cycle: 72%
MnTPPS$_4$: 98%, 7th cycle: 96%
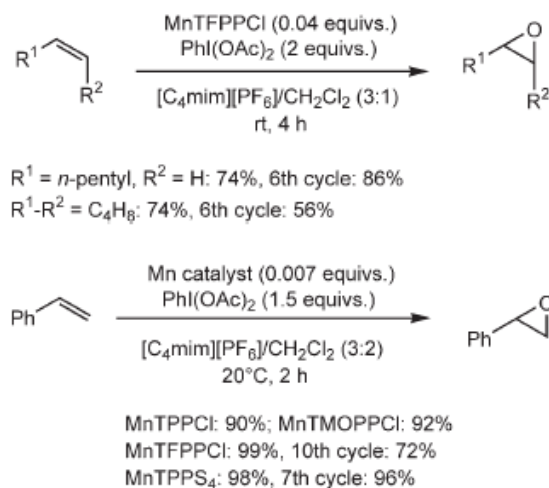
Scheme 6. Epoxidation with manganese porphyrins in ILs.

Since then, ILs have been successfully applied in olefin epoxidations, utilizing manganese(III) catalysts with porphyrins or Schiff base ligands.[158-161]

Moreover, effective epoxidation of various alkenes was accomplished at room temperature in [bmim][BF$_4$] with aqueous hydrogen peroxide, in the presence of catalytic amounts of manganese sulfate and a stoichiometric quantity of tetramethylammonium hydrogen carbonate. Good reactivities and high selectivities were generally obtained, except for the case of an unactivated terminal alkene such as 1-decene, which was unmodified, and 1-phenylcyclohexene. For recycling experiments, some amounts of MnSO$_4$ and Me$_4$NHCO$_3$ have to be added from time to time to restore the activity of the system.[162]

The asymmetric epoxidation of limonene was investigated by the group of Bernardo-Gusmao *et al*. They used the Jacobsen's Mn(salen) catalyst and hydrogen peroxide as oxygen source. The catalytic procedure was performed in [bmim][BF$_4$] and resulted in a high diastereomeric excess of 74% to the respective 1,2-epoxi-*p*-ment-8-enes, while the conversion was 70%.[163] Also a Mn(salen) catalyst was used for the oxidation of styrene with molecular oxygen to benzaldehyde.[164]

Finally, in 2010 Wong *et al*. reported a novel and robust IL system for the rapid epoxidation of a number of aliphatic terminal alkenes under relatively mild conditions using manganese(II) acetate as an effective ligand-free catalyst precursor, with peracetic acid as oxidant.[165]

1.3. Magnetism and EPR of manganese compounds

1.3.1. Molecular magnetism[166-168]

1.3.1.1. Magnetization and magnetic susceptibility

The use of magnetic properties as a tool for the determination of the structure of d-transition metal complexes has received considerable attention.

When a paramagnetic substance is exposed to a magnetic field H, the substance becomes magnetized with a magnetization M. The magnetic field within the substance is given by the magnetic induction B.

$$B = H + 4\pi M$$

In SI units the relationship between B, H and M is given using the permeability of free space, μ_0, as:

$$B = \mu_0(H + M)$$

The units of B are G (gauss) in cgs units and T (tesla) in SI units, with a conversion of 1 G = 10^{-4}T (Table 2).

The magnetization is defined as the variation of internal energy of a sample when it is perturbed by a magnetic field.

$$M = -\frac{\partial E}{\partial H}$$

Applying the Boltzmann distribution factors (P_n), the magnetization can be calculated as:

$$M = N \sum_n \mu_n P_n = N \frac{\sum_n (-\partial E_n/\partial H)\exp(-E_n/kT)}{\sum_n \exp(-E_n/kT)}$$

where k = Boltzmann constant, and N = Avogadro number.

Since the magnetic properties of the materials should be measured as a direct magnetization response to the applied magnetic field, the ratio of *M* to *H* is important:

$$\chi = \frac{\partial M}{\partial H}$$

This quantity, χ, is called "magnetic susceptibility", and is related to the degree to which a material can be magnetized in an external magnetic field. The magnetization of ordinary materials exhibits a linear function with *H*. Ordinary weak magnetic substances follow $M = \chi H$.

The unit of susceptibility is emu cm^{-3} Oe^{-1} in cgs units and it is dimensionless in SI units. In molecular magnetism, it is commonly used the molar magnetic susceptibility χ_M, whose units are emu mol^{-1} Oe^{-1} in cgs units and m^3 mol^{-1} in SI units.

$$\chi_M = \frac{N}{H}\frac{\sum_n (\partial E_n/\partial H)\exp(-E_n/kT)}{\sum_n \exp(-E_n/kT)}$$

In 1932 Van Vleck proposed a general method for calculating magnetic susceptibility,[169] based on some approximations, assuming the energy as an expansion in a series of the applied field: $E_n = E_n^{(0)} + E_n^{(1)}H + E_n^{(2)}H^2 + \ldots$ and $H/kT \ll 1$. This is fulfilled under the conditions of *H* not being too large and *T* not too low. The final Van Vleck equation is:

$$\chi_M = N\frac{\sum_n \left[(E_n^{(1)})^2/kT - 2E_n^{(2)}\right]\exp(-E_n^{(0)}/kT)}{\sum_n \exp(-E_n^{(0)}/kT)}$$

where $E_n^{(0)}$ is the energy in the zero field, and $E_n^{(1)}$ and $E_n^{(2)}$ are the first- and second-order Zeeman terms.

The latter equation can be simplified for mononuclear or polynuclear complexes formed for ions without orbital contribution ($E_n^{(2)} = 0$):

$$\chi_M = \frac{Ng^2\mu_B^2}{3kT}\frac{\sum_S S(S+1)(2S+1)\exp[-E_S^0/kT]}{\sum_S (2S+1)\exp[-E_S^0/kT]} + N\alpha$$

where S = total spin of each energy state $E_S^{(0)}$ and μ_B is the Bohr magneton.

Table 2. Units used in magnetism in the SI system and in the cgs system.

Quantity	Symbol	SI units		cgs units
Energy	E	10^{-7} J	= 1	erg
Magnetic induction	B	10^{-4} T	= 1	G
Magnetic field strength	H	$10^3/4\pi$ A m-1	= 1	Oe
Magnetization	M	10^{-3} A m^{-1} or J T^{-1} m^{-3}	= 1	Oe or emu cm^{-3}
Magnetic susceptibility	χ	4π	= 1	emu cm^{-3} or emu cm^{-3} Oe^{-1}
Molar susceptibility	χ_M	$4\pi \times 10^{-6}$ m^3 mol^{-1}	= 1	emu mol^{-1} or emu mol^{-1} Oe^{-1}
Mass susceptibility	χ_g	$4\pi \times 10^{-3}$ m^3 kg^{-1}	= 1	emu g^{-1} or emu g^{-1} Oe^{-1}

1.3.1.2. Magnetic properties of polynuclear transition metal complexes

In a polynuclear compound based on transition metals bounded through diamagnetic bridges, there is some overlap between the metallic orbitals with unpaired electrons. This is known as superexchange mechanism, which involves the ligand frontier orbitals and gives rise to magnetic coupling between metallic centers.

The simplest example is the magnetic coupling between two metallic centers with one unpaired electron each one, which interact to create two molecular orbitals. The two electrons can fill one molecular orbital (the one with lower energy) or two different molecular orbitals (Figure 12). In the first case, the resulting spin state is $S_T = 0$ (singlet), whereas in the second case is $S_T = 1$ (triplet). When the ground state is the singlet, the coupling is antiferromagnetic, whereas when the ground state is the triplet, the coupling is ferromagnetic. The difference in energy between the two states (S = 0 and S = 1) is known as the coupling constant J.
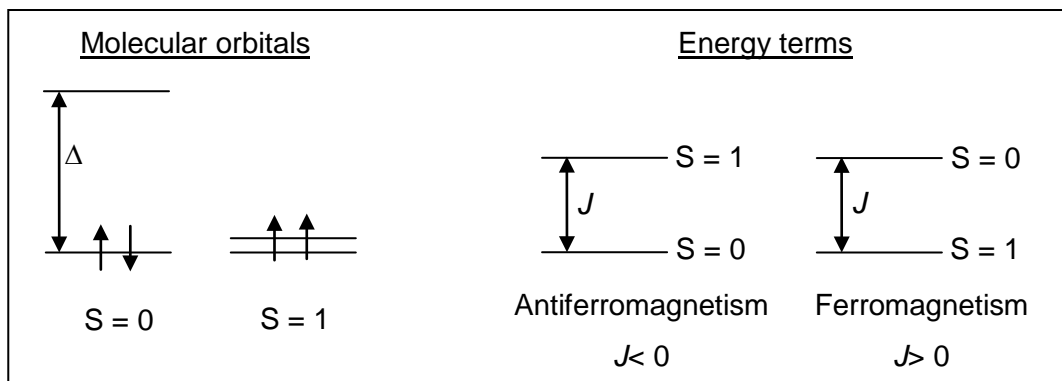
Figure 12. Possible arrangements of two electrons in two molecular orbitals of a dinuclear compound with one unpaired electron per metal. Molecular ferromagnetism and antiferromagnetism.

The spin-spin interaction can be described using the Heisenberg Hamiltonian, which allows to calculate the energy of the interaction between two or more ions as a function of J.

$$H = -J_{ij}S_iS_j$$

where S_i, S_j = spin operators, and J_{ij} = coupling constant between i and j.

For a dinuclear compound with two ions A and B, with spins S_A and S_B, the isotropic Hamiltonian is $H = -JS_AS_B$. Because $S = S_A + S_B$, $S^2 = S_A{}^2 + S_B{}^2 + 2S_AS_B$, $S_AS_B = (S^2 - S_A{}^2 - S_B{}^2)/2$:

$$H = -J/2(S^2 - S_A{}^2 - S_B{}^2)$$

This Hamiltonian has exact quantum solution:

$$E(S, S_A, S_B) = -J/2[S(S+1) - S_A(S_A + 1) - S_B(S_B + 1)]$$

With the change of the origin of the potential energy, considering $[-S_A(S_A + 1) - S_B(S_B + 1)]$ as the zero, we obtain that the energy for each value of S is:

$$E(S) = (-J/2)[S(S + 1)]$$

Applying this equation to each spin of the system (from $|S_A - S_B|$ to $|S_A + S_B|$) and using the simplified Van Vleck equation, it is possible to find an expression of χ_M as a

function of the temperature for any dinuclear compound. In the case of manganese (II), $S_A = S_B = 5/2$.

$$\chi_M = \frac{Ng^2\mu_B^2}{kT}\frac{110\exp(15x) + 60\exp(10x) + 28\exp(6x) + 10\exp(3x) + 2\exp(x)}{11\exp(15x) + 9\exp(10x) + 7\exp(6x) + 5\exp(3x) + 3\exp(x) + 1}$$

where $x = J/kT$, g = giromagnetic factor, μ_B = Bohr magneton.

For a linear trinuclear complex the interacting ions are not all equivalent and Kambe's method is used to determine the energies of the spin-states of the molecule. Assuming that only the interactions between nearest neighbours are important then the Hamiltonian representing the interaction can be written as:

$$H = -2J(S_1 \cdot S_2 + S_2 \cdot S_3) = -2JS_2(S_1 + S_3)$$

1.3.1.3. Zero Field Splitting

When a ground state of the system has more than one unpaired electron (S > 1/2), the spin-orbital coupling with the excited states can produce a splitting of the Zeeman components even in absence of external magnetic field. This phenomenon produces magnetic anisotropy and has profound effects on the magnetic properties. The Hamiltonian of the ZFS is:

$$H_D = S \cdot D \cdot S = D\left[S_z^2 - S(S+1)/3\right] + E(S_x^2 - S_y^2)$$

where D is the ZFS tensor (considered a diagonalized form, 3x3 matrix), and D and E are the ZFS parameters, the axial and the rhombic respectively.

The zero field splitting breaks the spin multiplicity degeneration as a function of S_Z (m_S) values. The Hamiltonian is a function of S_Z^2, consequently the energy of m_S = +1 is the same as the energy of m_S = -1 and both are different than the energy of m_S = 0.

Depending on the sign of D, the lower energy level will be the highest or lowest $|m_S|$. Figure 13 shows the effect of the axial ZFS ($E = 0$) in the z direction (parallel to the applied field) for the spin states S = 5/2 and S = 2, corresponding to manganese (II) and manganese (III) respectively.
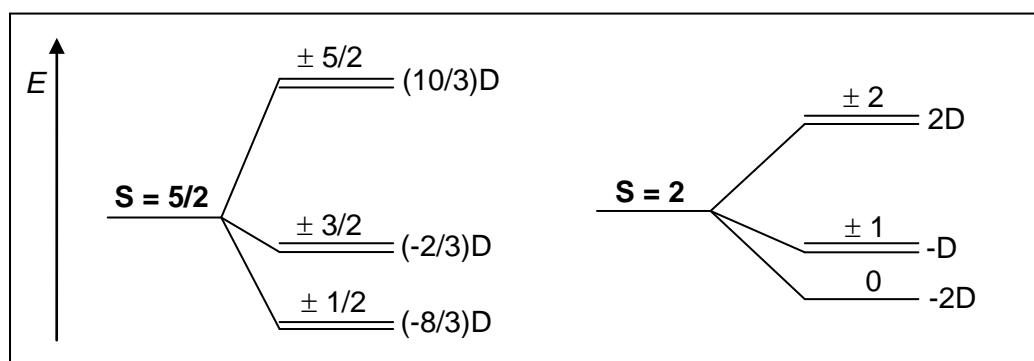
Figure 13. Zero Field Splitting of two spin states, S = 5/2 and S = 2, in an environment with axial distortion.

In ions with strictly cubic environment, such as the high spin d^5 (e.g. Mn(II)), the spin-orbital coupling partly splits the ground state. However, this zero field splitting in absence of geometrical distortion is a weak phenomenon, which doesn't create anisotropy. Nevertheless, any distortion of the octahedral environment, even small, decreases the symmetry and gives rise to a greater split of the Kramers doublets.

1.3.1.4. Magnetism of binuclear manganese compounds

Binuclear manganese complexes bridged by organic or inorganic units in general have attracted research interests, as far as electronic and magnetic studies are concerned. As organic connecting entities, nitrogen-containing aromatic heterocycles and carboxylates have been mainly investigated. The first type of bridges can adopt chelating and bis(chelating) coordination modes affording a plethora of extended magnetic systems,[170] while the second is present in some metalloenzymes and can adopt different coordination modes (μ-1,1 or μ-1,3 syn-anti, syn-syn or anti-anti).[171] Despite the magnetic interaction for this latest kind of compounds is weak, the interest lies in the versatility of their magnetic behaviour and its relationship with the distortion of the coordination polyhedra.[172-174] These type of compounds usually show weak antiferromagnetic coupling, although a ferromagnetic interaction is also possible depending on the type and degree of distortion around the manganese. As example of inorganic bridging units, halides are favored, with either ferro- or antiferromagnetic interactions.[175,176] Magneto-structural and electrochemical studies of these manganese binuclear complexes have been carried out.[177,178]

1.3.2. Electron paramagnetic resonance

1.3.2.1. Fundamentals of EPR

Electron paramagnetic resonance spectroscopy[167] is a technique that consists in applying a magnetic field over a sample (liquid or powder) with unpaired electrons, causing a splitting of the states due to the electronic Zeeman effect, and the study of the electronic transitions between these states.

It is usual to work by keeping the sample under irradiation of an energy source with a fixed frequency, ν, and performing a screening of magnetic field until the splitting of the states fits the energy of the source (see below), thus allowing the electronic transitions. The frequency necessary to observe the transitions is in the microwave region. The most commonly used frequencies are:

-X band: $\nu \approx 9.5$ GHz (≈ 0.3 cm^{-1}). Magnetic fields around 3000 Gauss.
-Q band: $\nu \approx 35$ GHz (≈ 1.16 cm^{-1}). Magnetic fields around 12000 Gauss.

Q-band is more sensitive than X-band but it is more difficult to obtain uniform magnetic fields. For this latest reason X-band is generally used.

When a magnetic field H is applied over a sample composed of atoms, molecules or ions having electrons with unpaired spins (S ≠ 0), there is a split of the spin states (Zeeman effect). In the simplest case of a sole electron (S = 1/2), the Zeeman Hamiltonian that expresses the interaction with the magnetic field is:

$$H_Z = g\mu_B HS$$

where: $g = 2.0023$ for the free electron
$\mu_B = 9.274096 \cdot 10^{-21}$ erg G^{-1} (electronic Bohr magneton)
H = applied magnetic field
S = Spin operator

At the considered system (S = 1/2), when the external magnetic field is applied, the splitting of the states leads to $m_S = +1/2$ and $m_S = -1/2$ with energies $g\mu_B H m_S$, as represented in Figure 14.
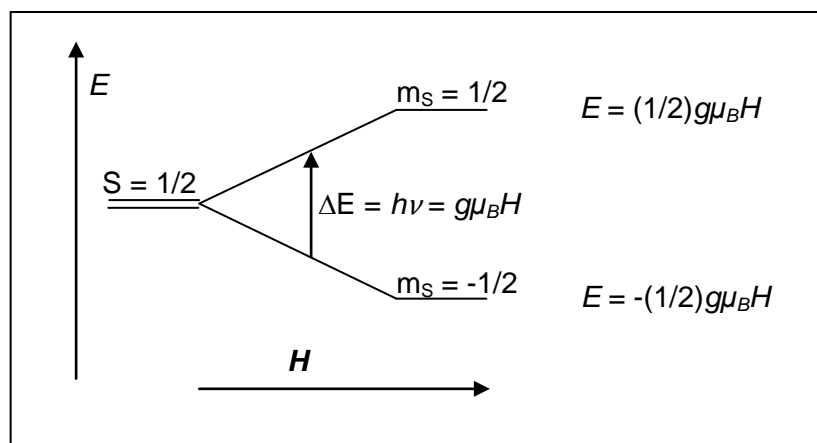
Figure 14. Splitting of the states $|\pm 1/2\rangle$ due to the Zeeman effect.

When a radiation with energy $h\nu$ is applied, an electronic transition is possible, with:

$$h\nu = g\mu_B H$$

The allowed transitions are those that fulfill $\Delta m_S = \pm 1$. In a system with a sole unpaired electron ($S = 1/2$) only one transition is possible (from -1/2 to +1/2) and consequently only one value of g is determined. In a manganese (II) mononuclear compound 5 transitions are allowed, although if the environment is isotropic ($g = 2$ in the three directions) every transition will have the same energy and will appear in the EPR spectrum as a sole band.

Knowing the working frequency of the apparatus and the value of the magnetic field where the transition takes place, it is possible to calculate the g value for any transition:

$$g = \frac{h\nu}{\mu_B H} = 714.6\frac{\nu}{H}$$

where ν is the working frequency (in GHz) and H is de magnetic field (in Gauss).

If the electron is in a symmetric environment, g is isotropic and its value is similar to that observed for the free electron (2.0023). However, if the compound is not symmetric it is possible to see different g values for each direction. Thus, if the compound has axial symmetry and anisotropy at the z direction, there will be a $g_{\parallel}$ (z direction) and a $g_{\perp}$ of double intensity (x and y directions), whereas if the compound is completely anisotropic there will be three different g values: g_x, g_y and g_z.

1.3.2.2. Hyperfine coupling

When the atom that has the unpaired electron also possesses a nuclear spin *I* different from zero, this can interact with the electronic spin *S* giving rise to the hyperfine coupling, described by the Hamiltonian:

$$H_A = g_n \mu_{Bn} HI + hSAI$$

where A is the hyperfine coupling tensor and μ_{Bn} is the nuclear Bohr magneton.

The first term of the equation is the nuclear Zeeman Hamiltonian, corresponding to the split of the nuclear spins when a magnetic field is applied. The second term describes the coupling between the nuclear and the electronic spins. For manganese (II), with I_{Mn} = 5/2, 6 bands can be observed due to the hyperfine coupling (see below).

1.3.2.3. Zero Field Splitting

If the compound has more than one unpaired electron, there can be zero field splitting due to the dipole-dipole magnetic interactions between unpaired electrons, the spin-orbit coupling and distortions from the ideal octahedral geometry. The energy of the spin states is modified depending on the parameters *D* (axial ZFS) and *E* (rhombic ZFS) according to the Hamiltonian:

$$H_D = S \cdot D \cdot S = D\left[S_z^2 - S(S+1)/3\right] + E(S_x^2 - S_y^2)$$

where **D** is the ZFS tensor.

In integer spin systems, if $D < h\nu$, EPR signals are observable at different fields, however, when the ZFS is important ($D > h\nu$) the EPR spectrum doesn't display any signal because the microwave radiation energy is not enough to produce transitions. This is the case of manganese (III) (S = 2), which is EPR silent.

Taking into account the Zeeman effect, the hyperfine interactions and the zero field splitting, the final Hamiltonian in EPR is:

$$H = g\mu_B HS + hSAI + D\left[S_z^2 - S(S+1)/3\right] + E(S_x^2 - S_y^2)$$

35

1.3.2.4. EPR of manganese compounds

In EPR, the *D*-values for mononuclear hexacoordinate Mn(II) complexes are rather small and the *g*-factors are close to 2.0.[179] The *D*-values increase with ligand sphere asymmetry. Magneto-structural studies of these mononuclear compounds have also been carried out.[7,180] The inclusion of the hyperfine term *SAI* for ^{55}Mn splits a single resonance into $2I + 1$ lines (Figure 15).
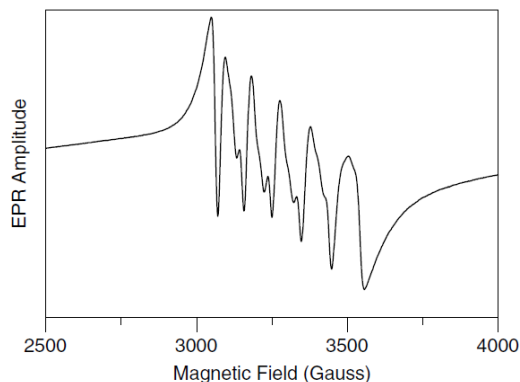
Figure 15. Hyperfine contribution in an EPR spectra of Mn(II) ($I = 5/2$).

As previously mentioned, Mn(III) (S = 2) is EPR silent when the ZFS is important ($D > h\nu$). On the other hand, Mn(IV) (S = 3/2) shows a broad absorption band at g ≈ 4.

For dinuclear manganese complexes with mixed-valence, the number of lines in the EPR spectrum increase. In the case of a di-µ-oxo Mn(III,IV) species, since the two Mn ions are in different oxidation states, the hyperfine contributions to the spectrum will be different for each ion. Thus, this system is an example of hyperfine anisotropy in EPR.[181] The typical 16-line spectrum (Figure 16) can be largely explained if $A_1 = 2A_2$.
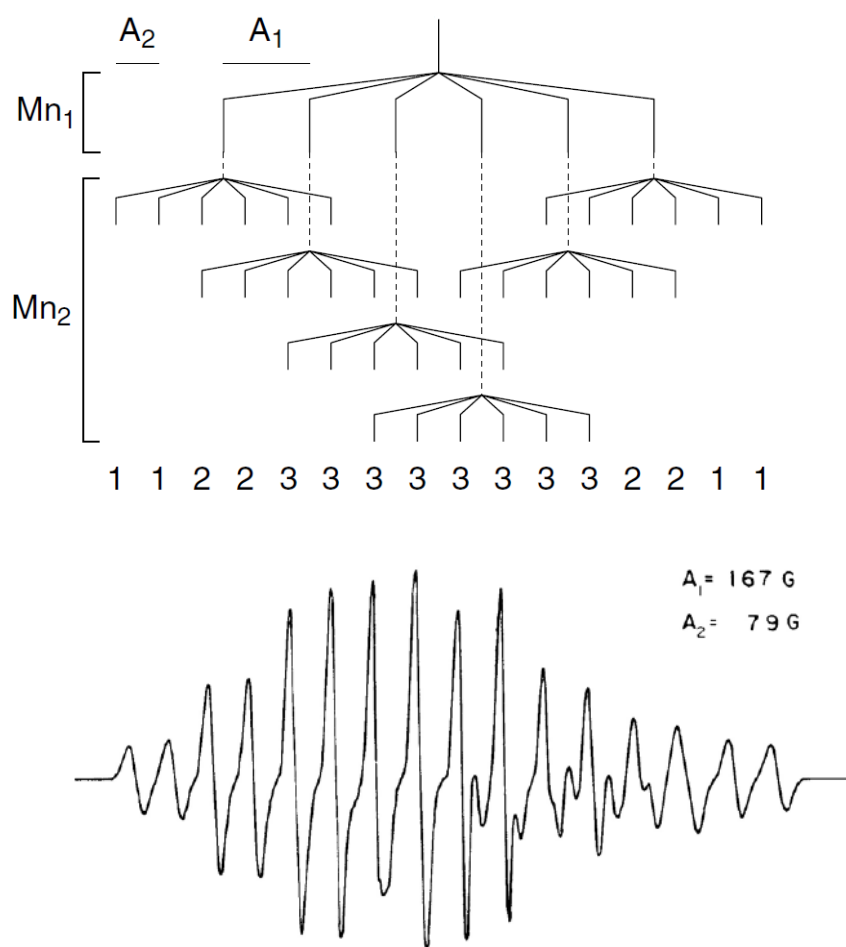
Figure 16. Splitting of the states for a mixed-valent dinuclear Mn complex.

1.4. References

[1] Greenwood, N.N.; Earnshaw A. *Chemistry of the elements*, 2nd ed., Elseiver Butterworth Heinemann, Oxford, **1997**, Ch 24.

[2] Cotton, F.A.; Wilkinson, G.; Murillo, C.A.; Bochmann, M. *Advanced Inorganic Chemistry*, 6th ed., John Wiley & Sons: New York, **1999**, Ch 17.

[3] Collomb, M.-N.; Deronzier, A. *Manganese: Inorganic & Coordination Chemistry*, in *Encyclopedia of Inorganic and Bioinorganic Chemistry*, John Wiley & Sons: New York, **2011**.

[4] Chiswell, B.; McKenzie, E.D.; Lindoy, L.F. *Comprehensive Coordination Chemistry*, Ed. Wilkinson, G.; Pergamon, Oxford, **1987**, vol. 4, Ch 41.

[5] Ganguly, S.; Karmakar, S.; Pal, C.K.; Chakravorty, A. *Inorg. Chem*. **1999**, *38*, 5984-5987.

[6] Saha, A.; Majumdar, P.; Goswami, S. *J. Chem. Soc., Dalton Trans.* **2000**, 1703-1708.

[7] Duboc, C.; Collomb, M.-N.; Neese, F. *Appl. Magn. Reson.* **2010**, *37*, 229-245.

[8] Lah, S.; Chun, H. *Inorg. Chem*. **1997**, *36*, 1782-1785.

[9] Dube, K.S.; Harrop, T.C. *Dalton Trans*. **2011**, *40*, 7496-7498.

[10] Deroche, A.; Morgenstern-Baradau, I.; Cesario, M.; Guilhem, J.; Keita, B.; Nadjo, L.; Houée-Levin, C. *J. Am. Chem. Soc*. **1996**, *118*, 4567-4573.

[11] Darensbourg, D.J.; Frantz, E.B. *Dalton Trans*. **2008**, 5031-5036.

[12] Romain, S.; Baffert, C.; Duboc, C.; Leprêtre, J.-C.; Deronzier, A.; Collomb, M.-N. *Inorg. Chem*. **2009**, *48*, 3125-3131.

[13] Romain, S.; Duboc, C.; Neese, F.; Rivière, E.; Hanton, L.R.; Blackman, A.G.; Philouze, C.; Leprêtre, J.-C.; Deronzier, A.; Collomb, M.-N. *Chem. Eur. J.* **2009**, *15*, 980-988.

[14] Weymüller, T.; Paine, T.K.; Bothe, E.; Bill, E; Chaudhuri, P. *Inorg. Chim. Acta* **2002**, *337*, 344-356.

[15] Rajendiran, T.M.; Kampf, J.W.; Pecoraro, V.L. *Inorg. Chim. Acta* **2002**, *339*, 497-502.

[16] Weiss, R.; Gold, A.; Trautwein, A.X.; Terner, J. *The Porphyrin Handbook*, Eds. Kadish, K.M.; Smith, K.M.; Guilard, R.; Academic Press, San Diego, CA, **2000**, Vol. 4, p. 65.

[17] Brudvig, G.W. *Phil. Trans. R. Soc. B* **2008**, *363*, 1211-1219.

[18] Limburg, J.; Vrettos, J.S.; Liable-Sands, L.M.; Rheingold, A.L.; Crabtree, R.H.; Brudvig, G.W. Science **1999**, *283*, 1524-1527.

[19] Poulsen, A.K.; Rompel, A.; Mckenzie, C.J. *Angew. Chem. Int. Ed.* **2005**, *44*, 6916-6920.

[20] Collomb, M.-N.; Deronzier, A. *Eur. J. Inorg. Chem.* **2009**, 2025-2046.

[21] Bhaduri, S.; Tasiopoulos, A.J.; Bolcar, M.A.; Abboud, K.A.; Streib, W.E.; Christou, G. *Inorg. Chem* **2003**, *42*, 1483-1492.

[22] Mukhopadhyay, S.; Mandal, S.K.; Bhaduri, S.; Armstrong, W.H. *Chem. Rev.* **2004**, 104, 3981-4026.

[23] Mukhopadhyay, S.; Armstrong, W.H. *J. Am. Chem. Soc.* **2003**, *125*, 13010-13011.

[24] Biava, H.; Palopoli, C.; Duhayon, C.; Tuchagues, J.P.; Signorella, S. *Inorg. Chem.* **2009**, 3205-3214.

[25] Koek, J.H.; Russell, S.W.; van der Wolf, L.; Hage, R.; Warnaar, J.B.; Spek, A.L.; Kerschner, J.; Del Pizzo, L. *J. Chem. Soc., Dalton Trans.* **1996**, 353-362.

[26] Horner, O.; Anxolabéhère-Mallart, E.; Charlot, M.-F.; Tchertanov, L.; Guilhem, J.; Mattioli, T.A.; Boussac, A.; Girerd, J.-J. *Inorg. Chem.* **1999**, *38*, 1222-1232.

[27] Wu, A.J.; Penner-Hahn, J. E.; Pecoraro, V.L. *Chem. Rev.* **2004**, *104*, 903-938.

[28] Bräuer, B.; Schaarshmidt, D.; Flohrer, C.; Rüffer, T.; Tripke, S.; Hildebrandt, D.; Walfort, B.; Sorace, L.; Lang, H. *Inorg. Chim. Acta* **2011**, *365*, 277-281.

[29] Smith, S.J.; Riley, M.J.; Noble, C.J.; Hanson, G.R.; Stranger, R.; Jayaratne, V.; Cavigliasso, G.; Schlenk, G.; Gahan, L.R. *Inorg. Chem.* **2009**, *48*, 10036-10048.

[30] Tasiopoulos, A.J.; Abboud, K.A.; Christou, G. *Chem. Commun.* **2003**, 580-581.

[31] Brechin, E.K.; Soler, M.; Davidson, J.; Hendrickson, D.N.; Parsons, S.; Christou, G. *Chem. Commun.* **2002**, 2252-2253.

[32] Stamatatos, T.C.; Poole, K.M.; Abboud, K.A.; Wernsdorfer, W.; O'Brien, T.A.; Christou, G. *Inorg. Chem.* **2008**, *47*, 5006-5021.

[33] Maayan, G.; Christou, G. *Inorg. Chem.* **2011**, *50*, 7015-7021.

[34] Manoli, M.; Prescimone, A.; Mishra, A.; Parsons, S.; Christou, G.; Brechin, E.K. *Dalton Trans.* **2007**, 532-534.

[35] Brockman, J.T.; Huffman, J.C.; Christou, G. *Angew. Chem., Int. Ed.* **2002**, *41*, 2506-2508.

[36] Langley, S.K.; Stott, R.A.; Chilton, N.F.; Moubaraki, B.; Murray, K.S. *Chem. Commun.* **2011**, *47*, 6281-6283.

[37] Sheldon, R.A.; Kochi, J.K. *Metal Catalyzed Oxidation of Organic Compounds*; Academic Press; New York, **1981**.

[38] Meunier, B. Ed. *Biomimetic Oxidations Catalyzed by Transition Metal Complexes*, Imperial College Press, **2000**.

[39] Bäckvall, J.E. *Modern Oxidation Methods*, Wiley-VCH: Weinheim, **2004**.

[40] Bruijnincx, P.C.A.; van Koten, G.; Gebbink, R.J.M.K. *Chem. Soc. Rev.* **2008**, 37, 2716-2744.

[41] Crabtree, R.H. *Oxidation Catalysis by Transition Metal Complexes*, in *Encyclopedia of Inorganic and Bioinorganic Chemistry*, John Wiley & Sons: New York, **2011**.

[42] Lippard, S.J.; Berg, J.M. *Principles of Bioinorganic Chemistry*, University Science Books: Mill Valley, California, **1994**.

[43] Pecoraro, V.L. Ed. *Manganese Redox Enzymes*, VCH Publisher: New York, **1992**.

[44] Riley, D.P. *Chem. Rev.* **1999**, *99*, 2573-2587.

[45] Dismukes, G.C.; van Willigen, R.T. *Manganese: The Oxygen-Evolving Complex & Models*, in *Encyclopedia of Inorganic and Bioinorganic Chemistry*, John Wiley & Sons: New York, **2011**.

[46] Zouni, A.; Witt, H.-T.; Kern, J.; Fromme, P.; Krauss, N.; Saenger, W.; Orth, P. *Nature* **2001**, *409*, 739-743.

[47] Loll, B.; Kern, J.; Saenger, W.; Zouni, A.; Biesiadka, J. *Nature* **2005**, *438*, 1040-1044.

[48] Waldo, G.S.; Penner-Hahn, J.E. *Biochemistry* **1995**, *34*, 1507-1512.

[49] Kono, Y.; Fridovich, I. *J. Biol. Chem.* **1983**, *258*, 6015-6019.

[50] Allgood, G.S.; Perry, J.J. *J. Bacteriol.* **1986**, *168*, 563-567.

[51] Antonyuk, S.V.; Melik-Adamyan, V.R.; Popov, A.N.; Lamzin, V.S.; Hempstead, P.D.; Harrison, P.M.; Artymiuk, P.J.; Barynin, V.V. *Crystallography Reports* **2000**, *45*, 105-116.

[52] Barynin, V.V.; Whittaker, M.M.; Antonyuk, S.V.; Lamzin, V.S.; Harrison, P.M.; Artymiuk, P.J.; Whittaker, J.W. *Structure* **2001**, *9*, 725-738.

[53] Ghanotakis, D.F.; Yocum, C.F. *Annu. Rev. Plant Physiol. Plant Mol. Biol.* **1990**, *41*, 255-276.

[54] Dismukes, G.C. *Chem. Rev.* **1996**, *96*, 2909-2926.

[55] Palopoli, C.; Bruzzo, N.; Hureau, C.; Ladeira, S.; Murgida, D.; Signorella, S. *Inorg. Chem.* **2011**, *50*, 8973-8983.

[56] Mathur, P.; Crowder, M.; Dismukes, G.C. *J. Am. Chem. Soc.* **1987**, *109*, 5227-5233.

[57] Sakiyama, H.; Okawa, H.; Suzuki, M. *J. Chem. Soc., Dalton Trans.* **1993**, 3823-3825.

[58] Higuchi, C.; Sakiyama, H.; Okawa, H.; Fenton, D.E. *J. Chem. Soc., Dalton Trans.* **1995**, 4015-4020.

[59] Wieghardt, K.; Bossek, U.; Nuber, B.; Weiss, J.; Bonvoisin, J.; Corbella, M.; Vitols, S.E.; Girerd, J.J. *J. Am. Chem. Soc.* **1988**, *110*, 7398-7411.

[60] Bossek, U.; Weyermüller, T.; Wieghardt, K.; Nuber, B.; Weiss, J. *J. Am. Chem. Soc.* **1990**, 112, 6387-6388.

[61] Meunier, B.; de Visser, S.P.; Shaik, S. *Chem. Rev.* **2004**, *104*, 3947-3980.

[62] Ayougou, K.; Bill, E.; Charnock, J.M.; Garner, C.D.; Mandon, D.; Trautwein, A.X.; Weiss, R.; Winkler, H. *Angew. Chem., Int. Ed. Engl.* **1995**, *34*, 343-346.

[63] Song, W.J.; Seo, M.S.; George, S.D.; Ohta, T.; Song, R.; Kang, M.-J.; Tosha, T.; Kitagawa, T.; Solomon, E.I.; Nam, W. *J. Am. Chem. Soc.* **2007**, *129*, 1268-1277.

[64] Tabushi, I.; Kodera, M.; Yokoyama, M. *J. Am. Chem. Soc.* **1985**, *107*, 4466-4473.

[65] Groves, J.T. *Cytochrome P450: Structure, Mechanism and Biochemistry*, 3rd ed., Ed. Ortiz de Montellano, P.R.; Kluwer Academic/Plenum Publishers: New York, **2005**, Ch 1.

[66] Sono, M.; Roach, M.P.; Coulter, E.D.; Dawson, J.H. *Chem. Rev.* **1996**, 96, 2841-2887.

[67] Bernadou, J.; Meunier, B. *Adv. Synth. Catal.* **2004**, *346*, 171-184.

[68] Meunier, B. *Chem. Rev.* **1992**, *92*, 1411-1456.

[69] Groves, J.T. *J. Inorg. Biochem.* **2006**, *100*, 434-447.

[70] Nam, W. *Acc. Chem. Res.* **2007**, *40*, 522-531.

[71] de Oliveira, F.T.; Chanda, A.; Banerjee, D.; Shan, X.; Mondal, S.; Que Jr., L.; Bominaar, E.L.; Münck, E.; Collins, T.J. *Science* **2007**, *315*, 835-838.

[72] Costas, M. *Coord. Chem. Rev.* **2011**, *255*, 2912-2932.

[73] Shaik, S.; Cohen, S.; Wang, Y.; Chen, H.; Kumar, D.; Thiel, W. *Chem. Rev.* **2010**, *110*, 949-1017.

[74] Lee, J.Y.; Lee, Y.-M.; Kotani, H.; Nam, W.; Fukuzumi, S. *Chem. Commun.* **2009**, 704-706.

[75] Lanucara, F.; Crestoni, M.E. *Chem. Eur. J.* **2011**, *17*, 12092-12100.

[76] Jacobsen, E. N.; Pfaltz, A.; Yamamoto, H. Eds. *Comprehensive Asymmetric Catalyses*, Springer: Berlin, **1999**.

[77] Ojima, I. Ed. *Catalytic Asymmetric Synthesis*, 2nd ed., John Wiley & Sons: New York, **2000**.

[78] Noyori, R.; Aoki, M.; Sato, K. *Chem. Commun.* **2003**, 1977-1986.

[79] Gagnon, S.D.H.F. *Encyclopedia of Polymer Science and Engineering*, 2nd ed., Eds. Mark, H.F.; Bikales, N.M.; Overberger, C.G.; Menges, G.; Kroschwitz, J.I.; John Wiley & Sons: New York, **1985**, Vol. 6, pp 273-307.

[80] de Faveri, G.; Ilyashenko, G.; Watkinson, M. *Chem. Soc. Rev.* **2011**, *40*, 1722-1760.

[81] Smith, J.G. *Synthesis* **1984**, 629-656.

[82] Jacobsen, E.N. *Acc. Chem. Res.* **2000**, *33*, 421-431.

[83] de Vries, E.J.; Janssen, D.B. *Curr. Opin. Biotechnol.* **2003**, *14*, 414-420.

[84] Muzart, J. *Eur. J. Org. Chem.* **2011**, 4717-4741.

[85] Katsuki, T.; Sharpless, K.B. *J. Am. Chem. Soc.* **1980**, *102*, 5974-5976.

[86] Brunel, J.M.; Kagan, H.B. *Bull. Soc. Chim. Fr.* **1996**, *133*, 1109-1115.

[87] Zhang, W.; Loebach, J.L.; Wilson, S.R.; Jacobsen, E.N. *J. Am. Chem. Soc.* **1990**, *112*, 2801-2803.

[88] Irie, R.; Noda, K.; Ito, Y.; Matsumoto, N.; Katsuki, T. *Tetrahedron Lett.* **1990**, *31*, 7345-7348.

[89] Katsuki, T. *Coord. Chem. Rev.* **1995**, *140*, 189-214.

[90] Katsuki, T. *J. Mol. Cat. A: Chem.* **1996**, *113*, 87-107.

[91] Groves, J.T.; Nemo, T.E.; Myers, R.S. *J. Am. Chem. Soc.* **1979**, *101*, 1032-1033.

[92] Guilmet, E.; Meunier, B. *Tetrahedron Lett.* **1980**, *21*, 4449-4450.

[93] Meunier, B.; Guilmet, E.; De Carvalho, M.E.; Poilblanc, R. *J. Am. Chem. Soc.* **1984**, *106*, 6668-6676.

[94] Katsuki, T. *Coord. Chem. Rev.* **1995**, *140,* 189-214.

[95] Gross, Z.; Ini, S. *J. Org. Chem.* **1997**, *62*, 5514-5521.

[96] Rose, E.; Andrioletti, B.; Zrig, S.; Quelquejeu-Ethève, M. *Chem. Soc. Rev.* **2005**, *34*, 573-583.

[97] Solati, Z.; Hashemi, M.; Ebrahimi, L. *Catal. Lett.* **2011**, *141*, 163-167.

[98] Barry, J.F.; Campell, L.; Smith, D.W.; Kodadek, T. *Tetrahedron* **1997**, *53*, 7753-776.

[99] Renaud, J.-P.; Battioni, P.; Bartoli, J.-F.; Mansuy, D. *J. Chem. Soc., Chem. Commun.* **1985**, 888-889.

[100] Battioni, P.; Renaud, J.P.; Bartoli, J.F.; Reina-Artiles, M.; Fort, M.; Mansuy, D. *J. Am. Chem. Soc.* **1988**, *110*, 8462-8470.

[101] Mohajer, D.; Solati, Z. *Tetrahedron Lett.* **2006**, *47*, 7007-7010.

[102] Collman, J.P.; Zhang, X; Lee, V.J.; Uffelman, E.S.; Braumann, J.I. *Science* **1993**, *261*, 1404-1411.

[103] Groves, J.T.; Viski, P. *J. Org. Chem.* **1990**, *55*, 3628-3634.

[104] Breslow, R.; Huang, Y.; Zhang, X.; Yang, J. *Proc. Natl. Acad. Sci. USA* **1997**, *94*, 11156-11158.

[105] Samsel, E.G.; Srinivasan, K.; Kochi, J.K. *J. Am. Chem. Soc.* **1985**, *107*, 7606-7617.

[106] Srinivasan, K.; Michaud, P.; Kochi, J.K. *J. Am Chem. Soc.* **1986**, *108*, 2309-2320.

[107] Irie, R.; Noda, K.; Ito, Y.; Katsuki, T. *Tetrahedron Lett.* **1991**, *32*, 1055-1058.

[108] Hosoya, N.; Irie, R.; Katsuki, T. *Synlett* **1993**, 261-263.

[109] Sasaki, H.; Irie, R.; Katsuki, T. *Synlett.* **1994**, 356-358.

[110] Jacobsen, E.N.; Zhang, W.; Muci, A.R.; Ecker, J.R.; Deng, L. *J. Am. Chem. Soc.* **1991**, *113*, 7063-7064.

[111] Pospisil, P.J.; Carsten, D.H.; Jacobsen, E.N. *Chem. Eur. J.* **1996**, *2*, 974-980.

[112] Deng, L.; Jacobsen, E.N. *J. Org. Chem.* **1992**, *57*, 4320-4323.

[113] Jacobsen, E.N.; Zhang, W.; Güler, M.L. *J. Am. Chem. Soc.* **1991**, *113*, 6703-6704.

[114] Larrow, J.F.; Jacobsen, E.N.; Gao, Y.; Hong, Y.; Nie, X.; Zepp, C.M. *J. Org. Chem.* **1994**, *59*, 1939-1942.

[115] Lee, N.H.; Muci, A.R.; Jacobsen, E.N. *Tetrahedron Lett.* **1991**, *32*, 5055-5058.

[116] Jacobsen, E.N.; Deng, L.; Furukawa, Y.; Martinez, L.E. *Tetrahedron* **1994**, *50*, 4323-4334.

[117] Lee, N.H.; Jacobsen, E.N. *Tetrahedron Lett.* **1991**, *32*, 6533-6536.

[118] Chang, S.; Lee, N.H.; Jacobsen, E.N. *J. Org. Chem.* **1993**, *58*, 6939-6941.

[119] Palucki, M.; Pospisil, P.J.; Zhang, W.; Jacobsen, E.N. *J. Am. Chem. Soc.* **1994**, *116*, 9333-9334.

[120] Martinez, L.E.; Leighton, J.L.; Carsten, D.H.; Jacobsen, E.N. *J. Am. Chem. Soc.* **1995**, *117*, 5897-5898.

[121] Hansen, K.B.; Leighton, J.L.; Jacobsen, E.N. *J. Am. Chem. Soc.* **1996**, *118*, 10924-10925.

[122] Leighton, J.L.; Jacobsen, E.N. *J. Org. Chem.* **1996**, *61*, 389-390.

[123] Martinez, L.E.; Nugent, W.A.; Jacobsen, E.N. *J. Org. Chem.* **1996**, *61*, 7963-7966.

[124] Bernardo, K.; Robert, A.; Dahan, G.; Meunier, B. *New J. Chem.* **1995**, *19*, 129-131.

[125] Bernardo, K.; Leppard, S.; Robert, A.; Commenges, G.; Dahan, F.; Meunier, B. *Inorg. Chem.* **1996**, *35*, 387-396.

[126] Murphy, A.; Dubois, G.; Stack, T.D.P. *J. Am. Chem. Soc.* **2003**, *125*, 5250-5251.

[127] Murphy, A.; Pace, A.; Stack, T.D.P. *Org. Lett.* **2004**, *6*, 3119-3122.

[128] Brinksma, J.; Rispens, M.T.; Hage, R.; Feringa, B.L. *Inorg. Chim. Acta* **2002**, *337*, 75-82.

[129] Guillemot, G.; Neuburger, M.; Pfaltz, A. *Chem. Eur. J.* **2007**, *13*, 8960-8970.

[130] Sheldon, R.A. *Green Chem.* **2005**, *7*, 267-278.

[131] Sheldon, R.A. *Pure Appl. Chem.* **2000**, *72*, 1233-1246.

[132] Earle, M.; Wasserscheid, P.; Schulz, P.; Olivier-Bourbigou, H.; Favre, F.; Vaultier, M.; Kirschning, A.; Singh, V.; Riisager, A.; Fehrmann, R.; Kuhlmann S. *Organic Synthesis*, in *Ionic Liquids in Synthesis*, 2nd ed., Eds. Wasserscheid, P.; Welton, T.; Wiley-VCH Verlag GmbH & Co. KGaA, Weinheim, Germany, **2008**, Ch 5.

[133] Welton, T. *Chem. Rev.* **1999**, *99*, 2071-2083.

[134] Wasserscheid, P.; Keim, W. *Angew. Chem. Int. Ed.* **2000**, *39*, 3772-3789.

[135] Sheldon, R. *Chem. Commun.* **2001**, 2399-2407.

[136] Welton, T. *Coord. Chem. Rev.* **2004**, *248*, 2459-2477.

[137] Liu, S.; Xiao, J. *J. Mol. Catal. A: Chem.* **2007**, *270*, 1-43.

[138] Parvulescu, V.; Hardacre, C. *Chem. Rev.* **2007**, *107*, 2615-2655.

[139] Fraile, J.M.; Garcia, J.I.; Mayoral, J.A. *Coord. Chem. Rev.* **2008**, *252*, 624-646.

[140] Ochsner, E.; Schneiders, K.; Junge, K.; Beller, M.; Wasserscheid, P. *Appl. Cat. A* **2009**, *364*, 8-14.

[141] Gu, Y.; Li, G. *Adv. Synth. Catal.* **2009**, *351*, 817-847.

[142] Gauchot, V.; Kroutil, W.; Schmitzer, A.R. *Chem. Eur. J.* **2010**, *16*, 6748-6751.

[143] Dupont, J.; de Souza, R.F.; Suarez, P.A. *Chem. Rev.* **2002**, *102*, 3667-3692.

[144] Freemantle, M. *Chem. Eng. News* **1998**, *76*, 32-37.

[145] Freemantle, M. *Chem. Eng. News* **2001**, *79*, 21-25.

[146] Jastorff, B.; Störmann, R.; Ranke, J.; Mölter, K.; Stock, F.; Oberheitmann, B.; Hoffmann, W.; Hoffmann, J.; Nüchter, M.; Ondruschka, B.; Filser, J. *Green Chem.* **2003**, *5*, 136-142.

[147] Wilkes, J.S. *J. Mol. Catal. A: Chem.* **2004**, *214*, 11-17.

[148] Ranke, J.; Stolte, S.; Störmann, R.; Arning, J.; Jastorff, B. *Chem. Rev.* **2007**, *107*, 2183-2206.

[149] Hagiwara, R.; Ito, Y. *J. Fluorine Chem.* **2000**, *105*, 221-227.

[150] Huddleston, J.G.; Visser, A.E.; Reichert, W.M.; Willauer, H.D.; Broker, G.A.; Rogers, R.D. *Green Chem.* **2001**, *3*, 156-164.

[151] de Bellefon, C.; Pollet, E.; Grenouillet, P. *J. Mol. Catal.* **1999**, *145*, 121-126.

[152] Böhm, V.P.W.; Herrmann, W.A. *Chem. Eur. J.* **2000**, *6*, 1017-1025.

[153] Song, C.E.; Roh, E.J. *Chem. Commun.* **2000**, 837-838.

[154] Smith, K.; Liu, S.; El-Hiti, G.A. *Catal. Lett.* **2004**, *98*, 95-101.

[155] Li, Z.; Xia, C.-G. *Tetrahedron Lett.* **2003**, *44*, 2069-2071.

[156] Li, Z.; Xia, C.-G. *J. Mol. Catal. A: Chem.* **2004**, *214*, 95-101.

[157] Li, Z.; Xia, C.-G.; Ji, M. *Appl. Catal. A: General* **2003**, *252*, 17-21.

[158] Liu, Y.; Zhang, H.-J.; Lu, Y.; Cai, Y.-Q.; Liu, X.-L. *Green Chem.* **2007**, *9*, 1114-1119.

[159] Zhang, H.-J.; Liu, Y.; Lu, Y.; He, X.-S.; Wang, X.; Ding, X. *J. Mol. Catal. A: Chem.* **2008**, *287*, 80-86.

[160] Tan, R.; Yin, D.; Yu, N.; Zhao, H.; Yin, D. *J. Catal.* **2009**, *263*, 284-291.

[161] Teixeira, J.; Silva, A.R.; Branco, L.C.; Afonso, C.A.M.; Freire, C. *Inorg. Chim. Acta* **2010**, *363*, 3321-3329.

[162] Tong, K.-H.; Wong, K.-Y.; Chan, T.H. *Org. Lett.* **2003**, *5*, 3423-3425.

[163] Pinto, L.D.; Dupont, J.; de Souza, R.F.; Bernardo-Gusmao, K. *Catal. Commun.* **2008**, *9*, 135-139.

[164] Zhang, Z.; Li, H.; Liu, Y.; Ye, Y. *Synth. React. Inorg. Met. Org. Nano Met. Chem.* **2009**, *39*, 144-148.

[165] Ho, K-P.; Wong, W-L.; Lee, L.Y.S.; Lam, K-M., Chan, T.H.; Wong K-Y. *Chem. Asian J.* **2010**, *5*, 1970-1973.

[166] Mabbs, F.E.; Machin, D.J. *Magnetism and Transition Metal Complexes*, Chapman and Hall, London, **1973**.

[167] Ribas, J. Ed. *Química de Coordinación*, Edicions UB – Ediciones Omega S.A., Barcelona, **2000**.

[168] Yamauchi, J. *Fundamentals of Magnetism*, in *Nitroxides: Applications in Chemistry, Biomedicine and Materials Science*, Eds. Likhtenshtein, G.I.; Yamauchi, J.; Nakatsuji, S.; Smirnov, A.I.; Tamura, R.; Wiley-VCH Verlag GmbH & Co. KGaA, Weinheim, Germany, **2008**.

[169] Van Vleck, J.H. *The Theory of Electric and Magnetic Susceptibilities*, Oxford University Press., Oxford, **1932**.

[170] Kahn, O. Ed. *Molecular Magnetism*, Wiley-VCH, Weinheim, Germany, **1993**.

[171] Rardin, R.L.; Tolman, W.B.; Lippard, S.J. *New J. Chem.* **1991**, *15*, 417-430.

[172] Gómez, V.; Corbella, M. *Eur. J. Inorg. Chem.* **2009**, 4471-4482.

[173] Gómez, V.; Corbella, M.; Font-Bardia, M.; Calvet, T. *Dalton Trans.* **2010**, *39*, 11664-11674.

[174] Gómez, V.; Corbella, M. *J. Chem. Crystallogr.* **2011**, *41*, 843-846.

[175] Romero, I.; Collomb, M.-N.; Deronzier, A.; Llobet, A.; Perret, E.; Pécaut, J.; Le Pape, L.; Latour, J.-M. *Eur. J. Inorg. Chem.* **2001**, 69-72.

[176] Qi, C.-M.; Sun, X.-X.; Gao, S.; Ma, S.-L.; Yuan, D.-Q.; Fan, C.-H.; Huang, H.-B.; Zhu, W.-X. *Eur. J. Inorg. Chem.* **2007**, 3663-3668.

[177] Pantazis, D.A.; Krewald, V.; Orio, M.; Neese, F. *Dalton Trans.* **2010**, *39*, 4959-4967.

[178] Bräuer, B.; Schaarschmidt, D.; Flohrer, C.; Rüffer, T.; Tripke, S.; Hildebrandt, A.; Walfort, B.; Sorace, L.; Lang, H. *Inorg. Chim. Acta* **2011**, *365*, 277-281.

[179] Boca, R. *Coord. Chem. Rev.* **2004**, *248*, 757-815.

[180] Duboc, C.; Collomb, M.-N.; Pécaut, J.; Deronzier, A.; Neese, F. *Chem. Eur. J.* **2008**, *14*, 6498-6509.

[181] Cooper, S.R.; Dismukes, G.C.; Klein, M.P.; Calvin, M. *J. Am. Chem. Soc.* **1978**, *100*, 7248-7252.

Chapter 2

General Objectives

2. General objectives

One of the main research lines of the group where this thesis has been developed is centered in the synthesis of new manganese and ruthenium complexes and their exhaustive characterization, as well as their evaluation as potential catalysts for different reactions such as epoxidation, water oxidation or hydrogenation, among others.

The objectives at the beginning of the thesis were the design of new families of manganese complexes with different types of N-pyridyl ligands (some of them chiral) and their subsequent evaluation in catalytic oxidation reactions (asymmetric in some cases).

- **Manganese complexes with a chiral bidentate ligand**

The ligand chosen for this former part of the work was the (–)pinene[5,6]bipyridine ((–)-**L**), where the pinene group can induce enantioselectivity in oxidation reactions as has been reported in the literature. The objectives were:

- The synthesis and thorough characterization of a new family of mononuclear and dinuclear manganese complexes bearing the bidentate ligand (–)pinene[5,6]bipyridine.

- The study of the magnetic properties of the binuclear complexes and the determination of the ZFS of the mononuclear complexes through EPR spectroscopy and computational calculations.

- The study of their reactivity with regard to the epoxidation of some aromatic and aliphatic alkenes and the study of the influence of additives in the catalytic media.

- The study of the active catalytic species present in the epoxidation reactions, with the idea of investigating the role of the Cl or triflate ligands in the formation of the intermediate species and thus rationalise the results obtained in terms of the performance of the catalysts in such catalytic reactions.

- Taking into account the importance of the reusability of the homogeneous systems and given the few studies reported to date in the literature concerning the use of Mn (II) compounds in ILs, we considered to study the catalytic epoxidation of alkenes in a ionic liquid:solvent media with the aim of studying the reusability of the catalysts in such media.

- **Manganese complexes with racemic and chiral N-tetradentate ligands**

The tetradentate N-donor ligands chosen are the combination of a chiral or racemic spirobi(chroman) skeleton, which gives flexibility and chirality to the ligand, and a pyridyl substituent with or without fused pinene rings, which can introduce a second chiral element. The objectives proposed in this section were:

- The synthesis and complete characterization of a new family of ligands (SPANimine), either chiral or racemic.

- The coordination of these ligands to different manganese salts to afford a new family of racemic and chiral manganese (II) complexes and the subsequent thorough characterization.

- The study of the catalytic activity of these complexes in the epoxidation of styrene as well as the influence of additives in the catalytic media, in addition to the study of the stereospecificity of the catalysts by means of experimental and computational results.

- **Manganese complexes with a bridging N-tetradentate ligand**

The 3,5-bis(pyridin-2-yl)-pyrazole (Hbpp) ligand has been extensively studied in our group and it has proved to be a good ligand for the synthesis of dinuclear ruthenium complexes able to oxidize water. The main objective of this section was the synthesis of a dinuclear manganese compound; however, the unexpected complex obtained made us to consider new objectives, such as:

- The full characterization of the resulting complexes through structural, analytical and spectroscopic techniques and the execution of a broad redox study together with a thorough magnetic characterization.

- The study of the ability of the obtained complex towards the catalytic epoxidation of a series of alkenes. This latest study would allow us to compare the activity observed with that of related mononuclear manganese complexes previously synthesized.

Chapter 3

Mn(II) complexes containing the polypyridylic chiral ligand (–)-pinene[5,6]bipyridine. Investigation of the Zero-Field Splitting by combining EPR Spectroscopy and Quantum Chemistry.

A series of mononuclear and dinuclear chiral manganese (II) complexes containing the neutral bidentate chiral nitrogen-donor ligand (–)-pinene[5,6]bipyridine, (–)-**L**, were prepared from different manganese salts. These complexes have been characterized through structural, analytical, spectroscopic and electrochemical techniques. The magnetic properties of the two binuclear complexes have been studied and display a weak antiferromagnetic coupling. The electronic properties of the six-coordinate mononuclear complexes, together with other six- and seven-coordinate mononuclear complexes synthesized previously, have been investigated by X- and Q-band EPR spectroscopy. The zero-field splitting (ZFS) parameters have been predicted by density functional theory (DFT) calculations using two types of functionals, BP86 and B3LYP.

TABLE OF CONTENTS

CHAPTER 3. Mn(II) complexes containing the polypyridylic chiral ligand (–)-pinene[5,6]bipyridine. Investigation of the Zero-Field Splitting by combining EPR Spectroscopy and Quantum Chemistry.

3.1. Introduction

3.1.1. Pinene-derived ligands

Transition-metal asymmetric catalysis is one of the most powerful tools for the synthesis of optically active compounds, and the development of new efficient and enantioselective chiral ligands represents a crucial part in this area since most asymmetric catalysts reported so far are metal complexes with this type of ligands. The nature of the chiral ligand plays a key role in the reactivity and selectivity of the catalytic reaction.

A wide range of enantiopure ligands with different coordinating atoms are known today and used extensively for all kinds of catalytic reactions.[1-4] However, just a few of them can create effective asymmetric environments and can be applied to a broad range of reactions and substrates. Some of these "privileged" families include BINAP,[5] DuPhos,[6] Bisoxazoline,[7-10] and Salen derivatives[11-13] (Figure 1). Thus, the design of new chiral ligands able to expand those families is still an important challenge.
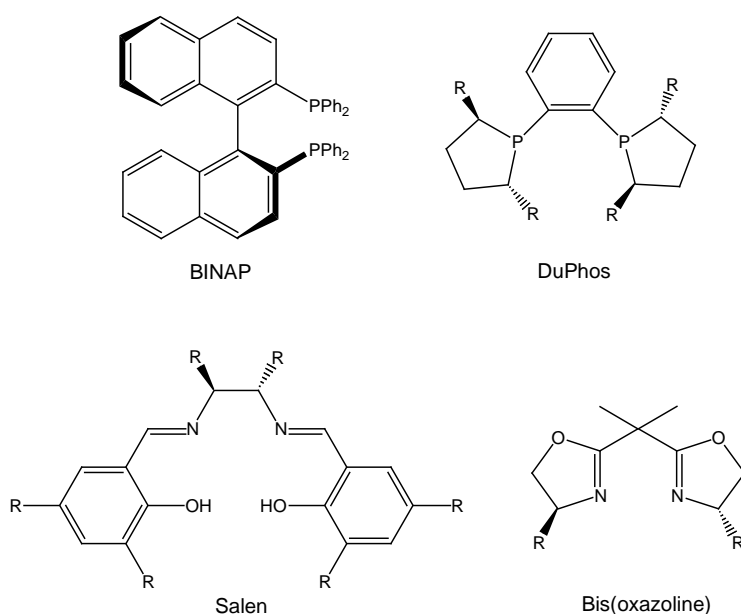
Figure 1. Examples of chiral ligands.

Enantiopure compounds are of central importance in many domains of chemistry. A classical method for the preparation of an enantiopure substance is the resolution of a racemate. However, much more effective is the selective synthesis of the desired stereoisomer. Predetermination of chirality at tetrahedral carbon centers has been the

central interest in synthetic organic chemistry for a long time. In this way, organic chemists have developed efficient methods for the creation of stereogenic centers with predetermined chirality.[14]

Transition metal complexes with sp^2-nitrogen atoms as the coordinating sites constitute an important class of chiral catalysts able to perform a wide range of asymmetric transformations.[15-18] Within this group, substituted oxazolines and bisoxazolines have received remarkable attention.[19,20] Apart from these successful chiral inducers, 2,2'-bipyridyl, 2,2':6'2''-terpyridines and 1,10-phenanthrolines can be envisaged as other potentially promising groups since they can be turned into chiral species by appending additional substituents.[21] However, despite their rich coordination chemistry, chiral polypyridylic ligands have not received much attention in asymmetric catalysis until the last two decades, when von Zelewsky attached a chiral α-pinene moiety to a pyridine ring.[22,23] Since then, a variety of pineno-annellated ligands have been described (Figure 2). [24 -34]

The pinene side groups are utilized to provide chiroptical properties to the ligand and, therefore, to the coordination complexes that can potentially induce enantioselectivity in catalytic processes based on prochiral substrates.
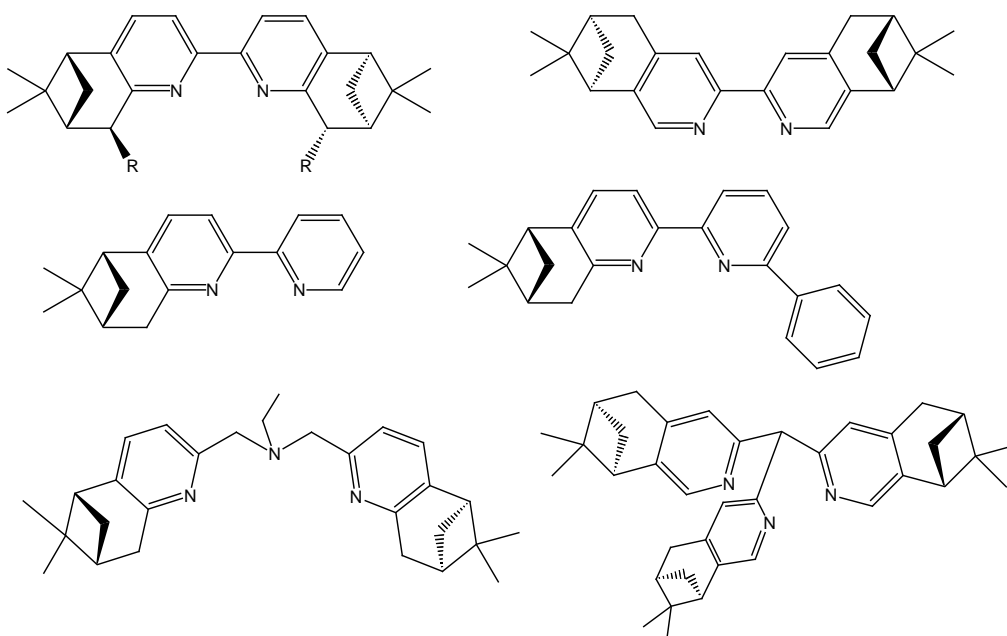
Figure 2. Some examples of pineno-fused ligands.

The modification of the structure of the catalysts with the aim of improving their stereoselectivity has proven to be a challenging task. Pioneering studies have demonstrated that small modifications to the structure of the ligands result in dramatic changes in the efficiency and selectivity of the catalysts.[21] Given these precedents, the modification of either the 4 and 5 or the 5 and 6 positions of the pyridine rings was a general strategy towards the design of a robust and more enantioselective catalyst.

[4,5]- and [5,6]-pineno-fused ligands are easily accessible in their enantiomerically pure forms starting from the commercially available (-)-α-pinene or (-)-myrtenal monoterpenes, respectively. Consequently, short and efficient syntheses of new optically active bipyridines have been carried out using these sources of chirality. The new bipyridines allow easy access to chiral helicating and caging ligands with sterically well defined shapes and properties.

Moreover, the pineno-fused ring can also be transformed by alkylation at the CH_2 ring positions as indicated in Figure 2 (R-substituted ligand).

3.1.2. Coordination chemistry of pinene derived ligands

In the last two decades, many new and interesting metal complexes of helicating and caging chiral ligands have been described.[35] Many of these ligands lead to chiral complexes or host-guest structures. However, a racemic mixture of the forms is usually produced. As such systems grow in size and number of chiral centers, the number of possible diastereoisomers and enantiomeric pairs increase exponentially, and it becomes necessary to develop new systems where the chirality is predetermined prior to the coordination so that the exact structure can be predicted in the supramolecular assemblies. For this reason, stereoselective synthesis of coordination compounds can be achieved through enantiopure chiral ligands.

The so-called "chiragen" (chirality generator) ligands have been designed to overcome these problems; these ligands contain a rigid chiral group in their pyridyl moieties, introduced by the use of a readily available natural product in their synthesis. These chiral polypyridylic pineno-fused ligands have been employed in a wide range of asymmetric transformations. Kishi and co-workers published the use of chiral pinene-bipyridine ligands in Ni/Cr-catalyzed coupling reactions.[24] Chelucci found application in Pd(0)-catalyzed allylic substitution.[36,37] Von Zelewsky demonstrated that mono- and bis-pinene-[5,6]-bipyridines are useful ligands in asymmetric Cu-catalyzed

cyclopropanation[28] and Pt-catalyzed substitution reactions.[29] He also coordinated these ligands to Co, Ag and Ru and studied their chiroptical properties.[30,38-40] Besides, Kocovsky used these ligands in coordination with Mo, Cu and Pd and evaluated their application in asymmetric allylic substitution, allylic oxidation and cyclopropanation.[31,32] Other polypyridylic pineno-fused ligands were coordinated to Ru, Fe and Mn and were applied as catalysts in oxidation reactions.[34,41-44]

In a similar way, pinene-derived mono- and bisphosphinite ligands have been applied in Rh-catalyzed hydrogenations.[45]

In general, the best results in asymmetric catalysis have been obtained when the pyridine is modified at the 6 position, probably due to the closest position of the chiral environment to the metal center.[31]

3.1.3. Zero-field splitting (ZFS) in mononuclear Mn^{II} complexes

In recent years, considerable attention has been paid to the precise determination of the zero-field splitting (ZFS) of transition-metal ion complexes with a total ground spin state $S > \frac{1}{2}$.[46-49] In fact, the ZFS is largely involved in the design of single-molecule magnets for which a large and negative axial ZFS (D parameter) represents an essential criterion to reach the desired magnetic characteristics.[50,51] Furthermore, for several transition-metal ions, it has been evidenced that the ZFS can probe their structural and electrostatic environment.[46] This is particularly true in the case of the Mn^{II} ion. Indeed, magnetostructural correlations have been proposed[52] based on the experimental investigation of a large number of mononuclear Mn^{II} complexes for which the structure has been resolved by X-ray diffraction, and the ZFS precisely determined by EPR spectroscopy. When the Mn^{II} ion is coordinated to at least one halide ligand, the nature of the halide controls the ZFS with $D_I > D_{Br} > D_{Cl}$.[53 -63] On the other hand, for five- and six-coordinate complexes with only nitrogen- and/or oxygen-based ligands, the ZFS is governed by the coordination number of the Mn^{II} atom with $|D_5| > |D_6|$.[64-66]

The rationalization of these experimental tendencies has required the understanding of the physical origin of the ZFS. This has been recently achieved by quantum chemistry in a DFT framework.[59,65,67,68] A good prediction of D has been obtained since the two physical factors that contribute to the bilinear term in the ZFS have been quantified: the direct dipole–dipole interaction of unpaired electrons (SSC) and the spin–orbit coupling

(SOC) of excited states into the ground state.[68,69] For the halide complexes, the major contribution to D arises from a cross term between the metal and halide SOC contributions that explains the strong effect of the nature of the halide on D.[59] In contrast, for the five- and six-coordinate N/O complexes, the physical origin of D is different since the major contribution in each case are the SOC and SSC parts, respectively.[65]

A deeper analysis of the ZFS for this latter class of compounds shows that the relative ratio between the N- and O-based ligands seems not to affect the D magnitude.[52] However, this conclusion is almost exclusively based on previous investigations performed on theoretical simplified models because of the limited experimental data available on compounds in a mixed N/O environment.[65] The large majority of mononuclear Mn^{II} complexes for which the D magnitude has been precisely determined by EPR spectroscopy are in N_6, N_5, O_6 and O_5 environments. Furthermore, the ZFS of only one seven-coordinate mononuclear complex has been investigated by EPR so far.[70] The reported D value for this N_6O complex falls in the range of the six-coordinate N/O complexes, but the prediction of the D value by DFT was rather poor. Thus, additional experimental and theoretical data on the ZFS of these compounds are required to evaluate whether or not the ZFS can be related to the ratio of N/O ligands and the coordination number of the Mn^{II} ion (6 vs. 7). These data should be also useful for the biochemical community since this type of coordination sphere reproduces those of the Mn^{II} ions contained at the active sites of several metalloenzymes.[71-75]

Based on the X-ray structures, it is also possible to predict the ZFS by quantum chemistry using a DFT approach. In previous works, performed on complexes that contained N/O ligand(s) and in some cases halide ligands, the BP86 functional was successfully used to calculate the ZFS.[59,65,67] Also, an improvement in the prediction of the ZFS for mononuclear Mn^{II} dihalide complexes has been recently achieved with B3LYP.[68]

3.2. Objectives

The research interests of our group in the latest few years include the synthesis of chiral pyridine derivative ligands and their coordination chemistry with some transition-metal ions. These ligands are potentially useful for enantioselective catalysis.

Continuing with the group interest in pinene-derived ligands, we considered to coordinate an asymmetric chiral sp^2-nitrogen donor ligand, (–)pinene[5,6]bipyridine (Chart 1), to different manganese (II) salts and fully characterize the resulting monuclear and/or binuclear complexes through structural, analytical, spectroscopic (IR, ESI-MS, UV-Vis) and electrochemical (CV) techniques.

(-)-L
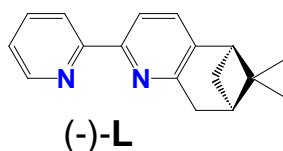
Chart 1. Ligand (–)pinene[5,6]bipyridine

Finally, other goals of this chapter were the study of the magnetic properties of the binuclear complexes and the determination of the ZFS of the mononuclear complexes through the help of X- and Q-band EPR spectroscopy, as well as computational calculations.

3.3. Results and discussion

3.3.1. Synthesis and characterization

The (–)-pinene[5,6]bipyridine chiral ligand, (–)-**L**, was synthesized following the method described in the literature (Scheme 1).[31] Oxidation of the pinene group with single oxygen leads to the (+)-pinocarvone intermediate that is subsequently condensated with a pyridinium salt under Krönke conditions.

The synthetic strategy followed for the preparation of Mn^{II} complexes **C1**-**C6**, containing (–)-**L**, is outlined in Scheme 2. Different Mn(II) salts were used as the starting material and then the (–)-**L** ligand was added stepwise. When an ethanolic solution of ligand (–)-**L** was added to MnCl$_2$ dissolved in water in a ligand:metal ratio of 0.85:1, the colourless solution turned pale yellow and the dinuclear complex, [{MnCl((–)-**L**)}$_2$(μ-Cl)$_2$] (**C1**), could be crystallized by slow evaporation of the solution. When the chiral ligand (–)-**L** was treated in ethanol with the Mn(OAc)$_2$·4H$_2$O and MnCl$_2$ salts in a 1:1 ratio, the dinuclear [{Mn((–)-**L**)}$_2$(μ-OAc)$_3$](PF$_6$) (**C2**) and the mononuclear [MnCl$_2$(H$_2$O)((–)-**L**)] (**C3**) complexes were respectively formed. When the metal:ligand ratio was 1:2, the mononuclear compounds [MnCl$_2$((–)-**L**)$_2$] (**C4**), [Mn(CF$_3$SO$_3$)$_2$((–)-**L**)$_2$] (**C5**) and [Mn(NO$_3$)(H$_2$O)((–)-**L**)$_2$)](NO$_3$) (**C6**) were respectively obtained starting from the corresponding Mn salts. Similar structures as those determined for complexes **C2**,[76] **C4**,[77] **C5**[78] and **C6**[79,80] (see below) have been already published with the parent bpy ligand.

Scheme 1. Synthesis of (–)-**L**.

X = Cl
$\xrightarrow{\text{EtOH / H}_2\text{O}}$ [{MnCl((-)-**L**)}$_2$(μ-Cl)$_2$] **C1**

X = OAc
$\xrightarrow{\text{EtOH}}$ [{Mn((-)-**L**)}$_2$(μ-OAc)$_3$](PF)$_6$ **C2**

X = Cl
$\xrightarrow{\text{EtOH}}$ [MnCl$_2$(H$_2$O)((-)-**L**)] **C3**

X = Cl
$\xrightarrow{\text{CH}_3\text{CN}}$ [MnCl$_2$((-)-**L**)$_2$] **C4**

X = CF$_3$SO$_3$
$\xrightarrow{\text{THF}}$ [Mn(CF$_3$SO$_3$)$_2$((-)-**L**)$_2$] **C5**

X = NO$_3$
$\xrightarrow{\text{EtOH / H}_2\text{O}}$ [Mn(NO$_3$)(H$_2$O)((-)-**L**)$_2$](NO$_3$) **C6**
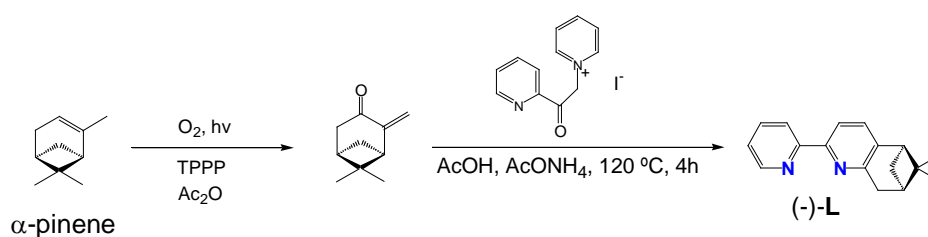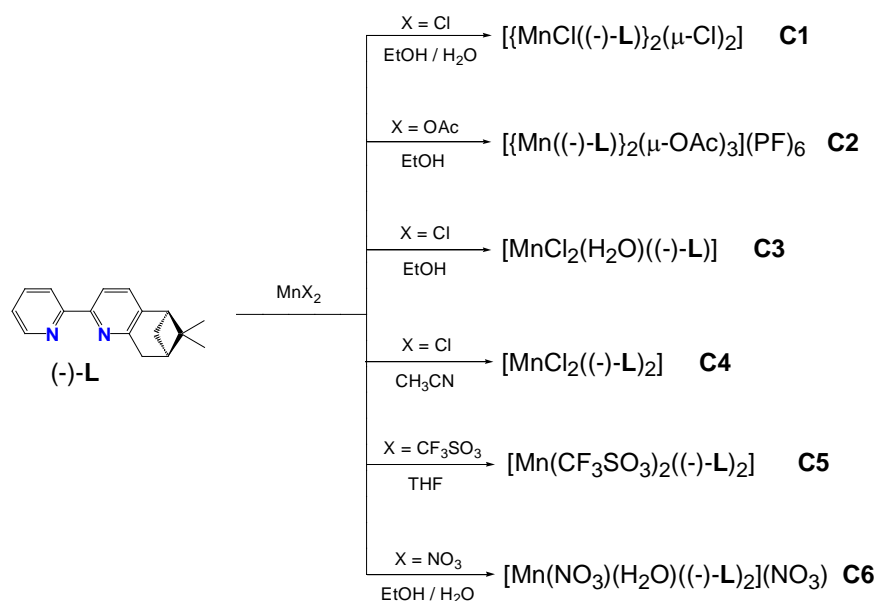
Scheme 2. Synthetic strategy for complexes **C1**-**C6**.

The crystal structures of complexes **C1**-**C6** have been solved by X-ray diffraction analysis. Figure 3 displays the molecular structures of the complexes whereas the principal bond lengths and angles are listed in Table 1 and Table 2. The main crystallographic data together with selected bond distances and angles can be found in the supporting information.

The dinuclear complex **C1** contains two pentacoordinated manganese (II) ions which are bridged by two chloro ligands. The three remaining coordination positions for each metal center are occupied by the two nitrogen atoms of the pinene ligand and a terminal chloride ion. It is worth mentioning that this compound constitutes the first example of a dinuclear complex with a {Mn$_2$(μ-Cl)$_2$}$^{2+}$ core where the Mn(II) ions adopt a pentacoordinate geometry; the other complexes described in the literature show hexacoordinate geometry around the central ion.[81-84] In addition, when the bpy ligand instead of (–)-**L** is used, a one-dimensional bis(μ-chloro) Mn(II) polymeric compound, [Mn(μ-Cl)$_2$(bpy)]$_n$ is obtained.[85] The geometry of each Mn(II) ion in **C1** is closer to distorted square pyramidal geometry than to trigonal bipyramid as ascertained by Reedijk's[86] τ factor of 0.39 for Mn1 and 0.44 for Mn2 (τ = 0 for a square-pyramid and τ = 1 for a trigonal bipyramid). The basal positions are occupied by two nitrogen atoms of the pinene ligand and by the two chloride bridges, and the axial position is occupied by the terminal chloro ligand. The bpy-pinene ligand shows a high degree of distortion (the N-C-C-N torsion angle is 12.4⁰ for the ligand bound to Mn2 and 7.8⁰ for the one coordinated to Mn1) and is also markedly tilted with regard to the Mn$_2$(μ-Cl)$_2$ core

plane. This remarkable distortion of the basal positions from planarity (Cl1-Mn2-N3 angle is 129.4º) allows moderate H-bonding interactions between H19A and Cl2 (d = 2.69 Å) and also between the two H atoms bound to C31 and two chloro ligands (d(H31a-Cl4) = 2.87 Å, d(H31b-Cl1) = 2.77 Å). The $Mn_2(\mu\text{-Cl})_2$ core is planar, with a Mn···Mn distance of 3.7 Å. The Mn-Cl bridging bond lengths are slightly different, 2.58 and 2.44 Å, and longer than the terminal Mn-Cl bond lengths, 2.33 and 2.34 Å, respectively. The two manganese atoms are non-equivalent since the complex has not any symmetry. One terminal Cl is orientated toward the methyl groups of the pinene ligand and the other one is directed away from these groups. The Mn-N distances are quite different for the two N atoms of the (–)-**L** ligand with an elongation of the Mn-N bond of the pyridine bearing the bulky pinene group (N_{pypi}). This elongation is also observed in complexes **C2**-**C6** (see below), as well as in other previously reported complexes with this ligand.[29,30]

Table 1. Principal bond lengths (Å) and angles (deg) for **C1**, **C2** and **C3**.

	Mn-N_{py}	Mn-N_{pypi}	Mn-X1[a]	Mn-X2[b]	Mn-X3[c]	Mn···Mn
C1	2.190	2.296	2.5772	2.4356	2.3293	3.736
	2.207	2.295	2.4519	2.5526	2.3390	
C2	2.186	2.234	2.159	2.175	2.034	3.433
C3	2.224	2.254	2.3822	2.3698	2.189	

[a] X1 = μ-Cl1 for **C1**, μ-O1 for **C2**, Cl1 for **C3**. [b] X2 = μ-Cl2 for **C1**, μ-O2* for **C2**, Cl2 for **C3**. [c] X3 = Cl3 for **C1**, μ-O3 for **C2**, O_{aqua} for **C3**.

In the cationic dinuclear complex **C2**, the Mn(II) ions are linked by three acetate bridging ligands, one of them in a *syn-syn* conformation and the other two in a *syn-anti* conformation. This complex adopts a symmetric structure. The two manganese atoms are equivalent since the complex has a C_2 symmetry axis passing through the C20 and C21 atoms of one of the acetate groups. Each manganese ion is bonded to two nitrogen atoms from a bidentate (–)-**L** ligand and three oxygen atoms of the acetate bridges, in a distorted square pyramidal geometry, with a τ factor[86] of 0.34. The equatorial plane is formed by N2 and the three oxygen atoms, O1, O2* and O3, and the apical position is occupied by N1. For the μ-acetate ligand in a *syn-syn* conformation, the Mn-O distances (d(Mn1-O3) = 2.04 Å) are shorter than the Mn-O distances for the carboxylate in a *syn-anti* conformation, where d(Mn1-O1$_{syn}$) = 2.16 Å and d(Mn1-O2*$_{anti}$) = 2.17 Å. The Mn1-O2*-C18-O1* dihedral angle is 96.4º. The *syn-*

anti disposition of two of the carboxylate bridges facilitates a weak interaction between one of the Mn(II) ions and the $O2_{anti}$ bound to the second Mn centre with a $Mn1 \cdots O2_{anti}$ distance of 2.48 Å. The $Mn \cdots Mn$ distance of 3.43 Å is shorter than those reported in the literature for other dinuclear Mn(II) complexes with the same $\{Mn_2(\mu\text{-RCOO})_3\}^+$ core. Different coordination modes of the carboxylate bridges are found for this kind of complexes. Four compounds show the three carboxylate bridges coordinated in a μ–1,3 mode: $[\{MnL'\}_2(\mu\text{-CH}_3\text{COO})_3](BPh_4)$ (L' = *N,N',N'*-trimethyl-1,4,7-triazacyclononane) ($d(Mn \cdots Mn)$ = 4.03 Å),[87] $[Mn_2(\mu\text{-Ph}_2\text{CH}_3\text{CCOO})_3(bpy)_2](PF_6)$, ($d(Mn \cdots Mn)$ = 3.69Å),[88] $[Mn_2(\mu\text{-CH}_3\text{COO})_3(bpea)_2](PF_6)$, ($d(Mn \cdots Mn)$ = 3.92 Å)[89] and $[\{Mn(Tp^{iPr2})\}(\mu\text{-C}_6\text{H}_5\text{COO})_3\{Mn(Tp^{iPr2}H)\}]$, ($d(Mn \cdots Mn)$ = 4.01 Å),[90] whereas four other complexes ($[\{Mn\{HB(3,5-Pr^i_2pz)_3\}(\mu\text{-C}_6\text{H}_5\text{COO})_3\{Mn(3,5-Pr^i_2pzH)_2\}]$ ($d(Mn \cdots Mn)$ = 3.75 Å),[91] $[Mn_2(baip)(\mu\text{-C}_6\text{H}_5\text{COO})_3(NCS)]$ ($d(Mn \cdots Mn)$ = 3.50 Å),[92] $[\{Mn(Tp^{iPr2})\}(\mu\text{-4-FC}_6\text{H}_4\text{COO})_3\{Mn(Pz^{iPr2}H)\}]$ ($d(Mn \cdots Mn)$ = 3.73 Å)[93] and $[\{Mn(bpy)\}_2(\mu\text{-CH}_3\text{COO})_3](ClO_4)$ ($d(Mn \cdots Mn)$ = 3.50 Å)[76]) show one of the carboxylate bridges coordinated in a μ-1,1 mode. For compound **C2**, the *syn-anti* conformation of two carboxylates and the pentacoordination of the Mn(II) ions make possible a weak interaction between the $O2^*_{anti}$ and the $Mn1^*$ ions and, as a result, a shorter $Mn \cdots Mn$ distance is observed.

The geometry around the Mn(II) ion in the mononuclear complex **C3** is a distorted trigonal bipyramid (Reedijk's[86] τ factor of 0.73), where the equatorial plane is occupied by the two monoatomic ligands, Cl1 and Cl2 and the N1 of the (–)-**L** ligand. The other nitrogen atom, N3, and the oxygen atom from the aquo ligand, O3, are in the axial positions. The spatially constrained nature of (–)-**L** produces geometrical distortions manifested in the N3-Mn-O3 angle equal to 163º compared to the theoretical value of 180º.

The mononuclear complexes **C4**, **C5** and **C6** present a distorted octahedral geometry. It is worth mentioning here that Mn(II) hexacoordination is achieved only in those complexes with two bipyridyl (–)-**L** ligands coordinated to the metal centre, probably due to the stronger π-acceptor capability of two aromatic ligands when compared to the pentacoordinated complexes **C1**-**C3** (either dinuclear or mononuclear), bearing only one of these ligands. The higher electron density withdrawing caused by the two (–)-**L** ligands might be partially compensated by the coordination of an additional monodentate anionic ligand.
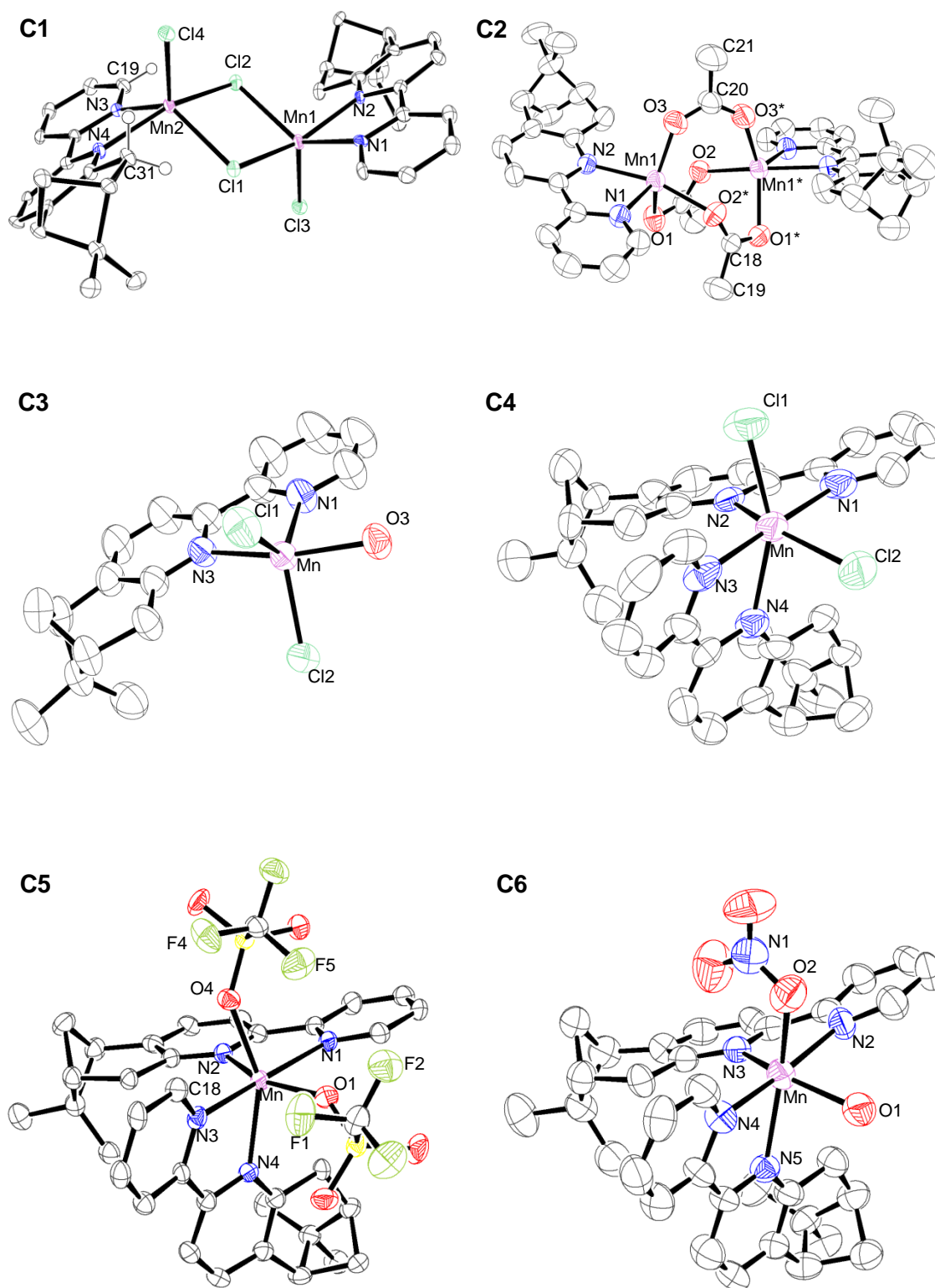
Figure 3. ORTEP plots (ellipsoids at 50% probability level) of complexes **C1**-**C6**.

In complexes **C4**-**C6** the Mn(II) ion is coordinated by four nitrogen atoms of the two (−)-**L** ligands and two monodentate ligands: two choride ions for **C4** and two oxygen atoms for **C5** and **C6**, in a *cis* position. The two choride or oxygen atoms are in all cases in *trans* position to a pyridine ring bearing a pinene group. The Mn-Cl and Mn-O_{aqua}/$O_{triflate}$/$O_{nitrate}$ bond distances are comparable to those found in [Mn(bpy)$_2$Cl$_2$],[77] [Mn(bpy)$_2$(CF$_3$SO$_3$)]$_2$,[78] [Mn(bpy)$_2$(NO$_3$)(H$_2$O)][79,80] and in other Mn(II) mononuclear complexes.[94]

Table 2. Principal bond lengths (Å) and angles (deg) for **C4**, **C5** and **C6**.

	Mn-N$_{py}$	Mn-N$_{pypi}$	Mn-X1[a]	Mn-X2[b]	N$_{py}$-Mn-N$_{pypi}$	X1-Mn-X2
C4	2.294	2.358	2.481	2.489	70.3	107.65
	2.290	2.387			70.4	
C5	2.265	2.280	2.168	2.186	72.80	98.20
	2.252	2.300			72.81	
C6	2.252	2.347	2.184	2.261	71.2	86.93
	2.246	2.321			71.7	

[a] X1 = Cl1 for **C4**, O1 for **C5**, O$_{aqua}$ for **C6**. [b] X2 = Cl2 for **C4**, O4 for **C5**, O$_{nitrate}$ for **C6**.

The spatial disposition of two (−)-**L** ligands and two monodentate ligands in an octahedral environment (as is the case of complexes **C4**-**C6**) could potentially lead to a set of four possible isomers, depicted in Scheme 3. The nomenclature *trans* or *cis* for the three first isomers refers to the relative position of the two monodentate ligands with regard to pyridyl rings bearing the pinene substituent. The nomenclature *trans(X)* for the fourth isomer indicates the relative disposition of the two monodentate X ligands.

trans,trans-[MnX$_2$((-)-L)$_2$]   *trans,cis*-[MnX$_2$((-)-L)$_2$]   *cis,cis*-[MnX$_2$((-)-L)$_2$]   *trans(X)*-[MnX$_2$((-)-L)$_2$]
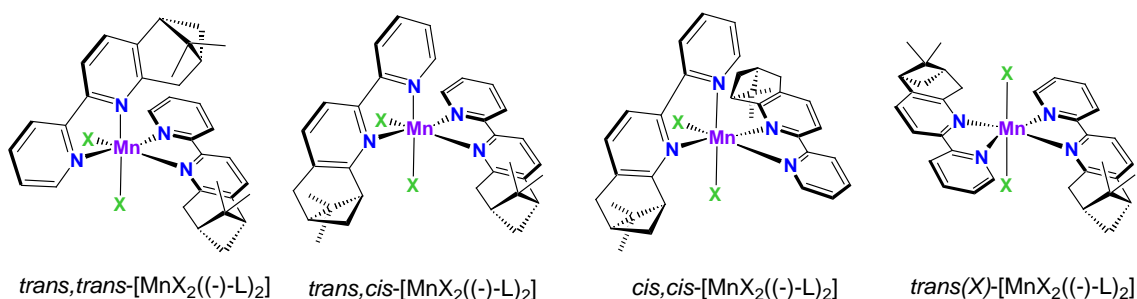
Scheme 3. Potential isomers for mononuclear octahedral complexes **C4**-**C6**.

(X = monodentate ligand)

The X-ray structures of complexes **C4**-**C6** reveal that, in all cases, the *trans,trans*-[MnX$_2$((−)-**L**)$_2$] is the isomer obtained. This evidence cannot be explained by steric arguments since the *trans,trans* isomer would probably be the most constrained one, given the relative disposition of the methyl substituents in both pinene groups, directed towards each other (see the X-ray structures in Figure 3). The specificity towards the *trans,trans* isomer can be interpreted in terms of the presence of H-bonding between the monodentate X ligands and the H atom in 2-position of the pyridyl rings in *cis*. Two such H-bonds can be formed in the *trans,trans* isomer whereas only one can be found in the *trans,cis* isomer, and none in the other two. The presence of *cis* H-bonding involving pyridyl rings in octahedral complexes has been found to be a determining factor in the exclusive formation of a geometrical isomer in ruthenium complexes,[95,96] as confirmed by DFT calculations.

Complexes **C4**-**C6** present a highly distorted geometry, mainly due to the spatially constrained nature of the (−)-**L** ligands coordinated to the metal. Thus, the N$_{py}$-Mn-N$_{pypi}$ angles are about 17° to 20° below the 90° for an ideal octahedron. Furthermore, a relatively high torsion N-C-C-N angles are found for the pinene-bipyridine ligands in the three mononuclear complexes (approximately 10.1°/12.1° for **C4**, 10.8°/2.5° for **C5** and 8.6°/1.6° for **C6**), which can be mainly due to the steric encumbrance of the methyl pinene groups that forces the second (−)-**L** ligand plane to tilt up to around 30° with respect to a regular octahedral geometry (see Figure S 2 in the supporting information section). However, in spite of this relatively high degree of distortion, the *cis* H-bonding interactions described above fall in the range between 2.4 and 2.7 Å.

3.3.2. Magnetic properties

Magnetic susceptibility data were recorded for the two dinuclear compounds **C1** and **C2** from room temperature to 4 K. The $\chi_M T$ vs *T* plots are shown in Figure 4. In both cases the $\chi_M T$ value is ca. 8.9 cm^3 mol^{-1} K in the range from room temperature to 70 K. This value is close to that expected for two uncoupled Mn(II) ions. The decrease in $\chi_M T$ value below this temperature for compound **C2**, and below 20 K for compound **C1**, may be the result of antiferromagnetic interactions (intra- or intermolecular) or of the ZFS (Zero Field Splitting), which is usually small for Mn(II) ions. The best fit, based on the spin hamiltonian $H = -J\, S_1\, S_2$, corresponds to $J = -0.22$ cm^{-1} and $g = 2.01$ (R = 4.04 10^{-4}) for **1** and $J = -0.85$ cm^{-1} and $g = 2.04$ (R = 5.87 10^{-4}) for **C2**.
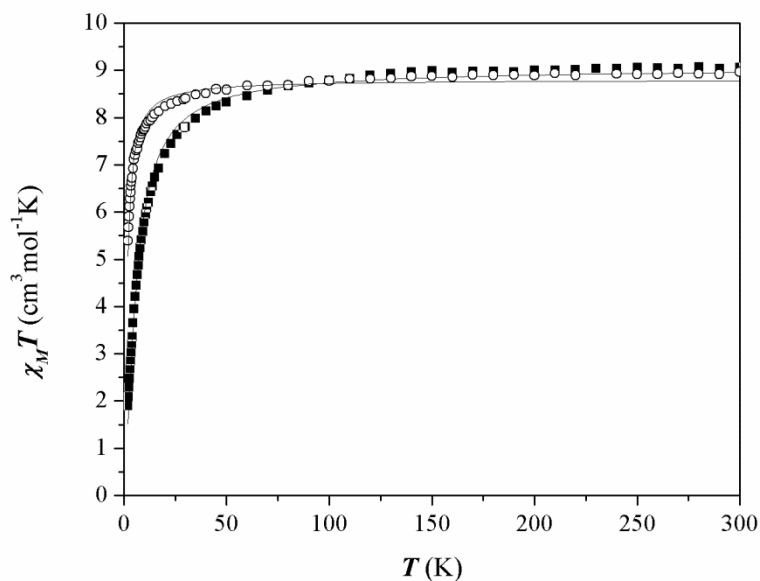
Figure 4. Temperature dependence of $\chi_M T$ for **C1** (○) and **C2** (■). Solid lines result from the least-squares fit using the parameters described in the text.

To the best of our knowledge, there are only other four Mn(II) dinuclear complexes with a $\{Mn_2(\mu\text{-Cl})_2\}^{2+}$ core magnetically and structurally characterized. Table 3 summarizes the magnetic coupling constants and the most important structural parameters for these complexes. All of them show a weak ferromagnetic coupling and octahedral coordination of the Mn(II) ions. As was indicated in the preceding section, the geometry around the Mn(II) ions in **C1** is a distorted square pyramid, with an average τ factor[86] of ~ 0.42.

Table 3. Comparison of the structural parameters (distances [Å] and angles [º]) and magnetic interaction (J [cm^{-1}], based in the spin hamiltonian $H = -J\,S_1\,S_2$) for dinuclear complexes with a $\{Mn_2(\mu\text{-Cl})_2\}^{2+}$ core.

	α(MnClMn)	d(Mn-Cl)	J	ref.
C1	96.4	2.44; 2.57	-0.22	
[{Mn(bpea)Cl}$_2$(μ-Cl)$_2$]	95.7	2.57; 2.54	+0.68	81
[{Mn(dpp)Cl(H$_2$O)}$_2$(μ-Cl)$_2$]	95.6	2.61; 2.52	+0.11	82
[{Mn(biz)$_2$}$_2$(μ-Cl)$_2$]Cl$_2$	93.5	2.57; 2.56	+0.33	83
[{Mn(mpbpa)Cl}$_2$(μ-Cl)$_2$]	96.4	2.60; 2.57	+1.10	84

The magnetic interaction in compounds with a $\{Mn_2(\mu\text{-Cl})_2\}^{2+}$ core is very sensitive to the relative orientation of the coordination polyhedra of the metallic centers.[81-84] In spite of the distortion around the Mn(II) ions in **C1**, the basal planes of the distorted square

pyramid environments contain the N atoms of the bpy-pinene ligand and the Cl bridges and, consequently, this complex could be described as two square pyramids sharing one edge, like in other dinuclear complexes with analogous core (but in octahedral coordination) reported in the literature.[81-84] The magnetic interaction through the chloride bridges with coplanar bases is very sensitive to the Mn-Cl-Mn angle (Table 3). In all cases, the angle is close to 90⁰, thus, close to the accidental orthogonality, and the magnetic coupling constant is small. For **C1** the magnetic coupling constant is very small and of opposite sign, probably due to the important distortion from the square pyramid towards trigonal bipyramid and to the fact that the basal planes of the square pyramid are not coplanar.

The exchange interaction in **C2** is antiferromagnetic and weak, similar to other dinuclear complexes with three carboxylate bridges (Table 4). In this kind of complexes, when one of the carboxylate ligands bridges the manganese ions in a μ-1,1 mode, the Mn$\cdots$Mn distance is shorter than if bridges are arranged in a μ-1,3 mode. The coordination mode of the carboxylate ligands in compound **C2** is μ-1,3 but due to the *syn-anti* disposition of two carboxylates and the weak Mn$\cdots$O$_{anti}$ interaction, the Mn$\cdots$Mn distance is the shortest found for this kind of compounds. However, there is not a good relationship between the coordination mode of the carboxylate and the Mn$\cdots$Mn distance with the magnetic coupling constant.

Table 4. Comparison of the structural parameters (distance [Å] and coordination mode of the bridging carboxylate ligand) and magnetic interaction (J [cm^{-1}], based on the spin hamiltonian $H = -J\,S_1\,S_2$) for Mn(II) dinuclear complexes with three carboxylate bridges.

	coordination mode	d(Mn$\cdots$Mn) Å	J (cm^{-1})	ref
C2	μ −1,3	3.43	-0.85	This work
[{Mn(bpea)}$_2$(μ-CH$_3$COO)$_3$](PF$_6$)	μ −1,3	3.92	-2.6	89
[{MnL'}$_2$(μ-CH$_3$COO)$_3$](BPh$_4$)	μ −1,3	4.03	-3.5	87
[{Mn(bpy)}$_2$(μ-CH$_3$COO)$_3$](ClO$_4$)	μ −1,3 μ −1,1	3.50	-0.4	76
[{Mn(bpy)}$_2$(μ-Ph$_2$CH$_3$CCOO)$_3$](PF$_6$)	μ −1,3	3.69	-0.4	88
[{Mn(bpy)}(μ-C$_6$H$_5$COO)$_3${Mn(bpy)(MeOH)](NO$_3$)	μ −1,3 μ −1,1	3.50	-2.2	88
[Mn$_2$(baip)(C$_6$H$_5$COO)$_3$(NCS)]	μ −1,3 μ −1,1	3.50	-3.46	92

3.3.3. Electrochemical properties

The redox potential of the compounds **C1**-**C6** have been determined by cyclic voltammetry (CV) in CH_3CN + 0.1 M $[(nBu)_4N]PF_6$. The cyclic voltammograms obtained for **C2**, **C3**, **C5** and **C6** are shown in the supporting information. For these compounds an irreversible Mn(III)/Mn(II) redox process is observed for compounds at a potential value ranging from 1.0 to 1.75 V (see experimental section and Figure S 3). In contrast, the redox processes of the chloro complexes **C1** and **C4** appear to be more reversible and are located at a slightly lower potential of $E_{1/2}$ = +0.90 and +0.83 V, respectively (Figure 5a and Figure 6a).
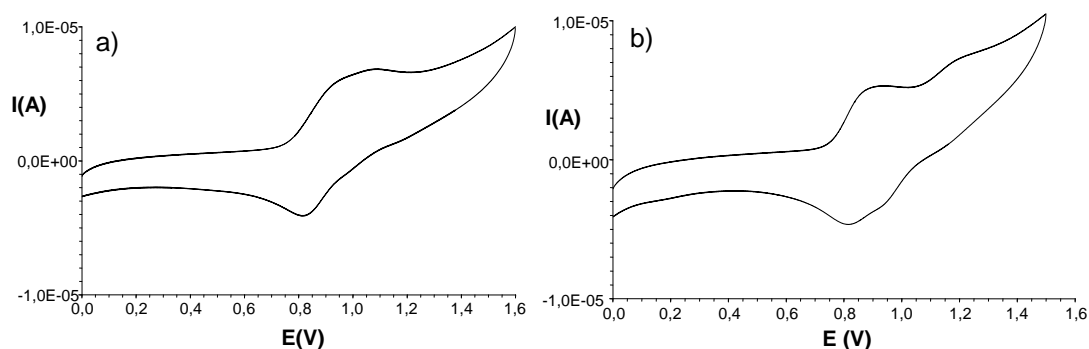
Figure 5. CV in CH_3CN +0.1M $[(nBu)_4N]PF_6$ of a 0.5 mM solution of: a) **C1**, b) **C1** after exhaustive oxidation at 1 V, at a platinum electrode (2 mm diameter); scan rate:100 mV/s.

Figure 6. CV in CH_3CN +0.1M $[(nBu)_4N]PF_6$ of a 0.5 mM solution of: a) **C4**, b) **C4** after exhaustive oxidation at 1 V, at a platinum electrode (2 mm diameter); scan rate:100 mV/s.
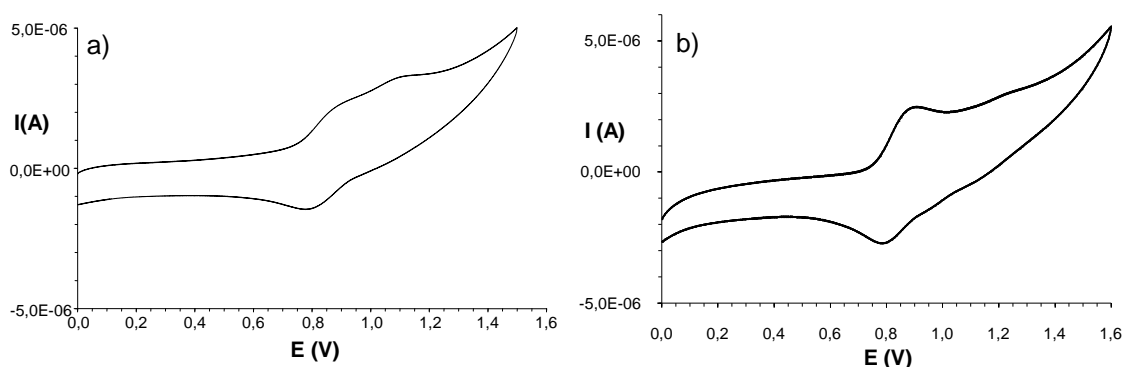
The electrochemical behaviour of complexes **C1** and **C4** has been investigated more thoroughly. The CV for **C4** (Figure 6a) exhibits the aforementioned one-electron reversible oxidation wave corresponding to the Mn^{III}/Mn^{II} redox system ($E_{1/2}$ = +0.83 V *vs* SSCE, ΔE_p = 110 mV; scan rate = 100 mV·s^{-1}) and a second irreversible oxidation wave at E_{pa} = +1.1 V *vs* SSCE with a very small intensity, that possibly corresponds to the oxidation of the chloride ions (generally E_{pa} = 1.1-1.4 *vs* SSCE).[97] Consequently, the oxidation process at $E_{1/2}$ = +0.83 V leads to the generation of $[Mn^{III}Cl_2((-)-\textbf{L})_2]^+$. The monoelectronic nature of the wave is confirmed by coulometric experiments carried out at E_{app} = +1 V, where 0.9 e$^-$ per mol of complex **C4** are transferred. After bulk electrolysis, the initial colourless solution turns green-olive and the UV-visible spectrum (Figure 7) shows two bands at λ_{max} = 577 and 388 nm. The latter transition is assigned to a Cl$^-$ → Mn(III) LMCT (ligand to metal charge transfer) transition on the basis of reported values for other Mn(III) complexes with nitrogen and chloro based ligands.[97-100] The transition observed at 577 nm is attributed to d-d Mn(III) transitions in agreement with the maximum absorbance wavelength theoretically expected for this type of process.[101,102]

A similar behaviour has been observed for **C1**. The initial CV (Figure 5a) exhibits a two-electron reversible oxidation wave corresponding to the $Mn^{III}Mn^{III}/$ $Mn^{II}Mn^{II}$ redox system ($E_{1/2}$ = +0.90 V *vs* SSCE, ΔE_p = 110 mV; scan rate = 100 mV·s^{-1}) and a second irreversible oxidation wave at E_{pa} = +1.1 V *vs* SSCE with a very small intensity. The bielectronic nature of the wave is confirmed on coulometric experiments carried out at E_{app} = +1 V, where 2.3 e$^-$ per mol of complex **C1** are transferred. After bulk electrolysis, the initial colourless solution also turns green-olive, giving a cyclic voltammogram similar to the one observed for **C4** after bulk electrolysis (compare Figure 5b and Figure 6b), and an identical UV-vis spectrum for the oxidized species (Figure 7). This fact indicates that the electrochemical oxidation of **C1** produces the breaking of the dinuclear compound obtaining a mononuclear Mn(III) species.

The triflate complex **C5** is oxidized at a very high potential compared to the structurally similar chloro complex **C4**. Indeed, the CV of **C5** in CH_3CN evidences two successive irreversible oxidation peaks at E_{pa} = +1.3 V and +1.75 V *vs* SSCE (Figure S 3c), a difference that can be explained in terms of the lower electron-donating capacity of the triflate anions with regard to chloride. It is consequently easier to oxidize complex **C4** than **C5**, which is in turn consistent with the higher valence of the intermediate species generated upon oxidation of **C4** with peracetic acid (described in Chapter 4).
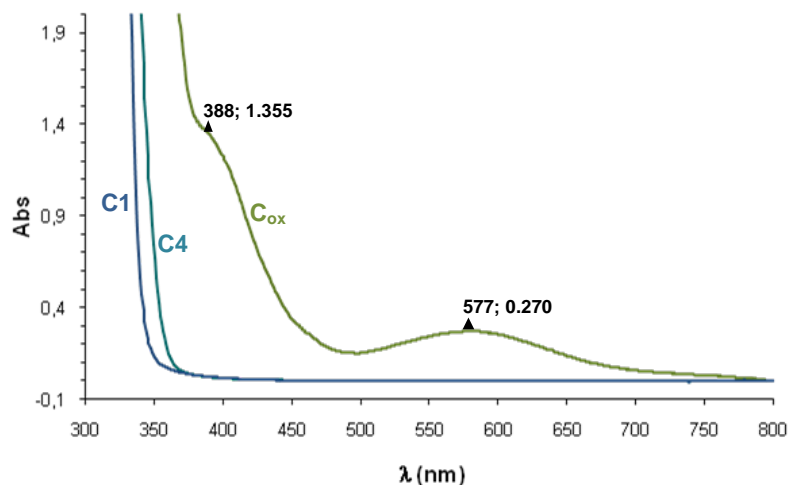
Figure 7. UV-vis spectra for complexes **C1**, **C4** and the species formed after exhaustive oxidation.

The formation of a mononuclear Mn(III) species has been confirmed recording EPR spectra on an acetonitrile solution of complex **C4** before and after the coulometric experiments (Figure 8). The X-band EPR spectrum of the initial Mn(II) compound recorded at 100K displays a signal centered at $g = 2.00$ characteristic of a mononuclear high-spin Mn^{II} complex (S = 5/2). Note that the presence of supporting electrolyte in solution allows observing the hyperfine splitting for the initial solution of **C4**. Upon exhaustive oxidation at 1 V, the EPR signal of the initial solution fully disappears in accordance with the formation of the X-band EPR silent high-spin Mn^{III} species ($S = 2$).
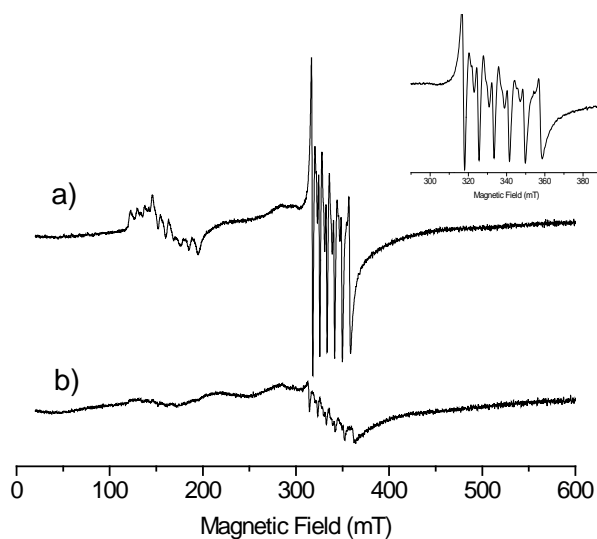
Figure 8. 100K X-band EPR spectra of a 0.8 mM solution of **C4** in CH$_3$CN + [(nBu)$_4$N]PF$_6$, a) initial solution, b) after exhaustive electrolysis at 1 V (formation of [Mn^{III}Cl$_2$((−)-**L**)$_2$]$^+$).

3.3.4. Investigation of the Zero-Field Splitting by combining EPR spectroscopy and quantum chemistry

Through the help of X- and Q-band EPR spectroscopy, the spin Hamiltonian parameters (SHPs) of a series of seven mononuclear Mn^{II} complexes in various mixed N/O and N/Cl coordination spheres (i.e., N_4Cl_2, N_4O_2, N_3O_3, and N_3O_4; Figure 9) have been determined. Complexes $[Mn((-)-L)_2Cl_2]$ (**C4**), $[Mn((-)-L)_2(CF_3SO_3)_2]$ (**C5**), $[Mn((-)L)_2(NO_3)(H_2O)](NO_3)$ (**C6**), $[Mn(bpy)_2(CF_3CO_2)_2]$ (**C7**) and $[Mn(terpy)(CF_3CO_2)_2(H_2O)]$ (**C8**) are six-coordinate, whereas $[Mn(terpy)(NO_3)_2(H_2O)]$ (**C9**) and $[Mn(bpea)(NO_3)_2]$ (**C10**) are seven-coordinate [terpy = 2,2':6,2''-terpyridine, (–)-**L** = (–)-pinene[5,6]bipyridine, bpy = 2,2'-bipyridine, bpea = N,N-bis(2-pyridylmethyl) ethylamine]. Based on the X-ray structures, the ZFS of **C4**–**C10** have also been predicted by quantum chemistry using a DFT approach.

Complexes **C4**-**C6** have been described in this chapter, whereas complexes **C7**-**C10** were previously synthesized and characterized.[94,103,104]

[Mn((-)-L)$_2$Cl$_2$] (**C4**)   [Mn((-)-L)$_2$(CF$_3$SO$_3$)$_2$] (**C5**)   [Mn((-)-L)(NO$_3$)(H$_2$O)](NO$_3$) (**C6**)

[Mn(bpy)$_2$(CF$_3$CO$_2$)$_2$] (**C7**)   [Mn(terpy)(CF$_3$CO$_2$)$_2$(H$_2$O)] (**C8**)   [Mn(terpy)(NO$_3$)$_2$(H$_2$O)] (**C9**)   [Mn(bpea)(NO$_3$)$_2$] (**C10**)
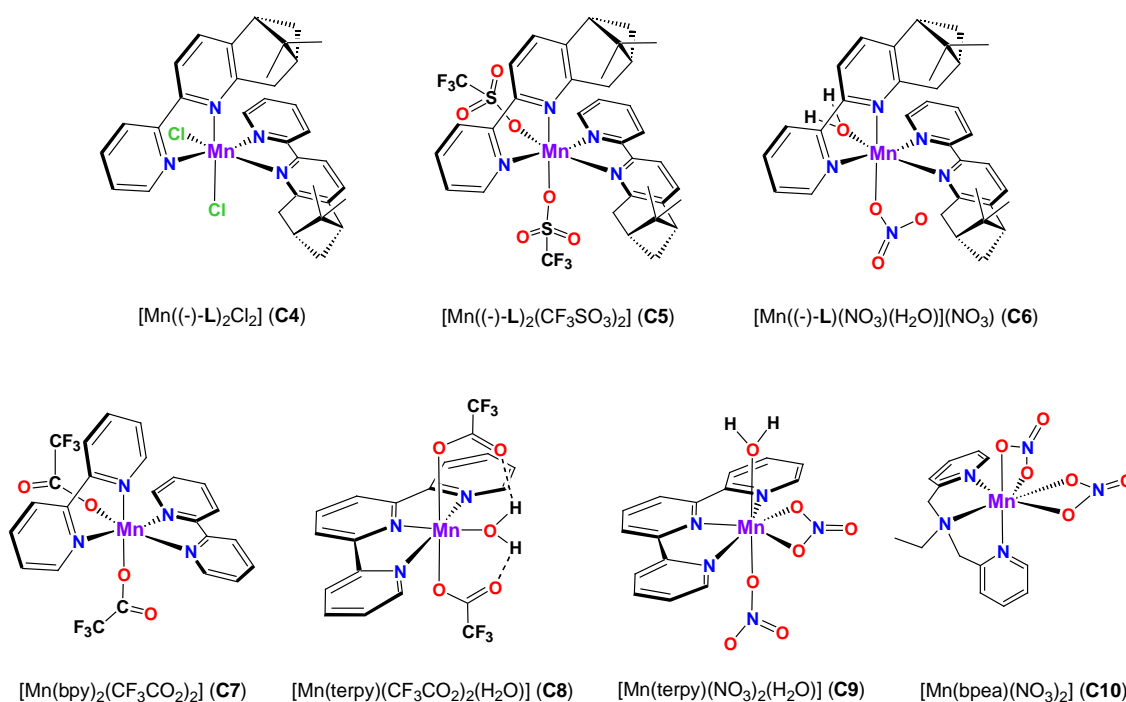
Figure 9. Schematic representation of complexes **C4**-**C10**.

3.3.4.1. X- and Q-band EPR spectroscopy experiments

Powder X- and Q-band EPR spectra have been recorded on each complex over a temperature range between 5 K and room temperature (Figure 10 to Figure 13). It clearly appears that the high-field limit condition is only reached at the Q-band frequency, which means that the D values of the complexes are generally smaller than the energy provided by the EPR spectrometer (i.e., 1.2 cm^{-1}). This is in accordance with the expected D values (< 0.22 cm^{-1}) for such complexes.[52] Such Q-band EPR-spectroscopy experiments have been already carried out on Mn^{II} complexes and in particular on a mononuclear Mn^{II}-containing enzyme.[105] The Q-band EPR spectra recorded under such high-field conditions are easily analyzable, and a direct estimation of the D and E values can be afforded as described elsewhere.[58] Actually, for high-spin Mn^{II} complexes, the shape of the EPR spectra only depends on the ZFS terms since the anisotropy of the Zeeman interaction is very small and leads to g values close to 2.[106,107]
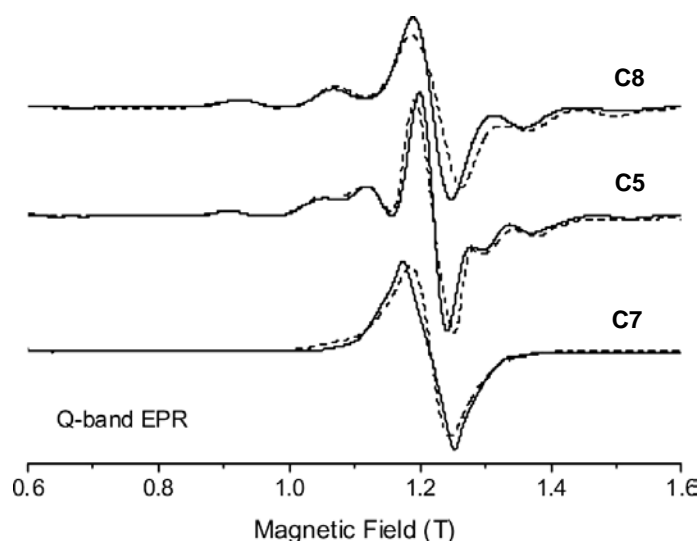
Figure 10. Experimental (solid line) and simulated (dashed line) Q- band EPR spectra recorded at room temperature on powder samples of complexes **C5**, **C7** and **C8**. The parameters used for the simulation are: g_{iso} = 2; for **C5**, D = −0.071 cm^{-1}, E/D = 0.070; for **C7**, D = −0.035 cm^{-1}, E/D = 0.154; for **C8**, D = 0.068 cm^{-1}, E/D = 0.308.

Figure 11. Experimental (solid line) and simulated (dashed line) Q-band EPR spectra recorded at low temperatures (10–30 K) on powder samples of complexes **C4**, **C5** and **C6**. The parameters used for the simulation are: g_{iso} = 2; for **C4**, $D = -0.150$ cm^{-1}, E/D = 0.113; for **C5**, D = +0.087 cm^{-1}, E/D = 0.138; for **C6**, $D = -0.078$ cm^{-1}, E/D = 0.077.

A comparable shape of the Q-band EPR spectra is observed for the whole series of complexes. Features are present around g = 2; these are associated with the $|^5/_2,-\frac{1}{2}>$ → $|^5/_2,+\frac{1}{2}>$ transitions along the x, y and z magnetic axes. The relative intensity of this central line varies as a function of the temperature and becomes prominent at room temperature to the detriment of the wings. Another common feature is the line located at 0.6 T (g = 4) observed at low temperature, which corresponds to the unique "forbidden" transition. On the other hand, the X-band EPR spectra (Figure 13) present a quite different shape depending on the complex and therefore seem to be very sensitive to the environment of the Mn^{II} ion. Nevertheless, the high-field limit condition not having been reached, their analysis is rendered delicate because of the mixture that occurs between the Zeeman levels.

The variable-temperature study has pointed out an interesting effect. In Figure 12, the 10 K spectrum recorded on **C10** presents a feature at 0.79 T that is shifted to 0.84 T at room temperature. A similar shift occurs for the 1.62 T transition at 10 K in the high-field wing that moves to 1.57 T at room temperature. These shifts are the signature of a slight decrease of the D value when the temperature increases and thus of small structural modifications of the Mn^{II} environment (see below). A similar behaviour has been observed for the rest of the complexes.
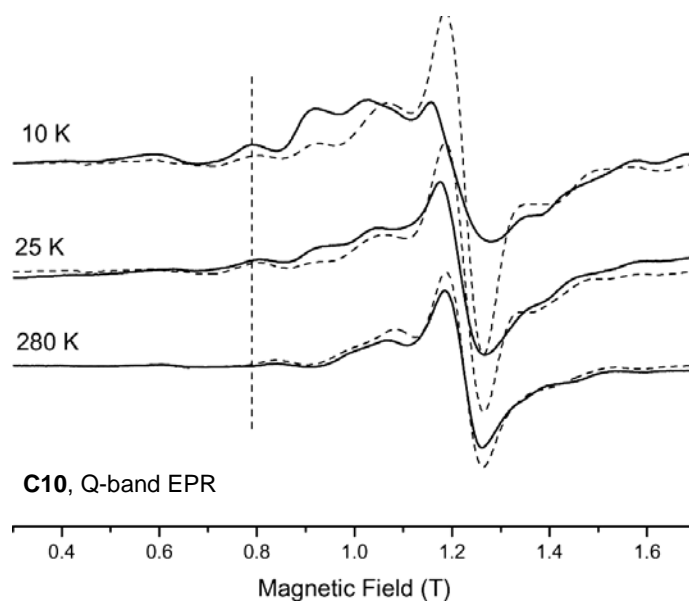
Figure 12. Experimental (solid line) and simulated (dashed line) Q-band EPR spectra recorded at different temperatures (10, 25 K and room temperature) on a powder sample of complex **C10**. The parameters used for the simulation are: g_{iso} = 2; at 10 K, D = +0.095 cm^{-1}, E/D = 0.152; at 25 K, D = +0.092 cm^{-1}, E/D = 0.147; at room temp. D = +0.086 cm^{-1}, E/D = 0.093.

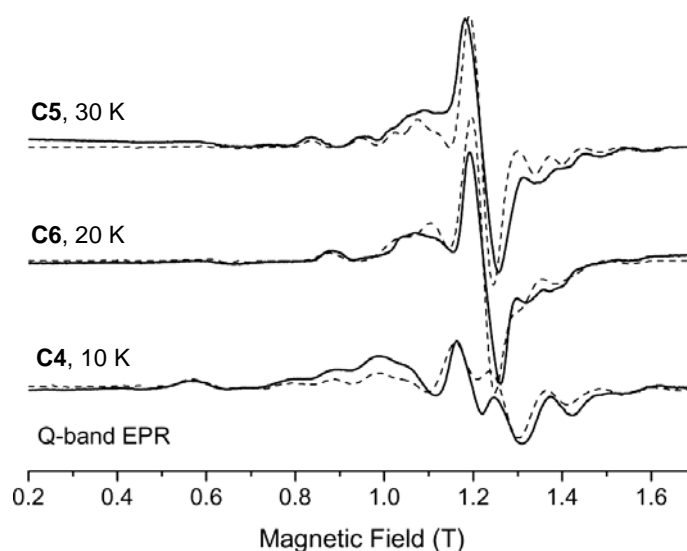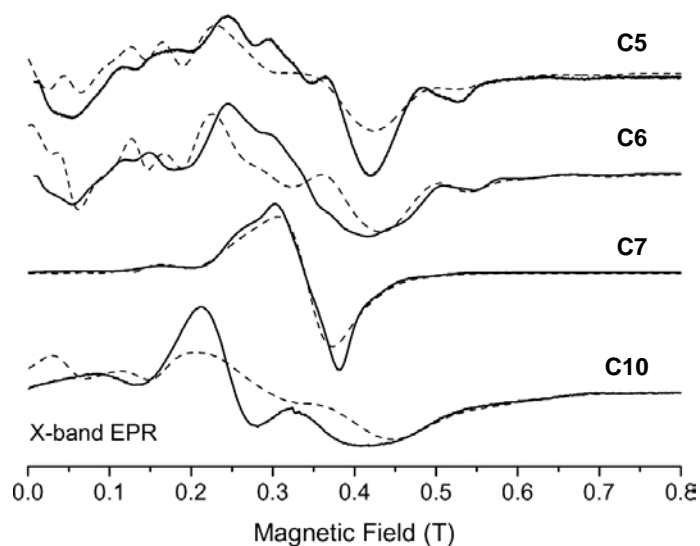**Figure 13.** Experimental (solid line) and simulated (dashed line) X-band EPR spectra recorded at room temperature on powder samples of complexes **C5**, **C6**, **C7** and **C10**. The parameters used for the simulation are: g_{iso} = 2; for **C5**, $|D|$ = 0.082 cm^{-1}, E/D = 0.122; for **C6**, $|D|$ = 0.087 cm^{-1}, E/D = 0.115; for **C7**, $|D|$ = 0.038 cm^{-1}, E/D = 0.132; for **C10**, $|D|$ = 0.092 cm^{-1}, E/D = 0.120.

For neat-powder EPR spectra, the ^{55}Mn hyperfine interaction is never resolved, presumably because of the intermolecular dipole–dipole interactions together with the *D* strain that contribute to the broadening of the line. As a consequence, the accurate determination of the spin Hamiltonian parameters can be obtained by simulating the experimental EPR spectra using a full-matrix diagonalization procedure of the simplified Hamiltonian displayed in Equation (1).

$$H = \mu_B \hat{B} \cdot [g] \cdot \hat{S} + D(\hat{S}_z^2 - 1/3\hat{S}^2) + E(\hat{S}_x^2 - \hat{S}_y^2) \qquad (1)$$

The first term represents the electronic Zeeman interaction. The last two terms define the second-order (bilinear) ZFS interaction with *D* and *E* representing the axial and rhombic parts, respectively. Table 5 summarizes all experimental *D* and *E/D* parameters at room temperature. The simulated EPR spectra nicely reproduce the experimental data even if a poorer quality of the simulations can be noticed in the case of the X-band EPR data (Figure 10,-Figure 13). This may be attributed to the difficulty of precisely calculating the relative intensity of the transitions since they occur between mixed Zeeman levels.

Table 5. Experimental and calculated ZFS parameters (*D* in cm^{-1} and *E/D*) of complexes **C4**-**C10** at room temperature.

Complex	Coordination no.	Coordination sphere	$D_{exptl.}$ [a]	$D_{calcd.}$ [b]	$E/D_{exptl.}$	$E/D_{calcd.}$
[Mn((–)-**L**)$_2$(Cl)$_2$] (**C4**)	6	N$_4$Cl$_2$	–0.146	–0.180 (+0.173)	0.116	0.283
[Mn((–)-**L**)$_2$(CF$_3$SO$_3$)$_2$] (**C5**)	6	N$_4$O$_2$	–0.071	–0.029 (–0.108)	0.070	0.134
[Mn((–)-**L**)$_2$(NO$_3$)(H$_2$O)](NO$_3$) (**C6**)	6	N$_4$O$_2$	–0.074	–0.050 (+0.147)	0.122	0.292
[Mn(bpy)$_2$(CF$_3$CO$_2$)$_2$] (**C7**)	6	N$_4$O$_2$	–0.035	–0.087 (–0.307)	0.154	0.059
[Mn(terpy)(CF$_3$CO$_2$)$_2$(H$_2$O)] (**C8**)	6	N$_3$O$_3$	0.068	–0.041 (+0.405)	0.308	0.328
[Mn(terpy)(NO$_3$)$_2$(H$_2$O)] (**C9**)	7	N$_3$O$_4$	–0.068	–0.090 (–0.077)	0.147	0.150
[Mn(bpea)(NO$_3$)$_2$] (**C10**)	7	N$_3$O$_4$	+0.086	+0.075 (+1.380)	0.093	0.094

[a] When determined, the sign of *D* is reported. [b] The basis used for the calculations is BP86; the results obtained with the B3LYP basis set are given in parentheses.

The sign of D has been unambiguously established from low-temperature Q-band EPR spectra for all complexes, except for **C8**, because of its large E/D value of 0.308.[108] For the whole series of complexes, the D values are within the magnitude range of 0.035–0.146 cm^{-1}. The largest value has been observed for complex **C4**, in which Mn^{II} is coordinated by two chloride anions. Previous studies have shown that the D magnitude is correlated to the nature of the halide in the case of the Mn^{II} ion, since a major contribution arises from the interference between metal- and halide-SOC contributions, proportional to $\zeta_{Mn}\zeta_X$. The D value of 0.146 cm^{-1} of **C4** is in the range found for the other chloro complexes (i.e., $0.110 < |D_{Cl}| < 0.319$ cm^{-1}).[52,62]

For the six-coordinate complexes **C5**–**C8**, with only N- and O-based ligands, the D values are between 0.035 and 0.074 cm^{-1}, which is a very narrow range that falls within the previously reported values for such complexes (0.001–0.175 cm^{-1}).[52] The N/O ratio of the coordination sphere of Mn^{II} seems to have no effect on D. Also, in agreement with previous observations done on six-coordinate Mn^{II} complexes with N_6, O_6 and N_5O coordination spheres, the E/D ratio can neither be rationalized in terms of the nature of the ligands, nor in terms of the N/O ratio.[52]

The seven-coordinate complexes **C9** and **C10** display smaller D values (0.068 and 0.086 cm^{-1}, respectively) than that determined for a previously reported seven-coordinate mononuclear Mn^{II} complex ($D = 0.127$ cm^{-1}).[70] However, all of these D values are in the same range as observed for the six-coordinate N/O complexes, and are also significantly smaller than previously reported values for five-coordinate N/O complexes $(0.2500 < |D_5| < 0.3000)$.[65]

3.3.4.2. DFT calculations

It has been previously shown that the DFT approach used here is suitable for the simulation of parameters on mononuclear Mn^{II} complexes that contain either halide ligands,[59,70] only N/O-based ligands[65,70] or S-based ligands.[109] In this work, DFT calculations have been performed on complexes **C4**–**C10**. The calculations were initiated from the crystal structures as well as from optimized structures in which only the positions of the hydrogen atoms were relaxed. Actually, the EPR parameters have not been calculated on fully optimized structures since they generally lead to a significant deterioration of the theoretical predictions.[67,68,110,111] It has already been demonstrated throughout several studies that D is very sensitive to small structural

modifications.[59,65] Therefore, the quality of the experimental structures is crucial for the success of the calculations. In particular, the position of the hydrogen atoms is not usually defined to high precision for structures resolved by X-ray diffraction experiments. The results obtained with the experimental structures are virtually indistinguishable from those where only the hydrogen atoms were optimized (less than 5 % of difference between the respective calculated D values). Thus, in Table 6, only a unique set of values corresponding to the optimized structures is reported.

Table 6. Spin-spin (D_{SSC}) and spin-orbit coupling (D_{SOC}) contributions to the D values together with the total D [cm^{-1}] obtained from DFT calculations.

Complex	D_{total}	D_{SOC}	$\alpha \rightarrow \alpha$	$\beta \rightarrow \beta$	$\alpha \rightarrow \beta$	$\beta \rightarrow \alpha$	D_{SSC}
C4	-0.180	-0.177	-0.012	-0.048	-0.118	0.000	-0.003
C5	-0.029	+0.002	-0.019	-0.016	+0.028	+0.009	-0.031
C6	-0.050	+0.020	-0.027	-0.030	+0.070	+0.006	-0.070
C7	-0.087	-0.057	+0.001	+0.003	-0.057	-0.004	-0.031
C8	-0.041	-0.039	+0.016	-0.007	-0.052	+0.004	-0.001
C9	-0.090	-0.062	-0.003	-0.012	-0.050	+0.003	-0.028
C10	+0.075	+0.056	-0.001	-0.011	+0.060	+0.008	+0.019

Two physical factors contribute to the bilinear term in the ZFS: the direct dipole–dipole interaction of unpaired electrons (SSC) and the spin–orbit coupling (SOC) of excited states into the ground state.[68,69] Systematic studies performed on Mn^{II} complexes have shown that the best approach to calculate the D_{SOC} part is provided by the coupled perturbed SOC approach,[112] whereas for the D_{SSC} contribution, slightly better predictions are reached with the DFT method based on the restricted open-shell Kohn–Sham (ROKS) reference determinants.[67,113]

With respect to the functional, recent results have shown an improvement in the prediction of the ZFS of mononuclear Mn^{II} dihalide complexes with B3LYP compared to BP86.[68] Thus, the D values have been calculated with both functionals to evaluate their respective performance. The results reported in Table 5 unambiguously show that B3LYP is not adapted to predict the ZFS for Mn^{II} complexes with only N/O-based ligands. This surprising result is an additional proof of the extreme complexity of accurately predicting the ZFS of the Mn^{II} ion since the choice of the functional depends on the nature of the Mn^{II} coordination sphere.

With BP86, the quality of the prediction is satisfactory with discrepancies between the experimental and calculated D values ranging between 13 and 60 %. However, the predicted magnitudes are alternatively under- or overestimated. For the six-coordinate complexes **C4**–**C8**, the best prediction is found for the chloro complex with an overestimation of the calculated magnitude of 19 %. This is in agreement with systematic studies performed for evaluating the performance of DFT to predict D in dihalide mononuclear Mn^{II} complexes.[67,68] With regard to **C5**–**C8**, the trend is not reproduced [i.e., the smallest experimental D magnitude found for **C7** (0.035 cm^{-1}) corresponds to the largest calculated D value (0.087 cm^{-1})].

In contrast to the previously reported seven-coordinate complex, for which the prediction of the D value was rather poor,[70] the calculated D values obtained here for complexes **C9** and **C10** reproduce the experimental D and E/D values well.

The E/D values of the six-coordinate complexes are overestimated except for complex **C7**, whereas for the seven-coordinate complexes they agree well with the experimental data. It has been previously shown that DFT is not reliable for predicting the sign of D for an E/D ratio larger than 0.2.[67] This is partly due to the small magnitudes of both D and E (a few tenths and hundredths of wavenumbers, respectively) that prevent the prediction, with sufficient precision, of the relatively small differences between the axial tensor components. From Table 5, it can be seen that the sign of D is correctly reproduced by DFT within the series when experimentally determined.

Table 6 reports the SSC and SOC contributions to the **D** tensor for complexes **C4**–**C10**. In the six-coordinate series (**C4**–**C8**) the percentage of the SSC interaction is randomly distributed. Indeed, for complex **C8** it represents only 2.5 %, whereas for **C5**, it represents 107 %. However, for complexes **C5**–**C7**, D_{SSC} is far too large to be negligible and determines the sign of D in the cases of **C5** and **C6**. It was previously shown that the four classes of excitation of D_{SOC} present comparable magnitudes with partially cancelling signs in the case of halide complexes. A different behaviour is observed through the series of the six-coordinate N/O-based ligands. The dominant contribution to D_{SOC} arises from the α → β excitation, whereas the β → α one is negligible.

Independently of the sign, the D_{SSC} and D_{SOC} parts are comparable for both seven-coordinate complexes, **C6** and **C7**, with D_{SSC} corresponding to 31 and 25 % of D, respectively. The major SOC contribution also originates from the α → β excitation.

3.4. Experimental section

3.4.1. Materials

All reagents used in the present work were obtained from Aldrich Chemical Co and were used without further purification. Reagent grade organic solvents were obtained from SDS and Scharlab and high purity de-ionized water was obtained by passing distilled water through a nano-pure Mili-Q water purification system.

3.4.2. Preparations

The (–)-pinene[5,6]bipyridine ligand, (–)-**L**,[31] and the complex $Mn(CF_3SO_3)_2$,[114] were prepared according to literature procedures. All synthetic manipulations were routinely performed under ambient conditions.

[{MnCl((–)-L)}$_2$(μ-Cl)$_2$], C1. To an aqueous solution of $MnCl_2$ (0.110 g, 0.874 mmol) (4 mL) an ethanolic solution of (–)-**L** (0.183 g, 0.746 mmol) (4 mL) was added under stirring. The resulting pale yellow solution was stirred for 2 h, then filtered and left to evaporate at room temperature. After one week, air-stable, colourless crystals of **1**, suitable for X-ray diffraction analysis, were obtained. Further amount of compound was obtained by addition of diethyl ether to the mother liquor. The solid (0.090 g, 32%) was filtered off, washed with diethyl ether and dried in air. Anal. found (Calcd.) for **C1·H$_2$O**: C, 53.20 (52.95); H, 5.20 (4.93); N, 7.15 (7.26). IR ν_{max}/cm^{-1} 2927 (ν (C-H)sp^3), 1603 (ν (C-N)sp^2), 1435 (ν (C-C)sp^2). $E_{1/2}$/V 0.90 *vs.* SSCE (CH$_3$CN + 0.1M [(nBu)$_4$N]PF$_6$). *m/z* (ESI-MS) 717 [Mn$_2$Cl$_3$(L)$_2$]$^+$.

[{Mn((–)-L)}$_2$(μ-OAc)$_3$](PF$_6$), C2. Solid (–)-**L** (0.060 g, 0.240 mmol) was added under stirring to a solution of Mn(OAc)$_2$·4H$_2$O (0.058 g, 0.240 mmol) (2 mL) in ethanol. The resulting pale yellow solution was stirred for 1 h, then filtered and reduced to 2 mL. Afterwards NH$_4$PF$_6$ was added and the product (0.088 g, 76%) was precipitated from the resulting solution by addition of diethyl ether. By recrystallization of the product in CH$_2$Cl$_2$, colourless plates of **2** suitable for X-ray diffraction were obtained. Anal. found (Calcd.) for **C2·0.5(C$_4$H$_{10}$O)**: C, 52.20 (52.01); H, 5.70 (5.20); N, 5.78 (5.77). IR ν_{max}/cm^{-1} 2969 (ν (C-H)sp^3), 1578 (ν (COO$^-$)as), 1428 (ν (COO)s), 833 (δ (COO). E_{pa}/V 1.3 *vs.* SSCE (CH$_3$CN + 0.1M [(nBu)$_4$N]PF$_6$).

[MnCl$_2$(H$_2$O)((–)-L)], C3. To a solution of $MnCl_2$ (0.110 g, 0.874 mmol) (4 mL) in ethanol, 0.218 g of (–)-**L** (0.874 mmol) were added under stirring. The resulting pale

yellow solution was stirred for 2 h and then filtered. After addition of diethyl ether a white product (0.23 g, 65%) was obtained that was filtered, washed with diethyl ether and dried in air. Colourless plates, suitable for X-ray diffraction were grown by recrystallization in ethanol. Anal. found (Calcd.) for **C3·0.5H₂O**: C, 48.59 (48.45); H, 4.60 (4.90); N, 6.73 (6.60). IR ν_{max}/cm^{-1} 3269 (ν (OH), 2926 (ν (C-H)sp^3), 1603 (ν (C-N)sp^2), 1436 (ν (C-C)sp^2). E_{pa}/V 1.25 *vs.* SSCE (CH$_3$CN + 0.1M [(nBu)$_4$N]PF$_6$).

[MnCl₂((–)-L)₂], C4. A solution of (–)-**L** (0.092 g, 0.365 mmol) and MnCl$_2$ (0.023 g, 0.183 mmol) in acetonitrile (4 mL) was stirred for 30 min at room temperature. A pale yellow precipitate (0.12 g, 86%) was obtained that was collected by filtration, washed thoroughly with diethyl ether and dried in air. By recrystallization in ethanol, colourless needles, suitable for X-ray diffraction, were obtained. Anal. found (Calcd.) for **C4·2.2H₂O**: C, 61.17 (61.30); H, 6.00 (6.11); N, 8.46 (8.41). IR ν_{max}/cm^{-1} 2890-2990 (ν (C-H)sp^3), 1600 (ν (C-N)sp^2), 1437 (ν (C-C)sp^2). $E_{1/2}$/V 0.83 *vs.* SSCE (CH$_3$CN + 0.1M [(nBu)$_4$N]PF$_6$). *m/z* (ESI-MS) 590.1 [MnCl(L)$_2$]$^+$.

[Mn(CF₃SO₃)₂((–)-L)₂], C5. A solution of (–)-**L** (0.110 g, 0.430 mmol) and Mn(CF$_3$SO$_3$)$_2$ (0.075 g, 0.215 mmol) in THF (2 mL) was stirred for one hour, at room temperature. A pale yellow precipitate (0.11 g, 63%) was obtained, that was collected by filtration, washed thoroughly with diethyl ether and dried in air. By recrystallization in CH$_2$Cl$_2$ colourless plates, suitable for X-ray diffraction were obtained. Anal. found (Calcd.) for **C5·H₂O**: C, 49.40 (49.59); H, 4.30 (4.13); N, 6.21 (6.41). IR ν_{max}/cm^{-1} 2900 (ν (C-H)sp^3), 1435 (ν (C-C)sp^2), 1200 (ν (S-O)sp^2). E_{pa}/V 1.3 and 1.75 *vs.* SSCE (CH$_3$CN + 0.1M [(nBu)$_4$N]PF$_6$). *m/z* (ESI-MS) 704.1 [Mn(CF$_3$SO$_3$)(L)$_2$]$^+$.

[Mn(NO₃)(H₂O)((–)-L)₂)](NO₃), C6. To an aqueous solution of Mn(NO$_3$)$_2$·4H$_2$O (0.23 g, 0.903 mmol) (2 mL) was added an ethanol solution of (–)-**L** (0.45 g, 1.81 mmol) under stirring. After one hour, a pale yellow precipitate (0.52 g, 42 %) was obtained that was collected by filtration, washed thoroughly with diethyl ether and dried in air. Suitable crystals as colourless blocks were grown by diffusion of ethyl ether into an acetone solution of the compound. Anal. Found (Calcd.) for **C6·0.5H₂O**: C, 57.52 (57.79); H, 5.62 (5.52); N, 11.81 (11.80). IR ν_{max}/cm^{-1} 2800-3000 (ν (C-H)sp^3), 1560-1600 (ν (NO$_2$)), 1437(ν (C-C)sp^2), 1322 (ν (C-N)sp^2). E_{pa}/V 1.0 *vs.* SSCE (CH$_3$CN + 0.1M [(nBu)$_4$N]PF$_6$). *m/z* (ESI-MS) 617 [Mn(NO$_3$)$_2$(L)$_2$]$^+$, 408 [Mn(NO$_3$)(L)$_2$]$^+$.

3.4.3. X-Ray structure determination

Measurement of the crystals were performed on a Bruker Smart Apex CCD diffractometer using graphite-monochromated Mo Kα radiation (λ = 0.71073Å) from an X-Ray tube. Data collection, Smart V. 5.631 (BrukerAXS 1997-02); data reduction, Saint+ Version 6.36A (Bruker AXS 2001); absorption correction, SADABS version 2.10 (Bruker AXS 2001) and structure solution and refinement, SHELXTL Version 6.14 (Bruker AXS 2000-2003). **Complex 2**: The displacement parameters for carbon atoms of the CH_2Cl_2 disordered solvent molecules were restrained to approximate to isotropic behaviour. **Complex 4**: The crystal was of poor quality, and so was the data. A high R_{int} Index was obtained, but no better crystals could be generated. The space group was checked with the PLATON[115] tool ADDSYM which didn't suggest any other symmetry. The New Symmetry tool of the same program suggested trying space groups Pmc21, P2cm and Pmcm. The data was processed in all those three space groups, but no better R_{int} index was obtained, and the crystal couldn't be satisfactory resolved in any of the three space groups. A considerable amount of electron density attributable to partially disordered solvent molecules was removed with the SQUEEZE option of PLATON.[115] This electron density couldn't be related to any chemical species. Displacement Parameters for atoms c2, c3, c4, c7, c9, c10, c21, c22, c23, c26, c16, c19, c27 and c36 were restrained to approximate to isotropic behaviour. C(sp3)-C(sp3) bond distance were restrained to 1.54(1)A for the bonds c15-c16, c15-c20, c15-c21, c16-c17, c16-c18, c31-c34. C(sp3)-C(sp2) bond distance was restrained to 1.51(1)A for the bonds c10-c11, c18-c19, c30-c31, c35-c36. **Complex 6**: The crystal was very weakly diffracting, and few reflections were collected although a large acquisition time was used. That made the Ratio Observed / Unique Reflections being too Low. The R_{int} is very large and the L.S. GooF smaller than 0.8. Close examination of the data was made to avoid mistakes in space group selection. The space group P212121 used to resolve the structure was checked with the ADDSYM and NEWSYM tools of PLATON[115] to be the correct one. This software didn't suggest any other possible space groups. The crystallographic data as well as details of the structure solution and refinement procedures are reported in Table S 1. Crystallographic data in CIF format can be found in the electronic supporting information or in CCDC: 720648 (**C1**), 720646 (**C2**), 720650 (**C3**), 720645 (**C4**), 720649 (**C5**), 720647 (**C6**).

3.4.4. Magnetic susceptibility study

Magnetic susceptibility measurements between 300-2 K were carried out in a SQUID magnetometer Quantum Design Magnetometer, model MPMP at the "Unitat de Mesures Magnètiques" (Universitat de Barcelona). Two different magnetic fields were used for the susceptibility measurements, 200 G (2-30 K) and 3000 G (2-300 K), with superimposable graphs. Pascal's constants were used to estimate the diamagnetic corrections for the compound. The fit was performed by minimizing the function $R = \Sigma[(\chi_M T)_{exp} - (\chi_M T)_{calc}]^2/\Sigma[(\chi_M T)_{exp}]^2$.

3.4.5. Theoretical calculations

All calculations were performed with the ORCA program package.[116] The ZFS parameters were calculated on X-ray structures as well as from optimized structures in which only the positions of the hydrogen atoms were relaxed. For a discussion of this point, see the literature.[67,68,110,111] The ZFS calculations based on DFT were performed with the hybrid B3LYP[117] and the nonhybrid BP86[118,119] functionals by using the TZVP basis set[120] and taking advantage of the RI approximation with the auxiliary TZV/J Coulomb fitting basis sets.[121] Four types of excitations were considered to calculate the D_{SOC} part.[69] Qualitatively, they take the form of (1) excitation of a spin-down (β) electron from a doubly occupied MO (DOMO) to a singly occupied MO (SOMO) that leads to states of the same spin S as the ground state ($\beta \rightarrow \beta$); (2) excitation of a spin-up (α) electron from a SOMO to a virtual MO (VMO), which also gives rise to states of total spin S ($\alpha \rightarrow \alpha$); (3) excitations between two SOMOs that are accompanied by a spin-flip and that give rise to states of $S' = S - 1$ ($\alpha \rightarrow \beta$); and (4) "shell-opening" transitions from a DOMO to a VMO that lead to states of $S' = S + 1$ ($\beta \rightarrow \alpha$).

3.4.6. Instrumentation and measurements

FT-IR spectra were taken in a Mattson-Galaxy Satellite FT-IR spectrophotometer containing a MKII Golden Gate Single Reflection ATR System. UV-vis spectroscopy was performed on a Cary 50 Scan (Varian) UV-vis spectrophotometer with 1 cm quartz cells. Cyclic voltammetric (CV) experiments were performed in an IJ-Cambria IH-660 potentiostat using a three electrode cell. Pt electrodes from BAS were used as working electrode, platinum wire as auxiliary and SSCE as the reference electrode. All cyclic

voltammograms presented in this work were recorded under nitrogen atmosphere. The $E_{1/2}$ values were estimated from cyclic voltammetry as the average of the oxidative and reductive peak potentials $(E_{pa}+ E_{pc})/2$ at a scan rate of 100 mV/s. Unless explicitly mentioned the concentration of the complexes were approximately 1 mM. Elemental analyses were performed using a CHNS-O Elemental Analyser EA-1108 from Fisons. ESI-MS experiments were performed on a Navigator LC/MS chromatograph from Thermo Quest Finigan, using acetonitrile as a mobile phase. Powder X-band EPR spectra were recorded with a Bruker EMX, equipped with an ER-4192 ST Bruker cavity and an ER-4131 VT for the 100 K experiments. Powder Q-band EPR spectra were recorded with an ER-5106 QTW Bruker cavity and an Oxford Instruments ESR-900 continuous-flow helium cryostat for the Q-band for the 4.5 K experiments.

3.5. Conclusions

A family of new Mn chiral complexes has been prepared and thoroughly characterized, among which there is a novel dinuclear $Mn_2(\mu\text{-}Cl)_2$ complex, **C1**, having pentacoordinated metal centers. Magnetic measurements have been performed for dinuclear complexes **C1** and **C2**, in both cases showing weak antiferromagnetic interactions.

Mononuclear complexes **C4**-**C6**, bearing two pinene-bipyridine ligands, display hexacoordination and are obtained as a sole isomer, *trans*,*trans*, which seems to be energetically favoured thanks to H-bonding interactions involving pyridyl groups and monodentate ligands.

The chlorocomplexes **C1** and **C4** exhibit reversible electrochemical redox processes whereas for **C2**, **C3**, **C5** and **C6** the cyclic voltammograms show irreversible processes. Through UV-vis and EPR experiments it has also been observed that, after bulk electrolysis, **C1** and **C4** lead to a similar mononuclear Mn^{III} species, with an identical UV-vis spectrum. This implies the breaking of the dinuclear complex **C1**.

The ZFS of a series of mononuclear Mn^{II} complexes, including six- and seven-coordinate compounds with N/O-based ligands (**C5**-**C10**), has been investigated by EPR spectroscopy as well as quantum chemistry. The experimental D values all fall within a small magnitude range of 0.035–0.086 cm^{-1}, which prevents the establishment of magnetostructural correlations with the coordination number of the Mn^{II} ion (6 *vs.* 7) or with the N/O ratio of their coordination sphere.

According to the results of this chapter, and together with previous investigations, we have confirmed that a good DFT prediction of the ZFS parameters requires precise calculations of the D_{SOC} and D_{SSC} contributions. More interestingly, this DFT study has also revealed that the choice of the functional is crucial to accurately predict the ZFS: B3LYP is the best functional in the case of halide complexes, whereas BP86 produces better results for complexes with only N/O-based ligands. This last result illustrates well the complexity of predicting the ZFS and the importance of such systematic studies.

3.6. References

[1] Noyori, R. Ed. *Asymmetric Catalysis in Organic Synthesis*, Wiley: New York, **1994**.

[2] Jacobsen, E. N.; Pfaltz, A.; Yamamoto, H. Eds. *Comprehensive Asymmetric Catalyses*, Springer: Berlin, **1999**.

[3] Ojima, I. Ed. *Catalytic Asymmetric Synthesis*, 2nd ed., John Wiley & Sons: New York, **2000**.

[4] Freixa, Z.; van Leeuwen, P.W.N.M. *Coord. Chem. Rev.* **2008**, *252*, 1755-1786.

[5] Noyori, R.; Takaya, H. *Acc. Chem. Res.* **1990**, *23*, 345-350.

[6] Burk, M.J. *Acc. Chem. Res* **2000**, *33*, 363-372.

[7] Pfaltz, A. *Acc. Chem Res.* **1993**, *26*, 339-345.

[8] Ghosh, A.K.; Mathivanan, P.; Cappiello, J. *Tetrahedron: Asymmetry* **1998**, *9*, 1-45.

[9] Johnson, J.S.; Evans, D.A. *Acc. Chem. Res.* **2000**, *33*, 325-335.

[10] Desimoni, G.; Faita, G.; Jorgensen, K.A. *Chem. Rev.* **2006**, *106*, 3561-3651.

[11] Palucki, M.; Finney, M.S.; Pospisil, P.J.; Güler, M.L.; Ishida, T.; Jacobsen, E.N. *J. Am. Chem. Soc.* **1998**, *120*, 948-954.

[12] Katsuky T *Adv. Synth. Catal.* **2002**, *344*, 131-147.

[13] Cozzi, P.G. *Chem. Soc. Rev.* **2004**, *33*, 410-421.

[14] Knof, U.; von Zelewsky, A. *Angew. Chem. Int. Ed.* **1999**, *38*, 302-322.

[15] Kizirian, J.-C. *Chem. Rev.* **2008**, *108*, 140-205.

[16] Fache, F.; Schulz, E.; Tommasino, L.; Lemaire, M. *Chem. Rev.* **2000**, *100*, 2159-2231.

[17] Hechavarría Fonseca, M.; König, B. *Adv. Synth. Catal.* **2003**, *345*, 1173-1185.

[18] Caputo, C.A.; Jones, N.D. *Dalton Trans.* **2007**, 4627-4640.

[19] Gómez, M.; Muller, G.; Rocamora, M. *Coord. Chem. Rev.* **1999**, *193*, 769-835.

[20] Hargaden, G.C.; Guiry, P.J. *Chem. Rev.* **2009**, *109*, 2505-2550.

[21] Chelucci, G.; Thummel, R.P. *Chem. Rev.* **2002**, *102*, 3129-3170.

[22] Hayoz, P.; von Zelewsky, A. *Tetrahedron Lett.* **1992**, *33*, 5165-5168.

[23] Hayoz, P.; von Zelewsky, A.; Stoeckli-Evans, H. *J. Am. Chem. Soc.* **1993**, *115*, 5111-5114.

[24] Chen, C.; Tagami, K.; Kishi, Y. *J. Org. Chem.* **1995**, *60*, 5386-5387

[25] Collomb, P.; von Zelewsky, A. *Tetrahedron: Asymmetry* **1995**, *6*, 2903-2904.

[26] Fletcher, N.C.; Keene, F.R.; Ziegler, M.; Stoeckli-Evans, H.; Viebrock, H.; von Zelewsky, A. *Helv. Chim. Acta* **1996**, *79*, 1192-1202.

[27] Mamula, O.; von Zelewsky, A.; Bark, T.; Bernardinelli, G. *Angew. Chem. Int. Ed.* **1999**, *38*, 2945-2948.

[28] Lötscher, D.; Rupprecht, S.; Stoeckli-Evans, H.; von Zelewsky, A. *Tetrahedron: Asymmetry* **2000**, *11*, 4341-4357.

[29] Kolp, B.; Abeln, D.; Stoeckli-Evans, H.; von Zelewsky, A. *Eur. J. Inorg. Chem.* **2001**, 1207-1220.

[30] Lötscher, D.; Rupprecht, S.; Collomb, P.; Belser, P.; Viebrock, H.; von Zelewsky, A.; Burger, P. *Inorg. Chem.* **2001**, *40*, 5675-5681.

[31] Malkov, A.V.; Baxendale, I.R.; Bella, M.; Langer, V.; Fawcett, J.; Russell, D.R.; Mansfield, D.J.; Valko, M.; Kocovský, P. *Organometallics* **2001**, *20*, 673-690.

[32] Malkov, A.V.; Pernazza, D.; Bell, M.; Bella, M.; Massa, A.; Teplý, F.; Meghani, P.; Kocovský, P. *J. Org. Chem.* **2003**, *68*, 4727-4742.

[33] Sauers, A.L.; Ho, D.M.; Bernhard, S. *J. Org. Chem.* **2004**, *69*, 8910-8915.

[34] Sala, X.; Rodríguez, A.M.; Rodríguez, M.; Romero, I.; Parella, T.; von Zelewsky, A.; Llobet, A.; Benet-Buchholz, J. *J. Org. Chem.* **2006**, *71*, 9283-9290.

[35] Piguet, C.; Bernardinelli, G.; Hopfgartner, G. *Chem. Rev.* **1997**, *97*, 2005-2062.

[36] Chelucci, G.; Caria, V.; Saba, A. *J. Mol. Catal.* **1998**, *130*, 51-55.

[37] Chelucci, G.; Pinna, G.A.; Saba, A. *Tetrahedron: Asymmetry* **1998**, *9*, 531-534.

[38] Ziegler, M.; von Zelewsky, A. *Coord. Chem. Rev.* **1998**, *177*, 257-300.

[39] Mamula, O.; von Zelewsky, A. *Coord. Chem. Rev.* **2003**, *242*, 87-95.

[40] Sala, X.; Poater, A.; von Zelewsky, A.; Parella, T.; Fontrodona, X.; Romero, I.; Solà, M.; Rodríguez, M.; Llobet, A. *Inorg. Chem.* **2008**, *47*, 8016-8024.

[41] Marchi-Delapierre, C.; Jorge-Robin, A.; Thibon, A.; Ménage, S. *Chem. Commun.* **2007**, 1166-1168.

[42] Gómez, L.; Garcia-Bosch, I.; Company, A.; Sala, X.; Fontrodona, X.; Ribas, X.; Costas, M. *Dalton Trans.* **2007**, 5539-5545.

[43] Sham, K.-C.; Yeung, H.-L.; Yiu, S.-M.; Lau, T.-C.; Kwong, H.-L. *Dalton Trans.* **2010**, *39*, 9469-9471.

[44] Gómez, L.; Garcia-Bosch, I.; Company, A.; Benet-Buchholz, J.; Polo, A.; Sala, X.; Ribas, X.; Costas, M. *Angew. Chem. Int. Ed.* **2009**, *48*, 5720-5723.

[45] Hobuß, D.; Hasenjäger, J.; Driessen-Hölscher, B.; Baro, A.; Axenov, K.V.; Laschat, S.; Frey, W. *Inorg. Chim. Acta* **2011**, *374*, 94-103.

[46] Boca, R. *Coord. Chem. Rev.* **2004**, *248*, 757-815.

[47] Neese, F. *Calculation of NMR and EPR Parameters,* Eds. Kaupp, M.B.M.; Malkin V.G.; Wiley-VCH, Heidelberg, **2004**.

[48] Neese, F.; Solomon, E.I. *In Magnetoscience – From Molecules to Materials*, vol. IV, Eds. Miller, J.S.; Drillon M.; Wiley-VCH, Weinheim, **2003**, p. 345.

[49] Krzysteck, J.; Ozarowski, A.; Telser, J. *Coord. Chem. Rev.* **2006**, *250*, 2308-2324.

[50] Gatteschi, D.; Sessoli, R. *Angew. Chem. Int. Ed.* **2003**, *42*, 268-297.

[51] Gatteschi, D.; Sessoli, R.; Villain, J. *Molecular Nanomagnets*, Oxford University Press, New York, **2006**.

[52] Duboc, C.; Collomb, M.-N.; Nesse, F. *Appl. Magn. Reson.* **2010**, *37*, 229-245.

[53] Birdy, R.B.; Goodgame, M. *Inorg. Chim. Acta* **1981**, 50, 183-187.

[54] Jacobsen, C.J.H.; Pedersen, E.; Villadsen, J.; Weihe, H. *Inorg. Chem.* **1993**, *32*, 1216-1221.

[55] Lynch, W.B.; Boorse, R.S.; Freed, J.H. *J. Am. Chem. Soc.* **1993**, *115*, 10909-10915.

[56] Wood, R.M.; Stucker, D.M.; Jones, L.M.; Lynch, W.B.; Misra, S.K.; Freed, J.H. *Inorg. Chem.* **1999**, *38*, 5384-5388.

[57] Goodgame, D.M.L.; El Mkami, H.; Smith, G.M.; Zhao, J.P.; McInnes, E.J.L. *Dalton Trans.* **2003**, 34-35.

[58] Mantel, C.; Baffert, C.; Romero, I.; Deronzier, A.; Pécaut, J.; Collomb, M.-N.; Duboc, C. *Inorg. Chem.* **2004**, *43*, 6455-6463.

[59] Duboc, C.; Phoeung, T.; Zein, S.; Pécaut, J.; Collomb, M.-N.; Neese, F. *Inorg. Chem.* **2007**, *46*, 4905-4916.

[60] Duboc, C., Phoeung, T.; Jouvenot, D.; Blackman, A.G.; McClintock, L.F.; Pécaut, J.; Deronzier, A.; Collomb, M.-N. *Polyhedron* **2007**, *26*, 5243-5249.

[61] Duboc, C.; Astier-Perret, V.; Chen, H.Y.; Pécaut, J.; Crabtree, R.H.; Brudvig, G.W.; Collomb, M.-N. *Inorg. Chim. Acta* **2006**, *359*, 1541-1548.

[62] Berggren, G.; Huang, P.; Eriksson, L.; Anderlund, M.F. *Appl. Magn. Reson.* **2009**, *36*, 9-24.

[63] The magnitude of D is between 0.9 and 1.2 cm^{-1} for the iodido complexes, 0.5 and 0.7 cm^{-1} for the bromido, and 0.16 and 0.30 cm^{-1} for the chlorido derivatives, except for the *cis*-dihalide six-coordinate systems, which are characterized by significantly smaller D values ($|D_I|$ = 0.6 cm^{-1}, $|D_{Br}|$ = 0.35 cm^{-1}, $|D_{Cl}|$ = 0.12 cm^{-1}.

[64] Mantel, C.; Philouze, C.; Collomb, M.-N.; Duboc, C. *Eur. J. Inorg. Chem.* **2004**, 3880-3886.

[65] Duboc, C.; Collomb, M.-N.; Pécaut, J.; Deronzier, A.; Neese, F. *Chem. Eur. J.* **2008**, *14*, 6498-6509.

[66] $0.2500 < |D_5| < 0.3000$, $0.0008 < |D_6| < 0.1750$ cm^{-1}

[67] Zein, S.; Duboc, C.; Lubitz, W.; Neese, F. *Inorg. Chem.* **2008**, *47*, 134-142.

[68] Zein, S.; Neese, F. *J. Phys. Chem. A* **2008**, *112*, 7976-7983.

[69] Neese, F. *J. Am. Chem. Soc.* **2006**, *128*, 10213-10222.

[70] Hureau, C.; Groni, S.; Guillot, R.; Blondin, G.; Duboc, C.; Anxolabéhère-Mallart, E. *Inorg. Chem.* **2008**, *47*, 9238-9247.

[71] Miller, A.F. *Curr. Opin. Chem. Biol.* **2004**, *8*, 162-168.

[72] Jackson, T.A.; Brunold, T.C. *Acc. Chem. Res.* **2004**, 37, 461-470.

[73] Barynin, V.V.; Whittaker, M.M.; Antonyuk, S.V.; Lamzkin, V.S.; Harrison, P.M.; Artymiuk, P.J.; Whittaker, J.W. *Structure* **2001**, *9*, 725–738.

[74] Ferreira, K.N.; Iverson, T.M.; Maghlaoui, K.; Barber, J.; Iwata, S. *Science* **2004**, *303*, 1831-1838

[75] Loll, B.; Kern, J.; Saenger, W.; Zouni, A.; Biesiadka, J. *Nature* **2005**, *438*, 1040-1044.

[76] Rardin, R.L.; Tolman, W.B.; Lippard, S.J. *New J. Chem.* **1991**, *15*, 417-430.

[77] McCann, S.; McCann, M.; Casey, R.M.T.; Jackman, M.; Devereux, M.; McKee, V. *Inorg. Chim. Acta* **1998**, *279*, 24-29.

[78] Smith, J.A.; Galán-Mascarós, J.R.; Clérac, R.; Sun, J.-S.; Ouyang, X.; Dunbar, K.R. *Polyhedron* **2001**, *20*, 1727-1734.

[79] Chen, C.; Zhu, H.; Huang, D.; Wen, T.; Liu, Q.; Liao, D.; Cui, J. *Inorg. Chim. Acta* **2001**, *320*, 159-166.

[80] Fernandez, G.; Corbella, M.; Alfonso, M.; Stoeckli-Evans, H.; Castro, I. *Inorg. Chem.* **2004**, *43*, 6684-6698.

[81] Romero, I.; Collomb, M.-N.; Deronzier, A.; Llobet, A.; Perret, E.; Pécaut, J.; Le Pape, L.; Latour, J.-M. *Eur. J. Inorg. Chem.* **2001**, 69-72.

[82] Armentano, D.; de Munno, G.; Guerra, F.; Faus, J.; Lloret, F.; Julve, M. *Dalton Trans.* **2003**, 4626-4634.

[83] Van Albada, G. A.; Mohamadou, A.; Driessen, W.L.; De Gelder, R.; Tanase, S.; Reedijk, J. *Polyhedron* **2004**, *23*, 2387-2391.

[84] Wu, J.-Z.; Bouwman, E.; Mills, A.M.; Spek, A.L.; Reedijk, J. *Inorg. Chim. Acta* **2004**, *357*, 2694-2702.

[85] Romero, I.; Rodríguez, M.; Llobet, A.; Corbella, M.; Fernández, G.; Collomb, M-N. *Inorg. Chim. Acta* **2005**, *358*, 4459-4465.

[86] Addison, A.W.; Rao, T.N.; Reedijk, J.; Rijn, J.V.; Verschoor, G.C. *J. Chem. Soc., Dalton Trans.* **1984**, 1349-1356.

[87] Wieghardt, K.; Bossek, U.; Nuber, B.; Weiss, J.; Bonvoisin, J.; Corbella, M.; Vitols, S.E.; Girerd, J.-J. *J. Am. Chem. Soc.* **1988**, *110*, 7398-7411.

[88] Matsushima, H.; Ishiwa, E.; Koikawa, M.; Nakashima, M.; Tokii, T. *Chem. Lett.* **1995**, 129-130.

[89] Romero, I.; Dubois, L.; Collomb, M.-N.; Deronzier, A.; Latour, J.-M.; Pécaut, J. *Inorg. Chem* **2002**, *41*, 1795-1806.

[90] Singh, U.P.; Singh, R.; Hikichi, S.; Akita, M.; Moro-oka, Y. *Inorg. Chim. Acta* **2000**, *310*, 273-278.

[91] Osawa, M.; Singh, U.P.; Tanaka, M.; Moro-oka, Y.; Kitajima, N. *J. Chem. Soc., Chem. Commun.* **1993**, 310-311..

[92] Yamami, M.; Tanaka, M.; Sakiyama, H.; Koga, T.; Kobayashi, K.; Miyasaka, H.; Ohba, M.; Okawa, H. *J. Chem. Soc., Dalton Trans.* **1997**, 4595-4601.

[93] Singh, U.P.; Sharma, A.K.; Tyagi, P.; Upreti, S.; Singh, R.K. *Polyhedron* **2006**, *25,* 3628-3638.

[94] Baffert, C.; Romero, I.; Pécaut, J.; Llobet, A.; Deronzier, A.; Collomb, M-N. *Inorg. Chim. Acta* **2004**, *357*, 3430-3436.

[95] Sala, X.; Poater, A.; von Zelewsky, A.; Parella, T.; Fontrodona, X.; Romero, I.; Solà, M.; Rodríguez, M.; Llobet, A. *Inorg. Chem.* **2008**, *47*, 8016-8024.

[96] Rodríguez, M.; Romero, I.; Llobet, A.; Deronzier, A.; Biner, M.; Parella, T.; Stoeckli-Evans, H. *Inorg. Chem.* **2001**, *40*, 4150-4156.

[97] Hureau, C.; Blondin, G.; Charlot, M.-F.; Philouze, C.; Nierlich, M.; Césario, M.; Anxolabéhère-Mallart, E. *Inorg. Chem.* **2005**, *44*, 3669-3683.

[98] Triller, M.U.; Pursche, D.; Hsieh, W.-Y.; Pecoraro, V.L.; Rompel, A.; Krebs, B. *Inorg. Chem.* **2003**, *42*, 6274-6283.

[99] Pascaly, M.; Duda, M.; Rompel, A.; Sift, B.H.; Meyer-Klaucke, W.; Krebs, B. *Inorg. Chim. Acta* **1999**, *291*, 289-299.

[100] Mantel, C.; Chen, H.Y.; Crabtree, R.H.; Brudvig, G.W.; Pecaut, J.; Collomb, M.-N.; Duboc, C. *Chemphyschem* **2005**, *6*, 541-546.

[101] Dingle, R. *Acta Chem. Scand.* **1966**, *20*, 33-44.

[102] Davis, T.S.; Fackler, J.P.; Weeks, M.J. *Inorg Chem.* **1968**, *7*, 1994-2002.

[103] Rich, J.; Castillo, C.E.; Romero, I.; Rodríguez, M.; Duboc, C.; Collomb, M.-N. *Eur. J. Inorg. Chem.* **2010**, 3658-3665.

[104] Andruh, M.; Hubner, K.; Noltemeyer, M.; Roesky, H.W. *Z. Naturforsch., Teil B* **1993**, *48*, 591-597.

[105] Smoukov, S.K.; Telser, J.; Bernat, B.A.; Rife, C.L.; Armstrong, R.N.; Hoffman, B.M. *J. Am. Chem. Soc.* **2002**, *124*, 2318-2326.

[106] Pilbrow, J.R. *Transition Ion Paramagnetic Resonance*, Clarendon Press, Oxford, **1990**.

[107] Mabbs, F.E.; Collison, D. *Electron Paramagnetic Resonance of d Transition Metal Compounds*, Elsevier, Amsterdam, **1992**, Ch 12.

[108] Abragam, A.; Bleaney, B. *Electron Paramagnetic Resonance of Transition Ions*, Oxford University Press, New York, **1970**.

[109] Tzima, T.D.; Sioros, G.; Duboc, C.; Kovala-Demertzi, D.; Melissas, V.S.; Sanakis, Y. *Polyhedron* **2009**, *28*, 3257-3264.

[110] Scheifele, Q.; Riplinger, C.; Neese, F.; Weihe, H.; Barra, A.L.; Juranyi, F.; Podlesnyak, A.; Tregenna-Piggott, P.L.W. *Inorg. Chem.* **2008**, *47*, 439-447.

[111] Bühl, M.; Reimann, C.; Pantazis, D.A.; Bredow, T.; Neese, F. *J. Chem. Theory Comput.* **2008**, *4*, 1449-1459.

[112] Neese, F. *J. Chem. Phys.* **2007**, *127*, 164112.

[113] Sinnecker, S.; Neese, F. *J. Phys. Chem. A* **2006**, *110*, 12267-12275.

[114] Inada, Y.; Nakano, Y.; Inamo, M.; Funashashi, S. *Inorg. Chem.* **2000**, *39*, 4793-4801.

[115] Spek, A.L (**2008**) *PLATON, A Multipurpose Crystallographic Tool,* Utrecht University, Utrecht, The Netherlands.

[116] F. Neese, University of Bonn, Bonn, Germany, **2007**.

[117] Becke, A.D. *J. Chem. Phys.* **1993**, *98*, 1372-1377.

[118] Becke, A.D. *Phys. Rev. A* **1988**, *38*, 3098-3100.

[119] Perdew, J.P. *Phys. Rev. B* **1986**, *33*, 8822-8824.

[120] Schäfer, A.; Huber, C.; Ahlrichs, R. *J. Chem. Phys.* **1994**, *100*, 5829-5835.

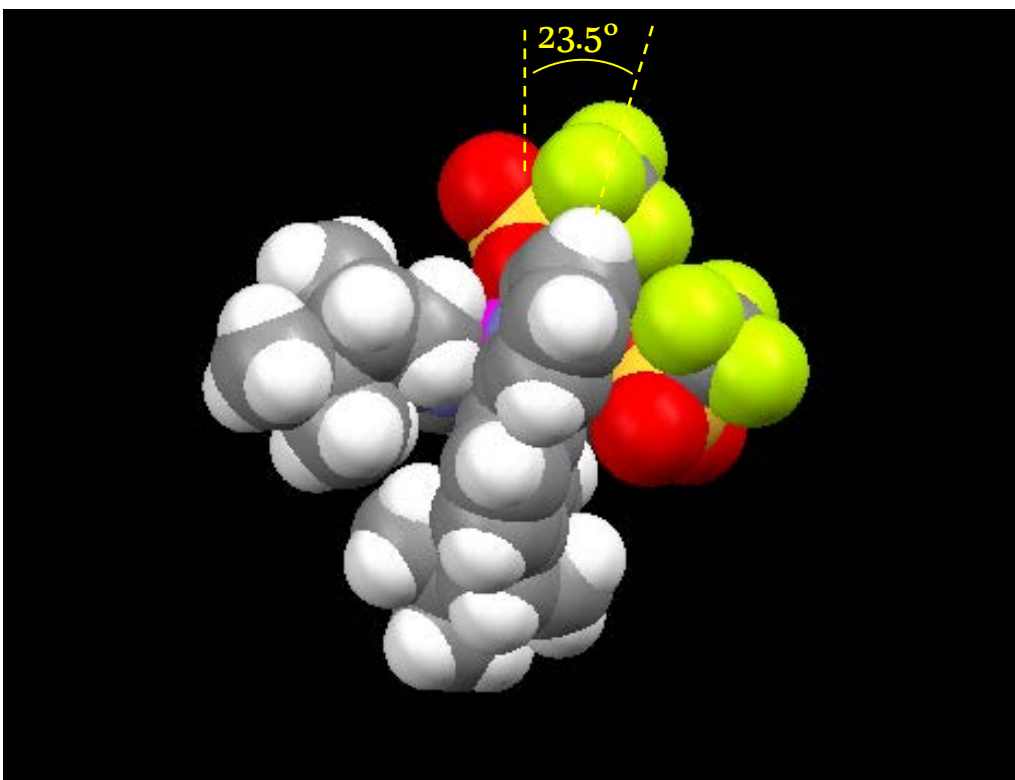[121] Weigend, F. *PhysChemChemPhys* **2006**, *8*, 1057-1065.

3.7. Supporting information
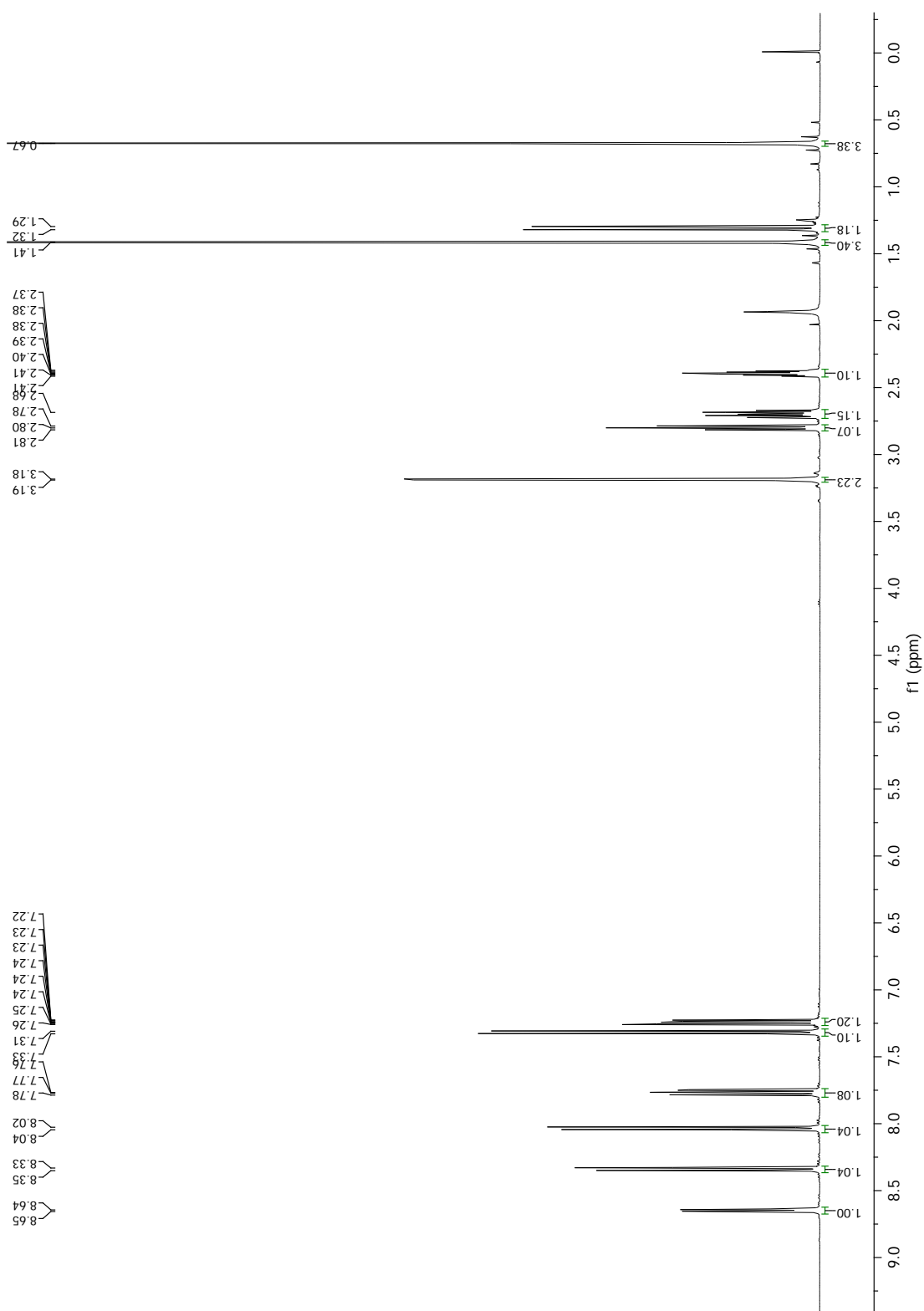
Figure S 1. ^{1}H-NMR of ligand (–)-**L**.
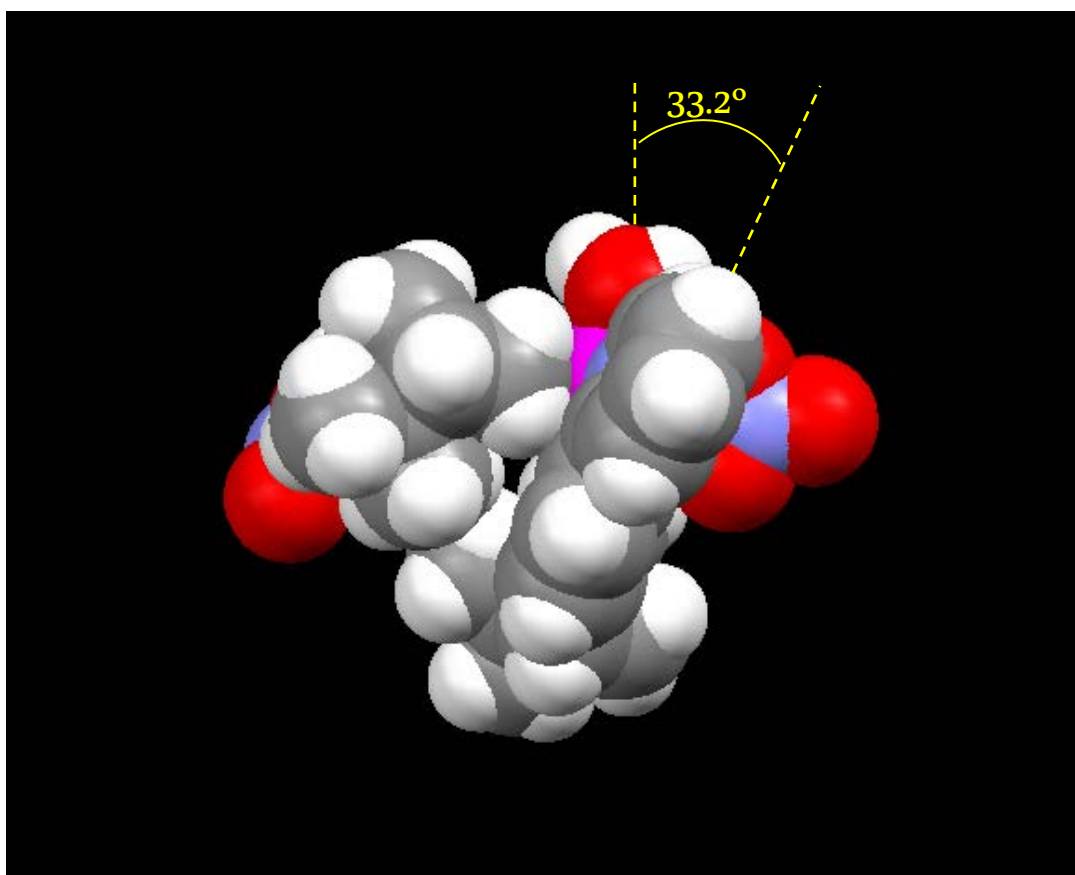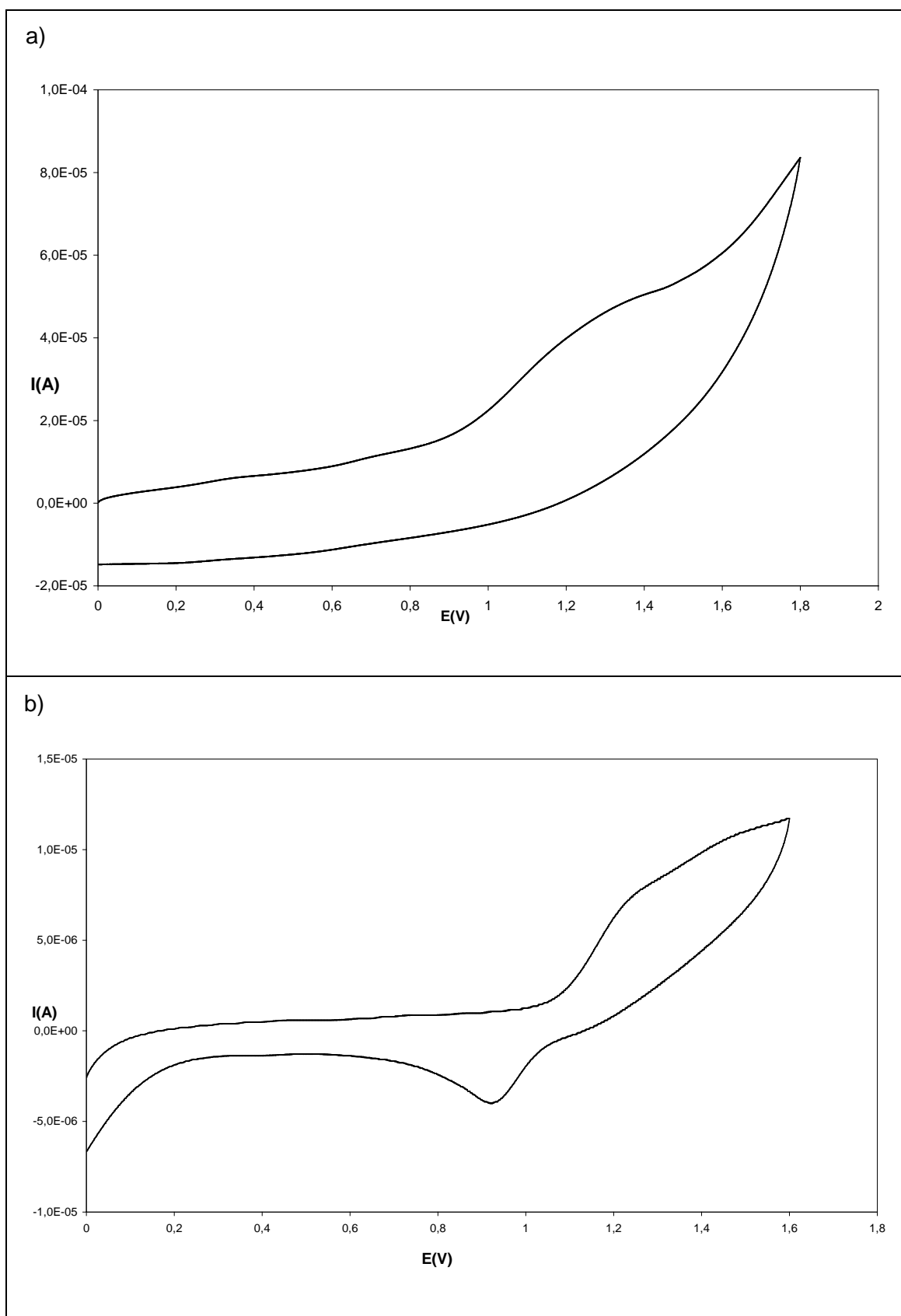
a)
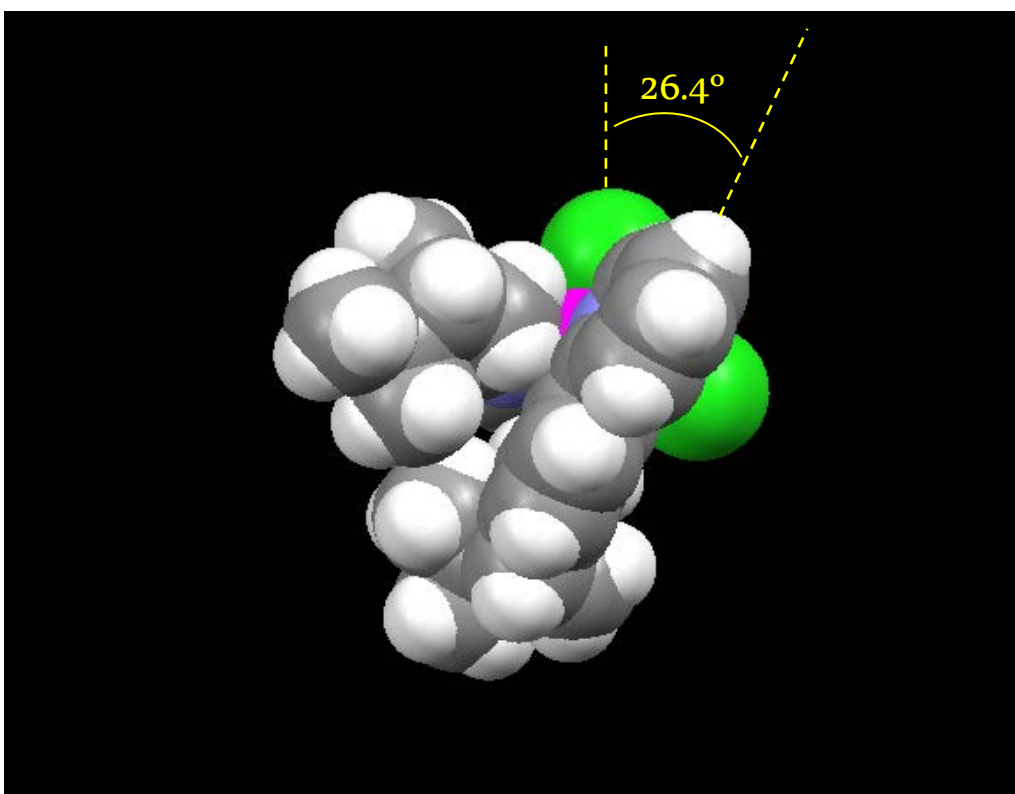
b)

c)

Figure S 2. Spacefill representations for the X-Ray diffraction structures of complexes a) **C4**, b) **C5** and c) **C6**. The angle manifesting the distortion with regard to regular octahedral environment is indicated in each case.
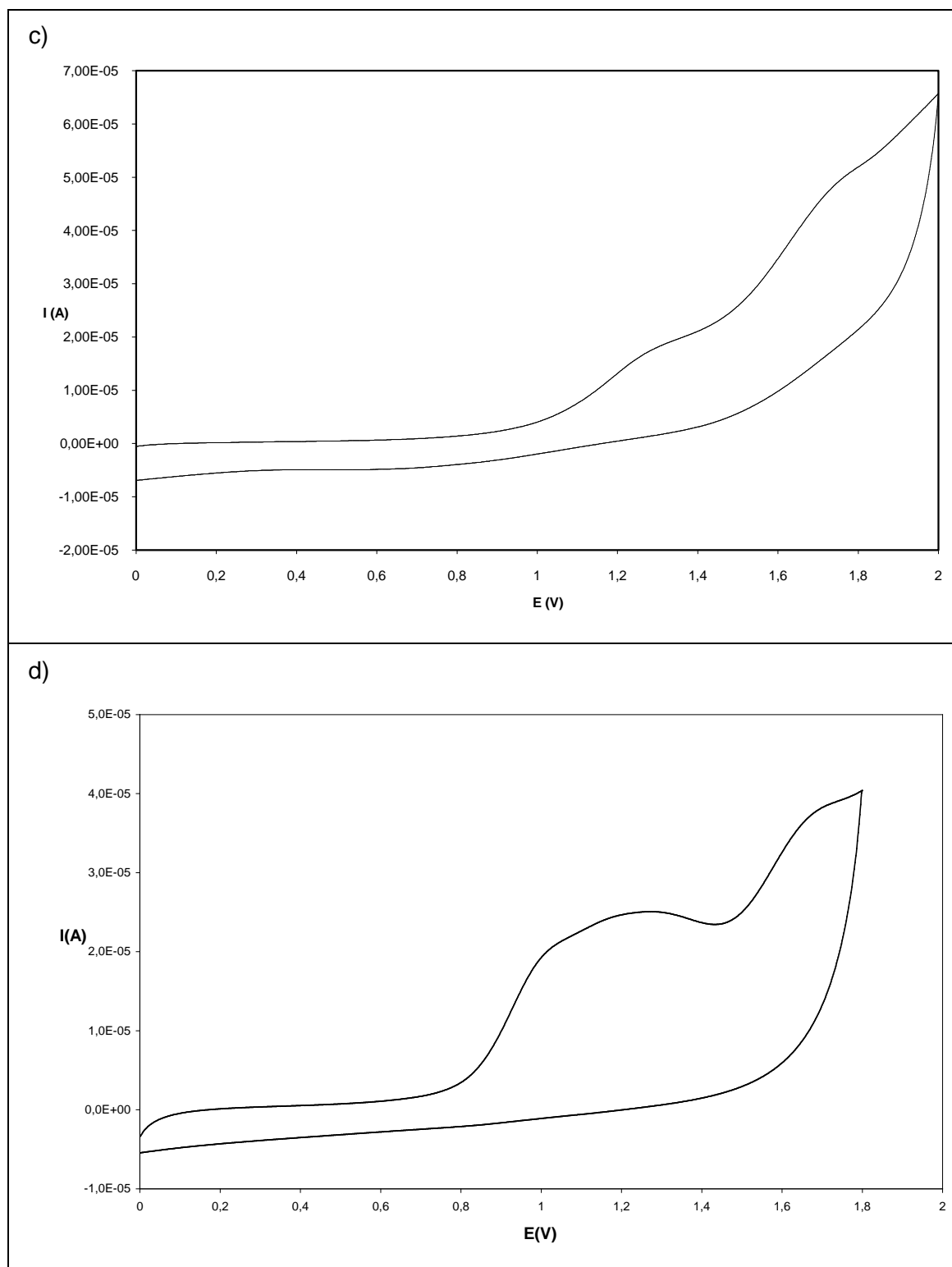
Figure S 3. CV in CH_3CN +0.1M $[(nBu)_4N]PF_6$ of a solution of a) **C2** , b) **C3**, c) **C5** and d) **C6**, at a platinum electrode (2 mm diameter); scan rate:100 mV/s.

Table S 1. Main crystallographic data for compounds **C1**-**C6**.

	C1	C2	C3	C4	C5	C6
Empirical formula	$C_{34}H_{36}Cl_4Mn_2N_4$	$C_{42}H_{49}Cl_4F_6Mn_2N_4O_6P$	$C_{17}H_{20}Cl_2MnN_2O$	$C_{34}H_{36}Cl_2MnN_4$	$C_{36}H_{36}F_6MnN_4O_6S_2$	$C_{34}H_{38}MnN_6O_9$
Formula weight	752.35	1102.5	394.19	626.51	853.75	729.64
Crystal system	monoclinic,	Orthorhombic	Orthorhombic	Orthorhombic	Orthorhombic	Orthorhombic
Space group	$P2_1$	P2(1)2(1)2	P212121	P212121	P212121	P212121
a [Å]	7.6452(13)	12.63(2)	8.189(5)	9.115(6)	9.340(5)	8.953(7)
b [Å]	8.4060(15)	18.08(3)	8.755(5)	15.739(11)	18.511(9)	12.691(10)
c [Å]	25.468(4)	10.392(18)	26.303(15)	25.528(17)	31.713(11)	31.31(2)
α [º]	90	90	90	90	90	90
β [º]	91.982(3)	90	90	90	90	90
γ [º]	90	90	90	90	90	90
Volume [Å^3]	1635.8(5)	2372(7)	1885.7(18)	3662(4)	3558(5)	3558(5)
Z	2	2	4	4	4	4
ρ_{calc} [Mg/m^3]	300(2)	100(2)	153(2)	300(2)	300(2)	300(2)
Temperature, K	1.527	1.544	1.389	1.136	1.362	1.362
μ [mm^{-1}]	1.130	0.865	0.988	0.532	0.432	0.432
Reflections collected/unique	25595 / 7938	33075 / 5860	29245 / 4602	57464 / 9018	54593 / 9293	55797 / 8934
R (int)	0.0513	0.0414	0.0557	0.2317	0.1081	0.3152
Final R indices [I>2 σ (I)]	R_1=0.0512 WR^2=0.1123	R_1= 0.0574 WR^2= 0.1691	R1 = 0.0366 wR2 = 0.0865	R_1=0.0885 WR^2=0.1897	R_1=0.0539 WR^2=0.1143	R_1=0.0546 WR^2=0.1020
R indices (all data)	R_1=0.0632 WR^2=0.1158	R_1=0.0740 WR^2=0.1826	R1 = 0.0563 wR2 = 0.0934	R_1=0.2524 WR^2=0.2396	R_1=0.1022 WR^2=0.1334	R_1=0.2931 WR^2=0.1461

$R_1 = \Sigma ||F_o| - |F_c||/\Sigma |F_o|$, $wR_2 = [\Sigma\{w(F_o^2-F_c^2)^2\}/\Sigma\{w(F_o^2)^2\}]^{½}$, where $w = 1/[\sigma^2(Fo^2) + (0.0042P)^2]$ and $P=(F_o^2+2F_c^2)/3$

Table S 2. Selected bond lengths [Å] and angles [deg] for **C1**.

Mn(1)-N(1)	2.190(4)	Mn(2)-Cl(1)	2.4519(14)
Mn(1)-N(2)	2.296(4)	Mn(2)-N(4)	2.295(4)
Mn(1)-Cl(3)	2.3293(13)	Mn(2)-Cl(2)	2.5526(13)
Mn(1)-Cl(2)	2.4356(14)	Mn(2)-N(3)	2.207(4)
Mn(1)-Cl(1)	2.5772(14)	Mn(2)-Cl(4)	2.3390(13)
Mn(1)···Mn(2)	3.736		
N(1)-Mn(1)-N(2)	73.76(15)	N(3)-Mn(2)-N(4)	73.90(15)
N(1)-Mn(1)-Cl(3)	115.34(10)	N(3)-Mn(2)-Cl(4)	120.22(11)
N(2)-Mn(1)-Cl(3)	98.82(10)	N(4)-Mn(2)-Cl(4)	98.76(10)
N(1)-Mn(1)-Cl(2)	132.10(10)	N(3)-Mn(2)-Cl(1)	129.40(11)
N(2)-Mn(1)-Cl(2)	93.62(10)	N(4)-Mn(2)-Cl(1)	94.90(11)
Cl(3)-Mn(1)-Cl(2)	112.17(5)	Cl(4)-Mn(2)-Cl(1)	110.15(15)
N(1)-Mn(1)-Cl(1)	90.15(10)	N(3)-Mn(2)-Cl(2)	88.11(10)
N(2)-Mn(1)-Cl(1)	155.50(10)	N(4)-Mn(2)-Cl(2)	104.71(5)
Cl(3)-Mn(1)-Cl(1)	104.83(5)	Cl(4)-Mn(2)-Cl(2)	83.65(4)
Cl(2)-Mn(1)-Cl(1)	83.46(4)	Cl(1)-Mn(2)-Cl(2)	83.65(4)
Mn(2)-Cl(1)-Mn(1)	95.91(5)	Mn(1)-Cl(2)-Mn(2)	96.97(5)

Table S 3. Selected bond lengths [Å] and angles [deg] for **C2**.

Mn(1)-N(1)	2.186(4)	Mn(1)-O(2*)	2.175(4)
Mn(1)-N(2)	2.234(4)	Mn(1)···O(2)	2.479(4)
Mn(1)-O(3)	2.034(4)	Mn(1)···Mn(1*)	3.433(4)
Mn(1)-O(1)	2.159(4)		
O(3)-Mn(1)-O(1)	142.87(15)	Mn(1*)-O(2)-Mn(1)	94.80(16)
O(3)-Mn(1)-O(2*)	94.45(14)	C(20)-O(3)-Mn(1)	136.3(3)
O(1)-Mn(1)-O(2*)	87.62(13)	C(18)-O(1)-Mn(1)	99.4(3)
O(3)-Mn(1)-N(1)	108.76(14)	C(18)-O(2)-Mn(1*)	127.6(3)
O(1)-Mn(1)-N(1)	108.30(14)	C(18)-O(2)-Mn(1)	84.4(3)
O(2*)-Mn(1)-N(1)	90.08(17)	N(1)-Mn(1)-O(2)	158.12(12)
O(3)-Mn(1)-N(2)	96.74(13)	N(2)-Mn(1)-O(2)	116.32(15)
O(1)-Mn(1)-N(2)	91.14(12)	O(1)-Mn(1)-O(2)	54.77(11)
O(2*)-Mn(1)-N(2)	162.97(11)	O(2*)-Mn(1)-O(2)	76.45(17)
N(1)-Mn(1)-N(2)	74.19(16)	O(3)-Mn(1)-O(2)	89.67(13)

Table S 4. Selected bond lengths [Å] and angles [deg] for **C3**.

Mn(1)-O(3)	2.189(2)	Mn(1)-Cl(2)	2.3698(13)
Mn(1)-N(1)	2.224(2)	Mn(1)-Cl(1)	2.3822(13)
Mn-(1)N(3)	2.254(2)		
O(3)-Mn(1)-N(1)	88.84(8)	N(3)-Mn(1)-Cl(2)	97.81(7)
O(3)-Mn(1)-N(3)	163.28(7)	O(3)-Mn(1)-Cl(1)	90.46(9)
N(1)-Mn(1)-N(3)	74.44(8)	N(1)-Mn(1)-Cl(1)	125.05(8)
O(3)-Mn(1)-Cl(2)	90.52(9)	N(3)-Mn(1)-Cl(1)	99.00(7)
N(1)-M(1)n-Cl(2)	119.96(8)	Cl(2)-Mn(1)-Cl(1)	114.99(5)

Table S 5. Selected bond lengths [Å] and angles [deg] for **C4**.

Mn(1)-N(1)	2.294(7)	Mn(1)-N(4)	2.387(6)
Mn(1)-N(2)	2.358(6)	Mn(1)-Cl(2)	2.489(3)
Mn(1)-N(3)	2.290(6)	Mn(1)-Cl(1)	2.481(3)
N(1)-Mn(1)-N(2)	70.3(3)	N(2)-Mn(1)-Cl(1)	88.48(16)
N(1)-Mn(1)-N(3)	179.0(3)	N(4)-Mn(1)-Cl(1)	156.05(19)
N(2)-Mn(1)-N(3)	110.6(2)	N(3)-Mn(1)-Cl(2)	89.93(17)
N(3)-Mn(1)-N(4)	70.4(2)	N(1)-Mn(1)-Cl(2)	89.2(2)
N(1)-Mn(1)-N(4)	109.9(2)	N(2)-Mn(1)-Cl(2)	153.91(18)
N(2)-Mn(1)-N(4)	84.25(19)	N(4)-Mn(1)-Cl(2)	88.00(16)
N(3)-Mn(1)-Cl(1)	91.07(17)	Cl(1)-Mn(1)-Cl(2)	107.65(10)
N(1)-Mn(1)-Cl(1)	88.86(16)		

Table S 6. Selected bond lengths [Å] and angles [deg] for **C5**.

Mn(1)-O(1)	2.168(3)	Mn(1)-N(1)	2.265(3)
Mn(1)-O(4)	2.186(3)	Mn(1)-N(2)	2.280(3)
Mn(1)-N(3)	2.252(3)	Mn(1)-N(4)	2.300(3)
O(1)-Mn(1)-O(4)	98.20(11)	N(1)-Mn(1)-N(2)	72.80(11)
O(1)-Mn(1)-N(3)	86.78(11)	O(1)-Mn(1)-N(4)	94.09(11)
O(4)-Mn(1)-N(3)	83.21(11)	O(4)-Mn(1)-N(4)	152.34(11)
O(1)-Mn(1)-N(1)	85.19(11)	N(3)-Mn(1)-N(4)	72.81(11)
O(4)-Mn(1)-N(1)	94.19(11)	N(1)-Mn(1)-N(4)	111.53(11)
N(3)-Mn(1)-N(1)	171.12 (11)	N(2)-Mn(1)-N(4)	91.86(11)
O(1)-Mn(1)-N(2)	157.86(11)	O(4)-Mn(1)-N(2)	86.01(11)
N(3)-Mn(1)-N(2)	115.34(11)		

Table S 7. Selected bond lengths [Å] and angles [deg] for **C6**.

Mn(1)-O(1)	2.184(4)	Mn(1)-N(4)	2.246(5)
Mn(1)-O(2)	2.261(5)	Mn(1)-N(2)	2.252(5)
Mn(1)-N(3)	2.347(5)	Mn(1)-N(5)	2.321(5)
N(4)-Mn(1)-N(2)	170.42(2)	N(2)-Mn(1)-N(5)	117.12(19)
O(1)-Mn(1)-N(4)	90.57(16)	O(2)-Mn(1)-N(5)	158.28(18)
O(1)-Mn(1)-N(2)	86.53(18)	O(1)-Mn(1)-N(3)	148.99(17)
O(1)-Mn(1)-O(2)	86.93(17)	N(4)-Mn(1)-N(3)	114.71(19)
N(4)-Mn(1)-O(2)	88.23(18)	N(2)-Mn(1)-N(3)	71.2(2)
N(2)-Mn(1)-O(2)	82.45 (17)	O(2)-Mn(1)-N(3)	110.35(17)
O(1)-Mn(1)-N(5)	85.12(16)	N(2)-Mn(1)-N(3)	170.42(2)
N(4)-Mn(1)-N(5)	71.7(2)		

Chapter 4

Catalytic activity of Mn(II) complexes containing the polypyridylic chiral ligand (–)-pinene[5,6]bipyridine: reusable catalytic systems for alkene epoxidation. Evidence of high-valent oxo-bridged binuclear Mn₂(IV,IV) and mixed-valent Mn₂(III,IV) active oxidant species.

The reactivity of the new complexes synthesized in the previous chapter has been tested with regard to the epoxidation of aromatic and aliphatic alkenes with peracetic acid as oxygen donor. The catalytic performance of the chloro complexes is enhanced by the use of additives (NaHCO$_3$ and imidazole) and also when a [bmim]:acetonitrile mixture (bmim = 1-butyl-3-methyl-imidazolium) is used as reaction media. The latter conditions allow for the recyclability of the catalytic system keeping good selectivity and conversion values. The nature of the intermediate catalytic species for three of the catalysts has been investigated through EPR, ESI-MS and UV-vis techniques. The results obtained point in all cases to the formation of binuclear [Mn(μ-O)$_2$Mn]$^{n+}$ species but displaying different oxidation states as a function of the starting Mn(II) complex ((IV,IV) for the chloro complexes; (III,IV) for the triflate complex), thus evidencing a significant role of the Cl or triflate ligands in the formation of the intermediate species.

TABLE OF CONTENTS

CHAPTER 4. Catalytic activity of Mn(II) complexes containing the polypyridylic chiral ligand (–)-pinene[5,6]bipyridine: reusable catalytic systems for alkene epoxidation. Evidence of high-valent oxo-bridged binuclear Mn$_2$(IV,IV) and mixed-valent Mn$_2$(III,IV) active oxidant species.

4.1. Introduction

4.1.1. Epoxidation catalysis

Metal-catalyzed oxidation is one of the most important transfer reactions in chemistry and biology.[1-4] Olefin epoxidation has received considerable interest from both academics and industry; concretely, enantiomerically pure epoxides play an eminent role as intermediates and buildings blocks in organic synthesis and materials science.[5-10] Although numerous procedures have been developed[11-13] the need to understand the mechanisms of metal-mediated oxygenation processes demands the synthesis of new stable and available catalysts. These reactions are known to proceed via oxo-, peroxo-, or peroxide metal intermediates. The exact nature of the oxygenating species and the mechanism of oxygen transfer to the substrate remain unclear, although the participation of multiple active oxidants has been proposed in most cases.[14-16] The efficiency of the oxygen transfer step is influenced by the coordination environment on the metal center; the ligands can sterically and chirally affect the approach of molecules toward the metal center and, hence, induce selectivity.

Chiral manganese complexes have been studied as catalysts for enantioselective oxidation reactions in combination with H_2O_2; this oxidizing agent is a good choice in terms of atom economy and does not produce environmentally undesirable by-products. The most developed systems are those based on Mn porphyrins[17-19] and Mn salen[20,21] complexes, which afford excellent enantioselectivities but suffer from a limited substrate scope and relatively high catalyst loadings (usually 2 – 5 %).

More recently, Stack and co-workers[22-24] described systems based on *in-situ* prepared mononuclear manganese(II) complexes by mixing $Mn(CF_3SO_3)_2$ and bi-, tri- or tetradentate nitrogen ligands in combination with peracetic acid as oxidizing agent, which is also a good and clean oxidant because it generates acetic acid as by-product. These systems provide rapid and efficient catalysts for the epoxidation of olefins with even higher activities than manganese complexes with Schiff base ligands, but they present poor stereoselectivity. Among the catalysts screened, the highest activity is obtained with $[Mn^{II}(R,R,-mcp)(CF_3SO_3)_2]$ (mcp = N,N'-dimethyl-N,N'-bis(2-pyridyl) cyclohexane-*trans*-1,2-diamine), $[Mn^{II}(bpy)_2(CF_3SO_3)_2]$ and $[Mn^{II}(phen)_2(CF_3SO_3)_2]$ compounds, which have been isolated and structurally characterized. Later studies demonstrated that trinuclear $[Mn_3(L)_2(OAc)_6]$ complexes, containing neutral bidentate nitrogen ligands, are also highly efficient catalysts in the epoxidation of alkenes using

peracetic acid.[25] Under the reaction conditions, these trinuclear complexes dissociate into mononuclear species which are assumed to be responsible for the observed activity. To improve the performance of these catalytic systems, namely the stereoselectivity, modification of Stack's catalyst [Mn^{II}(R,R,-mcp)(CF$_3$SO$_3$)$_2$] with chiral tetradentate ligands has been developed by fusing pinene groups to pyridine rings of mcp. These complexes demonstrate a remarkable stereoselectivity (up to 46%) in epoxidation[26] but an important limitation is still the complicated catalyst preparation. Pinene groups fused to bipyridine rings have also been used in diferric complexes that catalyze asymmetric olefin epoxidation reactions by peracetic acid with highly enantioselective epoxidation and high conversion yield.[27] On the other hand, a recently reported family of chiral supramolecular binuclear manganese complexes that also contain pinene type of ligands showed excellent activity in epoxidation reactions though no enantioselectivity was observed.[28]

A novel series of mononuclear Mn(II) complexes, containing enantiomerically pure ligands with both pyridyl and 2,2'-bipyridyl entities or mcp derivatives (mcp = N,N'-dimethyl-N,N'-bis(2-pyridylmethyl)cyclohexane-trans-1,2-diamine), have also been reported recently as efficient catalysts for alkene epoxidation with peracetic acid or H$_2$O$_2$/acetic acid mixture as oxidants.[29-31]

4.1.2. Influence of additives and ionic liquids

The use of additives is an important aspect of the metal-catalyzed epoxidation since often leads to an increase of the activity.[32-34] In the specific case of Mn(III) complexes the epoxidation activity is in some cases directly dependent on the basicity of the additives used.[33,34] Certain additives such as carboxylic acids, carboxylate or carbonate salts have been reported to cause increased chemoselectivity and diastereoselectivity in the catalytic epoxidation of chiral allylic alcohols by binuclear Mn(IV) complexes.[35,36]

Heterogeneization and reuse of catalysts are fields of unquestionable importance especially towards their application in large-scale processes.[37,38] Besides, in view of today's environmental consciousness, the use of environmentally benign reaction media is very important. In this context, room temperature ionic liquids (RTILs) have received in recent years a good deal of attention as potential cleaner, alternative solvents or co-solvents media in catalysis[39-46] given their potential benefits, particularly the ease of product separation and also the high recyclability of the catalyst.[47]

Numerous possible combinations of cations and anions (some examples are shown in Figure 1) offer convenient ways to fine-tune the physicochemical properties of ILs, such as polarity, viscosity and miscibility with others reagents. Most metal catalysts are soluble in ILs without modification of the ligands, and usually the noncoordinating anions of ILs leave the active sites of catalysts available for interaction with the substrates.

Epoxidation catalytic processes have been tested in ionic liquids with Mn(III) complexes containing porphyrin and Schiff base ligands[48-50] but, to the best of our knowledge, the only Mn(II) compound evaluated to date as epoxidation catalyst in such media is manganese (II) acetate, that has been tested in the epoxidation of aliphatic terminal alkenes.[51]
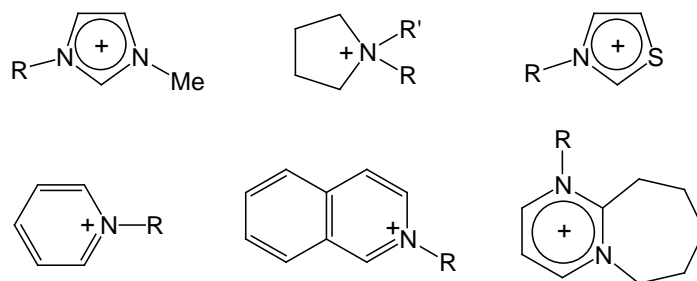
Anions: BF_4^-, PF_6^-, NO_3^-, ClO_4^-, Cl^-, Br^-

Figure 1. Commonly used cations and anions for ionic liquids.

4.2. Objectives

The main objective of this chapter was to study the reactivity of the asymmetric mononuclear and binuclear manganese (II) complexes containing the chiral bidentate nitrogen ligand (–)-pinene[5,6]bipyridine, ((–)-**L**, Chart 1), described in the previous chapter, with regard to the epoxidation of some aromatic and aliphatic alkenes using peracetic acid as the oxidant.

[{Mn((-)-**L**)Cl}₂(μ-Cl)₂] (**C1**)
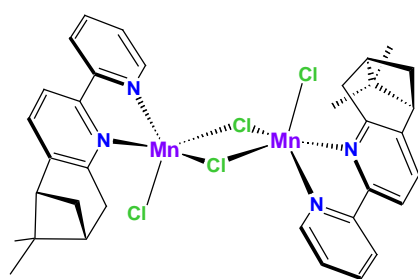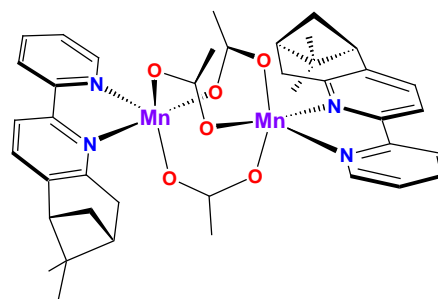
[{Mn((-)-**L**)}₂(μ-OAc)₃](PF)₆ (**C2**)
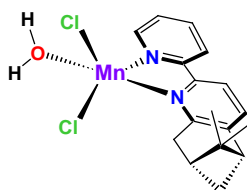
[Mn((-)-**L**)Cl₂(H₂O)] (**C3**)
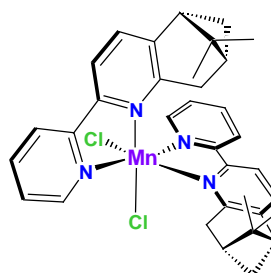
[Mn((-)-**L**)₂Cl₂] (**C4**)
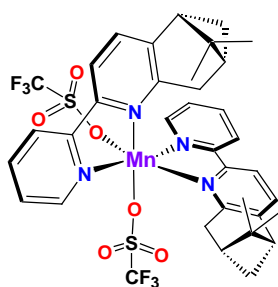
[Mn((-)-**L**)₂(CF₃SO₃)₂] (**C5**)
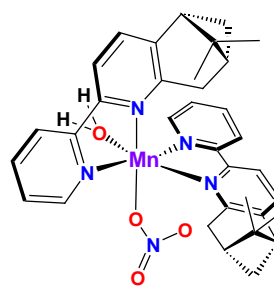
[Mn((-)-**L**)(NO₃)(H₂O)](NO₃) (**C6**)

Chart 1. Mn(II) complexes containing the chiral ligand (–)-**L**.

We also considered to study, after some initial catalytic tests, the performance of the best catalysts (which resulted to be the chloro complexes **C1** and **C4**) in epoxidation

catalysis carried out in the presence of additives such as imidazole or NaHCO$_3$, in order to study their influence on the catalytic performance.

We were also interested in the epoxidation activity of **C1** and **C4** in ionic liquid:solvent media (Chart 2) as well as in the study of their reusability, a system that constitutes the first example of polypyridyl Mn(II) complexes tested under these conditions.
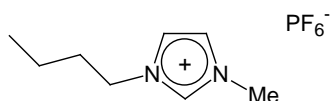

Chart 2. Ionic liquid [bmim]PF$_6$.

Finally, another objective was the analysis, by means of EPR, ESI-MS and UV-vis techniques, of the active catalytic species present in the epoxidation reactions catalyzed by the chloro complexes **C1** and **C4** and the triflate complex **C5**, with the idea of investigating the role of the Cl or triflate ligands in the formation of the intermediate species.

4.3. Results and discussion

4.3.1. Catalytic epoxidation of alkenes. Influence of additives

The catalytic activity of the manganese compounds described in the previous chapter (**C1**-**C6**) was investigated in the epoxidation of some aromatic alkenes using commercial peracetic acid (32%) as the oxidant. Table 1 reports the conversion, the yield of epoxide, selectivity and enantiomeric excess for the epoxide product using styrene as substrate. All complexes were tested under analogous conditions (catalyst:styrene:peracetic acid, 1:100:200). No epoxidation occurred in the absence of catalyst. Other previously reported complexes are also included in Table 1 for comparison purposes.

Table 1. Catalytic oxidation of styrene by Mn complexes using CH_3CO_3H as oxidant.[a]
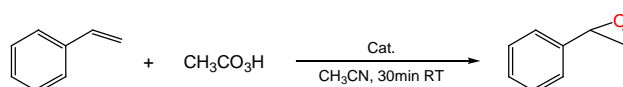
Entry	Compound	Conversion (%)	Epoxide yield (%)	Selectivity (%)	ee	ref.
1	**C1**	100	65	65	10	this chapter
2	**C1**[b]	3	3	100	21	this chapter
3	**C2**	10	10	100	19	this chapter
4	**C3**	10	7	70	20	this chapter
5	**C4**	52	30	57	10	this chapter
6	**C5**	18	6	33	15	this chapter
7	**C6**	19	10	53	19	this chapter
8	$[Mn(CF_3SO_3)(MCPP)]$[c]	100	80	80	40	26
9	$[Mn_3(ppei)_2(OAc)_6]$[c]	100	93	93	-	25
10	$[MnCl_2(L)]$[c,d]	89	43	48	-	29

[a] **Conditions** (see experimental section for further details): catalyst (2.5 µmol), substrate (250 µmol), CH_3CN (1 mL). Peracetic acid 32% (500 µmol) added in 3 minutes at 0ºC, then **30 min** of reaction at RT.
[b] Same conditions but temperature was kept at 0ºC along 30 minutes.
[c] Oxidant:substrate ratio of approximately 1:1.
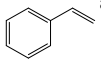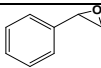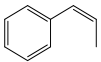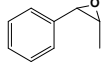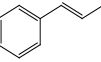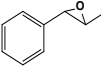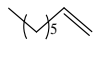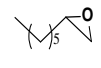[d] Not isolated catalyst, buffered oxidant, 7h reaction.

A first glance at entries 1-7 (complexes **C1**-**C6**) in Table 1 shows, after 30 minutes of reaction, moderate epoxide yields with low enantioselectivity, leading selectively to the *R* enantiomer. In most cases, minor amounts of side products (benzaldehyde) are formed. The two dinuclear (**C1** and **C2**) and the mononuclear **C3** complexes, which

possess pentacoordinated Mn(II) ions, show the highest selectivity for the epoxide, with **C2** exhibiting noticeable specificity (100% selective) with 19% enantioselectivity at room temperature. For the dinuclear compound **C1**, when the temperature is lowered to 0ºC, the conversion decreases as expected but the selectivity and the enantioselectivity increase (compare entries 1 and 2). Entries 3, 4, 6 and 7 show that the acetate, aquo, triflate, and nitrate compounds, **C2**, **C3**, **C5** and **C6** have similar performances regarding to the conversion of styrene under similar conditions, with moderate enantioselectivities (15-20%). The selectivity values of complexes **C1** and **C2** are higher than those presented by dinuclear iron complexes containing pinene groups (although the catalytic conditions are not exactly the same)[27] and, for our mononuclear compounds **C3**-**C6**, the values of selectivity are analogous or, in some cases, higher than those shown by other mononuclear Mn complexes. The epoxidation of aromatic olefins is known to be sluggish, leading to significant amounts of side products especially when the metal systems of Jacobsen or Stack are employed.[20-24,52]

The analysis of the performance of previously described compounds (entries 8-10) under relatively similar conditions (styrene epoxidation carried out with peracetic acid) shows that the best activities are shown by catalysts with highly labile ligands such as acetate or triflate. This is also a general trend for other previously reported catalysts when using different oxidants and substrates.[22-24,53] However, little is said about catalysts containing the $MnCl_2$ structural unit. Entry 10 in Table 1 reports a relatively good conversion value in styrene epoxidation under the mentioned conditions but using a non-isolated Mn chloro complex and after much longer reaction times. In sharp contrast, our Mn chloro complexes **C1** and **C4** (entries 1 and 5 in Table 1) show clearly higher conversions than their analogous triflate, nitrate or acetate complexes **C2**, **C3**, **C5** and **C6**, although the enantiomeric excesses are the lowest.

Better performances of the chloro complexes are also observed in the epoxidation of other alkenes. The results gathered in Table 2 allow the comparison between the chloro complex **C4** and the triflate complex **C5** for the epoxidation catalysis of aromatic and aliphatic alkenes with peracetic acid as the oxidant.

Table 2. Epoxidation tests performed with complexes **C4** and **C5**.

Substrate	Product	MnCl$_2$((−)-**L**)$_2$, **C4**		Mn(CF$_3$SO$_3$)$_2$((−)-**L**)$_2$, **C5**	
		Conv. (%)	Select. (%)	Conv. (%)	Select. (%)
[styrene][a]	[styrene oxide]	70	74	24	33
[cis-β-methylstyrene]	[epoxide]	37	95 c/t=100%[b]	30	62 c/t=100%[b]
[trans-β-methylstyrene]	[epoxide]	56	96	50	70
[1-octene]	[epoxide]	21	64	4	30

Conditions: catalyst (2.5 µmol), substrate (250 µmol), CH$_3$CN (1 mL). Peracetic acid 32% (500 µmol) added in 3 minutes at 0ºC, then **3 hours** of reaction at RT.
[a] **Time**: 2 hours. [b] c/t represents the percent of *cis* isomer obtained

It is remarkable that the conversion and selectivity values of chloro complex **C4** are higher than those presented by the triflate complex **C5** within the same time of reaction, thus indicating that the mechanism followed and/or the intermediate species involved in the catalytic cycle shall be distinctive for the two catalysts in spite of their structural similarity.

Complexes **C1** and **C4** are, to the best of our knowledge, the first examples of fully characterized Mn(II) chloro complexes with relatively simple N-donor ligands showing remarkable activity in epoxidation catalysis. For this reason a complete study of their catalytic performance has been developed.
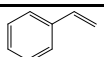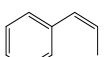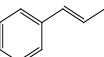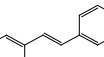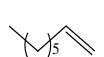
The catalytic activity of the manganese chloro complexes **C1** and **C4** was also investigated in the epoxidation of some alkenes in presence of two different additives, imidazole and NaHCO$_3$. Table 3 reports the conversion and selectivity values obtained for the corresponding epoxide products.

A first analysis of the catalytic activity, focusing the attention in the results obtained in epoxidation carried out without additives, shows that styrene conversions are excellent with good selectivity for the epoxide product. For *cis-* and *trans-*β-methylstyrene, conversions after 3 hours are moderate but with excellent selectivity for the epoxide in both cases and, in the case of *trans*-stilbene, only moderate activities and selectivities are observed, with formation of benzaldehyde by-product. The lower conversions are found for the aliphatic 1-octene although the selectivity is better than that for *trans*-

stilbene. For *trans*-β-methylcinnamate (data not shown), conversions are ≤5% after 20 hours and epoxidation leads to racemic mixtures in all cases. It is also interesting to observe a decrease of the conversions caused by the increase of the steric encumbrance of the aromatic substrates with regard to styrene.

Furthermore, still in absence of additives, complexes **C1** and **C4** oxidize *cis*-β-methylstyrene with high retention of configuration. The epoxidation of *cis*-β-methylstyrene by **C4** produced exclusively the corresponding *cis* epoxide stereoisomer, whereas only trace amounts (1%) of isomerized *trans* oxide product were observed in the case of complex **C1**. These reaction conditions seem to be an appropriate choice since the observed stereospecificity of the *cis/trans* epoxidation reaction excludes the presence of a long-lived free substrate radical during the oxygen transfer process.[21] Similar results had been observed previously with several manganese complexes with tetradentate nitrogen-donor ligands but containing triflate labile sites.[22-24,26,53]

Table 3. Epoxidation tests performed with complexes **C1** and **C4** in absence and presence of additives.

Substrate	[{MnCl((−)-**L**)}$_2$(μ-Cl)$_2$], **C1**						MnCl$_2$((−)-**L**)$_2$, **C4**					
	---		imidazole		NaHCO$_3$		---		imidazole		NaHCO$_3$	
	Conv. (%)	Select. (%)	Conv. (%)	Select. (%)	Conv. (%)	Select. (%)	Conv. (%)	Select. (%)	Conv. (%)	Select. (%)	Conv. (%)	Select. (%)
[styrene]	100[a]	65	100[a]	72	100[a]	79	70[b]	74	100[b]	98	100[b]	96
[*cis*-β-methylstyrene]	35	93 c/t=99%[c]	100	80 c/t=76%[c]	92	73 c/t=76%[c]	37	95 c/t=100%[c]	82	88 c/t=83%[c]	100	89 c/t=72%[c]
[*trans*-β-methylstyrene]	47	100	97	100	92	94	56	96	60	100	100	100
[stilbene]	20	8	62	64	91	67	22	27	36	61	85	84
[1-octene]	12	52	80	61	93	71	21	64	47	67	94	70

Conditions: catalyst (2.5 μmol), substrate (250 μmol), additive (25 μmol), CH$_3$CN (1 mL). Peracetic acid 32% (500 μmol) added in 3 minutes at 0°C, then **3 hours** of reaction at RT. After addition of an internal standard, an aliquot was taken for GC analysis.
[a] **Time**: 1 hour. [b] **Time**: 2 hours. [c] c/t represents the percent of *cis* isomer obtained.

As can be observed in Table 3, the conversion and selectivity values are considerably improved in the presence of additives, especially when NaHCO$_3$ is used. For the case of styrene, total consumption of the substrate is obtained with high epoxide yields particularly in the case of complex **C4**, which constitutes one of the most selective

catalysts described to date for the epoxidation of this substrate. *Cis*-β-methylstyrene also presents higher conversion in the presence of additives, but the process is less stereoselective for the formation of the *cis*-epoxide. Moreover, aliphatic alkenes such as 1-octene, which usually tend to be the least reactive olefins in metal-catalyzed epoxidation,[14] were readily epoxidized with both complexes **C1** and **C4**, again with sodium bicarbonate providing the best catalytic conditions from a conversion and selectivity perspectives. In terms of enantioselectivity, although the catalysts are chiral, no asymmetric induction has been observed (≤10% ee in all cases), as it was the case for other Mn complexes with pinene type of ligands.[28]
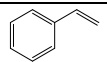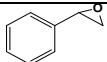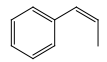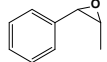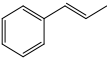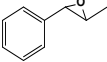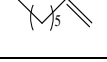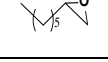
A comparison between the activities displayed by catalysts **C1** and **C4** evidences that both chloro complexes present similar performance degrees in the absence of additives for all the substrates tested, as well as a comparable increase of the conversion values in the presence of either imidazole or $NaHCO_3$. We can deduce from the results given in Table 3 that the epoxidation activity seems to be directly dependent on the basicity of the additives used (better results are obtained with sodium bicarbonate when compared to the less basic imidazole), and this basic character appears to be appropriate to achieve some enhanced catalytic activity when peracetic is used as oxidant. The basic nature of the additives can partially neutralize the acidity of the peracid added in large excess in the solution and thus prevent the decomposition of complexes into protonated ligand and free Mn^{2+}, as has been previously observed by Stack *et al.*[24] However, the coordinating character of imidazole might also play a role by partially blocking the active sites of the catalyst and thus slowing down the catalytic reaction, though with improved performance thanks to its basic character when compared to the same reaction performed in absence of additives.

4.3.2. Catalytic epoxidation of alkenes in ionic liquid:solvent media

The performance and reusability of catalysts **C1** and **C4** in ionic liquid:solvent media has been also tested. The ionic liquid (IL) used was the commercially available [bmim]PF_6 and the reaction conditions were initially optimized using different solvents and [bmim]PF_6:solvent ratios (see Table S 1 in the Supporting Information). Optimal performance was obtained using [bmim]PF_6:CH_3CN 1:1 as solvent and these conditions were used for the epoxidation of different alkenes. Table 4 reports the conversion and selectivity values obtained for the corresponding epoxide products. In general, remarkably better performances are observed in presence of the mixture ionic

liquid:acetonitrile when compared to acetonitrile, though a slight decrease of the selectivity is observed in some cases in the presence of ionic liquid. It is significant the enhancement in the performance for 1-octene when using ionic liquid media since, as has been reported,[51] the epoxidation of aliphatic terminal alkenes in IL is challenging due to the poor miscibility of alkenes among the reaction components, which often leads to slow reaction rates and low conversion yields. Our system [bmim]PF$_6$:CH$_3$CN 1:1 leads to three-fold conversion values when using both catalysts **C1** and **C4** with regard to the use of acetonitrile as sole solvent, keeping good selectivity values.

**Table 4.** Epoxidation tests performed with complexes **C1** and **C4** in [bmim]PF$_6$:CH$_3$CN media.

Substrate	Product	Complex **C1**		Complex **C4**	
		Conv. %	Select. %	Conv. %	Select. %
(styrene)	(styrene oxide)	86	66	95	71
(cis-β-methylstyrene)	(epoxide)	60	81 c/t=95%[a]	64	63 c/t=97%[a]
(trans-β-methylstyrene)	(epoxide)	75	77	91	81
(1-octene)	(1,2-epoxyoctane)	58	56	61	57

Conditions: catalyst (2.5 µmol), substrate (250 µmol), CH$_3$CN:[bmim]PF$_6$ 1:1 (2 mL). Peracetic acid 32% (500 µmol) added in 3 minutes at 0ºC, then **3 hours** of reaction at RT.
[a] c/t represents the percent of *cis* isomer obtained.

The recyclability of the catalytic systems has been investigated using different substrates. The results obtained for complex **C4** for a number of consecutive runs and employing different substrates are displayed in Figure 2, which reflects that the catalyst maintains a remarkable performance through up to 7-9 runs in all cases. The selectivity for the epoxide is also well maintained for 1-octene and *trans-* and *cis-*β-methylstyrene but it progressively decreases for styrene. The overall turnover numbers are 298 for styrene, 271 for *cis-*β-methylstyrene, 596 for *trans-*β-methylstyrene and 168 for 1-octene. In the case of epoxidation of *cis-*β-methylstyrene the stereoselectivity for the *cis-*epoxide is maintained through all the runs. The reusability of catalyst **C1** has been tested following an analogous procedure using styrene and 1-octene as substrates and the results obtained are shown in the supplementary information (Figure S 1).

We have tried a similar recycling procedure using CH_3CN as single solvent in absence of additives, but no conversion was obtained at the second run. Thus, the ionic liquid exerts a stabilizing effect on the catalyst that allows its reuse without loss of activity.
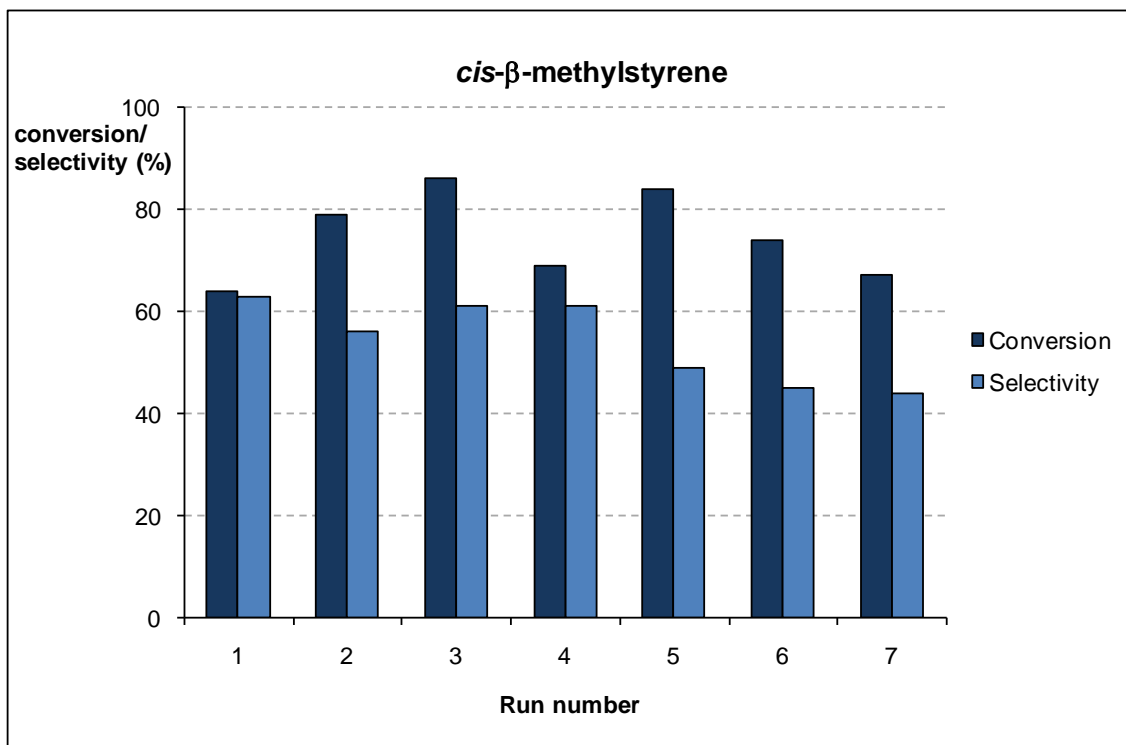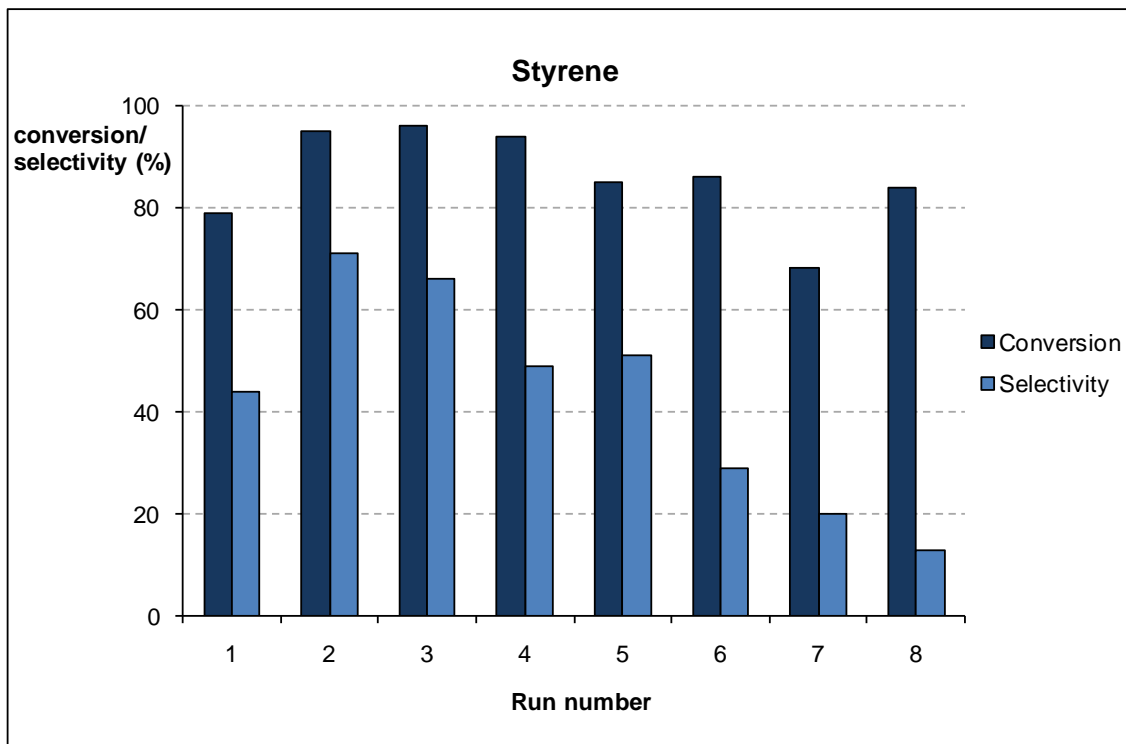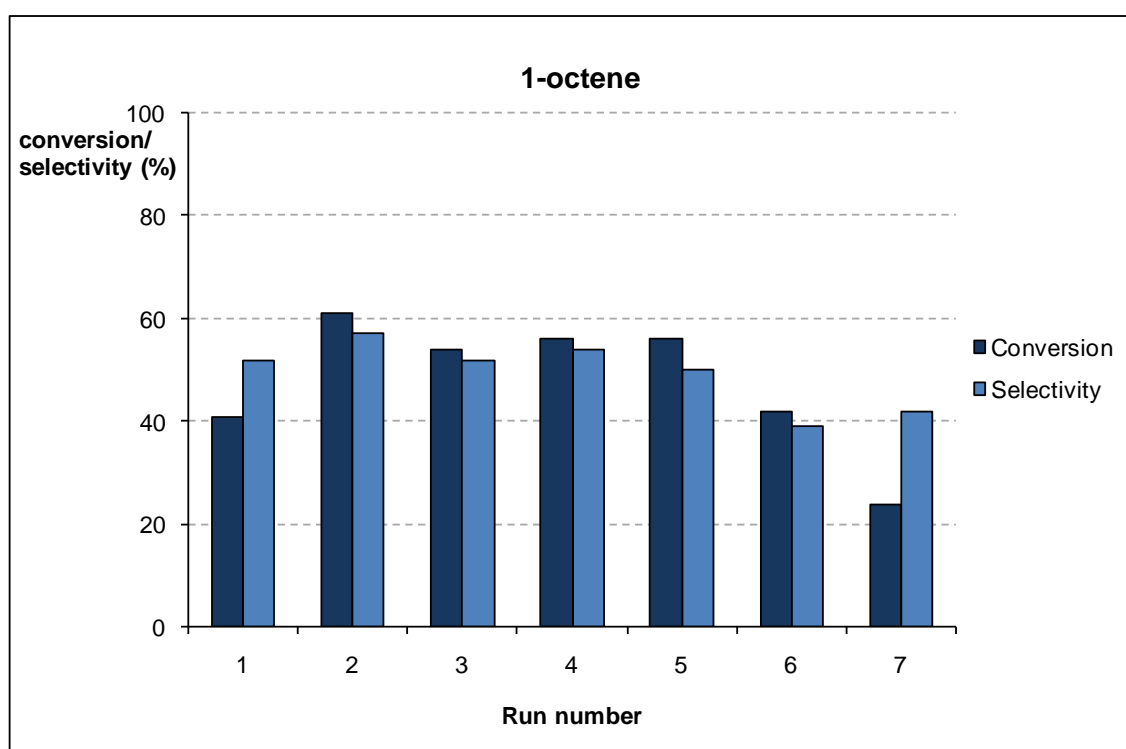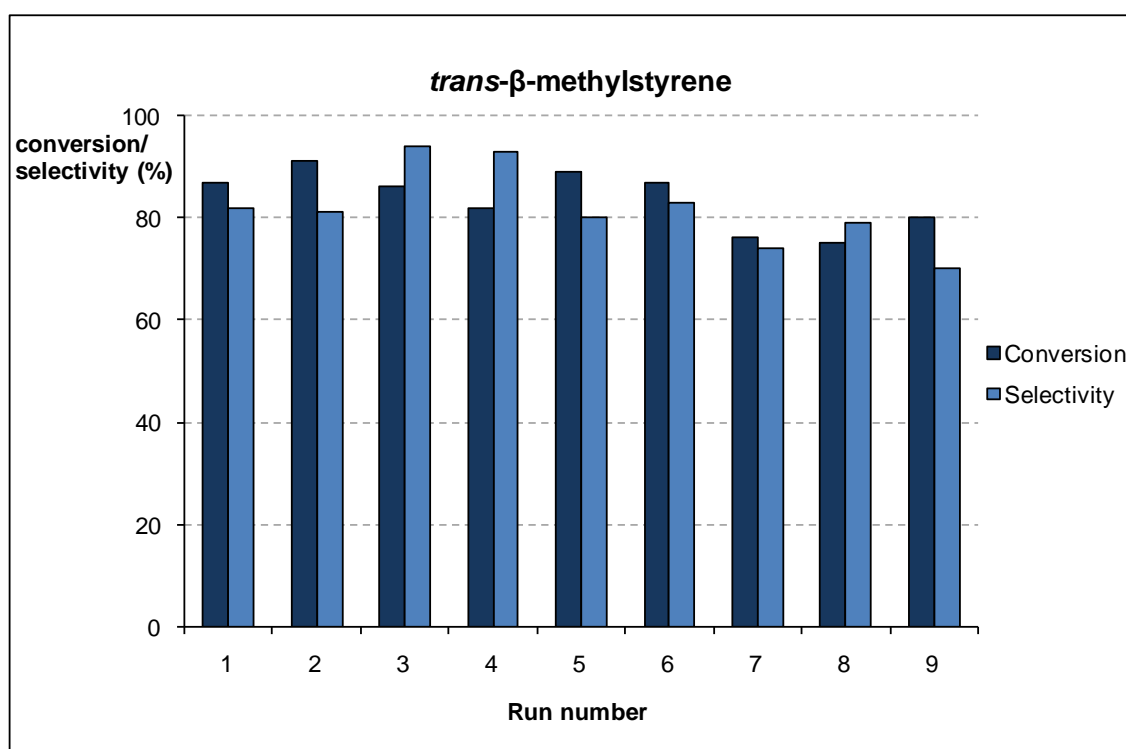
Figure 2. Conversion and selectivity values obtained throughout a number of consecutive reuses of complex **C4** in the epoxidation of different substrates in [bmim]PF$_6$:CH$_3$CN (see text for experimental conditions).

4.3.3. Determination of active oxidant species

In order to obtain further information about the nature of the reactive intermediates in the epoxidation catalysis, UV-vis, ESI-MS and EPR spectrophotometric measurements at low temperature were carried out using complexes $[\{Mn((-)-L)Cl\}_2(\mu-Cl)_2]$ (**C1**), $[Mn^{II}((-)-L)_2Cl_2]$ (**C4**) and $[Mn^{II}((-)-L)_2(CF_3SO_3)_2]$ (**C5**) as catalysts.

Figure 3 shows the evolution of the UV-vis spectrum of a solution of complex **C4** upon addition of oxidant at -40°C (solid lines) and subsequent addition of styrene after allowing the mixture to warm up to 15°C (dashed lines). The UV-visible spectrum of **C4** in CH$_3$CN is featureless, as expected for Mn(II) species. Addition of 2 eq. of peracetic acid causes the solution colour change from colourless to brown, with the appearance of two bands in the visible region at 670 nm and 550 nm (shoulder) as well as a strong increase of the absorbance below 500 nm. The shape and the maximum wavelength values of the spectrum obtained after oxidation of **C4** are very similar to those of di-μ-oxo binuclear Mn$_2$(IV,IV) complexes with polypyridyl ligands previously reported in the literature[54-58] and are also consistent with EPR and ESI-MS experiments performed on this system (see below). The absorption features observed can be assigned to Mn^{IV} d-d and oxo→Mn^{IV} LMCT transitions.[54-56]
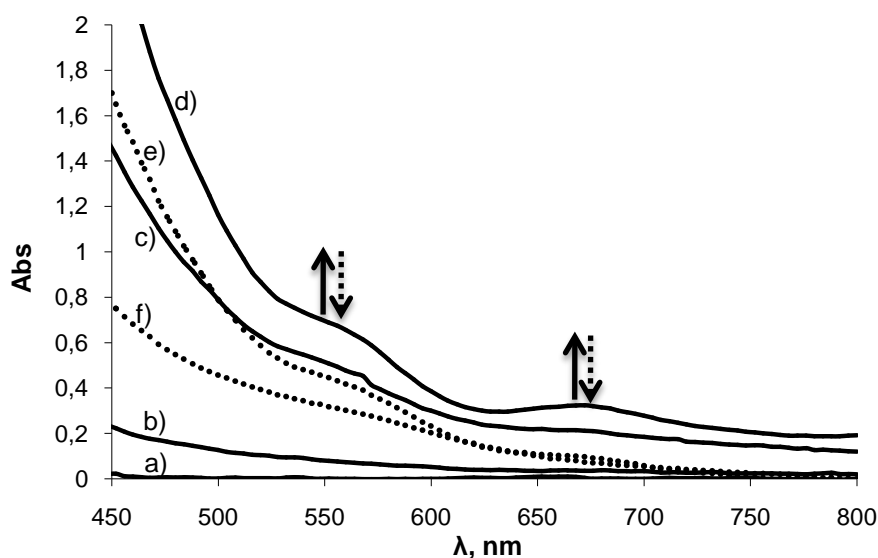
Figure 3. Evolution of UV-vis spectrum of complex **C4** in CH$_3$CN (2.5 mM), upon addition of 2 eq. of peracetic acid at -40ºC, warming up to 15ºC and subsequent addition of 10 eq. of styrene substrate. (a) initial, (b) 30 seconds after addition of peracetic acid, (c) 36 seconds after addition of peracetic acid, (d) 15 minutes after addition of peracetic acid, (e) 20 minutes after addition of styrene, (f) 21 hours after addition of styrene.

The absorption spectrum of the oxidized species formed was unchanged after 15 minutes at -40ºC and it was maintained after leaving the temperature raise up to 15ºC (or also to room temperature). Then 10 eq. of styrene were added and a decrease of the two visible bands was observed, leading to a new featureless spectrum that could correspond to the formation of low valent Mn species.

A similar UV-vis study has been done for complex **C4** in presence of $NaHCO_3$ as additive (see Figure S 2 in the Supporting Information) and a parallel evolution of the spectrum was observed, also with similar bands to the ones displayed in Figure 3. We can then assert that the same type of active oxidizing species is formed in presence and absence of additives and thus the main role of the additive should be the control of the pH into the catalytic media, as stated previously.

To obtain more concise information that allows confirming the existence of a high-valent binuclear Mn_2-µ-oxo compound during the catalysis, EPR spectra were monitored during the epoxidation of styrene. The X-band EPR spectrum of an acetonitrile solution of **C4** recorded at 100K is shown in Figure 4 (a). Complex **C4** displays an EPR signal characteristic of a mononuclear high-spin Mn(II) complex (S = 5/2) with octahedral geometry incorporating chloride ligands.[59,60]
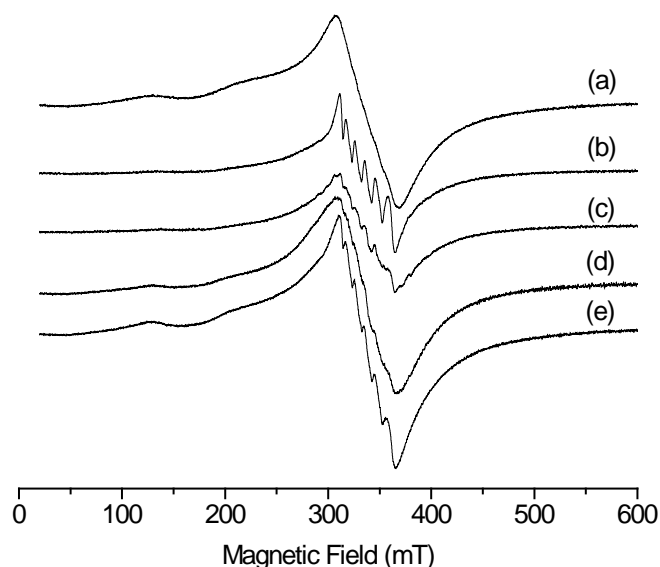

Figure 4. Evolution of the 100K X-band EPR spectrum of **C4** in CH_3CN at -40ºC (2 mM), upon addition of 2 eq. of peracetic acid and 10 eq. of styrene substrate: (a) initial, (b) 15 minutes after addition of peracetic acid, (c) 15 minutes after addition of styrene, (d) solution *c* after 3 hours at room temperature, and (e) 21 hours after addition of styrene at room temperature.

Upon addition of 2 eq. of peracetic acid at -40ºC, the EPR spectrum of the resulting brown solution (which displays the UV-vis spectrum shown in Figure 3 (d)) reveals the disappearance of the initial EPR signal with the concomitant appearance of a new 6-line signal centered at $g = 2.00$ (Figure 4 (b)), which corresponds to a new side-product Mn(II) mononuclear species probably present in low amount. The same solution has been recorded at 12 K (spectrum not shown) but no new features appear thus ruling out the formation of mononuclear Mn(IV) species. All these observations are consistent with the generation of a diamagnetic EPR-silent oxo-bridged Mn_2(IV,IV) binuclear complex as major species.[54-56] In such complexes, the two Mn ions are strongly antiferromagnetically coupled, leading to an S = 0 species.

After 3 hours at room temperature subsequently to the addition of styrene (Figure 4 (d)), the EPR spectra of the initial complex **C4** is restored.

To identify the nature of the catalytic brown species, ESI-MS on an acetonitrile solution of complex **C4** at 0ºC after addition of 2 equivalents of peracetic acid was carried out. The mass spectrum exhibits a ion peak at m/z = 746.9 whose mass and isotope distribution pattern corresponds to $[Mn_2^{IV,IV}((-)\text{-}\mathbf{L})_2O_2Cl_3]^+$ (Figure S 3 (a)), in accordance with the results yielded from EPR and UV-vis experiments that suggest the formation of bis-μ-O binuclear Mn(IV,IV) species. Note that the formation of this species has required the decoordination of one bidentate (–)-**L** ligand of complex **C4**.

The electrochemical oxidation of **C4** (seen in chapter 3), where a green solution of $[Mn^{III}Cl_2((-)\text{-}\mathbf{L})_2]^+$ was generated after bulk electrolysis, supports that the brown species formed by oxidation of **C4** with peracetic acid is not a simple electron transfer.

The same experiments were performed using complex **C1** instead of complex **C4**. Very similar UV-vis and EPR spectra have been obtained attesting that a similar di-μ-oxo Mn_2(IV,IV) active species is formed. This is confirmed by ESI-MS experiments with the detection of a peak at m/z = 771.2 whose mass and isotope distribution pattern corresponds to $[Mn_2^{IV,IV}((-)\text{-}\mathbf{L})_2O_2Cl_2(CH_3COO)]^+$ (Figure S 3 (b)).

UV-vis, ESI-MS and EPR spectrophotometric measurements at low temperature were also carried out using the mononuclear triflate complex **C5** as catalyst in a similar manner to that described above for complex **C4**, in order to gain insight into the nature of the reactive intermediates also in this case. Figure 5 shows the evolution of the UV-vis spectrum of an acetonitrile solution of complex **C5** upon addition of oxidant at -40°C

(solid lines) and subsequent addition of styrene at 15°C (dashed lines), monitored as previously described for complex **C4**. The spectrum obtained for the oxidized species differs from that obtained after oxidation of complex **C4** and displays a d-d transition around 640 nm, which is consistent with the presence of a mixed-valent Mn_2(III,IV) oxo-bridged species.[61,62] This point is also confirmed by EPR and ESI-MS experiments (see below).
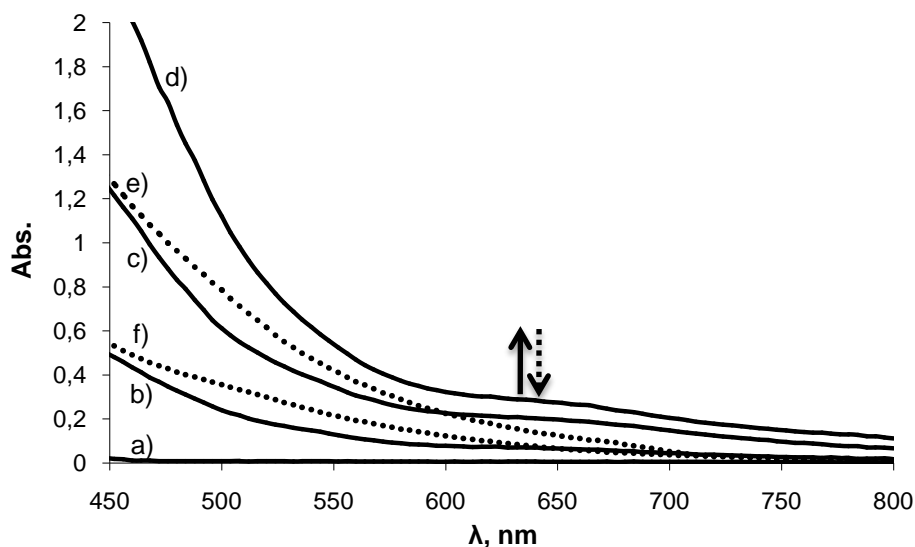

Figure 5. Evolution of UV-vis spectrum of complex **C5** in CH_3CN (2.5 mM), upon addition of 2 eq. of peracetic acid at -40ºC, warming up to 15ºC and subsequent addition of 10 eq. of styrene substrate. (a) initial, (b) 10 minutes after addition of peracetic acid, (c) 13 minutes after addition of peracetic acid, (d) 15 minutes after addition of peracetic acid, (e) 30 minutes after addition of styrene, (f) 24 hours after addition of styrene.

Upon addition of 2 eq. of peracetic acid to an acetonitrile solution of **C5** at -30ºC, the EPR spectrum of the resulting brown solution reveals a decrease of the intensity of the initial S = 5/2 signal to the benefit of a new multiline signal centered at $g = 2.00$ (Figure 6 (b)). This signal presents 16 lines regularly spaced by about 8 mT, highly characteristic of an oxo-bridged mixed-valent Mn_2(III,IV) binuclear complex.[54-56] In such complexes, the two Mn ions are strongly antiferromagnetically coupled, leading to an S = 1/2 species. The spectral width of 125 mT (from the first peak to the last one of the 16 line feature) is also consistent with a $[Mn^{III}(\mu\text{-}O)_2Mn^{IV}]$ core. The ESI-MS spectrum of this solution attests the formation of such species since two ion peaks at m/z = 760.2 and 850.2, assigned respectively to $[Mn_2^{III,IV}((-)\text{-}\mathbf{L})_2O_2(CH_3COO)_2]^+$ and $[Mn_2^{III,IV}((-)\text{-}\mathbf{L})_2O_2(CF_3SO_3)(CH_3COO)]^+$, are detected (Figure S 3 (c)). The peak corresponding to the mononuclear species $[Mn^{II}((-)\text{-}\mathbf{L})_2(CF_3SO_3)]^+$ is also detected at m/z = 704.3.

After addition of styrene to the reaction mixture at room temperature, the EPR 16-lines signal vanishes and the initial EPR spectra corresponding to complex **C5** is partially restored (Figure 6 (c-d)).
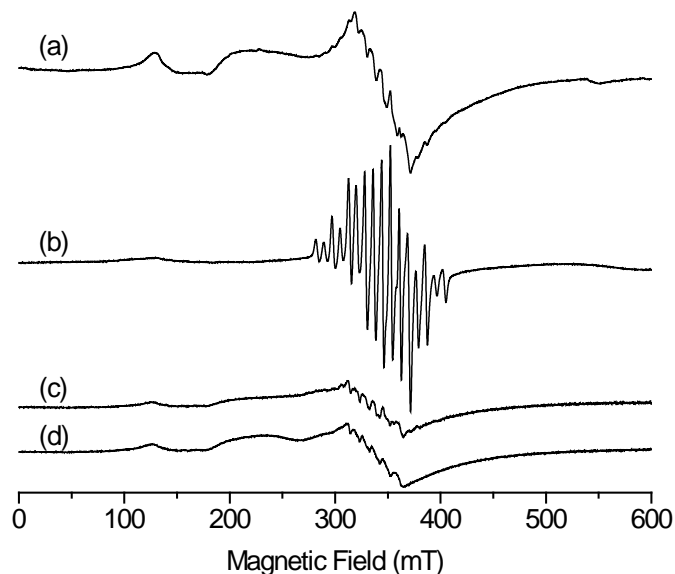

Figure 6. Evolution of the 100K X-band EPR spectrum of **C5** in CH_3CN at -30ºC (2.5 mM), upon addition of 2 eq. of peracetic acid and 10 eq. of styrene substrate: (a) initial, (b) 15 minutes after addition of peracetic acid, (c) after 3 hours subsequently to the addition of styrene at room temperature, and (d) 21 hours after addition of styrene at room temperature.

To the best of our knowledge, high-valent oxo-bridged or mononuclear oxo or peroxo manganese species have been proposed as active intermediates in some epoxidation reactions with peracids,[14,63-65] but not very clear evidences have been gained to this respect. The formation of high-valent di-µ-oxo binuclear complexes has been already evidenced in other catalytic oxidations mediated by Mn complexes using oxidants such as $^tBu\text{-}OOH$, H_2O_2 or hypochlorite,[66-69] with a mixed-valence (III,IV) dinuclear species postulated in most cases.

Based on UV-vis, ESI-MS and EPR spectroscopy results gathered for the oxidation of complexes **C1**, **C4** and **C5**, it can certainly be concluded that, for the epoxidation reactions carried out under the experimental conditions described above, a mixed-valent di-µ-oxo-bridged binuclear $Mn_2(III,IV)$ species operates as the active intermediate in epoxidation reactions mediated by the triflate compound **C5** whereas a di-µ-oxo-bridged binuclear $Mn_2(IV,IV)$ species is involved when using the chloro complexes **C1** and **C4**. These results are in line with the differences observed in the

catalytic performances for both categories of catalysts, chloro *vs* triflate, and also highlight the crucial importance that monodentate ligands seem to have in the fine tuning of the intermediate species formed during Mn oxidative catalysis, a topic that has been barely investigated to date.

The formation of the intermediate dinuclear species starting from the mononuclear complexes **C4** and **C5** involves the release of one of the bipyridyl ligands, which could be a consequence of steric restrains arising from the high volume of the pinene substituents. This is in accordance with the structure found for the dinuclear complex **C1**, where only one (–)-**L** ligand is bounded to each metal center, in contrast with other $\{Mn_2(\mu\text{-Cl})_2\}$ type of complexes bearing two smaller bidentate ligands at each Mn.[70,71]

4.4. Experimental section

4.4.1. Materials

All reagents used in the present work were obtained from Aldrich Chemical Co and were used without further purification. Reagent grade organic solvents were obtained from SDS and Scharlab and high purity de-ionized water was obtained by passing distilled water through a nano-pure Mili-Q water purification system.

4.4.2. Catalytic epoxidation

A CH_3CN (1 mL) solution of alkene (250 μmol), catalyst (2.5 μmol), additive (25 μmol) and biphenyl (250 μmol, internal standard) was prepared in a 10 mL flask and cooled in an ice bath. Afterwards, 32 % peracetic acid (500 μmol) was slowly added (over 3 minutes) via syringe under stirring at 0°C. The reaction vessel was then taken out of the ice bath (this is taken as the starting point of the catalysis) and allowed to progressively warm to RT. Each aliquot of the reaction taken for analysis was filtered through a basic alumina plug and was analyzed in a Shimadzu GC-2010 gas chromatography apparatus equipped with an Astec CHIRALDEX G-TA column and a FID detector, and quantification was achieved from calibration curves.

4.4.3. Catalytic epoxidation in ionic liquid:solvent media

Catalyst (2.5 μmol) and substrate (250 μmol) were dissolved in 2 mL of [bmim]PF_6:CH_3CN (1:1) (bmim = 1-butyl-3-methylimidazolium). 32% peracetic acid (500 μmol) was added via syringe over 3 minutes at 0°C. Afterward the solution was stirred at room temperature for 3 h. After completion, CH_3CN was rotavaporated and the resulting suspension was washed with diethylether (3x5 mL) to extract the epoxide (which is then analyzed by GC after addition of 250 μmol of biphenyl) and the oxidant by-products. The remaining mixture was washed with NaOH aqueous solution and dried in vacuo. A new load of substrate and oxidant dissolved in acetonitrile was then added and the mixture was left for an additional 3 h run. This procedure was repeated up to seven times.

4.4.4. Instrumentation and measurements

UV-vis spectroscopy was performed on a Cary 50 Scan (Varian) UV-vis spectrophotometer with 1 cm quartz cells. The low temperature control was performed with a cryostat from Unisoku Scientific Instruments, Japan. ESI-MS experiments were performed on a Navigator LC/MS chromatograph from Thermo Quest Finnigan, using acetonitrile as a mobile phase. X-band EPR spectra were recorded with a Bruker EMX, equipped with the ER 4116DM and ER-4192 ST Bruker cavity for the 12 K and 100 K experiments, respectively.

4.5. Conclusions

All the complexes synthesized in the previous chapter ([{Mn((−)-**L**)Cl}$_2$(μ-Cl)$_2$] (**C1**), [{Mn((−)-**L**)}$_2$(μ-OAc)$_3$](PF$_6$) (**C2**), [Mn((−)-**L**)Cl$_2$(H$_2$O)] (**C3**), [Mn((−)-**L**)$_2$Cl$_2$] (**C4**), [Mn((−)-**L**)$_2$(CF$_3$SO$_3$)$_2$] (**C5**) and [Mn((−)-**L**)$_2$)(NO$_3$)(H$_2$O)](NO$_3$) (**C6**)) have been tested in styrene epoxidation, being the chloro complexes **C1** and **C4** the ones exhibiting the highest conversion values. These chloro complexes have also been shown to catalyze epoxidation of other olefinic substrates with good efficiency and revealed to be specific for the *cis* epoxide when using *cis*-β-methylstyrene as substrate, in the absence of additives. Moreover, the epoxidation activity of these chloro complexes is strongly dependent on the steric encumbrance of the substrates employed. Complexes **C1** and **C4** constitute the first examples of Mn chloro complexes with simple N-ligands successfully applied in epoxidation catalysis.

The conversion and selectivity values of chloro complex **C4** are higher than those presented by the triflate complex **C5** with regard to the epoxidation of some aromatic and aliphatic alkenes under the same conditions.

Based on the UV-visible, ESI-MS and EPR spectroscopy results at low temperature, the active intermediate formed in situ is proposed to be an oxo-bridged binuclear Mn$_2$(IV,IV) species for the chloro complexes **C1** and **C4**, whereas a mixed-valent Mn$_2$(III,IV) species is found for the triflate compound **C5**. This is in accordance with the differences found in the catalytic performance particularly for the two mononuclear complexes **C4** and **C5** that pointed towards significant differences in the mechanism and/or the intermediate species involved in each case. This study revealed the crucial role of the monodentate ligands (chloro or triflate) attached to the metal center in the formation of the active intermediate species.

The formation of the intermediate dinuclear species starting from the mononuclear complexes **C4** and **C5** involves the release of one of the bipyridyl ((−)-**L**) ligands, which could be a consequence of steric restrains arising from the high volume of the pinene substituents.

New catalytic systems for the epoxidation of alkenes have been developed by using manganese chloro complexes as catalysts and peracetic acid as the oxidant in the presence of additives, which have shown to increase enormously the conversion and

selectivity values, especially for the case of NaHCO$_3$, when compared with the observed values in the absence of additives. The main role of the additives seems to be the control of the pH into the catalytic media because their basic nature can partially neutralize the acidity of the peracid added in large excess in the solution and thus prevent the decomposition of complexes into protonated ligand and free Mn^{2+}.

We have also investigated the Mn(II) chloro complexes **C1** and **C4** in epoxidation catalysis carried out in ionic liquid:solvent media ([bmim]PF$_6$:CH$_3$CN), a system that constitutes the first example of polypyridyl Mn(II) complexes tested under these conditions. Both catalysts display a remarkable effectiveness and selectivity for the epoxide product, with better results if compared to the use of acetonitrile as sole solvent. Both catalysts also show excellent reusability employing different substrates. The complex **C4** maintains a remarkable performance through up to 7-9 runs in all cases. The selectivity for the epoxide is well maintained for 1-octene and *trans*- and *cis*-β-methylstyrene but it progressively decreases for styrene. The overall turnover numbers are 298 for styrene, 271 for *cis*-β-methylstyrene, 596 for *trans*-β-methylstyrene and 168 for 1-octene. In the case of epoxidation of *cis*-β-methylstyrene the stereoselectivity for the *cis*-epoxide is maintained through all the runs. Catalyst **C1** also shows good reusability using styrene and 1-octene as substrates.

4.6. References

[1] Sheldon, R.A.; Kochi, J.K. *Metal Catalyzed Oxidation of Organic Compounds*; Academic Press; New York, **1981**.

[2] Gamez, P.; Aubel, P.G.; Driessen, W.L.; Reedjik, J. *Chem. Soc. Rev.* **2001**, *30*, 376-385.

[3] Robert, A.; Meunier, B. *Biomimetic Oxidations Catalyzed by Transition Metal Complexes*, Ed. Meunier, B.; Imperial College Press, **2000**, Ch. 12.

[4] Bruijnincx, P.C.A.; van Koten, G.; Gebbink, R.J.M.K. *Chem. Soc. Rev.* **2008**, 37, 2716-2744.

[5] Ko, S.Y.; Lee, A.W.M.; Masamune, S.; Reed, L.A.; Sharpless, K.B.; Walker, F.J. *Science* **1983**, *220*, 949-951.

[6] Nicolaou, K.C.; Winssinger, N.; Pastor, J.; Ninkovic, S.; Sarabia, F.; He, Y.; Vourloumis, D.; Yang, Z.; Li, T.; Giannakakou, P.; Hamel, E. *Nature* **1997**, *387*, 268-272.

[7] Gagnon, S.D.H.F. *Encyclopedia of Polymer Science and Engineering*, 2nd ed., Eds Mark, H.F.; Bikales, N.M.; Overberger, C.G.; Menges, G.; Kroschwitz, J.I.; John Wiley & Sons: New York, **1985**; Vol. 6, pp 273-307.

[8] Darensbourg, D.J.; Mackiewicz, R.M.; Phelps, A.L.; Billodeaux, D.R. *Acc. Chem. Res.* **2004**, *37*, 836-844.

[9] Ojima, I. Ed. *Catalytic Asymmetric Synthesis*, 2nd ed., Wiley & Sons: New York, **2000**.

[10] de Faveri, G.; Ilyashenko, G.; Watkinson, M. *Chem. Soc. Rev.* **2011**, *40*, 1722-1760.

[11] Jørgensen, K.A. *Chem. Rev.***1989**, *89*, 431-458.

[12] Katsuki, T. *Adv. Synth. Catal.* **2002**, *344*, 131-147.

[13] de Vos, D.E.; Sels, B.F.; Jacobs, P.A. *Adv. Synth. Catal.* **2003**, *345*, 457-473.

[14] Ho, K.-P.; Wong, W.-L.; Lam, K.-M.; Lai, C.-P.; Chan, T.H.; Wong, K.-Y. *Chem. Eur. J.* **2008**, *14*, 7988-7996.

[15] Groni, S.; Dorlet, P.; Blain, G.; Bourcier, S.; Guillot, R.; Anxolabéhère-Mallart, E. *Inorg. Chem.* **2008**, *47*, 3166-3172.

[16] Yin, G.; Danby, A.M.; Kitko, D.; Carter, J.D.; Scheper, W.M.; Busch, D.H. *Inorg. Chem.* **2007**, *46,* 2173-2180.

[17] Maruyama, K.; Tani, F.; Naruta, Y. *J. Chem Soc., Chem. Commun.* **1990**, 1378-1380.

[18] Groves, J.T.; Viski, P. *J. Org. Chem.* **1990**, *55*, 3628-3634.

[19] Meunier, B. *Chem. Rev.*, **1992**, *92*, 1411-1456.

[20] Jacobsen, E.N.; Zhang, W.; Muci, L.C.; Ecker, J.R.; Deng, L. *J. Am. Chem. Soc.* **1991**, *113*, 7063-7064.

[21] Palucki, M.; Finney, N.S.; Pospisil, P.J.; Güler, M.L.; Ishida, T.; Jacobsen, E.N. *J. Am. Chem. Soc.* **1998**, *120*, 948-954.

[22] Murphy, A.; Dubois, G.A.; Stack, T.D.P. *J. Am. Chem. Soc.* **2003**, *125*, 5250-5251.

[23] Murphy, A.; Stack, T.D.P. *J. Mol. Catal. A: Chem.* **2006**, *251*, 78-88;

[24] Murphy, A.; Pace, A.; Stack, T.D.P. *Org. Lett.* **2004**, *6*, 3119-3122.

[25] Kang, B.; Kim, M.; Lee, J.; Do, Y.; Chang, S. *J. Org. Chem.* **2006**, *71*, 6721-6727.

[26] Gómez, L.; Garcia-Bosch, I.; Company, A.; Sala, X.; Fontrodona, X.; Ribas, X.; Costas, M. *Dalton Trans.* **2007**, 5539-5545.

[27] Marchi-Delapierre, C.; Jorge-Robin, A.; Thibon, A.; Ménage, S. *Chem. Commun.* **2007**, 1166-1168.

[28] Sham, K-C.; Yeung, H-L.; Yiu, S-M.; Lau, T-C.; Kwong, H-L. *Dalton Trans.* **2010**, *39,* 9469-9471.

[29] Ilyashenko, G.; Sale, D.; Motevalli, M.; Watkison, M. *J. Mol. Catal. A: Chem.* **2008,** *296*, 1-8.

[30] Wu, M.; Wang, B.; Wang, S.; Xia, C.; Sun, W. *Org. Lett.* **2009**, *11*, 3622-3625.

[31] Ottenbacher, R.V.; Bryliakov, K.P.; Talsi, E.P. *Adv. Synth. Catal.* **2011**, *353*, 885-889.

[32] Lane, B.S.; Vogt, M.; DeRose, V.J.; Burgess, K. *J. Am. Chem. Soc.* **2002**, *124,* 11946-11954.

[33] Godbole, M.D.; Hotze A.C.G.; Hage, R.; Mills, A.M.; Kooijman, H.; Spek, A.L.; Bouwman, E. *Inorg. Chem.* **2005**, 9253-9266.

[34] Zhong, S.; Fu, Z.; Tan, Y.; Xie, Q.; Xie, F.; Xhou, X.; Ye, Z.; Peng, G.; Yin, D. *Adv. Synth. Catal.* **2008**, *350*, 802-806.

[35] de Boer, J.W.; Alsters, P.L.; Meetsma, A.; Hage, R.; Browne, W.R.; Feringa, B.L. *Dalton Trans.* **2008**, 6283-6295.

[36] Kilic H.; Adam, W.; Alsters P.l. *J. Org. Chem.* **2009**, *74*, 1135-1140.

[37] Centi, G.; Perathoner S. *Methods and Tools of Sustainable Industrial Chemistry: Catalysis,* in *Sustainable Industrial Chemistry,* Eds. Cavani, F.; Centi, G.; Perathoner, S.; Trifiró F.; Wiley-VCH Verlag GmbH & Co. KGaA, Weinheim, Germany, **2009**, Ch 2.

[38] Plechkova, N.V.; Seddon, K.R. *Chem. Soc. Rev.* **2008**, 37, 123-150.

[39] Earle, M.; Wasserscheid, P.; Schulz, P.; Olivier-Bourbigou, H.; Favre, F.; Vaultier, M.; Kirschning, A.; Singh, V.; Riisager, A.; Fehrmann, R.; Kuhlmann S. *Organic*

Synthesis, in *Ionic Liquids in Synthesis*, 2nd ed., Eds. Wasserscheid, P.; Welton, T.; Wiley-VCH Verlag GmbH & Co. KGaA, Weinheim, Germany, **2008**, Ch 5.

[40] Welton, T. *Coord. Chem. Rev.* **2004**, *248*, 2459-2477.

[41] Muzart, J. *Adv. Synth. Catal.* **2006**, *348*, 275-295.

[42] Parvulescu, V.; Hardacre, C. *Chem. Rev.* **2007**, *107*, 2615-2655.

[43] Fraile, J.M.; Garcia, J.I.; Mayoral, J.A. *Coord. Chem. Rev.* **2008**, *252*, 624-646.

[44] Gu, Y.; Li, G. *Adv. Synth. Catal.* **2009**, *351*, 817-847.

[45] Ochsner, E.; Schneiders, K.; Junge, K.; Beller, M.; Wasserscheid, P. *Appl. Cat. A* **2009**, *364*, 8-14.

[46] Betz, D.; Altmann, P.; Cokoja, M.; Herrmann, W.A.; Kühn, F.E. *Coord. Chem. Rev.* **2011**, *255*, 1518-1540.

[47] Liu, Y.; Zhang, H.-J.; Lu, Y.; Cai, Y.-Q.; Liu, X.-L. *Green Chem.* **2007**, *9*, 1114-1119.

[48] Zhang, H.-J.; Liu, Y.; Lu, Y.; He, X.-S.; Wang, X.; Ding, X. *J. Mol. Catal. A: Chem.* **2008**, *287*, 80-86.

[49] Tan, R.; Yin, D.; Yu, N.; Zhao, H.; Yin, D. *J. Catal.* **2009**, *263*, 284-291.

[50] Teixeira, J.; Silva, A.R.; Branco, L.C.; Afonso, C.A.M.; Freire, C. *Inorg. Chim. Acta* **2010**, *363*, 3321-3329.

[51] Ho, K-P.; Wong, W-L.; Lee, L.Y.S.; Lam, K-M.; Chan, T.H.; Wong, K-Y. *Chem. Asian J.* **2010**, *5*, 1970-1973.

[52] White, M.C.; Doyle, A.G.; Jacobsen, E.N. *J. Am. Chem. Soc.* **2001**, *123*, 7194-7195.

[53] Nehru, K.; Kim, S.J.; Kim, I.Y.; Seo, M.S.; Kim, Y.; Kim, S.-J.; Kim, J.; Nam, W. *Chem. Commun.* **2007**, 4623-4625.

[54] Baffert, C.; Dumas, S.; Chauvin, J.; Leprêtre, J.-C.; Collomb, M.-N.; Deronzier, A. *Phys. Chem. Chem. Phys.* **2005**, *7*, 202-210.

[55] Baffert, C.; Collomb, M.-N.; Deronzier, A.; Pécaut, J.; Limburg, J.; Crabtree, R.H.; Brudvig, G.W. *Inorg. Chem.* **2002**, *41*, 1404-1411.

[56] Romain, S.; Duboc, C.; Retegan, M.; Lepretre, J.-C.; Blackman, A.G.; Deronzier, A.; Collomb, M.-N. *Inorg. Chim. Acta* **2011**, *374*, 187-196.

[57] Baffert, C.; Collomb, M.-N.; Deronzier, A.; Kjaergaard-Knudsen, S.; Latour, J.-M.; Lund, K.H.; McKenzie, C.J.; Mortensen, M.; Nielsen L.P.; Thorup, N. *Dalton Trans.* **2003**, 1765-1772.

[58] Berggren, G.; Thapper, A.; Huang, P.; Eriksson, L.; Styring, S.; Ander, M.F. *Inorg. Chem.* **2011**, *50*, 3425-3430.

[59] Duboc, C.; Astier-Perret, V.; Chen, H.; Pécaut, J.; Crabtree, R.H.; Brudvig, G.W.; Collomb, M.-N. *Inorg. Chim. Acta* **2006**, *359*, 1541-1548.

[60] Rich, J.; Castillo, C.E.; Romero, I.; Rodriguez, M.; Duboc, C.; Collomb, M.-N. *Eur. J. Inorg. Chem.* **2010**, 3658-3665.

[61] Hureau, C.; Blondin, G.; Charlot, M.-F.; Philouze, C.; Nierlich, M.; Césario, M.; Anxolabéhère-Mallart, E. *Inorg. Chem.* **2005**, *44*, 3669-3683.

[62] Glerup, J.; Goodson, P.A.; Hazell, A.; Hazell, R.; Hodgson, D.J.; McKenzie, C.J.; Michelsen, K.; Rychlewska, U.; Toftlund, H. *Inorg. Chem.* **1994**, *33*, 4105-4111.

[63] Lee, S.H.; Xu, L.; Park, B.K.; Mironov, Y.V.; Kim, S.H.; Song, Y.J.; Kim, C.; Kim, Y.; Kim, S.-J. *Chem. Eur. J.* **2010**, *16*, 4678-4685.

[64] Ottenbacher, R.V.; Bryliakov, K.P.; Talsi, E.P. *Inorg. Chem.* **2010**, *49*, 8620-8628.

[65] Song, Y.J.; Lee, S.H.; Park, H.M.; Kim, S.H.; Goo, H.G.; Eom, G.H.; Lee, J.H.; Lah, M.S.; Kim, Y.; Kim, S.-J.; Lee, J.E.; Lee, H.-I.; Kim, C. *Chem. Eur. J.* **2011**, *17*, 7336-7344.

[66] Menage, S.; Collomb-Dunand-Sauthier, M.-N.; Lambeaux, C.; Fontecave, M. *J. Chem. Soc., Chem.Commun.* **1994**, 1885-1886.

[67] Tietz, T.; Limberg, C.; Stöber, R.; Ziemer, B. *Chem. Eur. J.* **2011**, *17*, 10010-10020.

[68] Bryliakov, K.P.; Kholdeeva, O.A.; Vanina, M.P.; Talsi, E.P. *J. Mol. Catal. A: Chem.* **2002**, *178*, 47-53.

[69] Campbell, K.A.; Lashley, M.R.; Wyatt, J.K.; Nantz, M.H.; Britt, R.D. *J. Am. Chem. Soc.* **2001**, *123*, 5710-5719.

[70] Van Albada, G.A.; Mohamadou, A.; Driessen, W.L.; De Gelder, R.; Tanase, S.; Reedijk, J. *Polyhedron* **2004**, *23*, 2387-2391.

[71] Wang, Z.M.; Yuan, M.; He, Z.; Liao, C.S.; Yan, C.H. *Acta Chim. Sinica* **2000**, *58*, 1615-1625.

4.7. Supporting information

Table S 1. Optimization of the procedure for the epoxidation of styrene as test substrate in ionic liquid:solvent media with $MnCl_2((-)\text{-}L)_2$, **C4**, as catalyst. Conditions: styrene (250 μmol), catalyst (2.5 μmol), peracetic acid (500 μmol), total volume = 2 ml, RT, 3h. Conversions and yields are evaluated by GC analysis with biphenyl as internal standard.

Entry	[bmim]PF$_6$:solvent ratio	Solvent	Washing with NaOH	Runs
1	1/0	-	No	1
2	1/1	CH$_3$CN	No	2
3	1/1	CH$_2$Cl$_2$	No	1
4	1/0	-	Yes	4[a]
5	1/1	CH$_3$CN	Yes	8
6[b]	1/1	CH$_3$CN	Yes	8[c]

[a] Good conversion, low selectivity.
[b] 275 μmol peracetic acid (110 eq.).
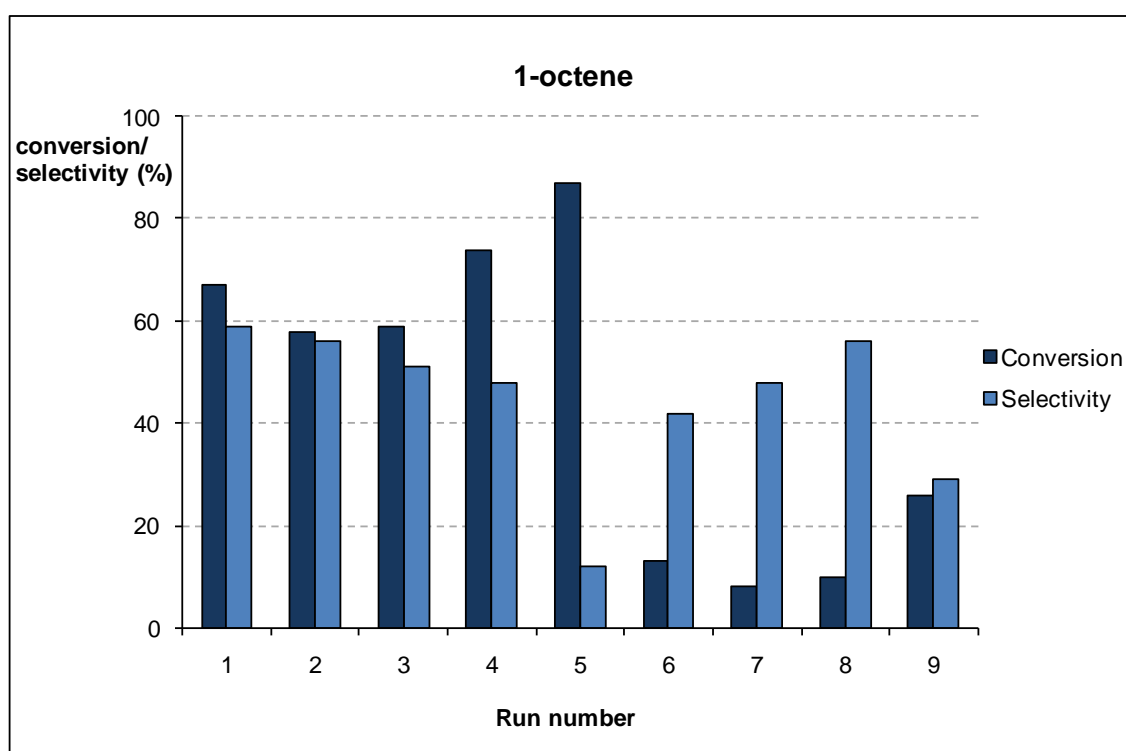[c] Lower conversion and selectivity than the obtained in entry 5.
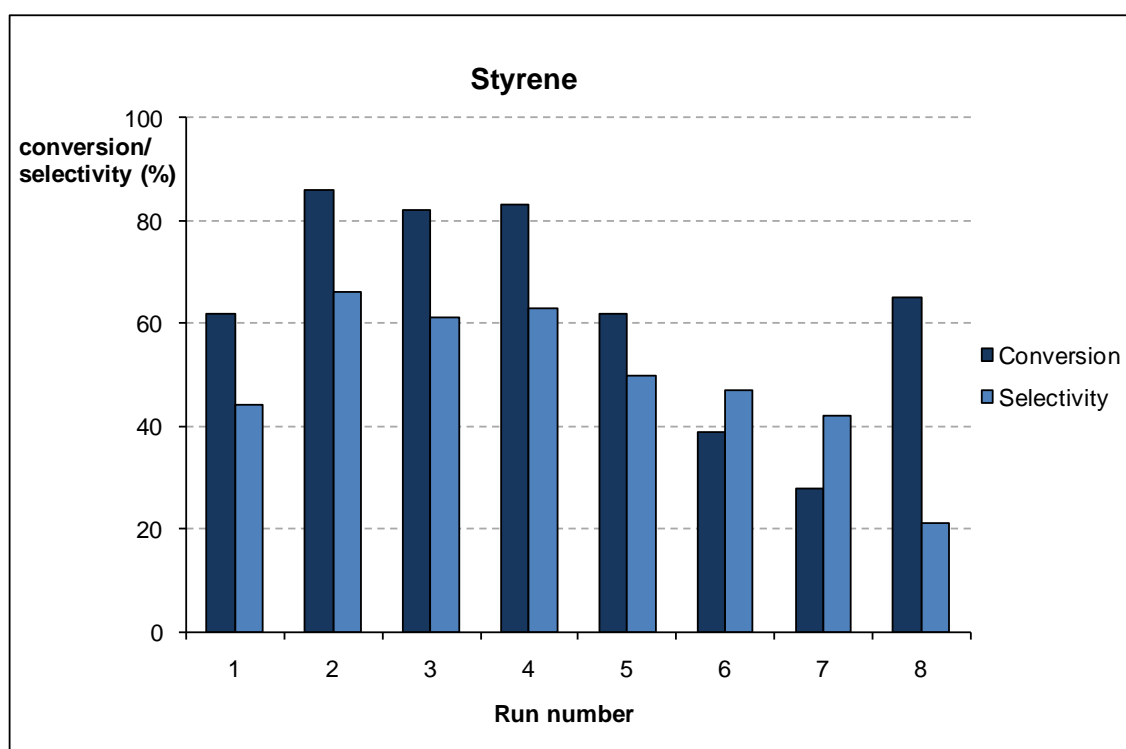
Figure S 1. Conversion and selectivity values obtained throughout a number of consecutive reuses of complex **C1** in the epoxidation of different substrates in [bmim]PF$_6$:CH$_3$CN.
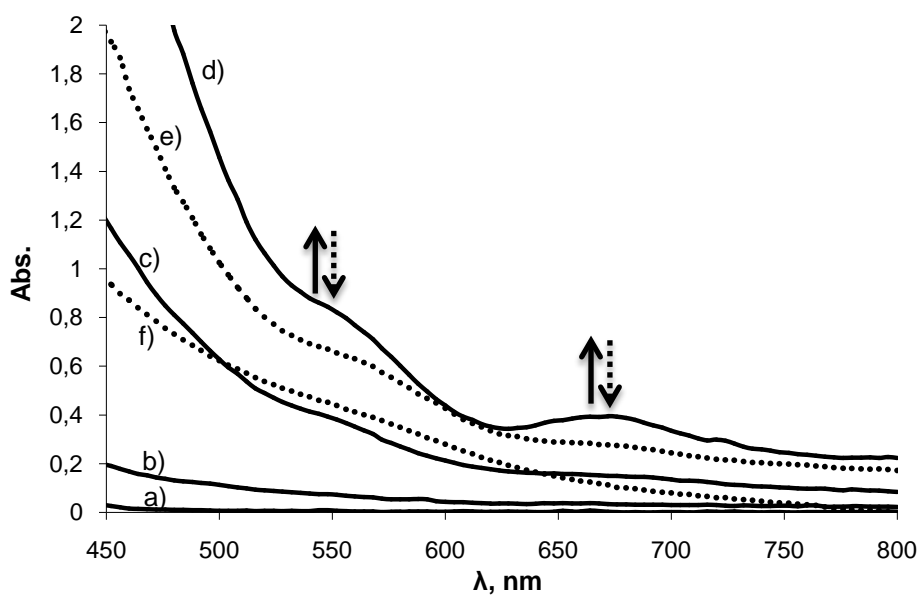
Figure S 2. Evolution of UV-vis spectrum of complex **C4** in CH$_3$CN (2.5 mM), upon addition of 2 eq. of peracetic acid at -40ºC, warming up to 15ºC and subsequent addition of 10 eq. of styrene substrate at 15ºC, in presence of NaHCO$_3$ as additive. (a) initial, (b) 24 seconds after addition of peracetic, (c) 30 seconds after addition of peracetic, (d) 15 minutes after addition of peracetic, (e) 1 hour after addition of styrene, (f) 41 hours after addition of styrene.

a)
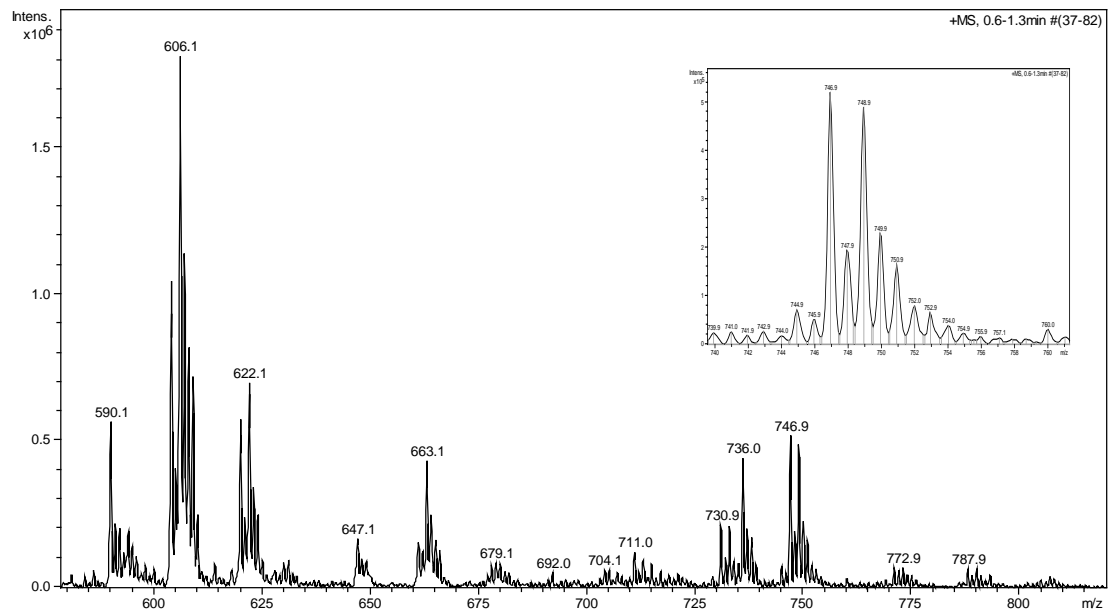
b)
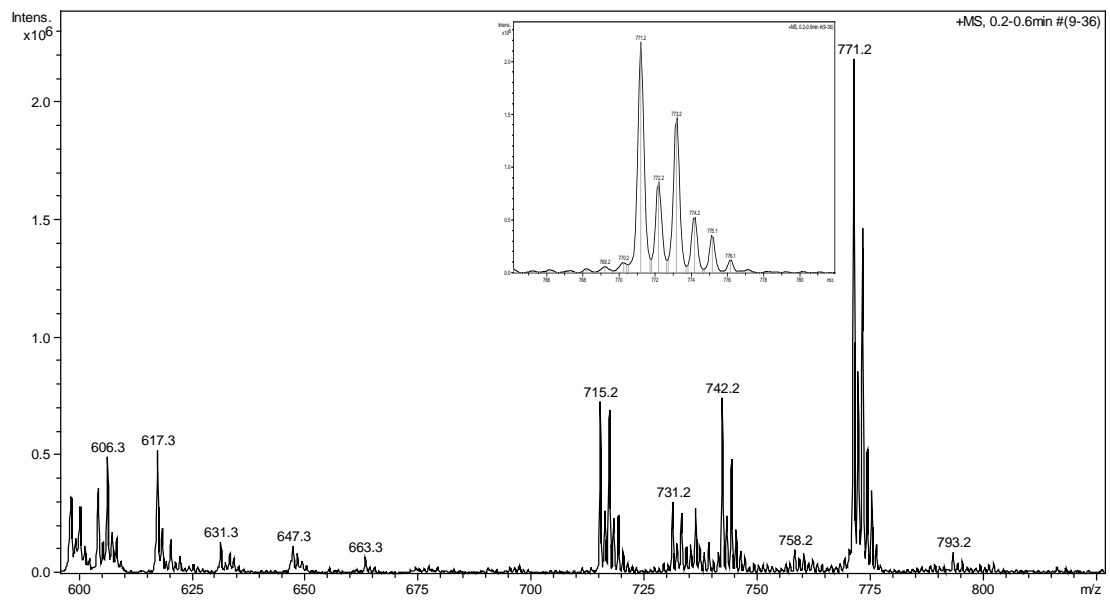
c)

Figure S 3. ESI-MS spectra formed after addition of 2 eq. of peracetic acid in a solution of the corresponding complex in CH_3CN at 0ºC (2.5 mM). a) Complex **C4**. b) Complex **C1**. c) Complex **C5**.
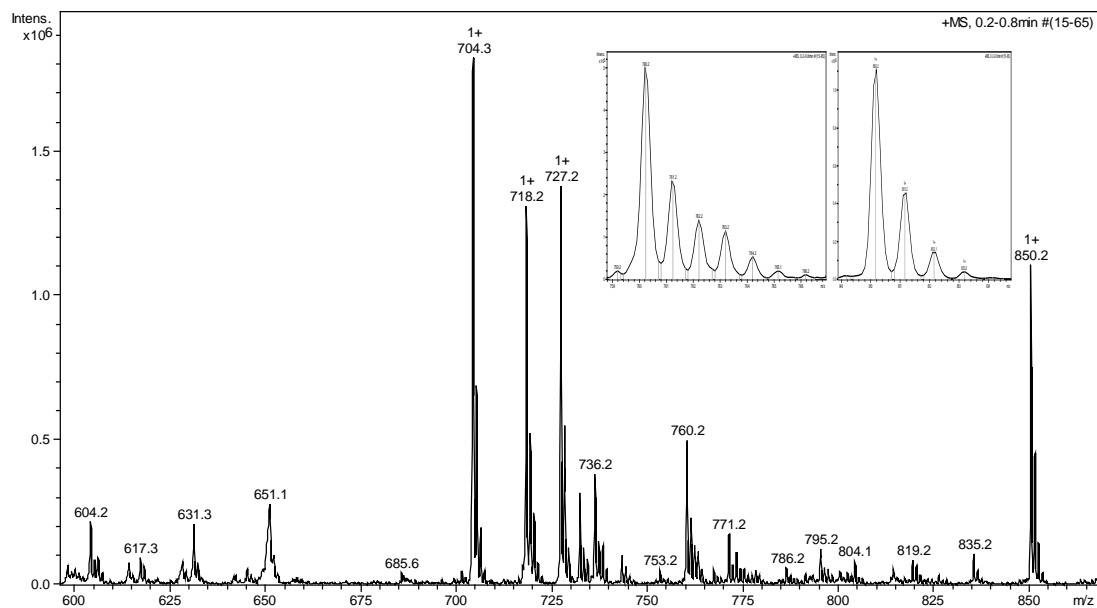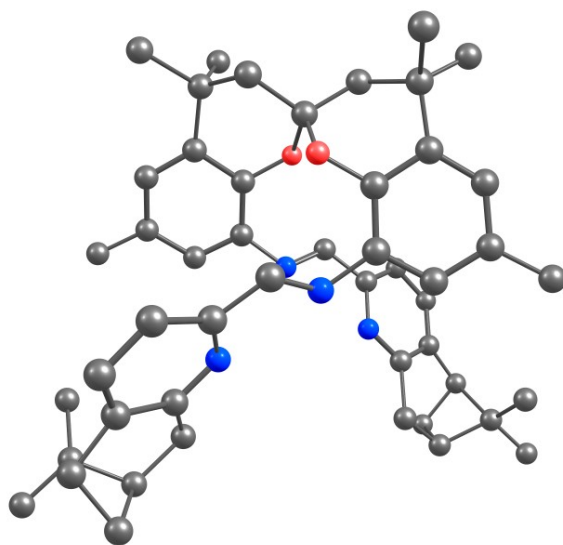
Chapter 5

New N-tetradentate SPANamine type of ligands and their Mn(II) complexes as catalysts for epoxidation of alkenes.

Five new tetradentate N-donor ligands with the spirobi(chroman) skeleton (either chiral or racemic) have been synthesized and fully characterized by NMR, ESI-MS and optical polarimetry. These ligands have been coordinated to a series of manganese salts affording a family of new chiral and racemic Mn (II) complexes, which have also been characterized through analytical and spectroscopic techniques. The crystallographic structure of five of them has been obtained by X-Ray diffraction, all showing distorted octahedral geometry with the ligand adopting a *cis*-α conformation over the Mn ion. All the complexes have been tested in the catalytic epoxidation of styrene and the conversion and selectivity values increase in presence of additives in the catalytic media. Experimental results and computational calculations demonstrate the stereospecificity for the *cis* epoxide in the epoxidation of *cis*-β-methylstyrene mediated by one of the complexes synthesized.

TABLE OF CONTENTS

CHAPTER 5. New N-tetradentate SPANamine type of ligands and their Mn(II) complexes as catalysts for epoxidation of alkenes.

5.1. Introduction

5.1.1. Spiro ligands

Great attention has been paid by the scientific community to metal-catalyzed asymmetric synthesis because it provides a powerful and economical tool for the synthesis of optically active organic compounds of biological importance such as chiral pharmaceuticals, agrochemicals, flavours, fragrances or advanced materials. In the past decades, enormous efforts have been dedicated to this important field and many efficient catalytic asymmetric reactions have been developed.[1,2] Concretely olefin epoxidation has received considerable interest from both academics and industry.[3,4] The discovery of more efficient and enantioselective chiral ligands and catalysts will undoubtedly promote the development of highly economical and environmental benign chiral technologies for the preparation of chiral compounds.

The development of new efficient chiral ligands is one of the most challenging tasks in asymmetric catalysis. Many aspects have to be considered for the ligand design such as an appropriate backbone for the ligand, an effective asymmetric environment, ease of ligand modification, coordinating sites to the metal, formation of a number of diastereoisomers, their separation and resolution, economical and short step synthesis, etc. Overall, the key for the development of asymmetric catalysts consists of an efficient chiral ligand with an appropriate affinity for the metal and a suitable chiral scaffold to construct an effective asymmetric environment.

A large number of studies during the past decades have led to thousands of chiral bidentate phosphines,[5-7] oxazolines,[8,9] diamines[10,11] and hybrid P,N ligands.[12] In the last 40 years, a huge number of efficient chiral metal catalysts bearing this type of ligands have been developed, but only a few of them, which can mediate efficiently and enantioselectively more than one unrelated reactions, can be considered "privileged chiral catalysts". Most of these catalysts are metal complexes containing relatively rigid chiral ligands, in particular the ones possessing a C_2-symmetric skeleton. Important members of privileged chiral catalysts include BINAP,[13] DuPhos,[14] Bisoxazoline,[15-18] and Salen derivatives, that have been extensively developed.[19-21]

In contrast, spiranes represent a new class of relatively less explored chiral ligands.[22,23] Molecules containing a spirocyclic backbone have a quaternary carbon atom (spiro

carbon), which joins two cyclic rings and makes them lie in perpendicular planes. The introduction of substituents on the rings of the spiro backbone usually generates a diversity of chiral derivatives and increases the difficulty in the synthesis of their optically pure forms (the resolution of racemates through fractional crystallization or chromatography is normally required for obtaining a pure enantiomer). However, the attachment of benzyl groups to the two perpendicular rings gives rise to the unique axial chirality (Figure 1). Apart of restricting the relative rotation of the two rings (thus giving rise to the axial chirality generally found in spiro compounds having substituents on the rings), this structural feature also increases molecular rigidity. This rigidity of the spirocyclic framework can minimize the number of possible conformations of the catalytic species and hence giving more selectivity in the asymmetric synthesis.

With these characteristics, axially chiral spiroskeleton, especially the C_2-symmetric spiranes, is an excellent scaffold for chiral ligands.

| C_2-symmetric achiral, rigid | C_2-symmetric axially and centrally chiral, rigid | C_2-symmetric axially chiral, highly rigid |
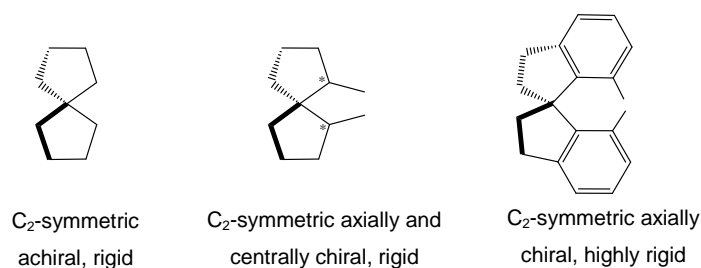
Figure 1. Spirane chirality.

The highly rigid chiral ligands having a spiro backbone such as spiro[4,4]nonane and spirobiindane (Figure 2) have emerged as a new class of efficient chiral ligands for a wide range of transition-metal-catalyzed asymmetric reactions. In 1992, Kumar used chiral spiro diols *cis,cis*-(+) and (-)-spiro[4,4]nonane-1,6-diol not as ligands but as chiral auxiliaries in the reduction of ketones with lithium aluminium hydride, leading to the corresponding alcohols with good enantioselectivities (85-90% ee).[24] In 1997, Chan and Jiang used the chiral spiro diol as a backbone to synthesize the chiral bis(phosphinite) ligand SpiroOP and reported the catalytic activity of rhodium catalysts bearing it, that displayed high efficiency and enantioselectivity (95-100% ee) in the asymmetric hydrogenation of α-dehydroamino acid derivatives.[25] This is the first example of spiro chiral catalysts applied in asymmetric reactions; this pioneering work initiated the search for alternative chiral ligands with a spiro skeleton.
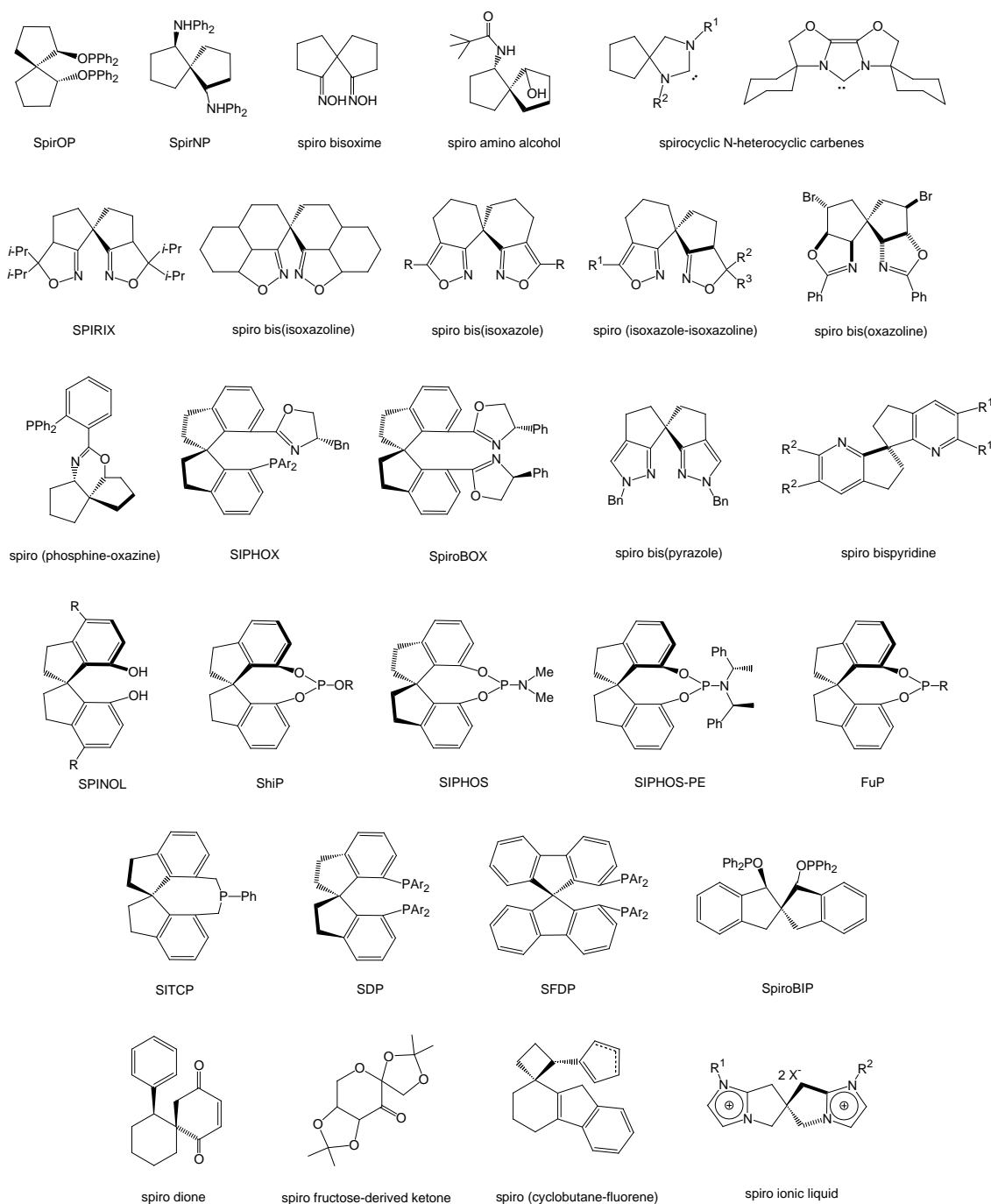
Figure 2. Chiral spiro ligands.

In this line, Sasai et al. reported a type of spiro bis(isoxazoline) ligands based on the spiro[4,4]nonane skeleton.[26-28] These new chiral spiro dinitrogen ligands, known as SPIRIX, showed excellent asymmetric induction in the palladium-catalyzed tandem Wacker-cyclization process, producing chiral bicyclic compounds. Zhou and Xie designed and synthesized a series of spiro chiral ligands bearing a spirobiindane or spirobifluorene backbone.[29] These spiro chiral ligands include monodentate phosphoramidites (SIPHOS),[30,31] diphosphines (SDP),[32,33] phosphine-oxazolines

(SIPHOX)[34] and bisoxazolines (SpiroBOX).[35] The transition metal complexes of these spiro chiral ligands exhibited excellent enantioselectivity and reactivity for a wide range of asymmetric reactions such as hydrogenation, carbon-carbon bond-forming reaction or carbon-heteroatom bond-forming reactions. Other research groups are involved in development of chiral spiro ligands and a variety of chiral ligands with different spiro backbones have been reported.[36-42] The corresponding metal complexes of these spiro chiral ligands were also efficient chiral catalysts for many asymmetric reactions.

As a summary, all the ligands shown in Figure 2 have been coordinated to transition metals such as Rh, Pd, Cu, Ru, Ir, Co, etc. Afterwards the catalysts were tested in asymmetric catalytic reactions such as hydrogenations, addition of arylboronic acids to aldehydes, hidrosilylation, allylic alkylations, hydrovinylation, Michael reactions, Diels-Alder reactions, Pauson-Khand reaction, ring opening, allylic oxidation, cyclopropanation, allylation of aldehydes, coupling reactions, cyclization reactions, carbon-heteroatom bond forming reaction, etc. All the complexes were efficient in the corresponding catalytic asymmetric reaction, obtaining excellent enantioselectivities (most of them between 90 and 100%).

It is also known an example of asymmetric epoxidation of *trans*-olefins with the fructose-derived ketone, which gives moderate yields and high enantioselectivities using oxone as oxidant and $NaHCO_3$ in CH_3CN-aqueous EDTA media. However, this reaction requires a high loading of ketone and it can't be considered a catalytic reaction (1 equivalent of substrate and 3 equivalents of ketone are used per mol of catalyst).[43]

It has been demonstrated that the enantioselectivities achieved with a chiral spiro skeleton with fused benzenes are distinctly superior to those obtained with other ligands having a different backbone. However, a large number of reactions still lack effective chiral ligands, and the enantioselectivities in many reactions are substrate-dependent.

The dramatic increment in the number of publications that have appeared in the last 10 years describing the design and synthesis of chiral spiro ligands and their utility in metal-catalyzed asymmetric reactions illustrates the rapid growth of this research area. Spiro ligands can emerge as a new class of chiral ligands in asymmetric catalysis and the development of efficient synthetic methods is an important task.

5.1.2. Spirobi(chroman) ligands (SPAN)

In the recent years, van Leeuwen *et al*. have developed a new series of preferentially trans-coordinating spirobi(chroman) diphosphanes (SPANphos), and their catalytic applications have been studied.[44-46] This spirobi(chroman) skeleton is flexible enough to allow for the formation of *cis* complexes when *trans* sites are not available. However, while the synthesis and catalytic application of spirobi(chroman) phosphorus ligands has been intensively investigated, nitrogen-containing analogous remain largely unexplored.

Van Leeuwen's group have also described a series of spirobi(chroman) amine and imine ligands (SPANamine, Figure 3). Their first application was the palladium catalyzed asymmetric resolution of phenylethanol by an oxidation reaction.[47] In 2011 they reported the catalytic asymmetric α-fluorination of β-keto esters in presence of nickel salts, with *ee* up to 63%. The same enantioselectivity was obtained when SPANamine was used as organocatalyst, although the reaction was much slower.[48]
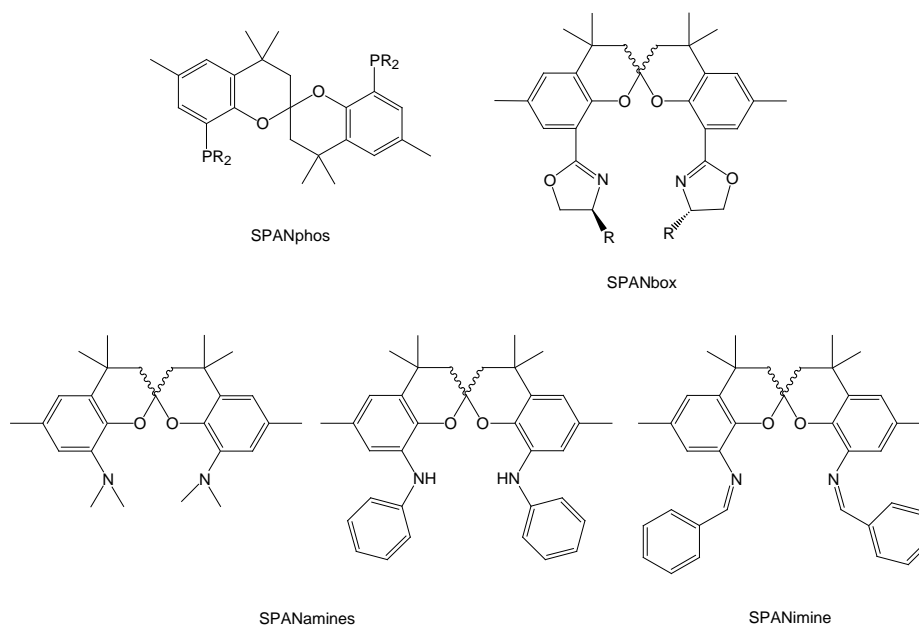

Figure 3. Spirobi(chroman) ligands.

In 2011 Ding *et al*. developed spirobi(chorman) bisoxazoline (SPANbox) ligands (Figure 3). They also tested the Zn complexes prepared "in situ" in hydroxylation of β-keto esters giving excellent activity and enantioselectivity (90-98% ee) with a catalyst loading of 0.1-5 mol %.[49]

5.1.3. Linear tetradentate N-donor ligands

Transition-metal complexes with ligands containing nitrogen-donor atoms constitute an important class of coordination compounds able to perform a wide range of asymmetric transformations.[11,50-52] Nitrogen-based ligands have well-known advantages such as chemical robustness, wide availability in enantiomerically pure form (from the chiral pool or through well-established racemate resolutions), rich coordination chemistry in combination with inexpensive first-row transition metals, and stabilization of high-oxidation-state transition-metal species (useful for oxidation catalysis). Among this type of ligands, those containing sp^2-hybridized nitrogen donor atoms such as chiral oxazolines[8,9] or pyridines,[53-55] porphyrines[56] and Salen[19-21] have received much attention during the last decades.

On the other hand, linear tetradentate N-donor ligands have been largely studied, combining amines or imines with N-heterocycles. This kind of linear ligands can coordinate to manganese in 3 different conformations (Figure 4).[57-62]

Cis-α   *Cis*-β   *Trans*
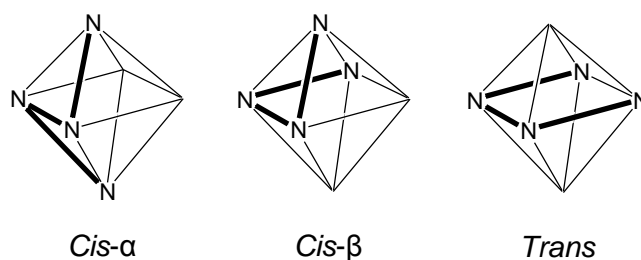
Figure 4. Different topologies that a linear tetradentate ligand can adopt.

Based on the success obtained with this kind of ligands, it appears that multidentate ligands containing nitrogen-donor sites (preferably pyridine) and a *cis* orientation of two labile coligands are desirable criteria in catalyst design. The *cis*-α geometries in transition metal complexes is believed to be important for high catalytic activity in oxidation reactions.

The efficiency of manganese complexes with tetradentate N-donor ligands (Figure 5) in oxidation reactions has been largely demonstrated.[63-68] Concretely, asymmetric epoxidation of olefins with H_2O_2 has been studied with chiral ligands obtaining high conversion and enantioselectivities, but these processes suffer from a limited substrate scope and relatively high catalyst loadings (usually 2-5%).

Recent studies also describe manganese (II) complexes with tetradentate N-donor ligands as catalysts in epoxidation reactions using peracetic acid as oxidant. In these cases the catalysts are very fast and efficient though the enantioselectivities obtained are relatively poor.[69]
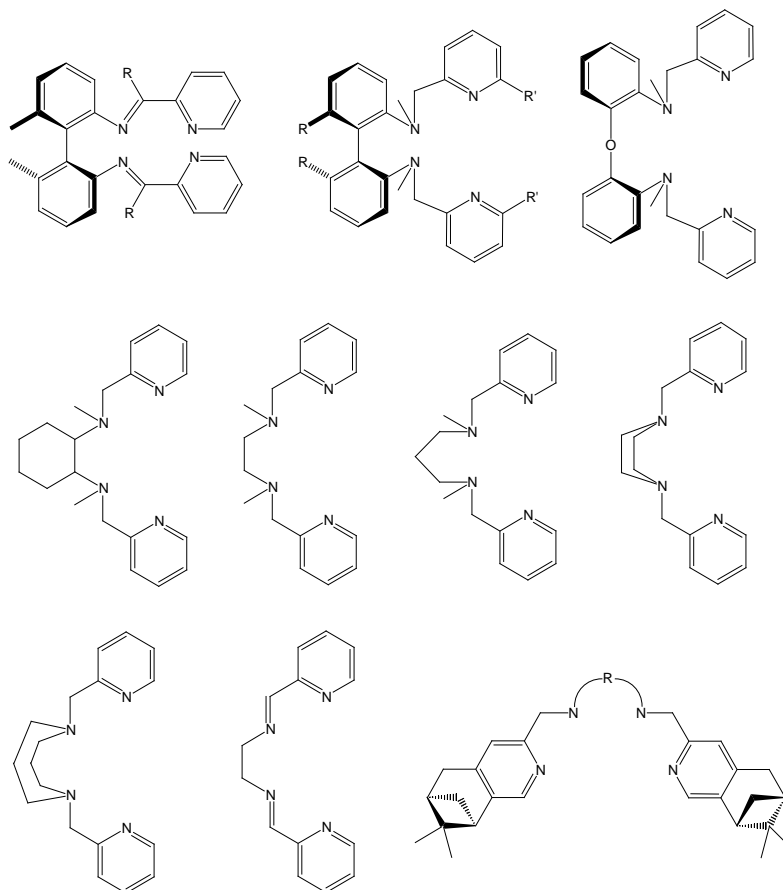
Figure 5. Amino and imino tetradentate N-heterocyclic ligands.

In the context of chiral ligand design, spiro backbone has been recognized as one of the privileged structures for the construction of chiral ligands. On the other hand, the efficient coordinative potential of N-heterocyclic ligands is well-established in inorganic chemistry. However, only few examples are known of chiral spiro ligands bearing N-heterocycles as metal coordinating units. Zhou et al decided to combine pyridyl and L-proline derived rings (Figure 6) together with a spiro skeleton.[70,71]

Figure 6. Amino and N-heterocyclic spiro ligands.

The proline derived ligand was used in asymmetric aldol reactions as organocatalyst, while the pyridyl ligands were coordinated to Co as bidentate ligands to be tested for Michael addition catalysis, giving in both cases good yields and moderate enantioselectivities.

5.2. Objectives

In the last decade, some chiral spiro ligands and tetradentate N-donor ligands have been developed. However, the combination of both features into an 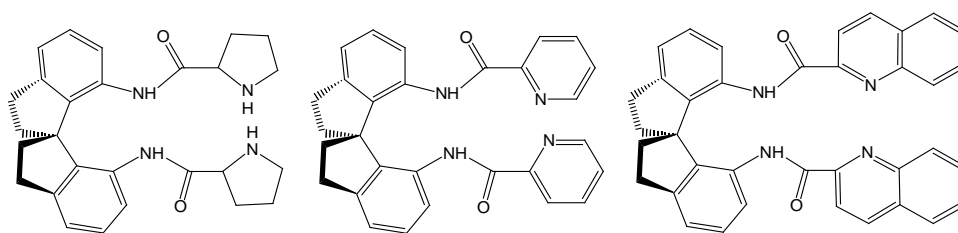unique type of ligand remains still unexplored. With all this in mind, we were interested in the development of chiral spiro ligands bearing N-heterocycles, as well as their behaviour in the coordination to transition metals and the catalytic activity of the complexes obtained.

Taking advantage of our experience with pinene groups fused to pyridines, we considered to combine the spirobi(chroman) backbone with different pyridine rings (Chart 1): (a) a simple pyridine, (b) a pyridine with a pinene group in the 4,5 position and (c) a pyridine with a pinene group in the 5,6 position. The introduction of such pinene groups provides two new chiral centers in the ligand structure.
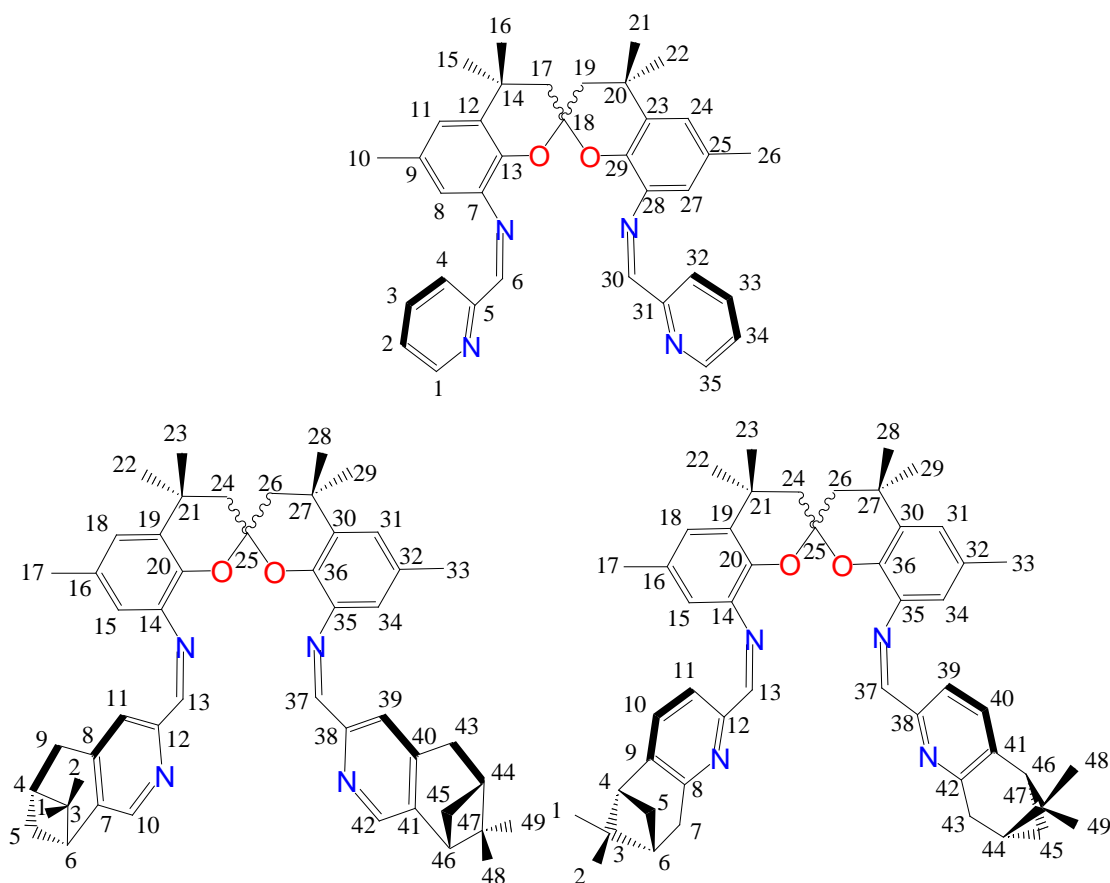
Chart 1. Ligands synthesized in this chapter.

Another goal of this chapter was to coordinate these ligands to different manganese (II) salts and fully characterize the resulting complexes through structural, analytical and

spectroscopic (IR, ESI-MS) techniques. The coordination of these ligands to manganese will provide a series of complexes potentially useful as catalysts for asymmetric reactions.

We were also interested in the reactivity of these compounds with regard to the asymmetric epoxidation of alkenes with the idea to evaluate the influece exerted by each ligand on the catalytic activity and the enantioselectivity. We also considered studying the influence of additives in the catalytic media.

Finally, we were concerned with the stereospecificity of the complexes in the epoxidation of *cis*-β-methylstyrene and we considered studying it by means of computational calculations.

5.3. Results and discussion

5.3.1. Synthesis and characterization of the ligands

Prior to the synthesis of the tetradentate N-donor spiro ligands (SPAN), the synthesis of two precursors was required: the spiroamine bi(chroman) backbone and the N-heterocyclic aldehydes bearing a pinene group.

The racemic and enantiopure spiroamine backbones (**1**, **(+)-1**, **(-)-1**) were synthesized by the van Leeuwen group following two different methods previously described by themselves (Scheme 1 and Scheme 2).[47,72]
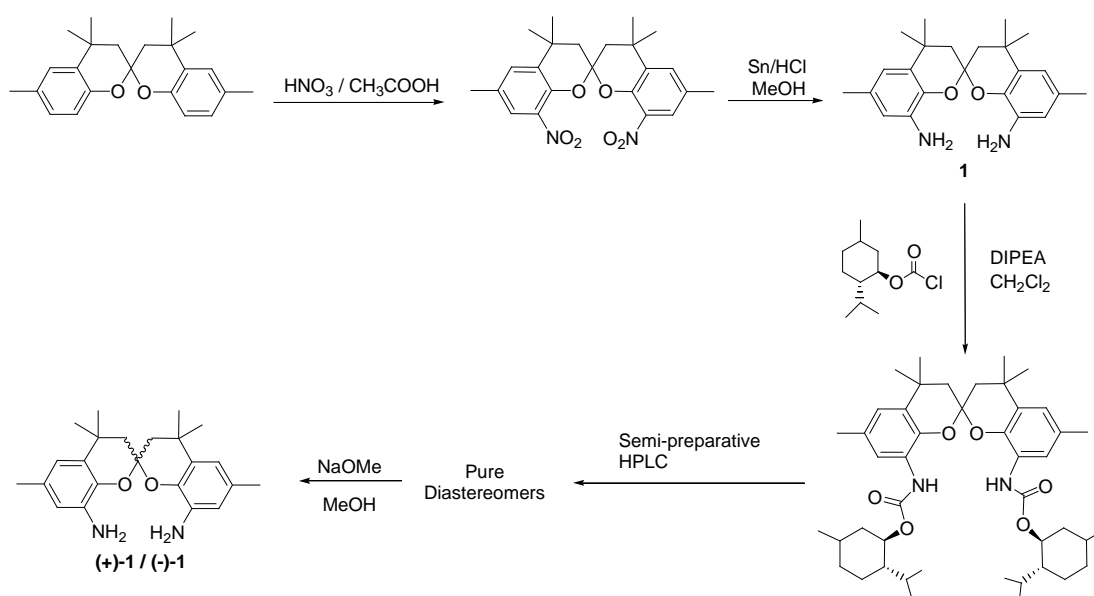
Scheme 1. Synthesis of the SPANamine backbone, route 1.
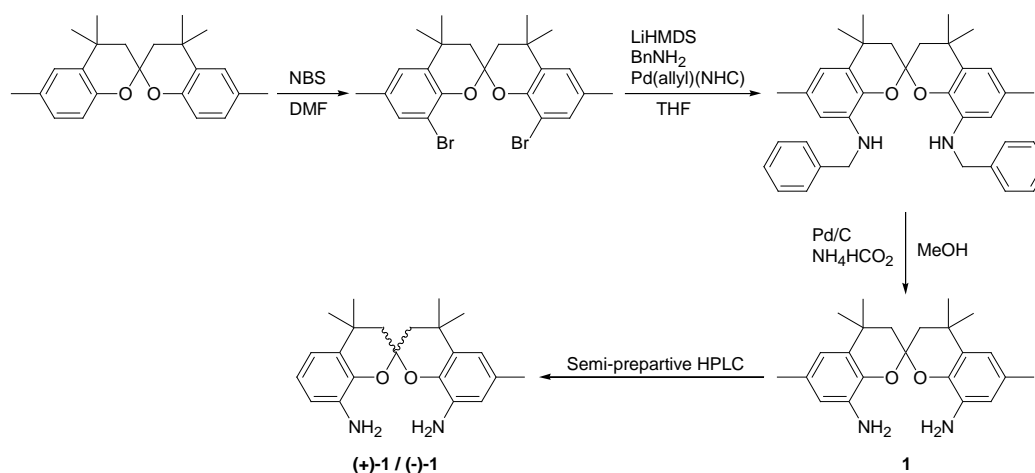
Scheme 2. Synthesis of the SPANamine backbone, route 2.

The two aldehydes bearing pinene groups were synthesized following two different procedures. The aldehyde **2**, containing the pinene group in the positions 5 and 6 of the pyridine, was prepared from the commercially available (-)-α-pinene following the method described in the literature (Scheme 3).[73]

Scheme 3. Synthesis of the aldehyde-pinene 5,6.

On the other hand, the aldehyde containing a pinene group in the positions 4 and 5 of the pyridine (**3**) was prepared from the commercially available (-)-myrtenal following the method described in the literature (Scheme 4).[74]
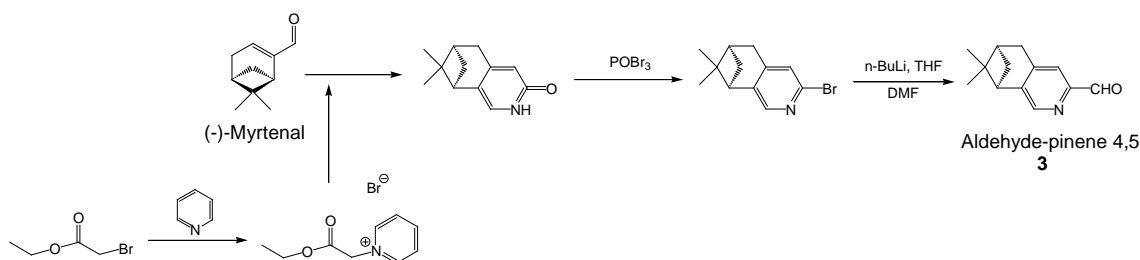
Scheme 4. Synthesis of the aldehyde-pinene 4,5.

SPANamines **1**, **(+)-1** and **(-)-1** have been employed as a racemic and enantiopure building blocks for the synthesis of tetradentate ligands in combination with the corresponding chiral (**2** and **3**) and n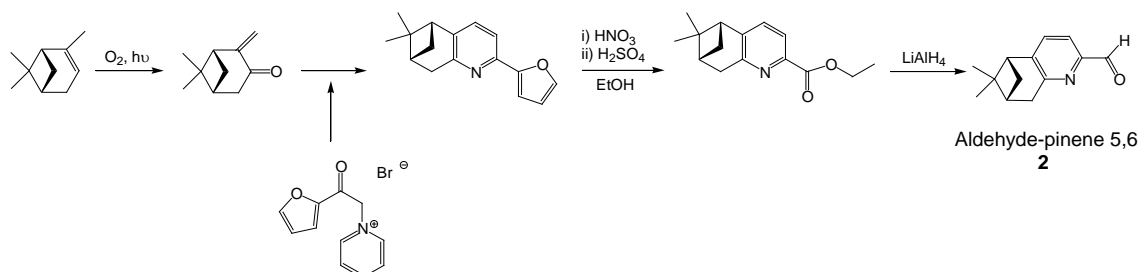on chiral aldehydes (Scheme 5). While **Lrac** is racemic, in **Lrac$_{5,6}$** a second chiral element is introduced via the pinene groups. In the case of **L(+)$_{4,5}$**, **L(+)$_{5,6}$** and **L(-)$_{5,6}$** the chirality is introduced by the bi(chroman) backbone (SPAN), as well as by the pinene groups.

These tetradentate new ligands have been prepared by one-step procedure via condensation between the diamines and the aldehydes. The condensation took place in a Dean-Stark apparatus with reflux of toluene for several hours (the synthesis was followed by thin layer chromatography). Afterwards, the solvent was removed until dryness obtaining a yellow precipitate. No further purification was possible due to their

high sensitivity to water. The yields of these reactions were nearly quantitative (between 87 and 97%).
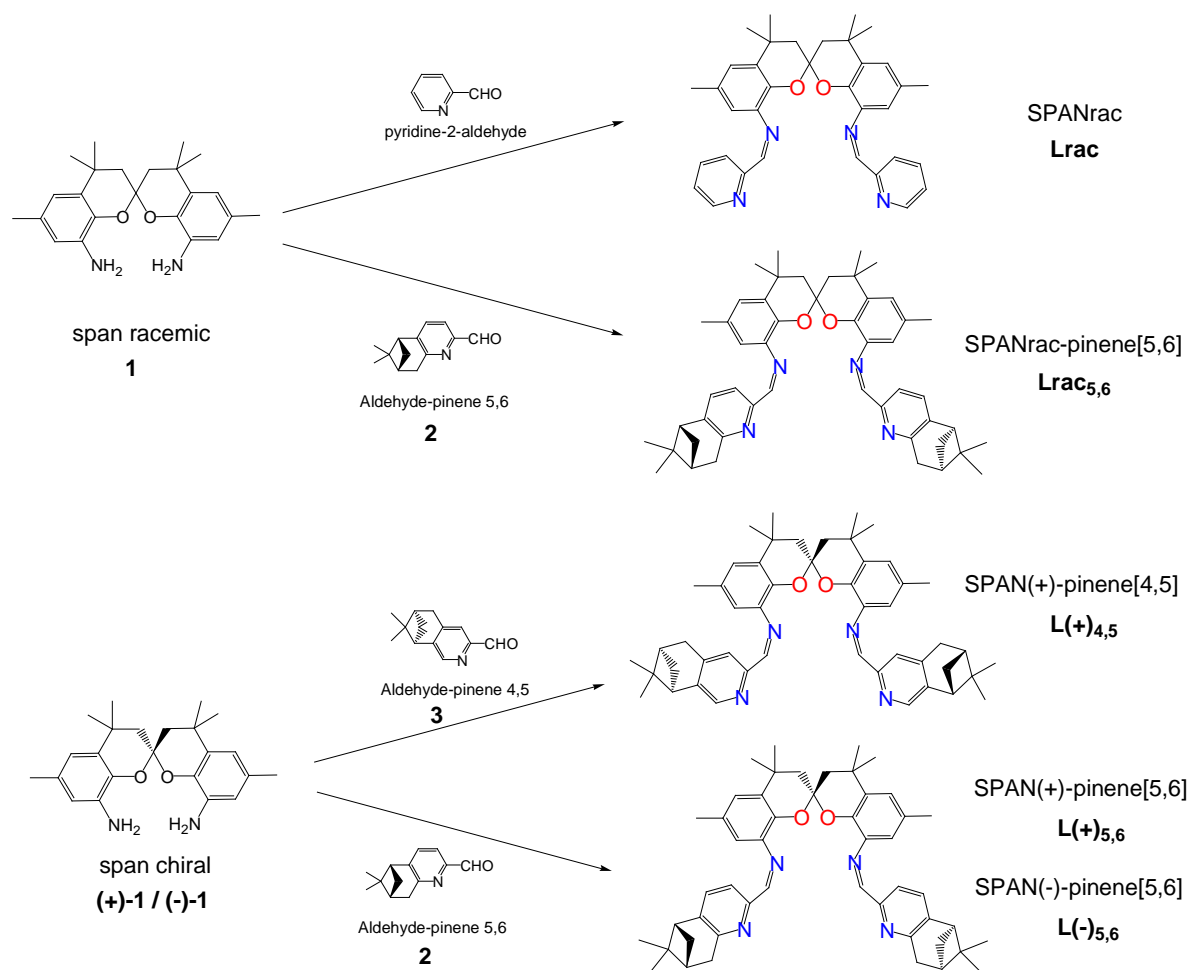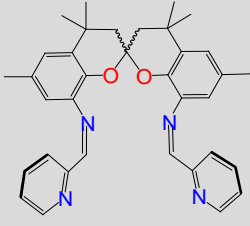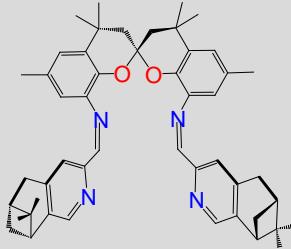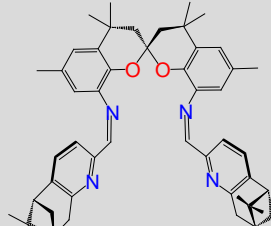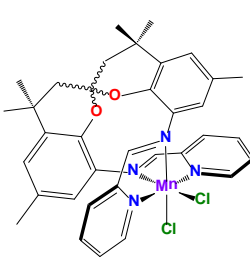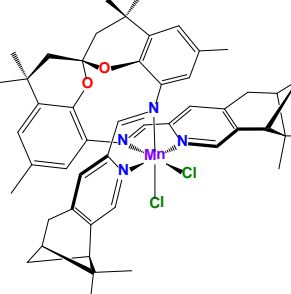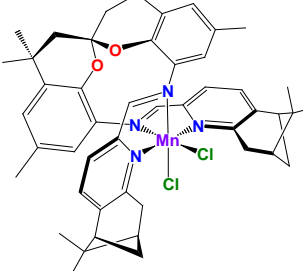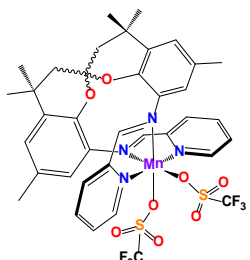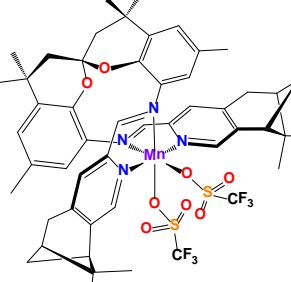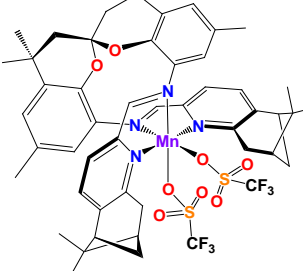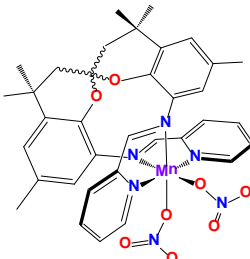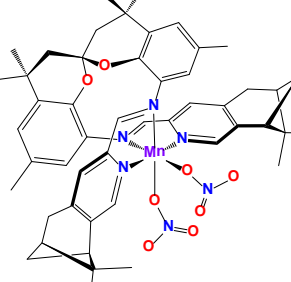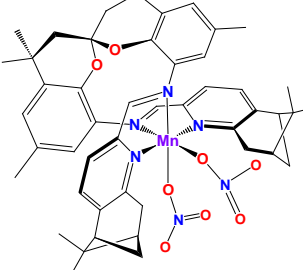
Scheme 5. Synthesis of the tetradentate SPAN ligands.

The five ligands were fully characterized by ^{1}H and ^{13}C-NMR, mass spectrometry and optical polarimetry. The signals observed in ^{1}H-NMR and ^{13}C-NMR were assigned to the corresponding protons and carbons after the analysis of the 1- and 2-dimensional (NOESY and HSQC) spectra (see supporting information). Numbering shown in Chart 1 has been used in the assignment.

5.3.2. Synthesis and characterization of the complexes

The synthesis of the complexes consists in the coordination of each of the five ligands to three different Mn(II) salts. The salts used were MnCl$_2$, Mn(CF$_3$SO$_3$)$_2$ and Mn(NO$_3$)$_2$·4H$_2$O. The three salts are commercially available and the corresponding anions will remain coordinated as mononuclear ligands in the final complex (Table 1).

Table 1. Manganese complexes synthesized in this work containing the different tetradentate ligands.

	Ligand		
Mn salt solvent	SPANrac (pyridine)	SPAN(+)-pinene[4,5]	SPANrac-pinene[5,6] SPAN(+)-pinene[5,6] SPAN(-)-pinene[5,6]
MnCl₂ CH₃CN	Mn(SPAN)Cl₂ **C1**	Mn(SPAN(+)-pinene[4,5])Cl₂ **C4**	Mn(SPANrac-pinene[5,6])Cl₂ – **C7** Mn(SPAN(+)-pinene[5,6])Cl₂ – **C10** Mn(SPAN(-)-pinene[5,6])Cl₂ – **C13**
Mn(CF₃SO₃)₂ THF	Mn(SPAN)(CF₃SO₃)₂ **C2**	Mn(SPAN(+)-pinene[4,5])(CF₃SO₃)₂ **C5**	Mn(SPANrac-pinene[5,6])(CF₃SO₃)₂ – **C8** Mn(SPAN(+)-pinene[5,6])(CF₃SO₃)₂ – **C11** Mn(SPAN(-)-pinene[5,6])(CF₃SO₃)₂ – **C14**
Mn(NO₃)₂·4H₂O EtOH	Mn(SPAN)(NO₃)₂ **C3**	Mn(SPAN(+)-pinene[4,5])(NO₃)₂ **C6**	Mn(SPANrac-pinene[5,6])(NO₃)₂ – **C9** Mn(SPAN(+)-pinene[5,6]) (NO₃)₂ – **C12** Mn(SPAN(-)-pinene[5,6]) (NO₃)₂ – **C15**

In all the cases, the metal:ligand ratio was 1:1, and the reactions took place at room temperature and under nitrogen atmosphere with anhydrous solvents. The general synthetic strategy followed for the preparation of the complexes was the slow addition of a solution of the corresponding ligand to a solution of the corresponding Mn(II) salt used as the starting material. After stirring the mixture, different procedures were followed to isolate the Mn(II) complexes.

For the complexes **C1**, **C2**, **C8**, **C11** and **C14**, an orange/yellow precipitate appeared in the mixture after 1 or 2 hours of stirring. For the complexes **C3-C7**, **C9**, **C10**, **C12**, **C13** and **C15** the solvent volume was reduced after 1 or 2 hours of stirring, and slow addition of diethyl ether produced the precipitation of an orange/yellow product. All of the complexes have been characterised by MALDI-MS and elemental analysis.

Suitable crystals for X-Ray diffraction of the complexes **C1**, **C2**, **C6**, **C8** and **C14** were obtained. The crystal structures are represented in Figure 7 and the most relevant bond lengths and angles are listed in Table 2. Their main crystallographic data together with selected bond distances and angles can be found in the supporting information.

The five structures are similar. The Mn(II) ions are coordinated by the four nitrogen atoms of the SPANimine ligands and two exogenous anions: chloride (**C1**), triflate (**C2**, **C8**, **C14**) or nitrate (**C6**). In all the structures the anions are in *cis* position and the two pyridine groups of SPANimine ligands are placed *trans* to one another. Consequently, the SPANimine ligand folds around the metal ion using the *cis*-α conformation usually observed within the family of twisted bis(iminopyridine) ligands.[57,75] Complexes present a crystallographic C_2 axis or pseudo axis (depending on the complex considered) that passes through the metal center and the spiro carbon (C16) of the SPAN skeleton. The geometries of the manganese centers are significantly distorted from the ideal octahedral geometry.

It is worth mentioning that the crystal structure of the compound **C8** contains the two diasteroisomers, **C8(+)** and **C8(-)**.

Figure 7. ORTEP plots (ellipsoids at 50% probability level) of complexes **C1**, **C2**, **C6**, **C8** (both diastereoisomers 8(+) and 8(-) are displayed) and **C14**.

In most complexes the Mn-N$_{imine}$ bond distances are somewhat longer than Mn-N$_{py}$ bond distances, thus indicating the different electronic nature of the donor atoms. For chloride and triflate compounds, the Mn-N$_{py}$ bond lengths are about the same value, but for the iminic nitrogen atoms they differ by 0.1 Å (2.378(2) Å for **C1** and 2.286(4) Å for **C2**) probably a consequence of the distinct *trans* influence exerted by chloride and triflate. In general, for the nitrate compound **C6** the Mn-N bond distances are slightly longer.

Table 2. Principal bond lengths (Å) and angles (deg) for the crystal structures of complexes **C1**, **C2**, **C6**, **C8** and **C14** (X = Cl, O$_{triflate}$, O$_{nitrate}$).

	C1	C2	C6[a]	C8[a]		C14[b]
				(+)	(-)	
Mn-N(1)	2.261(2)	2.264(4)	2.305	2.234(5)	2.252(6)	2.2825
Mn-N(4) or Mn-N(1)'	2.248(2)	2.264(4)	2.302	2.234(5)	2.252(6)	2.282
Mn-N(2)	2.359(2)	2.286(4)	2.370	2.288(6)	2.281(7)	2.2765
Mn-N(3) or Mn-N(2)'	2.378(2)	2.286(4)	2.372	2.288(6)	2.281(7)	2.293
Mn-X(1) or Mn-X(2)'	2.4466(8)	2.215(4)	2.228	2.159(6)	2.162(6)	2.148
Mn-X(2)	2.4571(8)	2.215(4)	2.205	2.159(6)	2.162(6)	2.154
X(1)-Mn-X(2) or X(2)'-Mn-X(2)	102.46(3)	95.7(2)	118.4	99.8(3)	93.0(3)	89.805
N(1)-Mn-N(4) or N(1)-Mn-N(1)'	160.25(9)	172.39(19)	158.4	171.3(3)	165.6(3)	166.74
N(2)-Mn-N(3) or N(2)-Mn-N(2)'	75.68(8)	78.98(18)	79.4	78.5(3)	81.1(3)	80.515
N(1)-Mn-N(2)	71.99(8)	72.08(15)	70.1	73.9(2)	73.2(2)	74.93

[a] The crystal contains the structures of the two diastereoisomers, **C8(+)** and **C8(-)**.

[b] The bond distances and angles are the average of the molecules present in the crystal structure.

Metal-ligand angles deviate significantly from the ideal value of 90º or 180º characteristic of a regular octahedron. Compared with chloride and nitrate compounds, the pyridine N atoms in the triflate compounds are bent towards the triflate ligands (N(1)-Mn-N(4) angle: 160.25(9)º in **C1**; 158.4 in **C6**; 172.39(19) in **C2**; 171.3(3) and

165.6(3) in **C8** and 166.74 in **C14**), probably due to H-bonding interactions between H1 and H35 (for **C2**) or H7 and H43 (for **C8** and **C14**) with oxygen and fluoride atoms from the triflate ligands.

The flexibility of this putative *trans*-coordinating ligand is demonstrated with the *cis*-chelating disposition around the Mn ion, with bite angle values (N(2)-Mn-N(3) or N(2)-Mn-N(2)') of 75-81º, lower than these observed for SPANphos ligands in *cis*-chelating complexes (around 97º)[46] and also considerably below the 90º expected for an ideal octahedral geometry. However, similar bite angles (73-74º) have been observed for another family of twisted bis(iminopyridine) ligands with a *cis*-α conformation.[75]

It is also remarkable the N_{py}-Mn-N_{imine} angle values of 70-75º, again lower than the ideal value of 90º, leading to an important distortion of the octahedral geometry.

In order to know whether the formation of one of the diastereoisomers is more favoured than the other in the coordination of a racemic ligand to Mn, an experiment was performed with $Mn(CF_3SO_3)_2$ and SPANrac-pinene[5,6] using a metal:ligand ratio of 0.5:1. The precipitate obtained after stirring the mixture showed an optical rotation of -244, similar to that of **C8** (-280) and far away from these shown by the pure diastereoisomers **C11** (+472) and **C14** (-880), thus indicating that there is no preference for one of the diastereoisomers.

5.3.3. Catalytic epoxidation of alkenes

The catalytic activity of the complexes described has been investigated in the epoxidation of styrene in acetonitrile using commercial 32% peracetic acid as the oxidant, in absence and in presence of additives (imidazole or $NaHCO_3$). The catalytic conditions used have been optimized after performing additional tests using other oxidants (such as iodosylbenzene diacetate or H_2O_2) and also a lower substrate:peracetic molar ratio (1:1.2 instead of the finally chosen 1:2), but low conversion values were obtained in most cases. Table 3 collects the conversion and selectivity values obtained for the epoxidation tests carried out using complexes **C1**-**C6** and **C9**-**C15**. In all the cases benzaldehyde has been detected as side product of the oxidation reaction.

Table 3. Catalytic epoxidation of styrene with complexes **C1**-**C6** and **C9**-**C15** using CH_3CO_3H as oxidant, in absence and presence of additives.

additive	---		imidazole		$NaHCO_3$	
complex	Conv. (%)	Select. (%)	Conv. (%)	Select. (%)	Conv. (%)	Select. (%)
$Mn(Lrac)Cl_2$, **C1**	100[a]	56	62[a]	92	100[a]	73
$Mn(Lrac)(CF_3SO_3)_2$, **C2**	58[a]	41	90[a]	69	100[a]	53
$Mn(Lrac)(NO_3)_2$, **C3**	86[a]	55	90[a]	76	97[a]	75
$Mn(L(+)_{4,5})Cl_2$, **C4**	80	67	100[b]	92	100	54
$Mn(L(+)_{4,5})(CF_3SO_3)_2$, **C5**	-	-	68	64	100[b]	82
$Mn(L(+)_{4,5})(NO_3)_2$, **C6**	82	63	99	48	100	81
$Mn(L(+)_{5,6})Cl_2$, **C10**	26	19	67	64	56	55
$Mn(L(+)_{5,6})(CF_3SO_3)_2$, **C11**	16	16	71	74	82	73
$Mn(L(+)_{5,6})(NO_3)_2$, **C12**	14	8	50	54	71	50
$Mn(L(-)_{5,6})Cl_2$, **C13**	21	13	100	75	100	77
$Mn(L(-)_{5,6})(CF_3SO_3)_2$, **C14**	18	5	70	68	99	62
$Mn(L(-)_{5,6})(NO_3)_2$, **C15**	10	11	58	57	68	47

Conditions: catalyst (2.5 µmol), substrate (250 µmol), additive (25 µmol), CH_3CN (1 mL). Peracetic acid 32% (500 µmol) added in 3 minutes at 0ºC, then **3 hours** of reaction at RT. After addition of an internal standard, an aliquot was taken for GC analysis.
[a] **Time**: 2 hours reaction. [b] **Time**: 30 minutes reaction.

As can be observed in Table 3, only moderate performances are obtained when carrying out the catalytic experiments in acetonitrile without the use of additives. A first glance at the conversion values obtained under such conditions allows observing that complexes **C10**-**C15**, bearing the span ligands with the bulky 5,6-pinene groups in close proximity to the labile sites, display considerably lower conversion rates than the analogous complexes containing the $L_{4,5}$ or the pyridyl analogues (particularly for the latter, for which the values reported have been registered after 2h reaction). A similar degree of performance is observed when comparing sets of related complexes containing a central (+) or (-) spiro building block (complexes **C10**-**C12** and **C13**-**C15** respectively). The conversions and selectivities obtained are also comparable as expected to those exhibited by complexes **C7**-**C9**, synthesized with the corresponding span-racemic mixtures (data not shown).

On the other hand, a comparison between related complexes with different monodentate ligands reveals that chloro complexes exhibit better conversion and selectivity values than the analogous triflate or nitrate compounds when the catalytic essays are performed in absence of additives. A parallel behaviour has been observed in chapter 4 when using related Mn catalysts also bearing pinene type of ligands.

The chloro complex **C1** has also been tested in the epoxidation of *cis*-β-methylstyrene under similar conditions leading to a conversion of 25% (100% yield) with total retention of the *cis* configuration in the epoxide product. This result indicates that, if an alkene-localized radical species was formed as intermediate, the closure of the ring would be much faster than the C-C rotation at the radical intermediate that would lead to the *trans* epoxide product. This hypothesis is in accordance with the results yielded by DFT theoretical calculations (see below).

In most cases the use of 10 equivalents of an additive such as imidazole or $NaHCO_3$ remarkably increases the conversion, especially when sodium bicarbonate is used. The selectivity for the epoxide product is increased as well in a similar extent for both types of additive. The improvement of catalytic performance through the use of additives has already been stated for analogous catalytic Mn-based systems and this positive effect is in some cases related to an increase in the pH value (when using peracids as oxidant, as in the case of chapter 4) that may lead to longer half-time life of the intermediate species formed,[76] though coordination of additives to Mn *prior* to the oxygen transfer step (leading to alternative, more effective intermediate species) has also been postulated.[77] In our case, the significant increase in the selectivity when using either imidazole or sodium bicarbonate indicates that the mechanistic pathway leading to the epoxide should be favored with regard to alternative non-desired routes and thus the additives might have an active role in the choice of the preferred mechanistic path.

Finally, the enantioselectivity in the epoxide formation has been evaluated in all cases but resulted in low values (between 1 and 14% ee). This might be partially due to the distant placement of the chiral pinene groups with regard to the potential active sites, considered as the vacant sites arising from decoordination of monodentate ligands (see Figure S 23 for spacefilling views of potential pentacoordinate species generated upon triflate release in complex **C8**). On the other hand, although SPAN backbone has been reported to induce a wide range of enantioselectivities (from 0 to 99% ee) in diverse catalytic processes with structurally similar compounds,[47-49] the irregular

coordination environment that Mn complexes can present, together with a certain flexibility of the spiro backbone in the ligand, might lead to a low restriction in the spatial arrangement of the atoms and orbitals involved in the key epoxidation step, thus conditioning the orientation of the olefin substrate in an almost inappreciable extent.

5.3.4. Computational calculations

DFT calculations have initially been performed on the geometry of **C1** and the optimized structure is overall in excellent agreement with the X-ray structure (rmsd 0.021 Å on distances and 0.7° on angles) [Standard deviations for distances and angles: $s_{n-1} = [\Sigma_{i=1 \to N} (CV - EV)^2/(N - 1)]^{1/2}$, where CV means calculated value, EV means experimental value (X-ray data), and N is the number of distances or angles taken into account]. Starting from the substitution of both chloride ligands of **C1** by oxo ligands we envisaged calculations to get insight into the epoxidation pathway using *cis*-β-methylstyrene as substrate. The most favourable pathway for the epoxidation might follow the scheme designed recently by Comba *et al.*[78] though the presence of two oxo ligands instead of one recommends the study of alternative pathways.[79] For all studied complexes the ground state is quadruplet. However, the doublet is in some cases located no further than 2 kcal/mol above the corresponding quadruplet ground state, thus forcing to check the ground state for each optimized intermediate or transition state.

The experimental results indicate that the Mn^{IV} catalyzed epoxidation reaction on *cis*-β-methylstyrene is stereospecific with no detection of the *trans* isomer. DFT is used here to shed some light on the reasons for these results. The most feasible mechanism is shown in Scheme 6. It consists of a mechanism in which an oxygen atom from the Mn complex is inserted into the C-C double bond generating the epoxide product. However, this insertion is not likely to take place in a single step so the alkene is first asymmetrically attacked by the Mn^{IV}=O oxidant to produce the radical intermediate **II**. The next step involves the cyclization to get the epoxidized complex **III** that afterwards will release a molecule of epoxide. Thus, to reach the epoxidized species **III** in Scheme 6 from the naked bis-oxo Mn^{IV} catalyst it is required to overcome two energy barriers of 8.1 and 0.1 kcal/mol, with intermediate **II** placed 12.9 kcal/mol below in energy with respect to the starting catalyst **I**. The main geometrical parameters of the optimized intermediates and transition states displayed in Scheme 6 are collected in Figure S 24.
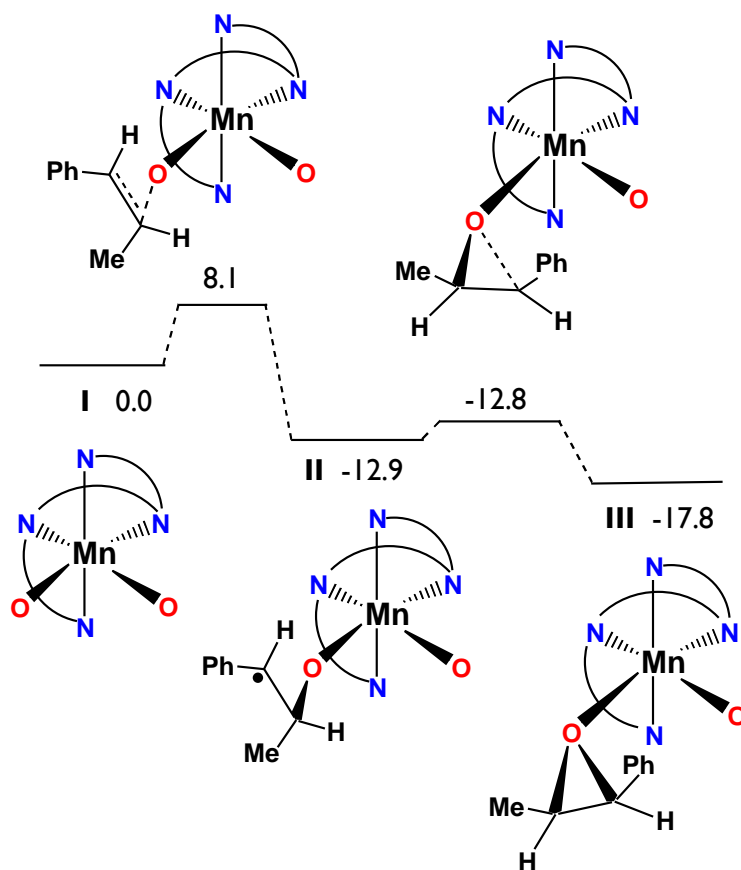
Scheme 6. Reaction pathway for the epoxidaton of the *cis*-β-methylstyrene substrate by the catalyst $[Mn^{IV}(O)_2]$ (energies in kcal/mol).

Alternative routes apart from the pathway displayed in Scheme 6 were also studied. First, because of the asymmetry of the substrate the formation of the radical **II** could also take place at the β carbon atom of methylstyrene, i.e. on the –CHMe moiety instead of the –CHPh one. This intermediate was not located due to its unstability in agreement with previous results of Comba *et al.*[78] Another point that was considered is the orientation of the alkene with regard to the Mn atom once bounded to the catalytic species (Figure S 25). The results obtained indicate that sterical hindrance together with H-bonding involving the alkene and the 'passive' oxo ligand lead to the orientation finally used as the most favoured one (see Figure S 24). Finally, no other radical species similar to **II** were located.

Alternative pathways were evaluated, such as the mechanism that would involve the concerted insertion of an oxygen atom from the Mn complex into the C-C double bond. The profile for this concerted step was computed by systematically varying the O-C_α and O-C_β distances. However the higher energy point on the potential energy surface

did not lead to a concerted transition state but to transition state **I-II** already determined for the stepwise reaction in Scheme 6.

The *cis-trans* isomerization in epoxidation processes involving *cis* alkenes is a common phenomenon due to the higher thermodynamic stability of the *trans* epoxides. To undergo such isomerization, a rotation around the C_α-C_β bond in the radical complex **II** is required. Computational calculations on this possibility allowed the location of the corresponding transition state **II$_{isomer1}$-II$_{isomer1trans}$** (Scheme 7), that displays an energy barrier of 4.2 kcal/mol and yields the radical species **II$_{isomer1trans}$**, indeed 0.2 kcal/mol above in energy with respect to **II**. However, this step does not take place because the barrier is 4.1 kcal/mol higher in energy with respect to the transformation **II → III** (Scheme 6) that requires just 0.1 kcal/mol. This supports the absence of the *trans* epoxide in experimental epoxidation on *cis*-β-methylstyrene, and thus demonstrates the stereospecificity of the catalyst.

II$_{isomer1}$-II$_{isomer1trans}$	**II$_{isomer1trans}$**	**II$_{isomer1}$-IV$_{isomer1}$**	**IV$_{isomer1}$**
-8.7	-12.7	-7.5	-49.3
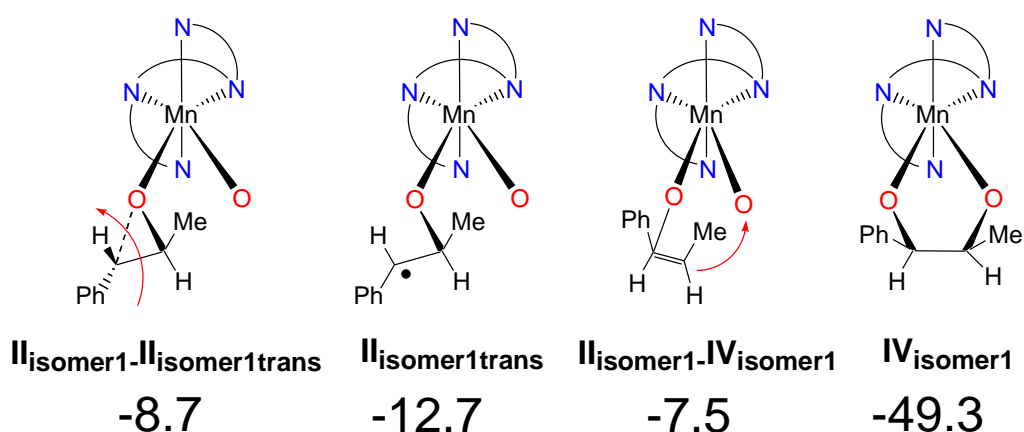
Scheme 7. Species involved in a potential *cis-trans* isomerization and in diol formation (energies in kcal/mol).

In Scheme 7 one can also envisage an alternative pathway that might be potentially competitive with **II-III** (Scheme 6) involving the non-reactive Mn-oxo moiety and that would lead to the formation of a diol product: instead of closing the epoxide (transition state **II-III)**, the interaction of the radical carbon with the non-reactive Mn-oxo moiety gives as a result the transition state **II$_{isomer1}$-IV$_{isomer1}$** which however is still 5.3 kcal/mol higher in energy with respect to the transition state **II-III**. Overcoming this transition state, the new intermediate **IV$_{isomer1}$** would be extremely more stable than complex **I**, indeed 49.3 kcal/mol. However, the formation of the diol product has not been detected experimentally.

5.4. Experimental section

5.4.1. Materials

All reagents used in the present work were obtained from Aldrich Chemical Co and were used without further purification. Reagent grade organic solvents were obtained from SDS and Scharlab. Solvents were purified and dried by passing through an activated alumina purification system (MBraun SPS-800) and high purity de-ionized water was obtained by passing distilled water through a nano-pure Mili-Q water purification system.

All synthetic manipulations were performed under nitrogen atmosphere using Schlenk tubes and vacuum line techniques.

5.4.2. Preparations

Synthesis of ligands

The racemic and chiral ligands 8,8'-diamino-4,4,4',4',6,6'-hexamethylspiro-2,2'-bichroman (**1**, **(+)-1** and **(-)-1**)[47,72] and the aldehydes **2**[73] and **3**[74] were prepared according to literature procedures. Pyridine-2-aldehyde is commercially available.

8,8'-bis[(2-pyridilmethylene)-imino]-4,4,4',4',6,6'-hexamethylspiro-2,2'-bichroman, SPANrac, Lrac. To a stirred solution of **1** (0,7 g, 1,91 mmol) in toluene (15 ml) was added pyridine-2-aldehyde (0,37 mL, 3,87 mmol) in toluene (5 ml). The mixture was refluxed in a Dean-Stark apparatus and monitored by TLC to establish completion. The solvent was then evaporated under reduced pressure to give **Lrac** as a yellow solid. Yield: 0.90 g, 87%. $[\alpha]_D^{25}$ = 14 (c = 0.1 g/ml, CH$_2$Cl$_2$). ^{1}H NMR (400 MHz, CDCl$_3$) δ 1.31 and 1.55 (s, 6H + 6H, H(15, 16, 21 and 22)), 2.05 (d, 2H, H(17 and 19)), 2.13 (s, 6H, H(10 and 26)), 2.19 (d, 2H, H(17 and 19)), 6.53 (s, 2H, H(8 and 27)), 6.76 (s, 2H, H(11 and 24)), 7.29 (dd, 2H, H(2 and 34)), 7.69 (t, 2H, H(3 and 33)), 7.89 (d, 2H, H(4 and 32)), 8.02 (s, 2H, H(6 and 30)), 8.62 (d, 2H, H(1 and 35)) ppm. ^{13}C NMR (400 MHz, CDCl$_3$) δ 20.96 (CH$_3$, C(10 and 26)), 31.36 (C, C(14 and 20)), 32.39 and 33.05 (CH$_3$, C(15, 16, 21 and 22)), 46.85 (CH$_2$, C(17 and 19)), 97.96 (C, C(18)), 117.69 (CH, C(8 and 27)), 121.67 (CH, C(2 and 34)), 121.84 (CH, C(11 and 24)), 124.47 (CH, C(4 and 32)), 124.69 (CH, C(3 and 33)), 127.97 (C, C(9 and 25)), 130.80 (C, C(12 and 23)),

136.16 (C, C(7 and 28)), 137.19 (C, C(13 and 29)), 149.34 (CH, C(1 and 35)), 150.37 (C, C(5 and 31)), 160.88 (CH, C(6 and 30)) ppm. ESI-MS: m/z = 567.3 [M + Na]$^+$.

8, 8' - bis[(2-(4,5-pinenepyridyl)methylene)-imino] - 4, 4, 4', 4', 6, 6' − hexamethyl-spiro - 2, 2'-bichroman, SPAN(+)-pinene[4,5], L(+)$_{4,5}$. To a stirred solution of **(+)-1** (0,190 g, 0,519 mmol) in 15 ml of toluene, a solution of aldehyde-pinene 4,5 (**3**, 0.2243 g, 1.1154 mmol in 5 ml of toluene) was slowly added and the reaction mixture was refluxed in a Dean-Stark apparatus for 12 h. The solvent was then removed under reduced pressure to give **L(+)$_{4,5}$** as a yellow solid. Yield: 0,368 g, 97 %. $[\alpha]_D^{25}$ = -301 (c = 0.1 g/ml, CH$_2$Cl$_2$). ^{1}H NMR (400 MHz, CDCl3) δ 0.63 (s, 6H, H(1 and 48)), 1.23 (d, 2H, H(4 and 44)), 1.33 (s, 6H, H(23 and 29)), 1.44 (s, 6H, H(2 and 49)), 1.55 (s, 6H, H(22 and 28)), 2.05 and 2.28 (d, 2H + 2H, H(24 and 26)), 2.20 (s, 6H, H(17 and 33)), 2.35 and 2.74 (m, 2H + 2H, H(5 and 45)), 2.92 (t, 2H, H(6 and 46)), 3.05 (d, 4H, (9 and 43)), 6.32 (s, 2H, H(15 and 34)), 6.51 (s, 2H, H(18 and 31)), 7.77 (s, 2H, H(11 and 39)), 8.14 (s, 2H, H(13 and 37)), 8.32 (s, 2H, H(10 and 42)) ppm. ^{13}C NMR (400 MHz, CDCl$_3$) δ 21.25 (CH$_3$, C(17 and 33)), 21.49 (CH$_3$, C(1 and 48)), 26.05 (CH$_3$, C(2 and 49)), 29.96 (C, C(21 and 27)), 31.20 (CH$_2$, C(5 and 45)), 31.53 (CH$_3$, C(23 and 29)), 32.11 (CH$_2$, C(9 and 43)), 33.03 (CH$_3$, C(22 and 28)), 39.25 (C, C(3 and 47)), 40.03 (CH, C(4 and 44)), 45.14 (CH, C(6 and 46)), 48.21 (CH$_2$, C(24 and 26)), 98.80 (C, C(25)), 114.18 (CH, C(15 and 34)), 116.07 (CH, C(18 and 31)), 121.27 (CH, C(11 and 39)), 130.98 (C, C(16 and 32)), 132.23 (C, C(19 and 30)), 135.97 (C, C(14 and 35)), 136.42 (C, C(20 and 36)), 145.92 (C, C(7 and 41)), 146.90 (C and CH, C(8 and 40, 10 and 42)), 148.27 (CH, C(13 and 37)), 152.00 (C, C(12 and 38)) ppm. ESI-MS: m/z = 733.5 [M + H]$^+$.

8, 8' - bis[(2-(5,6-pinenepyridyl)methylene)-imino] - 4, 4, 4', 4', 6, 6' − hexamethyl-spiro - 2, 2'-bichroman, SPANrac-pinene[5,6], L(rac)$_{5,6}$. To a stirred solution of **1** (0,200 g, 0,546 mmol) in 15 ml of toluene a solution of aldehyde-pinene 5,6 (**2**, 0,247 g, 1,229 mmol in 5 ml of toluene) was slowly added and the reaction mixture was refluxed in a Dean-Stark apparatus for 15 h. The solvent was then removed under reduced pressure to give **L(rac)$_{5,6}$** as a yellow solid. Yield: 0.356 g, 89%. ESI-MS: m/z = 795.5 [M + Na + CH$_3$CN]$^+$. NMR spectroscopy for this mixture is described below, separately for each diastereoisomer.

8, 8' - bis[(2-(5,6-pinenepyridyl)methylene)-imino] - 4, 4, 4', 4', 6, 6' − hexamethyl-spiro - 2, 2'-bichroman, SPAN(+)-pinene[5,6], L(+)$_{5,6}$ and L(-)$_{5,6}$. To a stirred solution of **(+)-1** or **(-)-1** (0,202 g, 0,553 mmol) in 15 ml of toluene a solution of aldehyde-pinene

5,6 (**2**, 0,250 g, 1,244 mmol in 5 ml of toluene) was slowly added and the reaction mixture was refluxed in a Dean-Stark apparatus for 25 h. The solvent was then removed under reduced pressure to give **L(+)$_{5,6}$** or **L(-)$_{5,6}$** as a yellow solid. **L(+)$_{5,6}$**: Yield: 0,369 g, 91%. $[\alpha]_D^{25}$ = -143 (c = 0.105 g/ml, CH$_2$Cl$_2$). ^{1}H NMR (400 MHz, CDCl3) δ 0.69 (s, 6H, H(2 and 49)), 1.26 (d, 2H, H(6 and 44)), 1.31 (s, 6H, H(23 and 29)), 1.43 (s, 6H, H(1 and 48)), 1.59 (s, 6H, H(22 and 28)), 2.03 and 2.07 (d, 2H + 2H, H(24 and 26)), 2.13 (s, 6H, H(17 and 33)), 2.40 and 2.71 (m, 2H + 2H, H(5 and 45)), 2.80 (t, 2H, H(4 and 46)), 3.14 (d, 4H, (7 and 43)), 6.54 (s, 2H, H(15 and 34)), 6.76 (s, 2H, H(18 and 31)), 7.21 (d, 2H, H(11 and 39)), 7.58 (d, 2H, H(10 and 40)), 8.01 (s, 2H, H(13 and 37)) ppm. ^{13}C NMR (400 MHz, CDCl$_3$) δ 21.25 (CH$_3$, C(17 and 33)), 21.43 (CH$_3$, C(2 and 49)), 26.10 (CH$_3$, C(1 and 48)), 29.86 (C, C(21 and 27)), 31.20 (CH$_2$, C(5 and 45)), 31.69 (CH$_3$, C(23 and 29)), 32.09 (CH$_2$, C(7 and 43)), 36.56 (CH$_3$, C(22 and 28)), 39.65 (C, C(3 and 47)), 40.14 (CH, C(6 and 44)), 47.14 (CH, C(4 and 46)), 48.21 (CH$_2$, C(24 and 26)), 98.28 (C, C(25)), 114.17 (CH, C(15 and 34)), 116.06 (CH, C(18 and 31)), 119.82 (CH, C(11 and 39)), 130.97 (C, C(16 and 32)), 132.23 (C, C(19 and 30)), 133.33 (C, C(14 and 35)), 133.72 (CH, C(10 and 40)), 135.97 (C, C(20 and 36)), 147.80 (C, C(9 and 41)), 150.93 (C, C(12 and 38)), 158.09 (C, C(8 and 42)), 161.42 (CH, C(13 and 37)) ppm. ESI-MS: *m/z* = 795.5 [M + Na + CH$_3$CN]$^+$. **L(-)$_{5,6}$**: Yield: 0,381 g, 94%. $[\alpha]_D^{25}$ = -52 (c = 0.15 g/ml, CH$_2$Cl$_2$) ^{1}H NMR (400 MHz, CDCl3) δ 0.66 (s, 6H, H(2 and 49)), 1.29 (d, 2H, H(4 and 46)), 1.33 (s, 6H, H(22 and 28)), 1.44 (s, 6H, H(1 and 48)), 1.55 (s, 6H, H(23 and 29)), 2.08 (d, 2H, H(24 and 26)), 2.15 (d, 2H, H(24 and 26)), 2.20 (s, 6H, H(17 and 33)), 2.44 (m, 2H, H(5 and 45)), 2.73 (m, 2H, H(5 and 45)), 2.88 (t, 2H, H(6 and 44)), 3.21 (d, 4H, (7 and 43)), 6.31 (s, 2H, H(15 and 34)), 6.52 (s, 2H, H(18 and 31)), 7.37 (d, 2H, H(11 and 39)), 7.69 (d, 2H, H(10 and 40)), 8.01 (s, 2H, H(13 and 37)) ppm. ^{13}C NMR (400 MHz, CDCl$_3$) δ 21.25 (CH$_3$, C(17 and 33)), 21.42 (CH$_3$, C(2 and 49)), 26.10 (CH$_3$, C(1 and 48)), 29.85 (C, C(21 and 27)), 31.20 (CH$_2$, C(5 and 45)), 31.69 (CH$_3$, C(22 and 28)), 32.10 (CH$_2$, C(7 and 43)), 36.55 (CH$_3$, C(23 and 29)), 39.65 (C, C(3 and 47)), 40.14 (CH, C(6 and 44)), 47.13 (CH, C(4 and 46)), 48.21 (CH$_2$, C(24 and 26)), 98.33 (C, C(25)), 114.16 (CH, C(15 and 34)), 116.05 (CH, C(18 and 31)), 119.81 (CH, C(11 and 39)), 130.96 (C, C(16 and 32)), 132.22 (C, C(19 and 30)), 133.22 (C, C(14 and 35)), 133.72 (CH, C(10 and 40)), 135.97 (C, C(20 and 36)), 147.79 (C, C(9 and 41)), 150.93 (C, C(12 and 38)), 158.08 (C, C(8 and 42)), 161.56 (CH, C(13 and 37)) ppm. ESI-MS: *m/z* = 795.5 [M + Na + CH$_3$CN]$^+$.

Synthesis of complexes

The complex Mn(CF$_3$SO$_3$)$_2$ was prepared according to the literature procedure.[80]

[Mn(SPANrac)Cl$_2$], C1. A solution of the ligand **Lrac** (65 mg, 0,12mmol) in acetonitrile (4 mL) was added to a solution of MnCl$_2$ (15 mg, 0,12 mmol) in 2 mL of acetonitrile and the mixture was stirred for 1 hour at room temperature. After reduction of the volume, an orange precipitate was obtained. The precipitate was collected by filtration, washed with diethyl ether and dried under vacuum (yield: 42 mg, 50%). Suitable crystals for X-ray diffraction were grown by diffusion of diethyl ether into an acetone solution of the compound. MALDI-MS (*m/z*) 636,3 [Mn(Lrac)Cl]$^+$. Anal. found (Calcd.) for **C1·1.7H$_2$O**: C, 59.82 (59.95); H, 5.04 (5.66); N, 7.68 (7.99). IR ν_{max}/cm^{-1} 2800-3000 (ν (C-H)sp^3), 1600 (ν (C-N)sp^2), 1400 (ν (C-C)sp^2).

[Mn(SPANrac)(CF$_3$SO$_3$)$_2$], C2. A solution of the ligand **Lrac** (31 mg, 0,06mmol) in THF (0,5 mL) was added to a solution of Mn(CF$_3$SO$_3$)$_2$ (20 mg, 0,06 mmol) in 1,5 mL of THF and the mixture was stirred for 1 hour at room temperature. A yellow precipitate was obtained and collected by filtration, washed with diethyl ether and dried under vacuum (yield: 41 mg, 74%). Suitable crystals for X-ray diffraction were grown by diffusion of diethyl ether into a CH$_2$Cl$_2$ solution of the compound. MALDI-MS (*m/z*) 748,2 [Mn(Lrac)(CF$_3$SO$_3$)]$^+$. Anal. found (Calcd.) for **C2·2H$_2$O**: C, 47.28 (47.59); H, 3.90 (4.31); N, 5.87 (5.99); S, 6.46 (6.72). IR ν_{max}/cm^{-1} 2800-3000 (ν (C-H)sp^3), 1600 (ν (C-N)sp^2), 1400 (ν (C-C)sp^2), 1000-1400 (CF$_3$SO$_3$).

[Mn(SPANrac)(NO$_3$)$_2$], C3. A solution of **Lrac** (32 mg, 0,06mmol) in EtOH$_{abs}$ (2 mL) was added to a solution of Mn(NO$_3$)$_2$·4H$_2$O (15 mg, 0,06 mmol) in 1 mL of EtOH$_{abs}$ and the mixture was stirred for 1 hour at room temperature. Then the mixture was filtered, the solvent volume was reduced and, after addition of diethylether, a yellow precipitate was obtained, that was washed with diethyl ether and dried under vacuum (yield: 29 mg, 62%). MALDI-MS (*m/z*) 661,3 [Mn(Lrac)(NO$_3$)]$^+$. Anal. found (Calcd.) for **C3·1.2EtOH**: C, 57.28 (57.67); H, 5.20 (5.59); N, 10.39 (10.79). IR ν_{max}/cm^{-1} 2800-3000 (ν (C-H)sp^3), 1600 (ν (C-N)sp^2), 1400 (ν (C-C)sp^2), 1300 (ν (NO$_2$)).

[Mn(SPAN(+)-pinene[4,5])Cl$_2$], C4. A solution of the ligand **L(+)$_{4,5}$** (58 mg, 0,08 mmol) in acetonitrile (2 mL) was added to a solution of MnCl$_2$ (10 mg, 0,08 mmol) in 2 mL of acetonitrile and the mixture was stirred for 30 minutes at room temperature. Then the mixture was filtered and after addition of diethyl ether an orange precipitate was obtained. It was collected by filtration, washed with diethyl ether and dried under vacuum (yield: 22 mg, 30%). MALDI-MS (*m/z*) 822,4 [Mn(L(+)$_{4,5}$)Cl]$^+$. Anal. found (Calcd.) for **C4·2.3H$_2$O**: C, 65.1 (65.37); H, 6.40 (6.78); N, 5.95 (6.22). IR ν_{max}/cm^{-1} 2800-3000 (ν (C-H)sp^3), 1600 (ν (C-N)sp^2), 1400 (ν (C-C)sp^2).

[Mn(SPAN(+)-pinene[4,5])(CF$_3$SO$_3$)$_2$], C5. This compound was prepared following a method analogous to that described for C4, using **L(+)$_{4,5}$** (30 mg, 0,04 mmol) in THF (2

mL) and $Mn(CF_3SO_3)_2$ (15 mg, 0,04 mmol) in THF (2 mL) to afford a yellow precipitate (yield: 34 mg, 76%). MALDI-MS (*m/z*) 936,3 $[Mn(L(+)_{4,5})(CF_3SO_3)]^+$. Anal. found (Calcd.) for **C5·2.1H₂O**: C, 54.05 (54.50); H, 5.04 (5.40); N, 4.52 (4.99); S, 5.52 (5.70). IR ν_{max}/cm^{-1} 2800-3000 (ν (C-H)sp^3), 1600 (ν (C-N)sp^2), 1400 (ν (C-C)sp^2), 1000-1400 (CF_3SO_3).

[Mn(SPAN(+)-pinene[4,5])(NO₃)₂], C6. This compound was prepared following a method analogous to that described for C3, using **L(+)₄,₅** (42 mg, 0,06 mmol) in EtOH$_{abs}$ (2 mL) and $Mn(NO_3)_2$·$4H_2O$ (14 mg, 0,06 mmol) in EtOH$_{abs}$ (2 mL) to afford a yellow precipitate (yield: 32 mg, 57 %). By recristallization in ethanol, suitable crystals for X-Ray diffraction were obtained. MALDI-MS (*m/z*) 849,5 $[Mn(L(+)_{4,5})(NO_3)]^+$. Anal. found (Calcd.) for **C6·0.8EtOH**: C, 63.52 (64.05); H, 6.20 (6.45); N, 8.53 (8.85). IR ν_{max}/cm^{-1} 2800-3000 (ν (C-H)sp^3), 1600 (ν (C-N)sp^2), 1400 (ν (C-C)sp^2), 1300 (ν (NO$_2$)).

[Mn(SPANrac-pinene[5,6])Cl₂], C7. A solution of **Lrac₅,₆** (58 mg, 0,08 mmol) in acetonitrile (3 mL) was added to a solution of $MnCl_2$ (10 mg, 0,08 mmol) in acetonitrile (2 mL) and the mixture was stirred for 1 hour at room temperature. Then the mixture was filtered, the solvent volume was reduced and, after addition of diethylether, a yellow precipitate was obtained, that was washed with diethyl ether and dried under vacuum (yield: 39 mg, 55%). MALDI-MS (*m/z*). 822,4 $[Mn(Lrac_{5,6})Cl]^+$. Anal. found (Calcd.) for **C7·1.8H₂O**: C, 65.75 (66.03); H, 6.46 (6.73); N, 5.99 (6.28). IR ν_{max}/cm^{-1} 2800-3000 (ν (C-H)sp^3), 1600 (ν (C-N)sp^2), 1400 ν (C-C)sp^2).

[Mn(SPANrac-pinene[5,6])(CF₃SO₃)₂], C8. A solution of **Lrac₅,₆** (30 mg, 0,04 mmol) in THF (2 mL) was added to a solution of $Mn(CF_3SO_3)_2$ (15 mg, 0,04 mmol) in THF (2 mL) and the mixture was stirred for 1 hour at room temperature. A yellow precipitate was obtained and collected by filtration, washed with diethyl ether and dried under vacuum (yield: 19 mg, 44%). Suitable crystals for X-ray diffraction were grown by diffusion of diethyl ether into a CH_2Cl_2 solution of the compound. MALDI-MS (*m/z*) 936,2 $[Mn(Lrac_{5,6})(CF_3SO_3)]^+$. Anal. found (Calcd.) for **C8·0.9H₂O**: C, 55.23 (55.57); H, 5.56 (5.28); N, 4.90 (5.08); S, 5.31 (5.81). IR ν_{max}/cm^{-1} 2800-3000 (ν (C-H)sp^3), 1600 (ν (C-N)sp^2), 1400 (ν (C-C)sp^2), 1000-1400 (CF_3SO_3).

[Mn(SPANrac-pinene[5,6])(NO₃)₂], C9. This compound was prepared following a method analogous to that described for C3, using **Lrac₅,₆** (42 mg, 0,06 mmol) in EtOH$_{abs}$ (2 mL) and $Mn(NO_3)_2$·$4H_2O$ (14 mg, 0,06 mmol) in EtOH$_{abs}$ (2 mL) and stirring 2 hours to afford an orange precipitate (yield: 23 mg, 40%). MALDI-MS (*m/z*) 849,4 $[Mn(Lrac_{5,6})(NO_3)]^+$. Anal. found (Calcd.) for **C8·0.9EtOH·0.6H₂O**: C, 62.88 (63.28); H, 6.06 (6.54); N, 8.55 (8.71). IR ν_{max}/cm^{-1} 2800-3000 (ν (C-H)sp^3), 1600 (ν (C-N)sp^2), 1400 (ν (C-C)sp^2), 1300 (ν (NO$_2$)).

[Mn(SPAN(+)-pinene[5,6])Cl$_2$], C10. This compound was prepared following the same procedure to that described for C7, with the ligand **L(+)$_{5,6}$** (yield: 33 mg, 46%). MALDI-MS(*m/z*) 822,5[Mn(L(+)$_{5,6}$)Cl]$^+$. Anal. found (Calcd.) for **C10·1.6H$_2$O**: C, 66.69 (66.30); H, 6.26 (6.72); N, 6.53 (6.32). IR ν_{max}/cm^{-1} 2800-3000 (ν (C-H)sp^3), 1600 (ν (C-N)sp^2), 1400 (ν (C-C)sp^2).

[Mn(SPAN(+)-pinene[5,6])(CF$_3$SO$_3$)$_2$], C11. This compound was prepared following the same procedure to that described for C8, with the ligand **L(+)$_{5,6}$** and stirring 2 hours (yield: 13 mg, 30%). MALDI-MS (*m/z*) 936,5[Mn(L(+)$_{5,6}$)(CF$_3$SO$_3$)]$^+$. Anal. found (Calcd.) for **C11·1.1H$_2$O**: C, 55.25 (55.39); H, 5.33 (5.30); N, 5.27 (5.06); S, 5.42 (5.79). IR ν_{max}/cm^{-1} 2800-3000 (ν (C-H)sp^3), 1600 (ν (C-N)sp^2), 1400 (ν (C-C)sp^2), 1000-1400 (CF$_3$SO$_3$).

[Mn(SPAN(+)-pinene[5,6])(NO$_3$)$_2$], C12. This compound was prepared following the same procedure to that described for C9, with the ligand **L(+)$_{5,6}$** and obtaining a yellow precipitate (yield: 37 mg, 63%). MALDI-MS (*m/z*) 886,2 [Mn(L(+)$_{5,6}$)(NO$_3$)(H$_2$O)$_2$]$^+$. Anal. found (Calcd.) for **C8·1.2EtOH·0.5H$_2$O**: C, 62.91 (63.23); H, 6.17 (6.62); N, 8.25 (8.60). IR ν_{max}/cm^{-1} 2800-3000 (ν (C-H)sp^3), 1600 (ν (C-N)sp^2), 1400 (ν (C-C)sp^2), 1300 (ν (NO$_2$)).

[Mn(SPAN(-)-pinene[5,6])Cl$_2$], C13. This compound was prepared following the same procedure to that described for C7, with the ligand **L(-)$_{5,6}$** (yield: 66 mg, 91%). MALDI-MS (*m/z*) 822,3 [Mn(L(-)$_{5,6}$)Cl]$^+$.)]$^+$. Anal. found (Calcd.) for **C13·0.5Et$_2$O·0.5H$_2$O**: C, 67.41 (67.69); H, 5.93 (6.19); N, 5.33 (5.48); S, 6.88 (6.90). IR ν_{max}/cm^{-1} 2800-3000 (ν (C-H)sp^3), 1600 (ν (C-N)sp^2), 1400 (ν (C-C)sp^2).

[Mn(SPAN(-)-pinene[5,6])(CF$_3$SO$_3$)$_2$], C14. This compound was prepared following the same procedure to that described for C8, with the ligand **L(-)$_{5,6}$** (yield: 31 mg, 63%). Suitable crystals for X-ray diffraction were grown by diffusion of diethyl ether into a CH$_2$Cl$_2$ solution of the compound. MALDI-MS (*m/z*) 936,3[Mn(L(-)$_{5,6}$)(CF$_3$SO$_3$)]$^+$)]$^+$. Anal. found (Calcd.) for **C14·2THF·1H$_2$O**: C, 56.81 (56.77); H, 4.57 (4.88); N, 6.08 (5.97); S, 5.14 (5.13). IR ν_{max}/cm^{-1} 2800-3000 (ν (C-H)sp^3), 1600 (ν (C-N)sp^2), 1400 (ν (C-C)sp^2), 1000-1400 (CF$_3$SO$_3$).

[Mn(SPAN(-)-pinene[5,6])(NO$_3$)$_2$], C15. This compound was prepared following the same procedure to that described for C9, with the ligand **L(-)$_{5,6}$** and obtaining a yellow precipitate (yield: 41 mg, 73%). MALDI-MS (*m/z*) 886,2 [Mn(L(-)$_{5,6}$)(NO$_3$)(H$_2$O)$_2$]$^+$. Anal. found (Calcd.) for **C8·0.7EtOH**: C, 64.61 (64.11); H, 6.08 (6.42); N, 8.54 (8.90). IR ν_{max}/cm^{-1} 2800-3000 (ν (C-H)sp^3), 1600 (ν (C-N)sp^2), 1400 (ν (C-C)sp^2), 1300 (ν (NO$_2$)).

5.4.3. X-Ray structure determination

Crystals of **C2**, **C6** and **C8** were used for room temperature (300(2) K) X-ray structure determination and a crystal of **C1** for low temperature (100(2) K) determination. The measurements were carried out on a *BRUKER SMART APEX CCD* diffractometer using graphite-monochromated Mo $K\alpha$ radiation (λ = 0.71073 Å) from an x-Ray Tube. Full-sphere data collection was carried out with ω and φ scans. Programs used: data collection, Smart;[81] data reduction, Saint +;[82] absorption correction, SADABS.[83] Structure solution and refinement was done using SHELXTL.[84] The structure were solved by direct methods and refined by full-matrix least-squares methods on F^2. The non-hydrogen atoms were refined anisotropically. The H-atoms were placed in geometrically optimized positions and forced to ride on the atom to which they are attached.

The measured crystal of **C14** was prepared under inert conditions immersed in perfluoropolyether as protecting oil for manipulation. Crystal structure determinations were carried out using a Bruker-Nonius diffractometer equipped with an APPEX 2 4K CCD area detector, a FR591 rotating anode with MoK$_\alpha$ radiation, Montel mirrors as monochromator and a Kryoflex low temperature device (T = -173 $^{\circ}$C). Full-sphere data collection was used with ω and φ scans. Programs used: Data collection, APEX-2;[85] data reduction, Bruker Saint V/.60A;[86] absorption correction, TWINABS[87]. Crystal structure solution was achieved using direct methods as implemented in SHELXTL[88] and visualized using the program XP. Missing atoms were subsequently located from difference Fourier synthesis and added to the atom list. Least-squares refinement on F^2 using all measured intensities was carried out using the program SHELXTL. All non hydrogen atoms were refined including anisotropic displacement parameters. Crystallographic data in CIF format can be found in the electronic supporting information.

5.4.4. Catalytic epoxidation

A CH_3CN (1 mL) solution of alkene (250 μmol), catalyst (2.5 μmol), additive (25 μmol) and biphenyl (250 μmol, internal standard) was prepared in a 10 mL flask and cooled in an ice bath. Afterwards, 32 % peracetic acid (500 μmol) was slowly added via syringe under stirring. The reaction vessel was then taken out of the ice bath and allowed to progressively warm to RT. Each aliquot of the reaction taken for analysis was filtered through a basic alumina plug and was analyzed in a Shimadzu GC-2010 gas

chromatography apparatus equipped with an Astec CHIRALDEX G-TA column and a FID detector, and quantification was achieved from calibration curves. GC conditions: initial temperature 40 ºC for 5 min, ramp rate 10 ºC/min, final temperature 170 ºC, injection temperature 250 ºC, detector temperature 250 ºC, carrier gas He at 25 mL/min.

5.4.5. Instrumentation and measurements

FT-IR spectra were taken in a Mattson-Galaxy Satellite FT-IR spectrophotometer containing a MKII Golden Gate Single Reflection ATR System. Elemental analyses were performed using a CHNS-O Elemental Analyser EA-1108 from Fisons. ESI-MS experiments were performed on a Navigator LC/MS chromatograph from Thermo Quest Finnigan, using acetonitrile as a mobile phase. MALDI-TOF spectra were recorded in a Bruker Daltonics autoflex. Specific optical rotation measurements were carried out on a Jasco P-1030 model polarimeter equipped with a PMT detector using the Sodium line at 589 nm. Optical rotations were recorded in CH_2Cl_2 at 25ºC with an error of less than ±0.1. $[\alpha]_D$ values are given in 10^{-1} deg cm^2 g^{-1}. NMR spectra were recorded in $CDCl_3$ on a 400 MHz NMR spectrometer from Bruker. Chemical Shifts (δ) for ^1H and ^{13}C were referred to internal solvent resonances. $CDCl_3$ was dried by passing through alumina.

5.4.6. Computational calculations

The density functional calculations were performed on all the systems at the GGA level with the Gaussian09 set of programs,[89] with BP86 correlation-exchange functional. For BP86 calculations, gradient corrections were taken from the work of Becke and Perdew.[90-92] The electronic configuration of the molecular systems was described by the standard SVP basis set, *i.e.* the split-valence basis set with polarization functions of Ahlrichs and co-worker, for H, C, N, and O.[93] For Mn we used the small-core, quasi-relativistic Stuttgart/Dresden effective core potential (standard SDD basis set in gaussian09) basis set, with an associated valence basis set.[94-96]

The geometry optimizations were performed without symmetry constraints, and the nature of the extrema was checked by analytical frequency calculations. Furthermore, all the extrema were confirmed by calculation of the intrinsic reaction paths. The

energies discussed throughout the text contain thermal and ZPE corrections. Solvent effects have been estimated in single point calculations on the gas phase optimized structures, based on the polarizable continuous solvation model PCM using acetonitrile as a solvent.[97,98] The cavity is created via a series of overlapping spheres.

5.5. Conclusions

Five new tetradentate N-donor ligands containing the spiro-2,2'-bi(chroman) backbone (SPANimine) have been synthesized and fully characterized by NMR (1-dimensional ^{1}H and ^{13}C, and 2-dimensional NOESY and HSQC), mass spectrometry and optical polarimetry.

With these ligands a family of new racemic and chiral Mn (II) complexes has been prepared and thoroughly characterized with analytical and spectroscopic (IR and MALDI-MS) techniques. The X-Ray structures for five of the complexes have been obtained. In all cases, the Mn ion is coordinated by four nitrogen atoms of the SPANimine ligand and two labile anions. These two anions are in *cis* relative position and the SPANimine ligand folds around the metal ion adopting a *cis*-α conformation. The complexes present a crystallographic C_2 axis or pseudo axis (depending on the complex considered) that passes through the metal center and the spiro carbon (C16) of the SPAN skeleton. The geometries around the manganese centers are significantly distorted from the ideal octahedral geometry due to the flexibility of the ligands, which present small bite angles (75-81º).

Optical spectrometry experiments have allowed to determine that, in the case of the racemic ligands, there is no preference for any of the diastereoisomers.

All the complexes synthesized have been tested in the catalytic epoxidation of styrene in acetonitrile, with only moderate performances when carrying out the catalytic experiments without the use of additives. The chloro complexes exhibit better conversion and selectivity values than the analogous triflate or nitrate compounds when the catalytic essays are performed under such conditions. In all the cases benzaldehyde was detected as side product of the oxidation reaction.

The complexes **C10**-**C15**, bearing the span ligands with the bulky 5,6-pinene groups in close proximity to the labile sites, display considerably lower conversion rates than the analogous complexes containing the $L_{4,5}$ or the pyridyl analogues. A similar degree of performance is observed when comparing sets of related complexes containing a central (+) or (-) spiro building block (complexes **C10**-**C12** and **C13**-**C15** respectively).

The use of additives such as imidazole or NaHCO$_3$ remarkably increases the conversion and the selectivity for the epoxide product. The significant increase in the selectivity indicates that the mechanistic pathway leading to the epoxide should be favoured with regard to alternative non-desired routes and thus the additives might have an active role in the choice of the preferred mechanistic path.

The chloro complex **C1** has also been tested in the epoxidation of *cis*-β-methylstyrene and the catalyst has proved to be selective and stereospecific for the formation of the *cis* epoxide. This result is in accordance with the computational results which postulate a lower barrier for the closure of the ring (0.1 kcal/mol) than for the C-C bond rotation leading to *cis-trans* isomerization (4.1 kcal/mol). This supports the absence of the thermodynamically more stable *trans* epoxide in experimental epoxidation.

5.6. References

[1] Jacobsen, E.N.; Pfaltz, A.; Yamamoto, H. Eds. *Comprehensive Asymmetric Catalyses*, Springer: Berlin, **1999**.

[2] Ojima, I. Ed. *Catalytic Asymmetric Synthesis*, 2nd ed., John Wiley & Sons: New York, **2000**.

[3] Sheldon, R.A.; Kochi, J.K. *Metal Catalyzed Oxidation of Organic Compounds.* Academic Press, New York, **1981**.

[4] Robert, A.; Meunier, B. *Biomimetic Oxidations Catalyzed by Transition Metal Complexes*, Ed. Meunier, B.; Imperial College Press, London, **2000**, Ch. 12.

[5] Tang, W.; Zhang, X. *Chem. Rev.* **2003**, *103*, 3029-3070.

[6] Freixa, Z.; van Leeuwen, P.W.N.M. *Coord. Chem. Rev.* **2008**, *252*, 1755-1786.

[7] Birkholz, M.-N.; Freixa, Z.; van Leeuwen, P.W.N.M. *Chem. Soc. Rev.* **2009**, *38*, 1099-1118.

[8] Gómez, M.; Muller, G.; Rocamora, M. *Coord. Chem. Rev.* **1999**, *193*, 769-835.

[9] Hargaden, G.C.; Guiry, P.J. *Chem. Rev.* **2009**, *109*, 2505-2550.

[10] Bennani, Y.L.; Hanessian, S. *Chem Rev.* **1997**, *97*, 3161-3196.

[11] Kizirian, J.-C. *Chem. Rev.* **2008**, *108*, 140-205.

[12] McManus, H.A.; Guiry, P.J. *Chem. Rev.* **2004**, *104*, 4151-4202.

[13] Noyori, R.; Takaya, H. *Acc. Chem. Res.* **1990**, *23*, 345-350.

[14] Burk, M.J. *Acc. Chem. Res* **2000**, *33*, 363-372.

[15] Pfaltz, A. *Acc. Chem Res.* **1993**, *26*, 339-345.

[16] Ghosh, A.K.; Mathivanan, P.; Cappiello, J. *Tetrahedron: Asymmetry* **1998**, *9*, 1-45.

[17] Johnson, J.S.; Evans, D.A. *Acc. Chem. Res.* **2000**, *33*, 325-335.

[18] Desimoni, G.; Faita, G.; Jorgensen, K.A. *Chem. Rev.* **2006**, *106*, 3561-3651.

[19] Palucki, M.; Finney, M.S.; Pospisil, P.J.; Güler, M.L.; Ishida, T.; Jacobsen, E.N. *J. Am. Chem. Soc.* **1998**, *120*, 948-954.

[20] Katsuky T *Adv. Synth. Catal.* **2002**, *344*, 131-147.

[21] Cozzi, P.G. *Chem. Soc. Rev.* **2004**, *33*, 410-421.

[22] Bajracharya, G.B.; Arai, M.A.; Koranne, P.S.; Suzuki, T.; Takizawa, S.; Sasai, H. *Bull. Chem. Soc. Jpn.* **2009**, *82*, 285-302.

[23] Zhou, Q.-L.; Xie, J.-H. *Topics in Organometallic Chemistry,* Ed. Ma, S.; Springer Berlin, **2011**, Ch. 36, 1-28.

[24] Srivastava, N.; Mital, A.; Kumar, A. *Chem. Commun.* **1992**, 493-494.

[25] Chan, A.S.C.; Hu, W.; Pai, C.-C.; Lau, C.-P.; Jiang, Y.; Mi, A.; Yan, M.; Sun, J.; Lou, R.; Deng, J. *J. Am. Chem. Soc.* **1997**, *119*, 9570-9571.

[26] Arai, M.A.; Arai, T.; Sasai, H. *Org. Lett.* **1999**, *1*, 1795-1797.

[27] Arai, M.A.; Kuraishi, M.; Arai, T.; Sasai, H. *J. Am. Chem. Soc.* **2001**, *123*, 2907-2908.

[28] Takenaka, K.; Nagano, T.; Takizawa, S.; Sasai, H. *Tetrahedron: Asymmetry* **2010**, *21*, 379-381.

[29] Xie, J.H.; Zhou, Q.-L. *Acc. Chem. Res.* **2008**, *41*, 581-593.

[30] Hu, A.-G.; Fu, Y.; Xie, J.-H.; Zhou, H.; Wang, L.-X.; Zhou, Q-L. *Angew. Chem., Int. Ed.* **2002**, *41*, 2348-2350.

[31] Zhou, H.; Wang, W.-H.; Fu, Y.; Xie, J.-H.; Shi, W.-J.; Wang, L.-X.; Zhou, Q.-L. *J. Org. Chem.* **2003**, *68*, 1582-1584.

[32] Xie, J.-H.; Wang, L.-X.; Fu, Y.; Zhu, S.-F.; Fan, B.-M.; Duan, H.-F.; Zhou, Q.-L. *J. Am. Chem. Soc.* **2003**, *125*, 4404-4405.

[33] Xie, J.-H.; Duan, H.-F.; Fan, B.-M.; Cheng, X.; Wang, L.-X.; Zhou, Q.-L. *Adv. Synth. Catal.* **2004**, *346*, 625-632.

[34] Zhu, S.-F.; Xie, J.-B.; Zhang, Y.-Z.; Li, S.; Zhou, Q.-L. *J. Am. Chem. Soc.* **2006**, *128*, 12886-12891.

[35] Liu, B.; Zhu, S.-F.; Wang, L.-X.; Zhou, Q.-L. *Tetrahedron: Asymmetry* **2006**, *17*, 634-641.

[36] Lait, S. M.; Parvez, M.; Keay, B.A. *Tetrahedron: Asymmetry* **2004**, *15*, 155-158.

[37] Varela, J.A.; Castedo, L.; Saá, C. *Org. Lett.* **1999**, *1*, 2141-2143.

[38] Ebeling, G.; Gruber, A.S.; Burrow, R.A.; Dupont, J.; Lough, A.J.; Farrar, D.H. *Inorg. Chem. Commun.* **2002**, *5*, 552-554.

[39] Langli, G.; Romming, C.; Undheim, K. *J. Organomet. Chem.* **2006**, *691*, 356-360.

[40] Lavallo, V.; Canac, Y.; Präsang, C.; Donnadieu, B.; Betrand, G. *Angew. Chem., Int. Ed.* **2005**, *44*, 5705-5709.

[41] Kandula, S.-R.V.; Puranik, V.G.; Kumar, P. *Tetrahedron Lett.* **2003**, *44*, 5015-5017.

[42] Patil, M.L.; Rao, C.V.L.; Yonezawa, K.; Takizawa, S.; Onitsuka, K.; Sasai, H. *Org. Lett.* **2006**, *8*, 227-230.

[43] Tu, Y.; Wang, Z.-X.; Shi, Y. *J. Am. Chem. Soc.* **1996**, *118*, 9806-9807.

[44] Freixa, Z.; Beentjes, M.S.; Batema, G.D.; Dieleman, C.B.; van Strijdonck, G.P.F.; Reek, J.N.H.; Kamer, P.C.J.; Fraanje, J.; Goubitz, K; van Leeuwen, P.W.N.M. *Angew. Chem., Int. Ed.* **2003**, *42*, 1284-1287.

[45] Freixa, Z.; Kamer, P.C.J.; Lutz, M.; Spek, A.L.; van Leeuwen, P.W.N.M. *Angew. Chem., Int. Ed.* **2005**, *44*, 4385-4388.

[46] Jiménez-Rodríguez, C.; Roca, F. X.; Bo, C.; Benet-Buchholz, J.; Escudero-Adán, E.C.; Freixa, Z.; van Leeuwen, P.W.N.M. *Dalton Trans.* **2006**, 268-278.

[47] Sala, X.; García Suárez, E.J.; Freixa, Z.; Benet-Buchholz, J.; van Leeuwen, P.W.N.M. *Eur. J. Org. Chem.* **2008**, 6197-6205.

[48] Jacquet, O.; Clément, N.D.; Freixa, Z.; Ruiz, A.; Claver, C.; van Leeuwen, P.W.N.M. *Tetrahedron:Asymmetry* **2011**, *22*, 1490-1498.

[49] Li, J.; Chen, G.; Wang, Z.; Zhang, R.; Zhang, X.; Ding, K. *Chem. Sci.* **2011**, *2*, 1141-1144.

[50] Fache, F.; Schulz, E.; Tommasino, L.; Lemaire, M. *Chem. Rev.* **2000**, *100*, 2159-2231.

[51] Hechavarría Fonseca, M.; König, B. *Adv. Synth. Catal.* **2003**, *345*, 1173-1185.

[52] Caputo, C.A.; Jones, N.D. *Dalton Trans.* **2007**, 4627-4640.

[53] von Zelewsky, A.; Mamula, O. *J. Chem. Soc., Dalton Trans.* **2000**, 219-231.

[54] Chelucci, G.; Thummel, R.P. *Chem. Rev.* **2002**, *102*, 3129-3170.

[55] Rich, J.; Rodríguez, M.; Romero, I.; Vaquer, L.; Sala, X.; Llobet, A.; Corbella, M.; Collomb, M.-N.; Fontrodona, X. *Dalton Trans.* **2009**, 8117-8126.

[56] Meunier, B. *Chem. Rev.* **1992**, *92*, 1411-1456.

[57] Goodson, P.A.; Glerop, J.; Hodgson, D.J.; Michelsen, K.; Weihe, H. *Inorg. Chem.* **1991**, *30*, 4909-4914.

[58] Ratilainen, J.; Airola, K.; Frohlich, R.; Nieger, M.; Rissanen, K. *Polyhedron* **1999**, *18*, 2265-2273.

[59] Schoumacker, S.; Hamelin, O.; Pécaut, J.; Fontecave, M. *Inorg. Chem.* **2003**, *42*, 8110-8116.

[60] Hureau, C.; Blondin, G.; Charlot, M.-F.; Philouze, C.; Nierlich, M.; Césario, M.; Anxolabéhère-Mallart, E. *Inorg. Chem.* **2005**, *44*, 3669-3683.

[61] Britovsek, G.J.P.; England, J.; White, A.J.P. *Dalton Trans.* **2006**, 1399-1408.

[62] Ebralidze, I.; Leitus, G.; Shimon, L.J.W.; Wang, Y.; Shaik, S.; Neumann, R. *Inorg. Chem. Acta* **2009**, *362*, 713-4720.

[63] Louloudi, M.; Nastopoulos, V.; Gourbatsis, S.; Perlepes, S.P.; Hadjiliadis, N. *Inorg. Chem. Commun.* **1999**, *2*, 479-483.

[64] Murphy, A.; Dubois, G.; Stack, T.D.P. *J. Am. Chem. Soc.* **2003**, *125*, 5250-5251.

[65] Garcia-Bosch, I.; Company, A.; Fontrodona, X.; Ribas, X.; Costas, M. *Org. Lett.* **2008**, *10*, 2095-2098.

[66] Wu, M.; Wang, B.; Wang, S.; Xia, C.; Sun, W. *Org. Lett.* **2009**, *11*, 3622-3625.

[67] Garcia-Bosch, I.; Ribas, X.; Costas, M. *Adv. Synth. Catal.* **2009**, *351*, 348-352.

[68] Ottenbacher, R.V.; Bryliakov, K.P.; Talsi, E.P. *Adv. Synth. Catal.* **2011**, *353*, 885-889.

[69] Gómez, L.; Garcia-Bosch, I.; Company, A.; Sala, X.; Fontrodona, X.; Ribas, X.; Costas, M. *Dalton Trans.* **2007**, 5539-5545.

[70] Chen, C.; Zhu, S.-F.; Wu, X.-Y.; Zhou, Q.-L. *Tetrahedron: Asymmetry* **2006**, *17*, 2761-2767.

[71] Jiang, M.; Zhu, S.-F.; Yang, Y.; Gong, L.-Z.; Zhou, X.-G.; Zhou, Q.-L. *Tetrahedron: Asymmetry* **2006**, *17*, 384-387.

[72] Jacquet, O.; Clement, N.D.; Martínez, O.; Serrano, M.; Claver, C.; van Leeuwen, P.W.N.M. unpublished work.

[73] Sauers, A.L.; Ho, D.M.; Bernhard, S. *J. Org. Chem.* **2004**, *69*, 8910-8915.

[74] Sala, X.; Rodríguez, A.M.; Rodríguez, M.; Romero, I.; Parella, T.; von Zelewsky, A.; Llobet, A.; Benet-Buchholz, J. *J. Org. Chem.* **2006**, *71*, 9283-9290.

[75] Vedder, C.; Schaper, F.; Brintzinger, H.H.; Kettunen, M.; Babik, S.; Fink, G. *Eur. J. Inorg. Chem.* **2005**, 1071-1080.

[76] Murphy A.; Pace A.; Stack, T.D.P. *Org. Lett.* **2004**, *6*, 3119–3122.

[77] Campbell, K.A.; Lashley, M.R.; Wyatt, J.K.; Nantz, M.H.; Britt, R.D. *J. Am. Chem. Soc.* **2001**, *123*, 5710-5719.

[78] Benet-Buchholz, J.; Comba, P.; Llobet, A.; Roeser, S.; Vadivelu, P.; Wadepohl, H.; Wiesner, S. *Dalton Trans.* **2009**, 5910-5923.

[79] Torrent, M.; Deng, L.; Duran, M.; Solà, M.; Ziegler, T. *Can. J. Chem.* **1999**, *77*, 1476-1491]

[80] Inada, Y.; Nakano, Y.; Inamo, M.; Funashashi, S. *Inorg. Chem.* **2000**, *39*, 4793-4801.

[81] Bruker Advanced X-ray Solutions. SMART: Version 5.631, 1997-2002.

[82] Bruker Advanced X-ray Solutions. SAINT +, Version 6.36A, 2001.

[83] Sheldrick, G. M. *Empirical Absorption Correction Program*, Universität Göttingen, **1996**. Bruker Advanced X-ray Solutions. SADABS Version 2.10, 2001.

[84] Sheldrick, G.M. *Program for Crystal Structure Refinement*, Universität Göttingen, **1997**. Bruker Advanced X-ray Solutions. SHELXTL Version 6.14, 2000-2003.

[85] Data collection with APEX II versions v1.0-22, v2009.1-0 and v2009.1-02. Bruker (2007). Bruker AXS Inc., Madison, Wisconsin, USA.

[86] Data reduction with Bruker SAINT versions V.2.10(2003), V/.60A and V7.60A. Bruker (2007). Bruker AXS Inc., Madison, Wisconsin, USA.

[87] TWINABS Version 2008/4 Bruker AXS; Blessing, Acta Cryst. (1995) A51 33-38.

[88] Sheldrick, G.M. *Acta Cryst.* **2008** A64, 112-122. SHELXTL versions V6.12 and 6.14.

[89] Gaussian 09, Revision A.1, Frisch, M.J.; Trucks, G.W.; Schlegel, H.B.; Scuseria, G.E.; Robb, M.A.; Cheeseman, J.R.; Scalmani, G.; Barone, V.; Mennucci, B.; Petersson, G.A.; Nakatsuji, H.; Caricato, M.; Li, X.; Hratchian, H.P.; Izmaylov, A.F.; Bloino, J.; Zheng, G.; Sonnenberg, J.L.; Hada, M.; Ehara, M.; Toyota, K.; Fukuda, R.; Hasegawa, J.; Ishida, M.; Nakajima, T.; Honda, Y.; Kitao, O.; Nakai, H.; Vreven, T.; Montgomery, Jr., J.A.; Peralta, J.E.; Ogliaro, F.; Bearpark, M.; Heyd, J.J.; Brothers, E.; Kudin, K.N.; Staroverov, V.N.; Kobayashi, R.; Normand, J.; Raghavachari, K.; Rendell, A.; Burant, J.C.; Iyengar, S.S.; Tomasi, J.; Cossi, M.; Rega, N.; Millam, N.J.; Klene, M.; Knox, J.E.; Cross, J.B.; Bakken, V.; Adamo, C.; Jaramillo, J.; Gomperts, R.; Stratmann, R.E.; Yazyev, O.; Austin, A.J.; Cammi, R.; Pomelli, C.; Ochterski, J.W.; Martin, R.L.; Morokuma, K.; Zakrzewski, V.G.; Voth, G.A.; Salvador, P.; Dannenberg, J.J.; Dapprich, S.; Daniels, A.D.; Farkas, Ö.; Foresman, J.B.; Ortiz, J.V.; Cioslowski, J.; Fox, D.J. Gaussian, Inc., Wallingford CT, **2009**.

[90] Becke, A. *Phys. Rev. A* **1988**, *38*, 3098-3100.

[91] Perdew, J.P. *Phys. Rev. B* **1986**, *33*, 8822-8824.

[92] Perdew, J.P. *Phys. Rev. B* **1986**, *34*, 7406-7406.

[93] Schaefer, A.; Horn, H.; Ahlrichs, R. *J. Chem. Phys.* **1992**, *97*, 2571-2577.

[94] Haeusermann, U.; Dolg, M.; Stoll, H.; Preuss, H. *Mol. Phys.* **1993**, *78*, 1211-1224.

[95] Kuechle, W.; Dolg, M.; Stoll, H.; Preuss, H. *J. Chem. Phys*. **1994**, *100,* 7535-7542.

[96] Leininger, T.; Nicklass, A.; Stoll, H.; Dolg, M.; Schwerdtfeger, P. *J. Chem. Phys*. **1996**, *105*, 1052-1059.

[97] Barone, V.; Cossi, M. *J. Phys. Chem. A* **1998**, *102*, 1995-2001

[98] Tomasi, J.; Persico, M. *Chem. Rev.* **1994**, *94*, 2027-2094.

5.7. Supporting Information
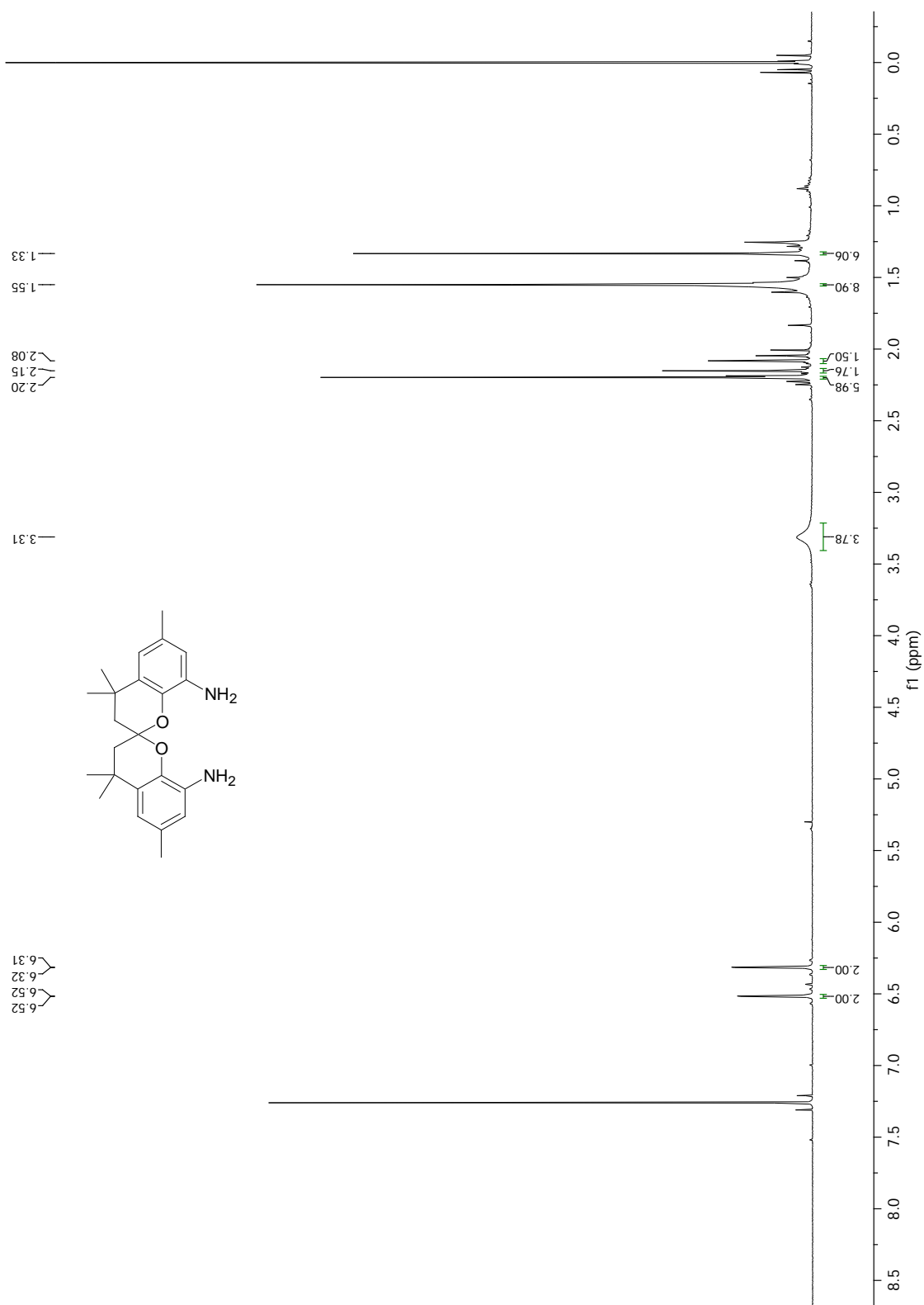
Figure S 1. ^{1}H-NMR of **1**.
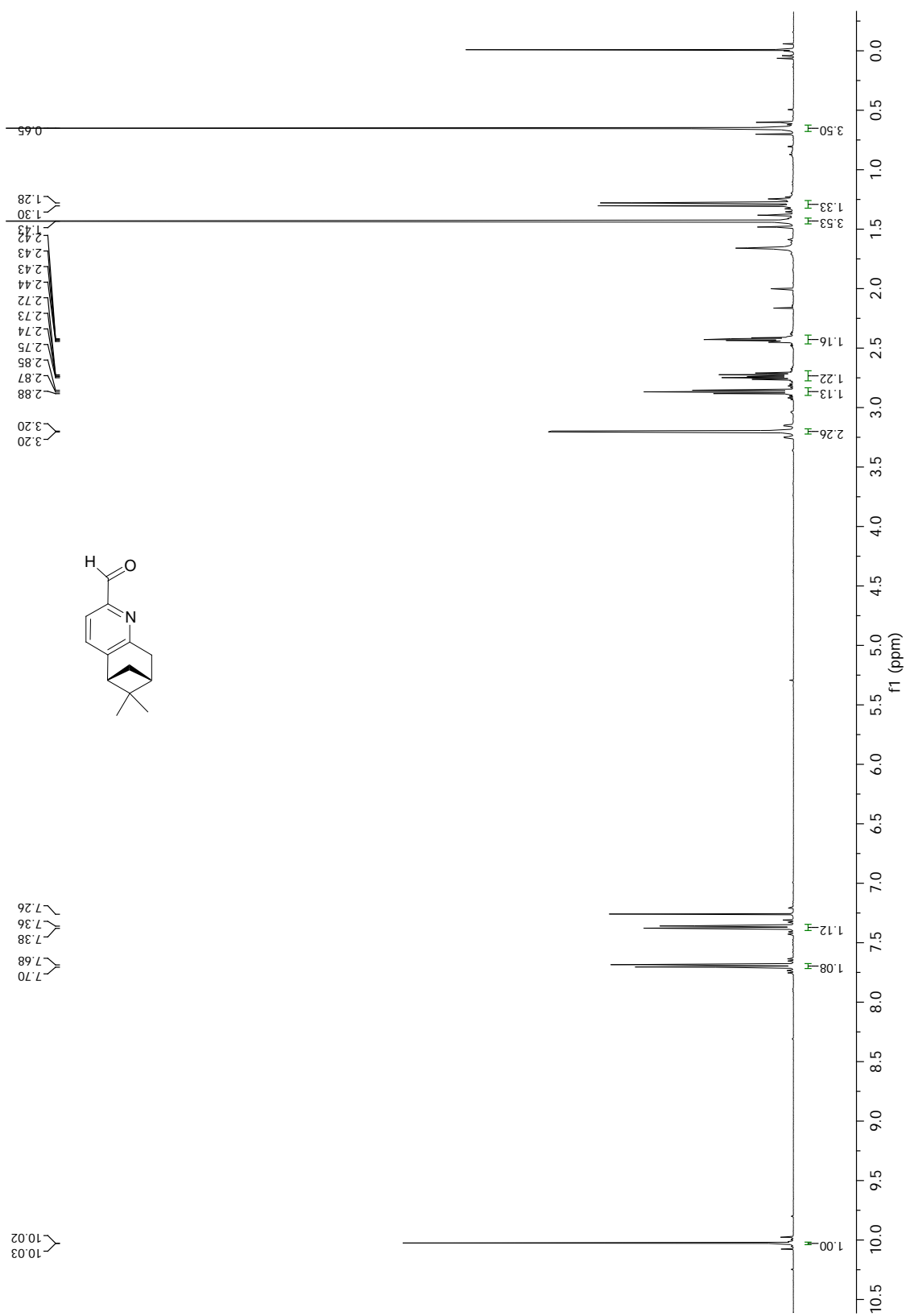
Figure S 2. ^{1}H-NMR of **2**.
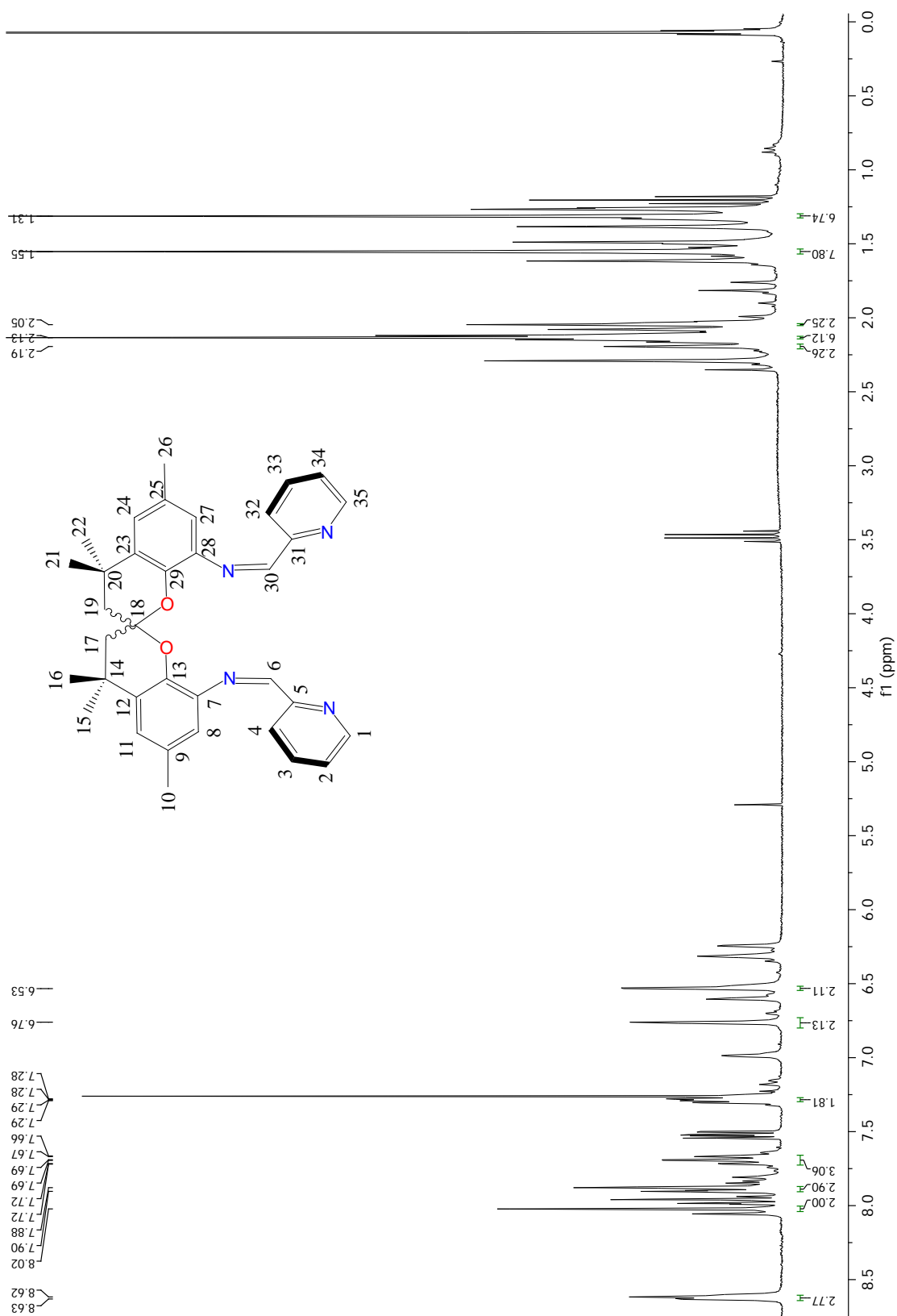
Figure S 3. ^{1}H-NMR of **Lrac**.
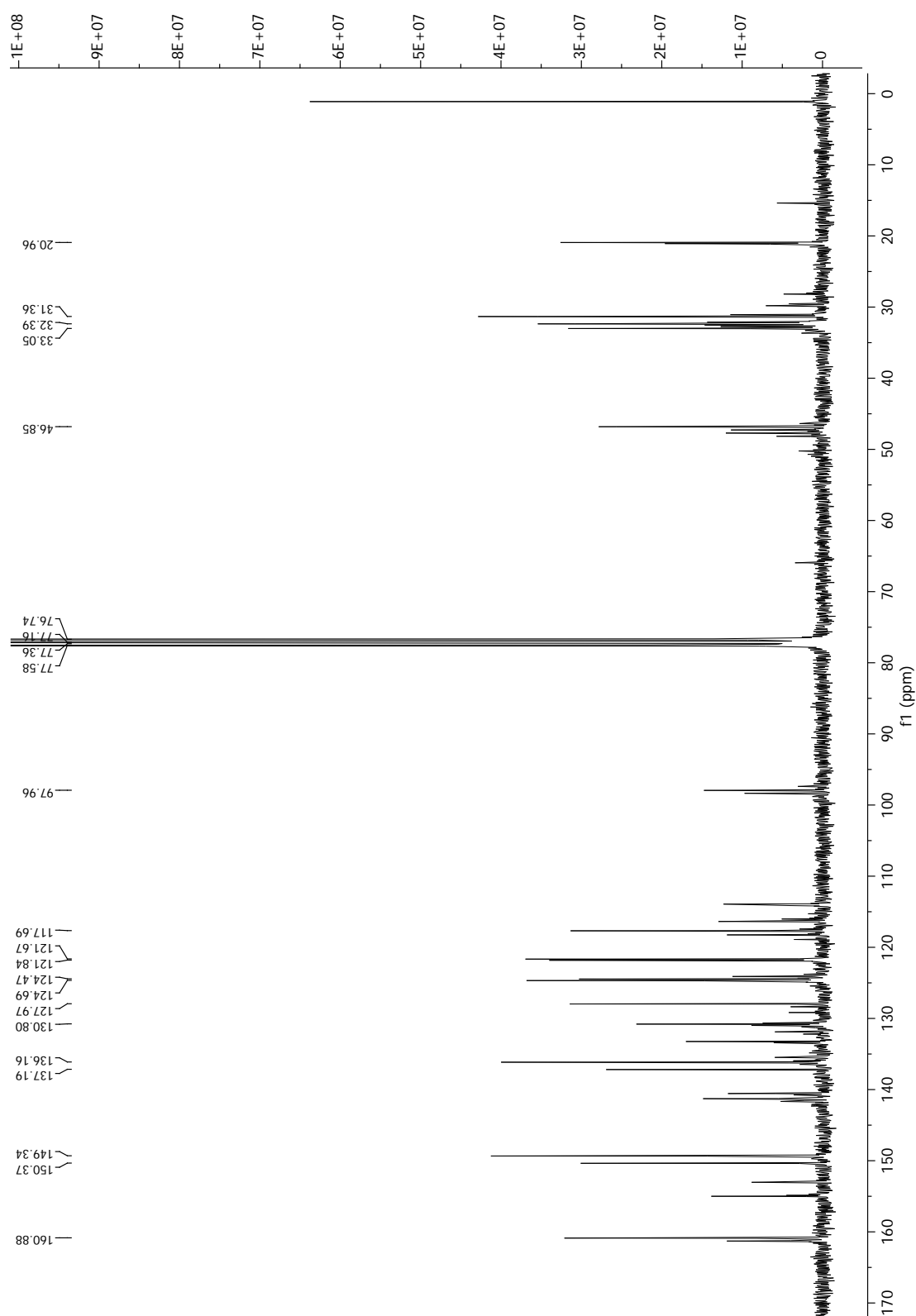
Figure S 4. ^{13}C-NMR of **Lrac**.
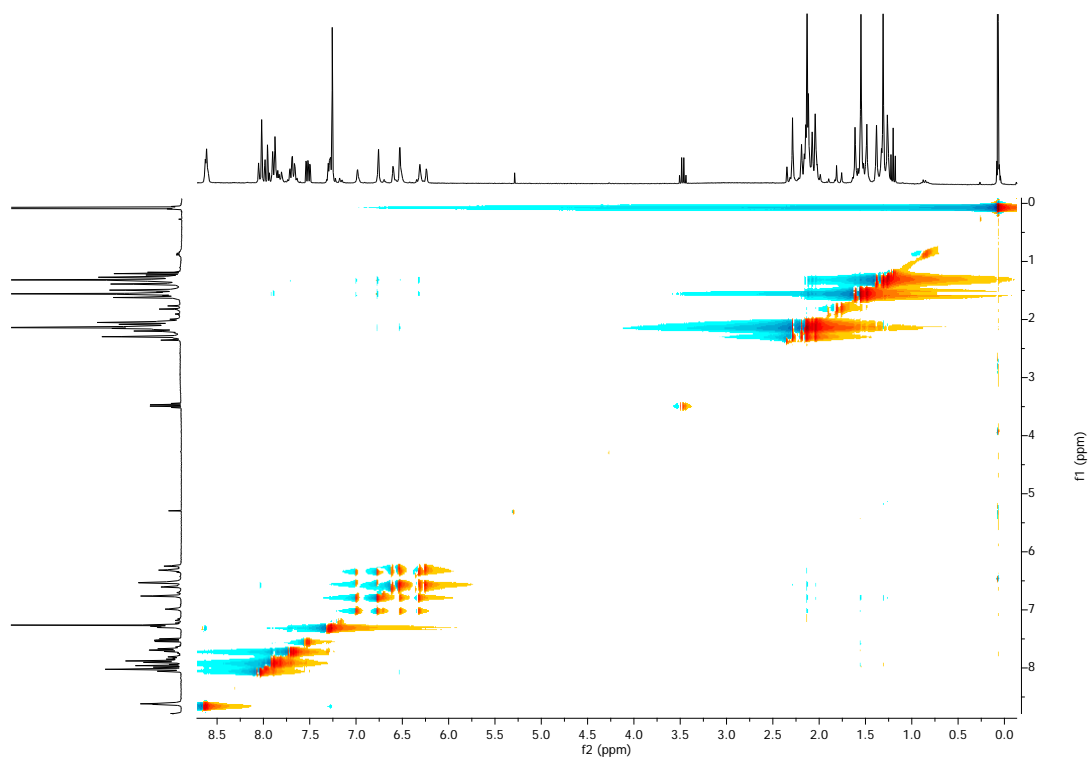
Figure S 5. NOESY of **Lrac**.
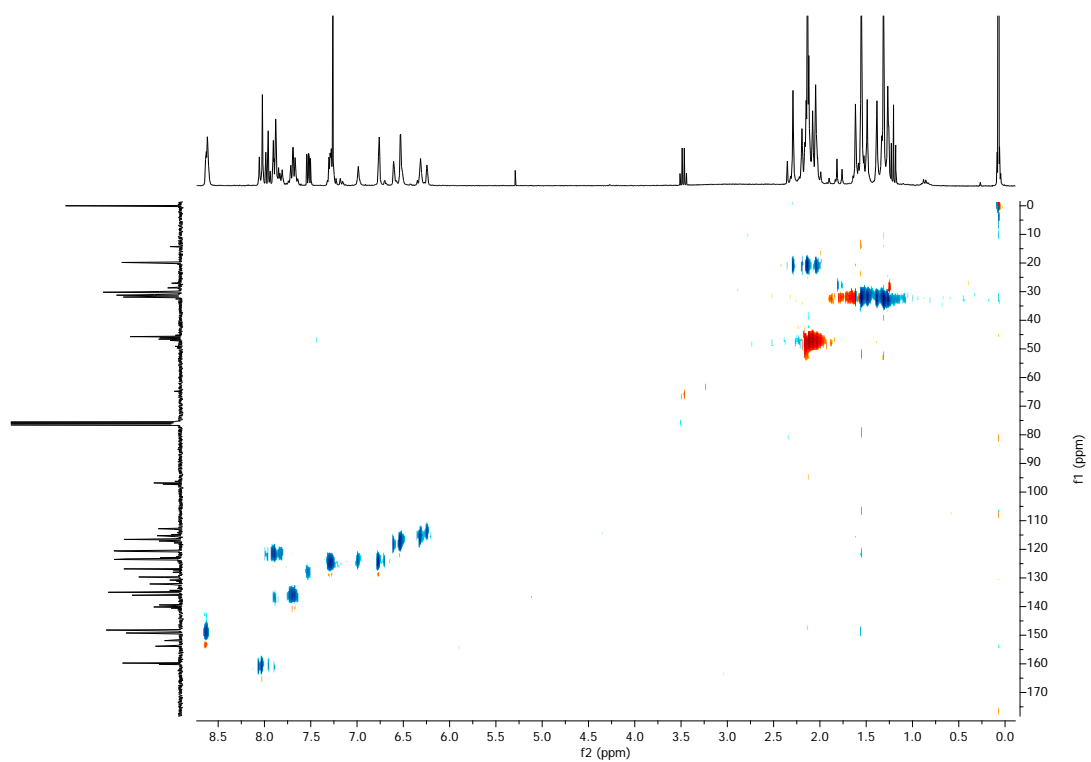
Figure S 6. HSQC of **Lrac**.
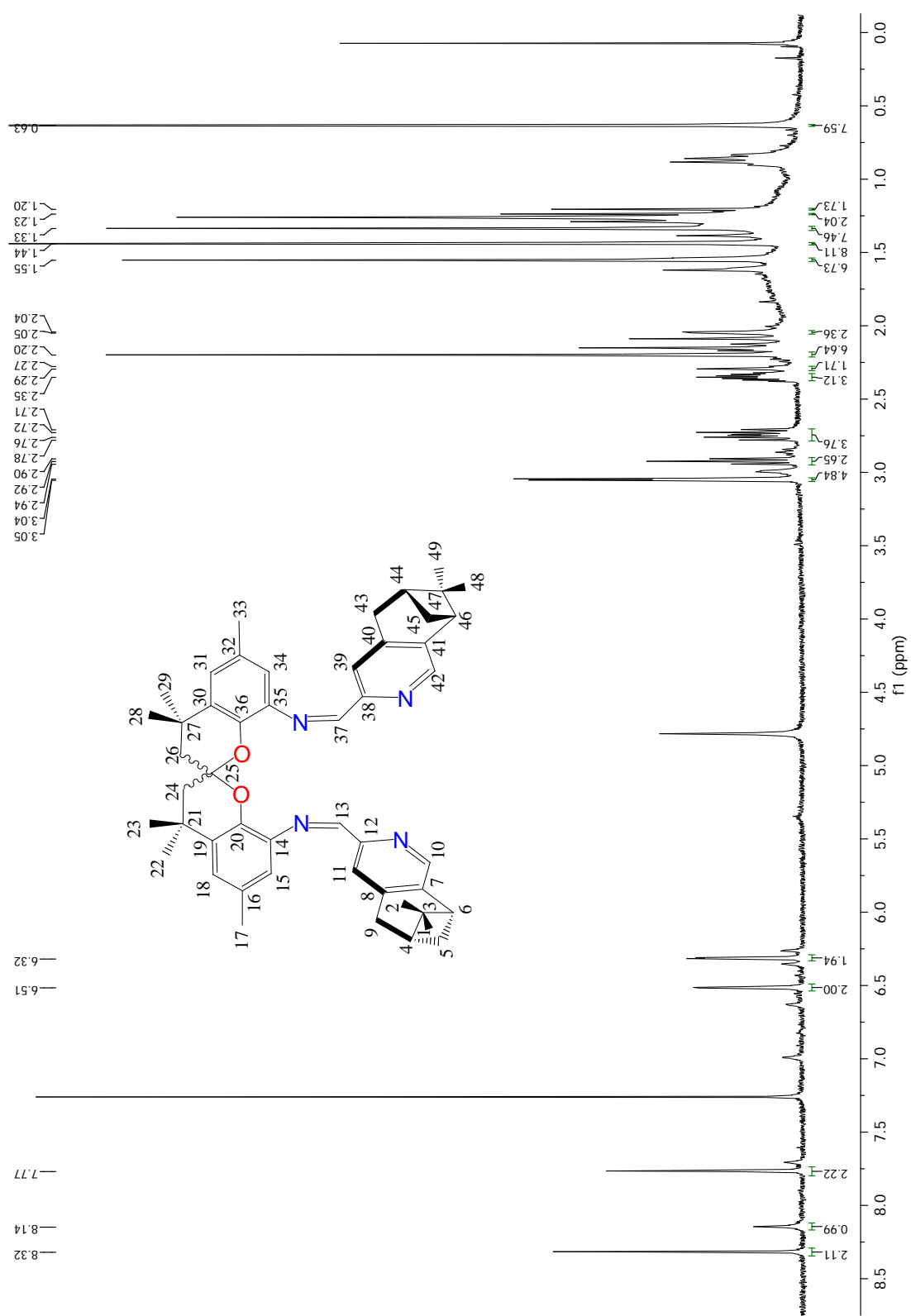
Figure S 7. ^{1}H-NMR of **L(+)4,5**.

Figure S 8. ^{13}C-NMR of **L(+)$_{4,5}$**.

Peak labels (ppm):
21.25, 21.49, 26.05, 29.86, 31.20, 31.53, 32.11, 33.03, 39.25, 40.03, 45.14, 48.21, 98.80, 114.18, 116.07, 121.27, 130.98, 132.23, 135.97, 136.42, 145.92, 146.90, 148.27, 152.00
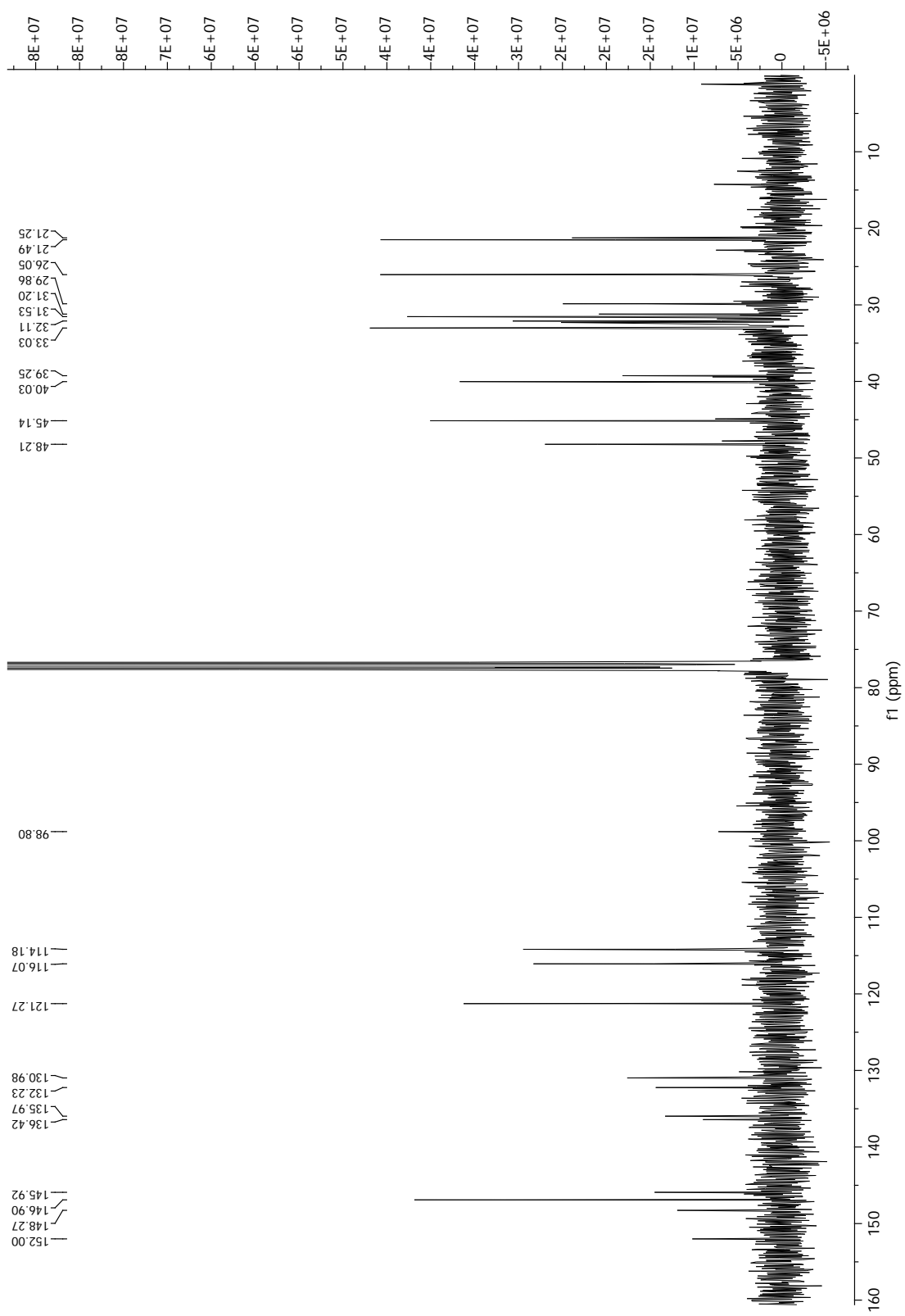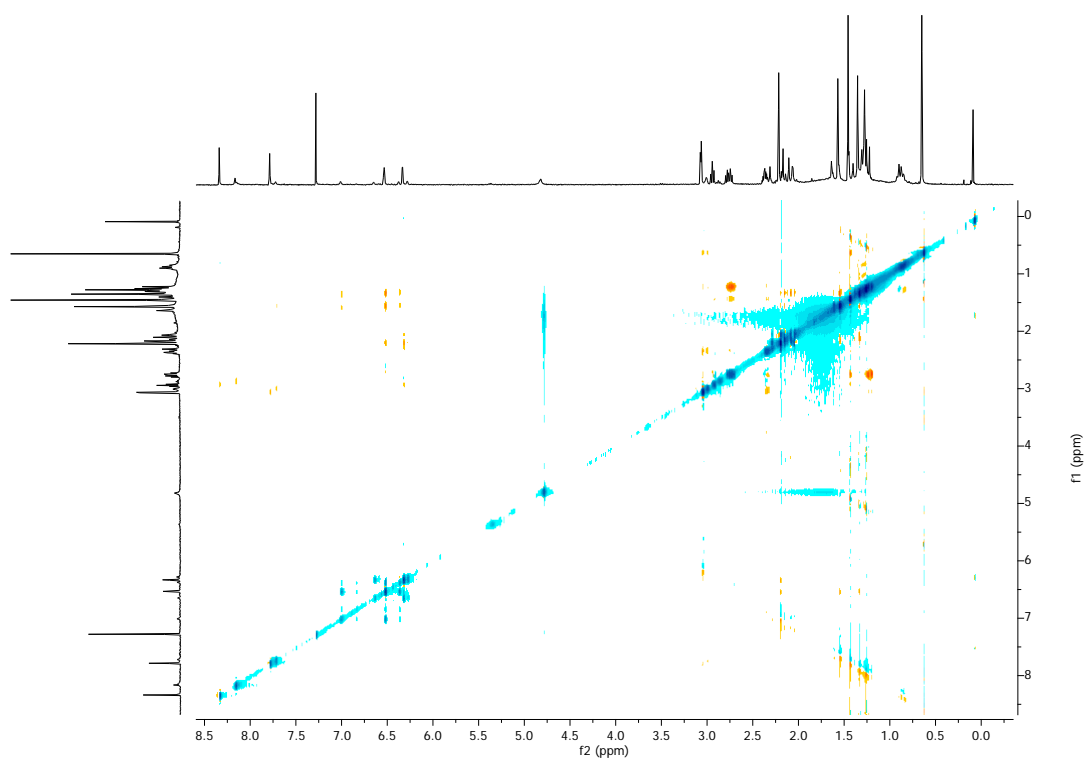
Figure S 9. NOESY of **L(+)**$_{4,5}$.
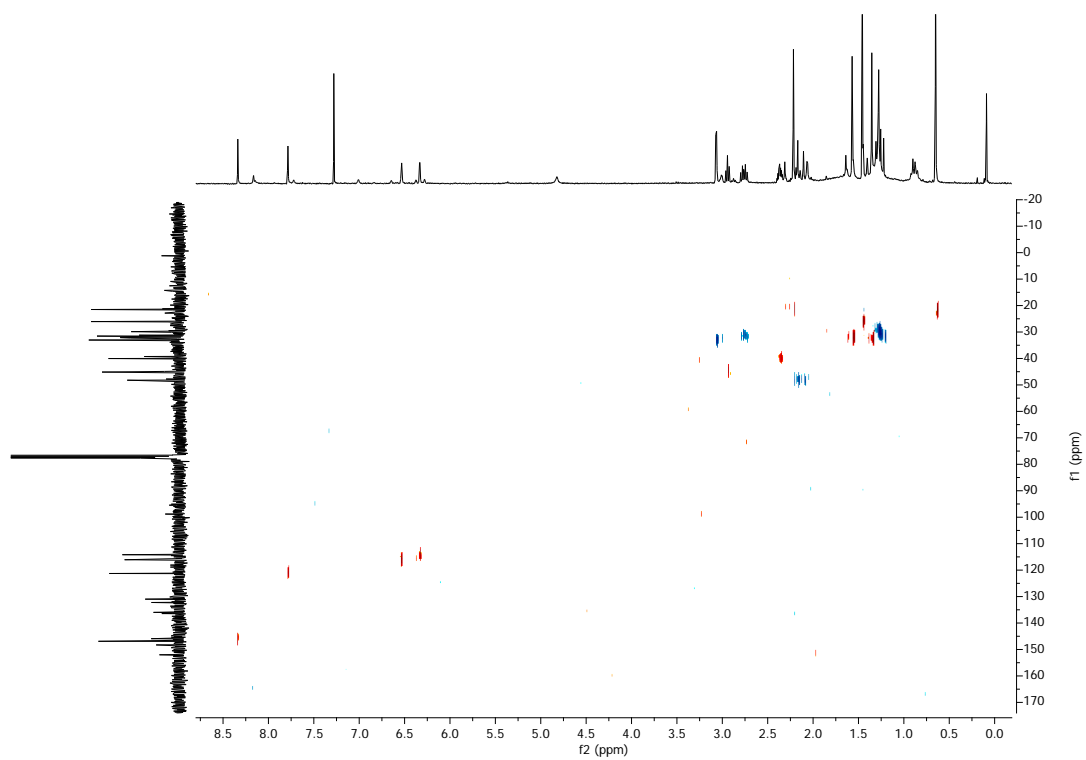
Figure S 10. HSQC of **L(+)**$_{4,5}$.
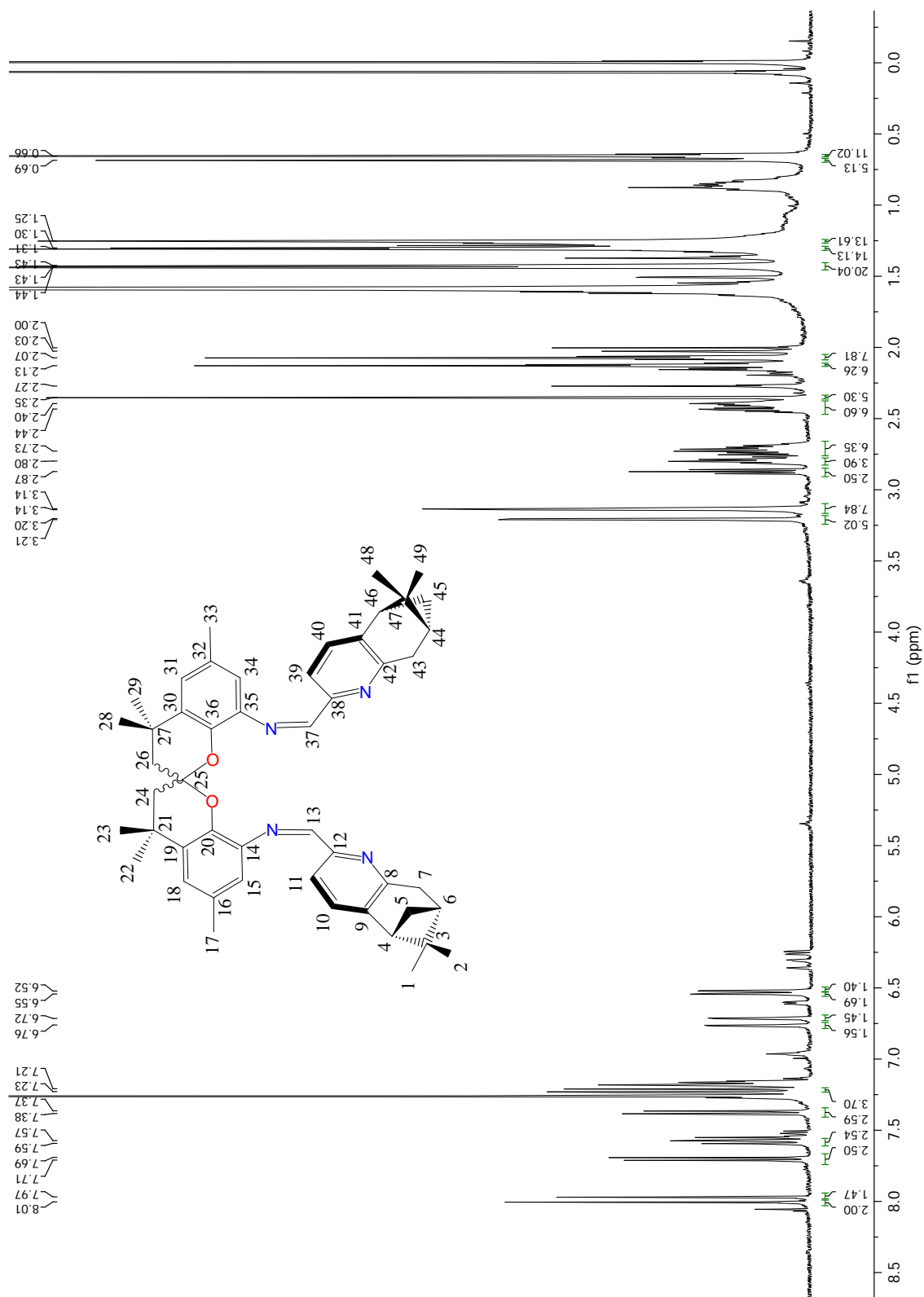
Figure S 11. ^{1}H-NMR of **Lrac$_{5,6}$**.
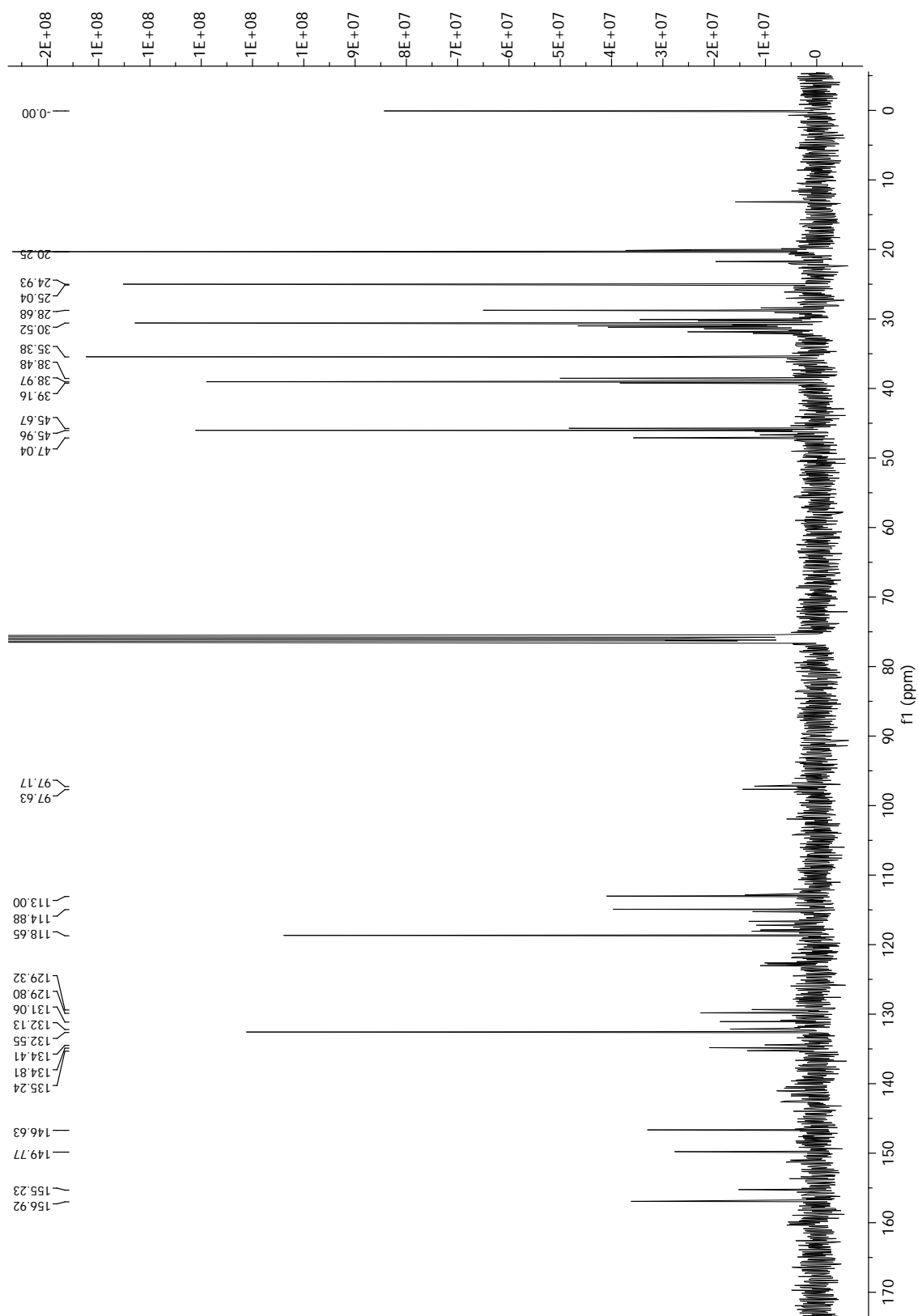
Figure S 12. ^{13}C-NMR of **Lrac$_{5,6}$**.
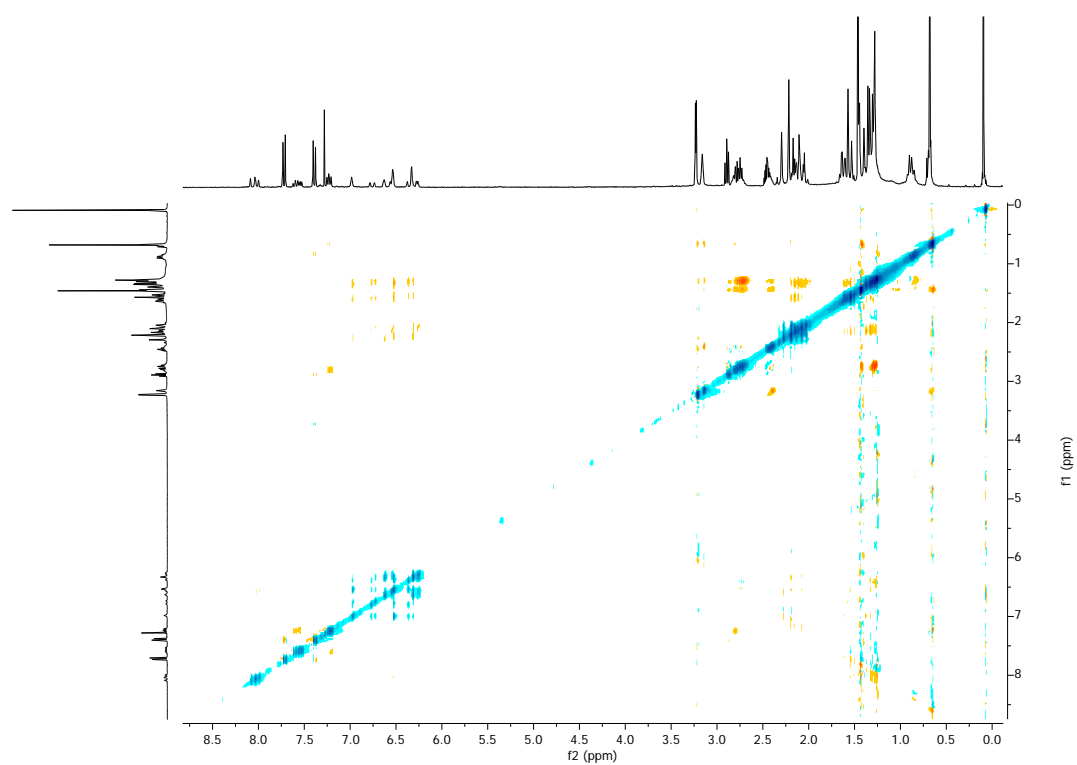
Figure S 13. NOESY of **Lrac$_{5,6}$**.
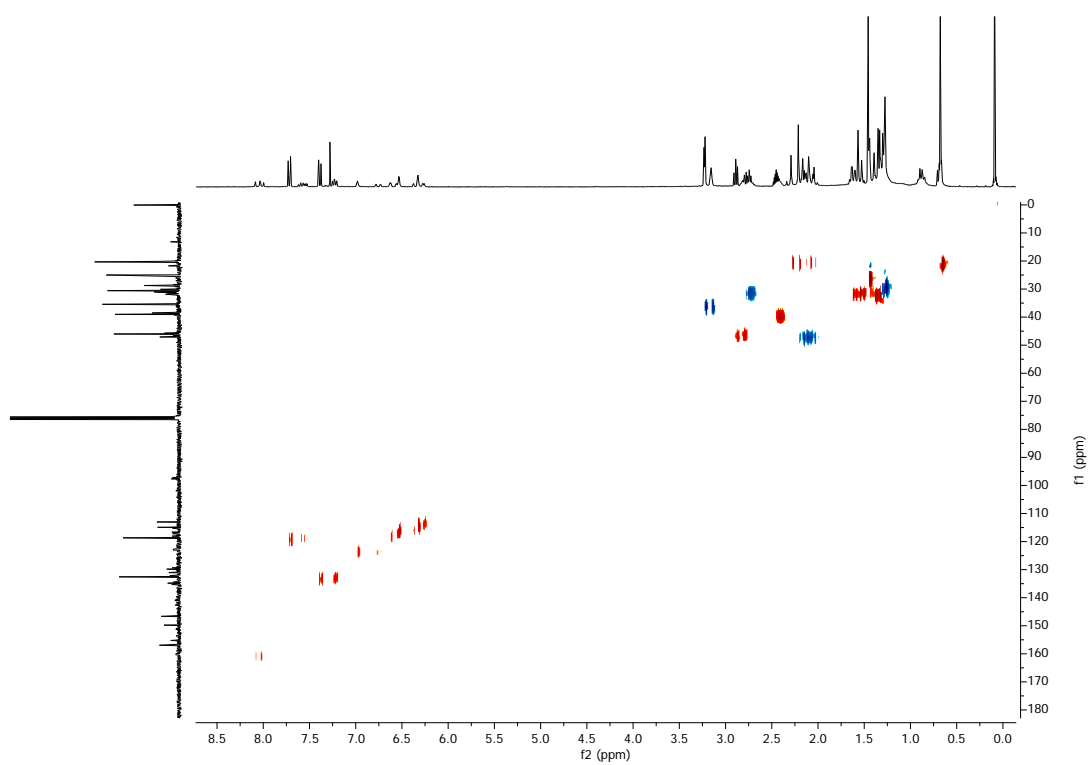
Figure S 14. HSQC of **Lrac$_{5,6}$**.
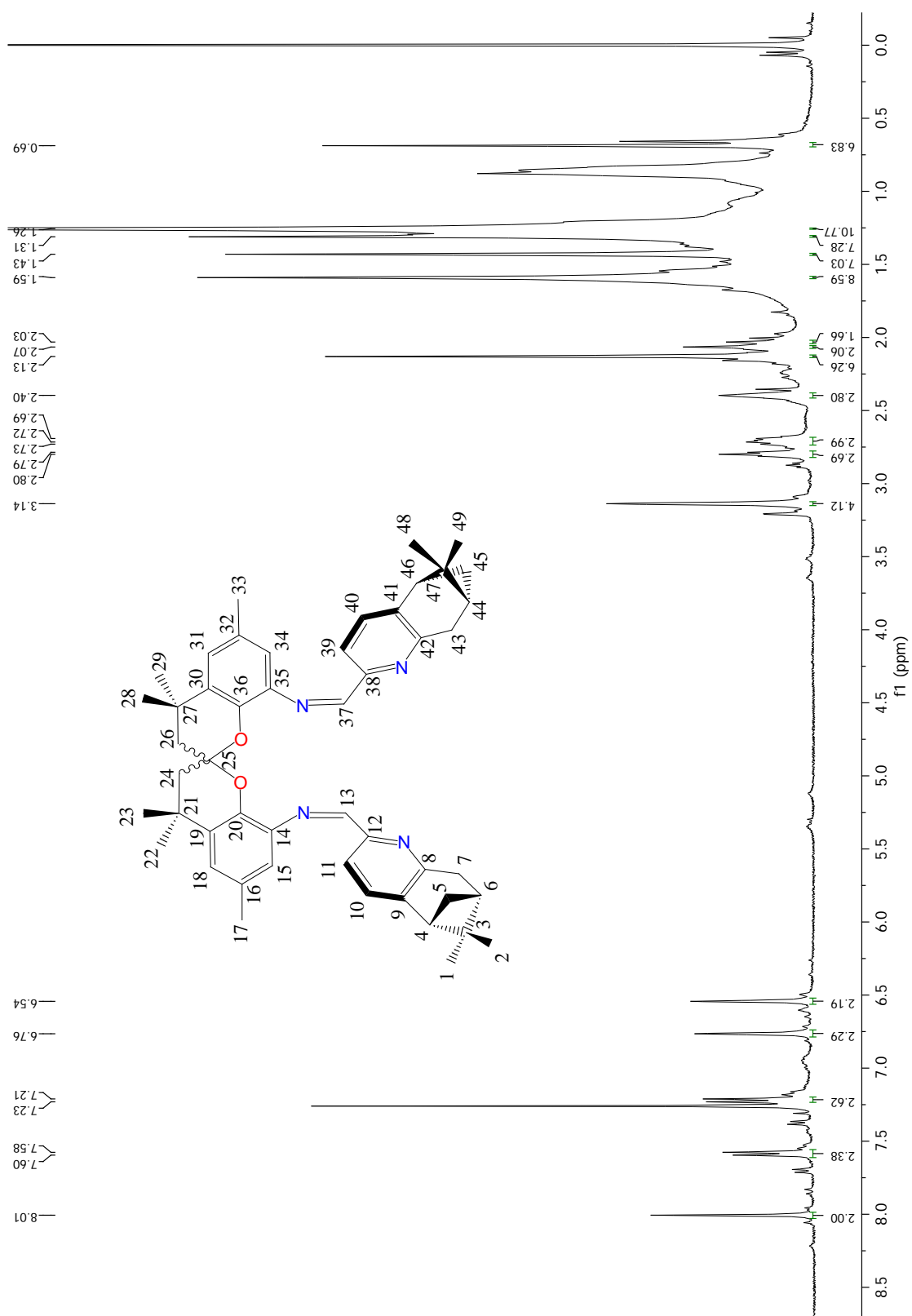
Figure S 15. ^{1}H-NMR of **L(+)$_{5,6}$**.
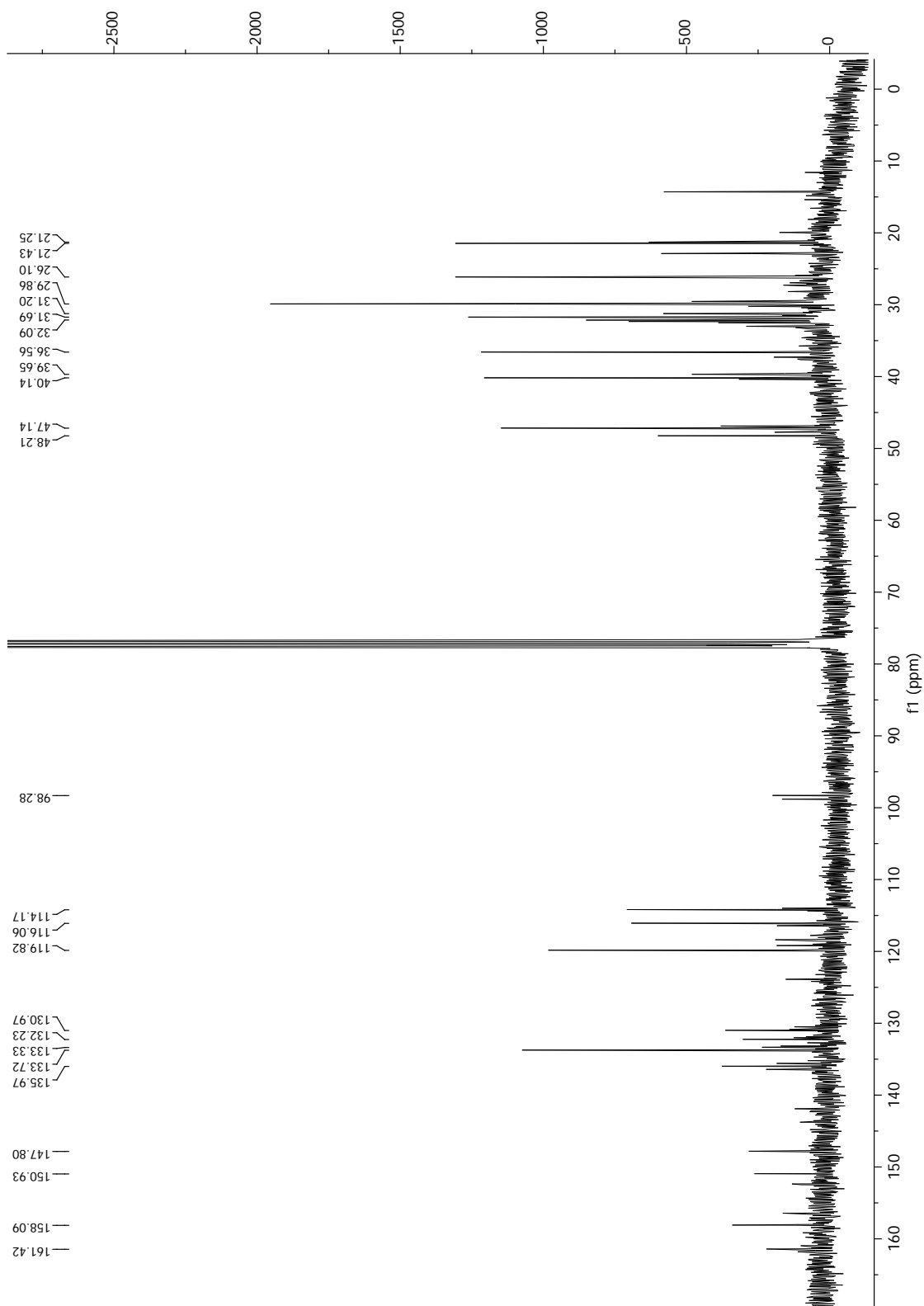
Figure S 16. ^{13}C-NMR of **L(+)$_{5,6}$**.
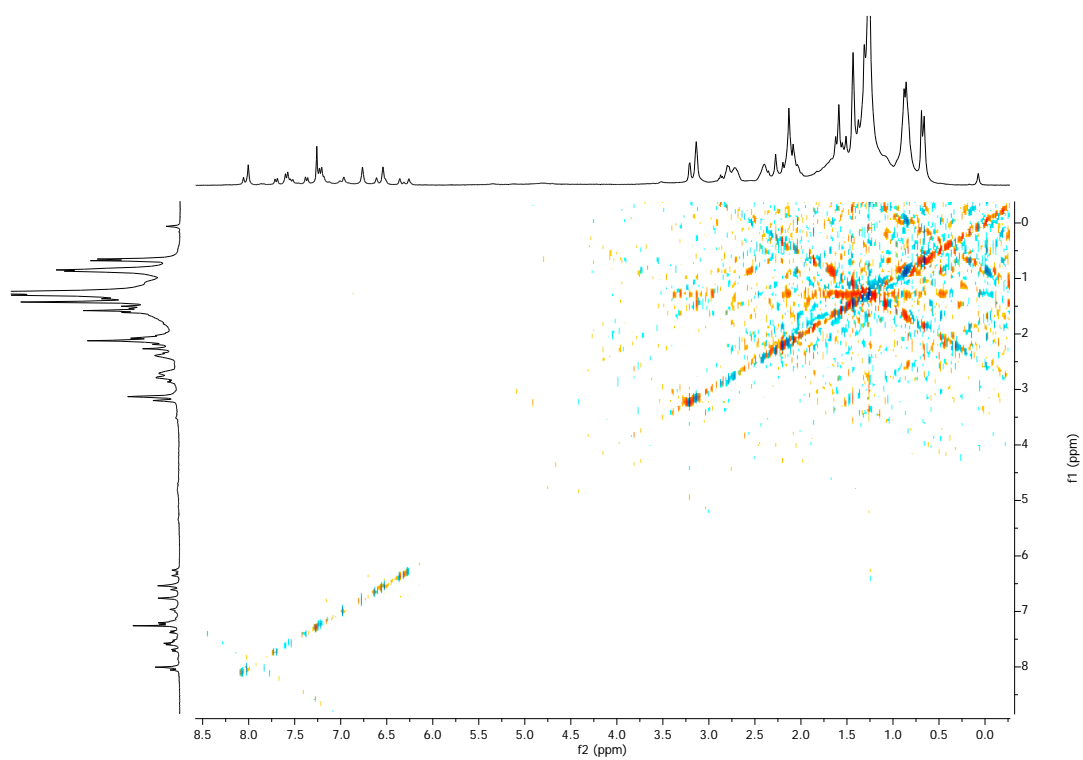
Figure S 17. NOESY of **L(+)₅,₆**.
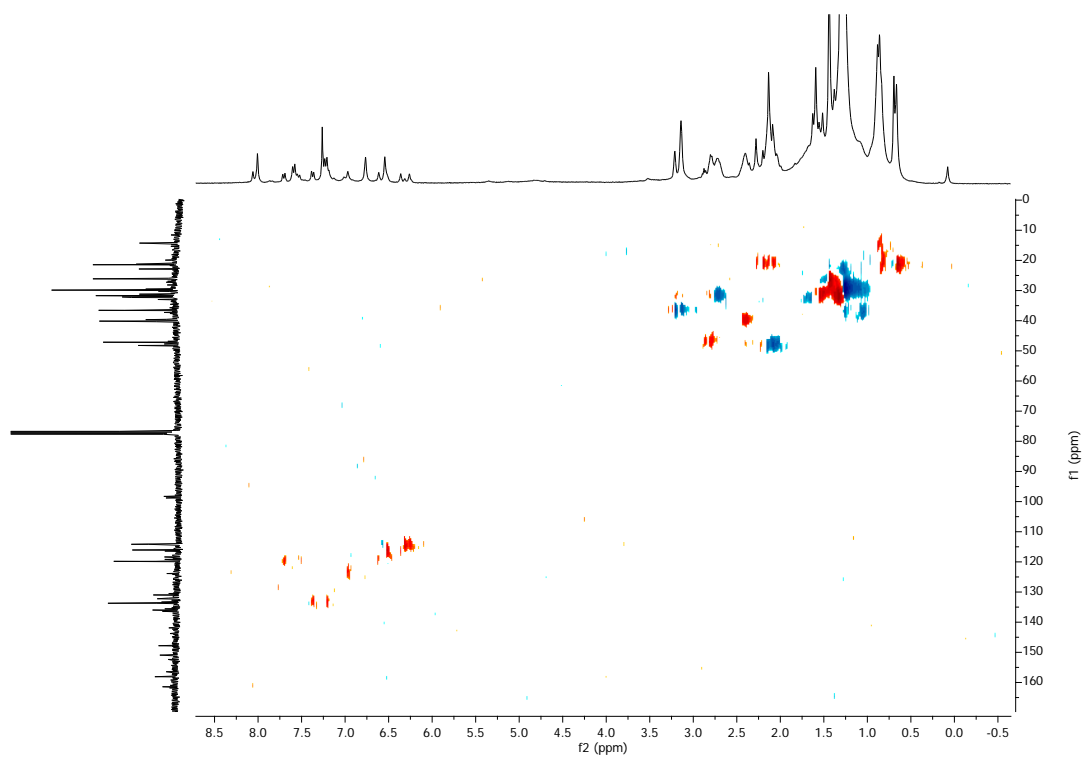
Figure S 18. HSQC of **L(+)₅,₆**.

Figure S 19. ^{1}H-NMR of **L(-)$_{5,6}$**.

21.25
21.42
26.10
29.85
31.20
31.69
32.10
36.55
39.65
40.14

47.13
48.21

98.33

114.16
116.05
119.81

130.96
132.22
133.22
133.72
135.97

147.79

150.93

158.08
161.56
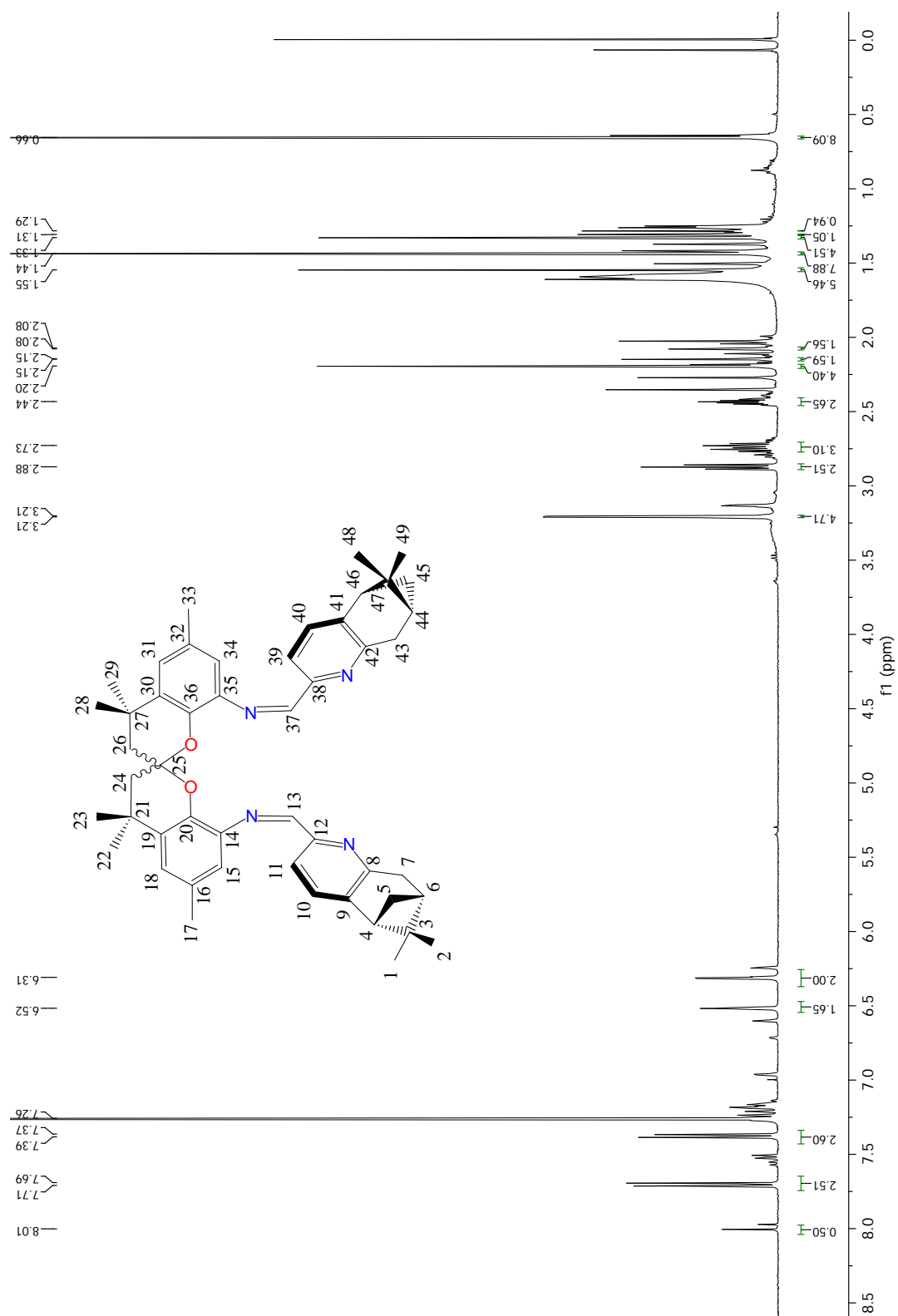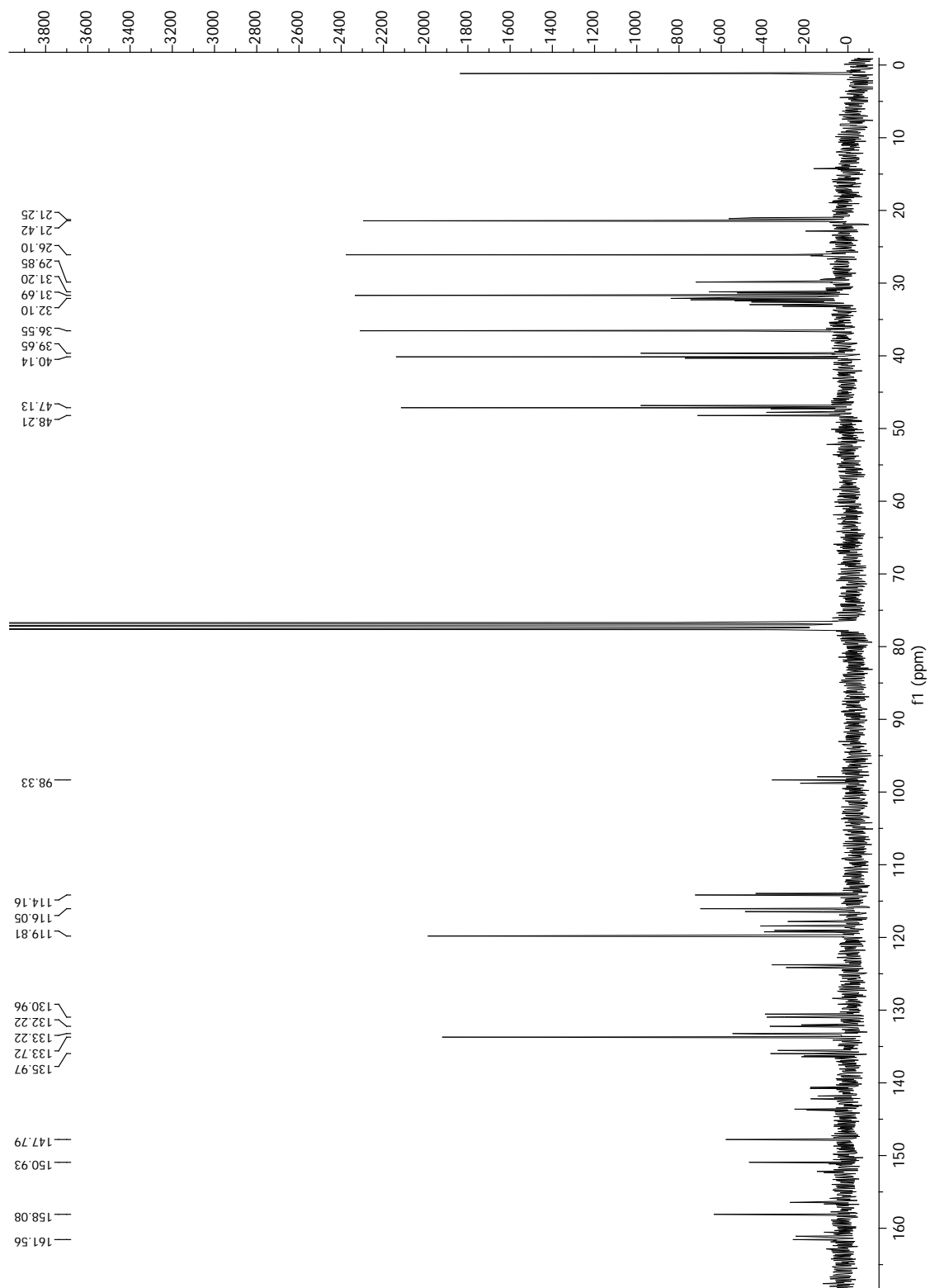
Figure S 20. ^{13}C-NMR of **L(-)₅,₆**.
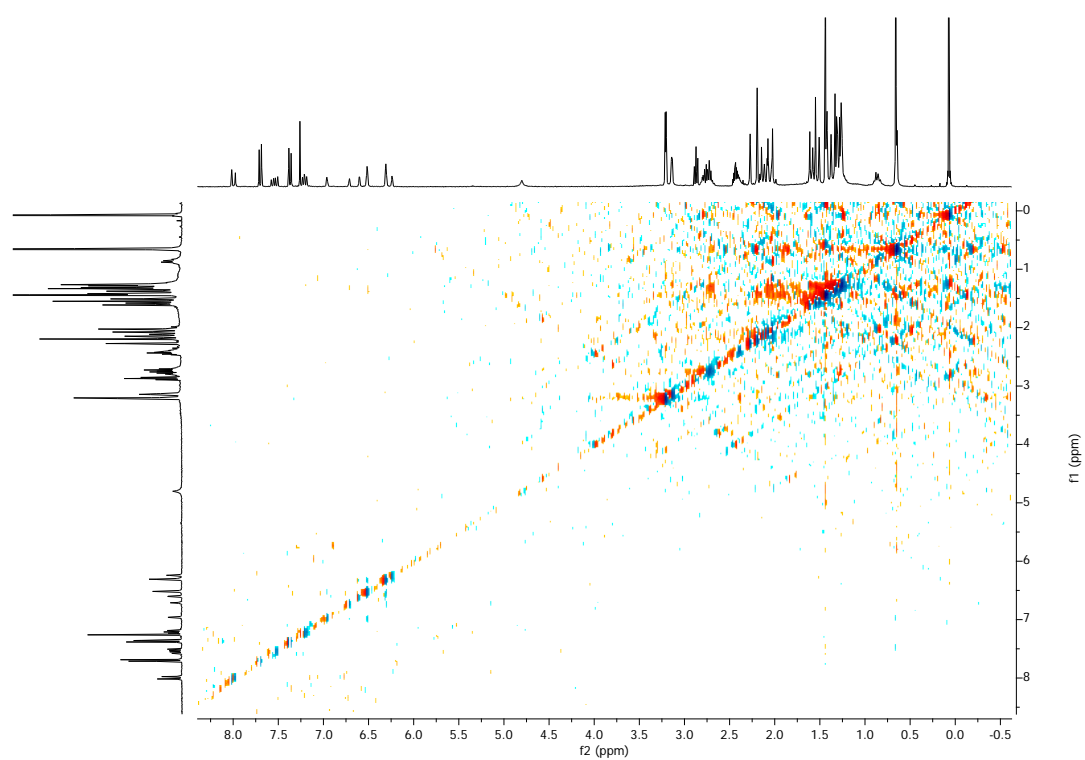
Figure S 21. NOESY of **L(-)$_{5,6}$**.
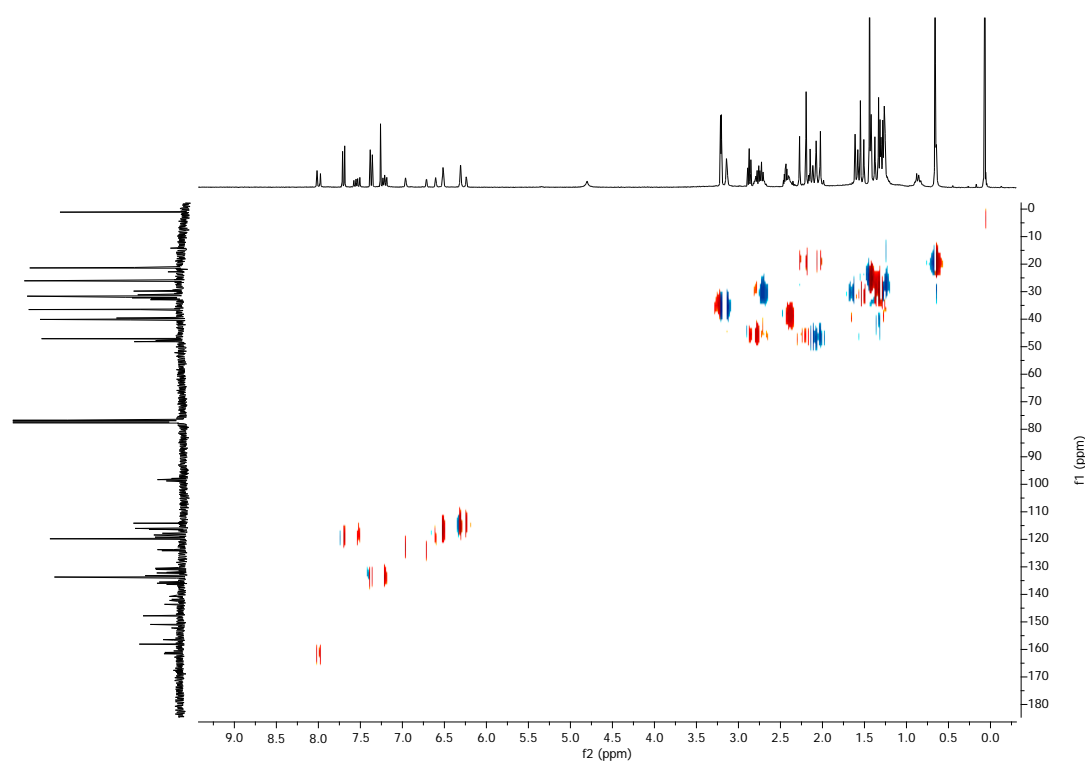
Figure S 22. HSQC of **L(-)$_{5,6}$**.
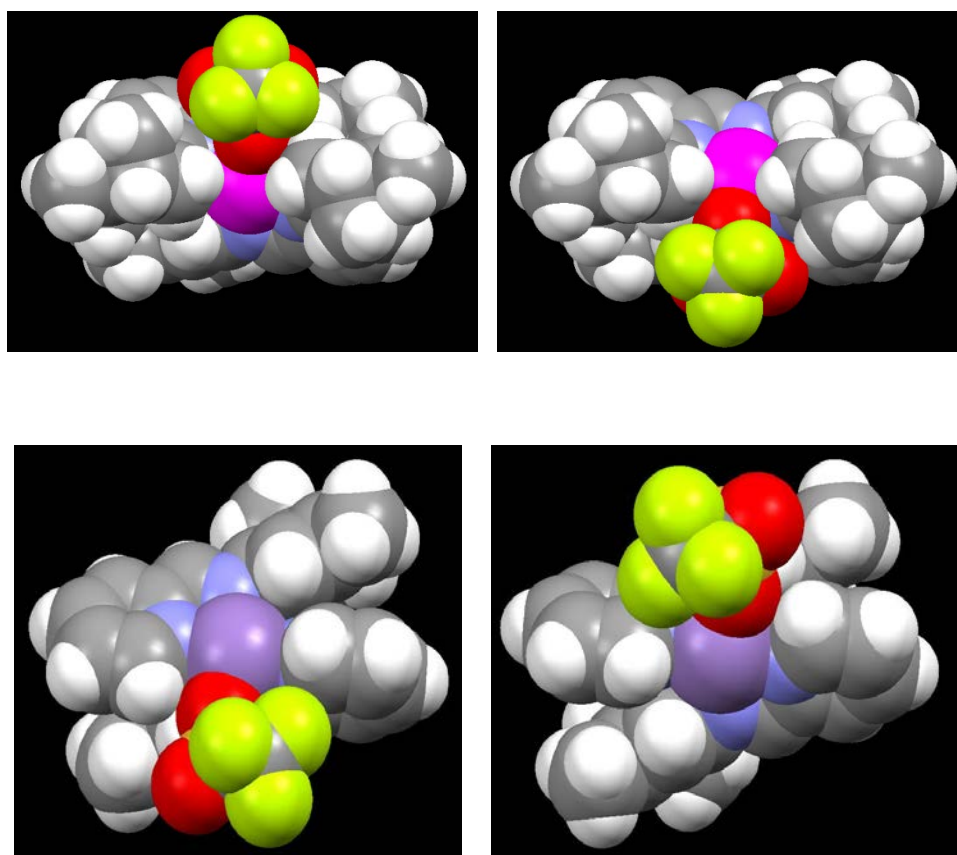
Figure S 23. Spacefilling perspectives of complex **C8** where one of the triflate ligands has been removed in each case.

Figure S 24. Optimized intermediate species and transition states of the [Mn^{IV}(O)$_2$] catalyzed epoxidation of *cis*-β-methyl-styrene.
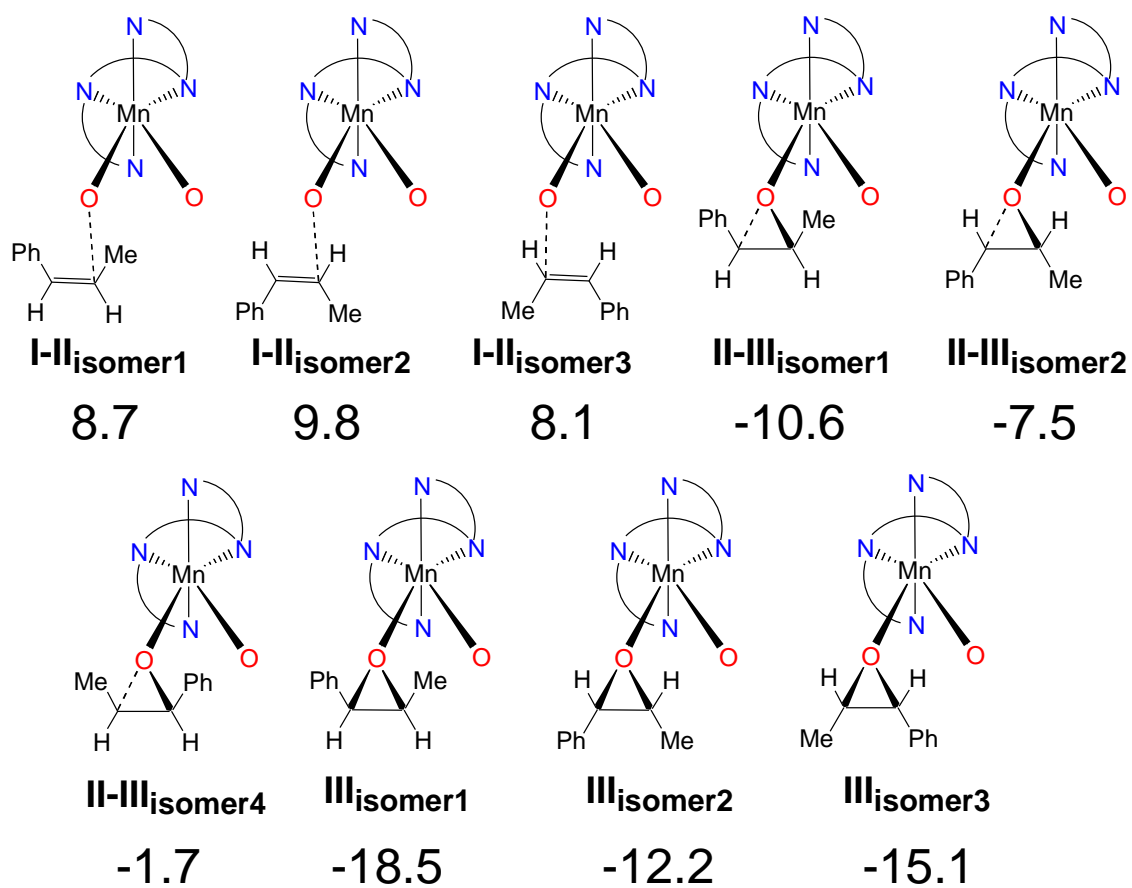
Figure S 25. Isomers of the **I-II**, **II-III** and **III** species (energies in kcal/mol).

Table S 1. Main crystallographic data for complexes **C1**, **C2**, **C6**, **C8** and **C14**.

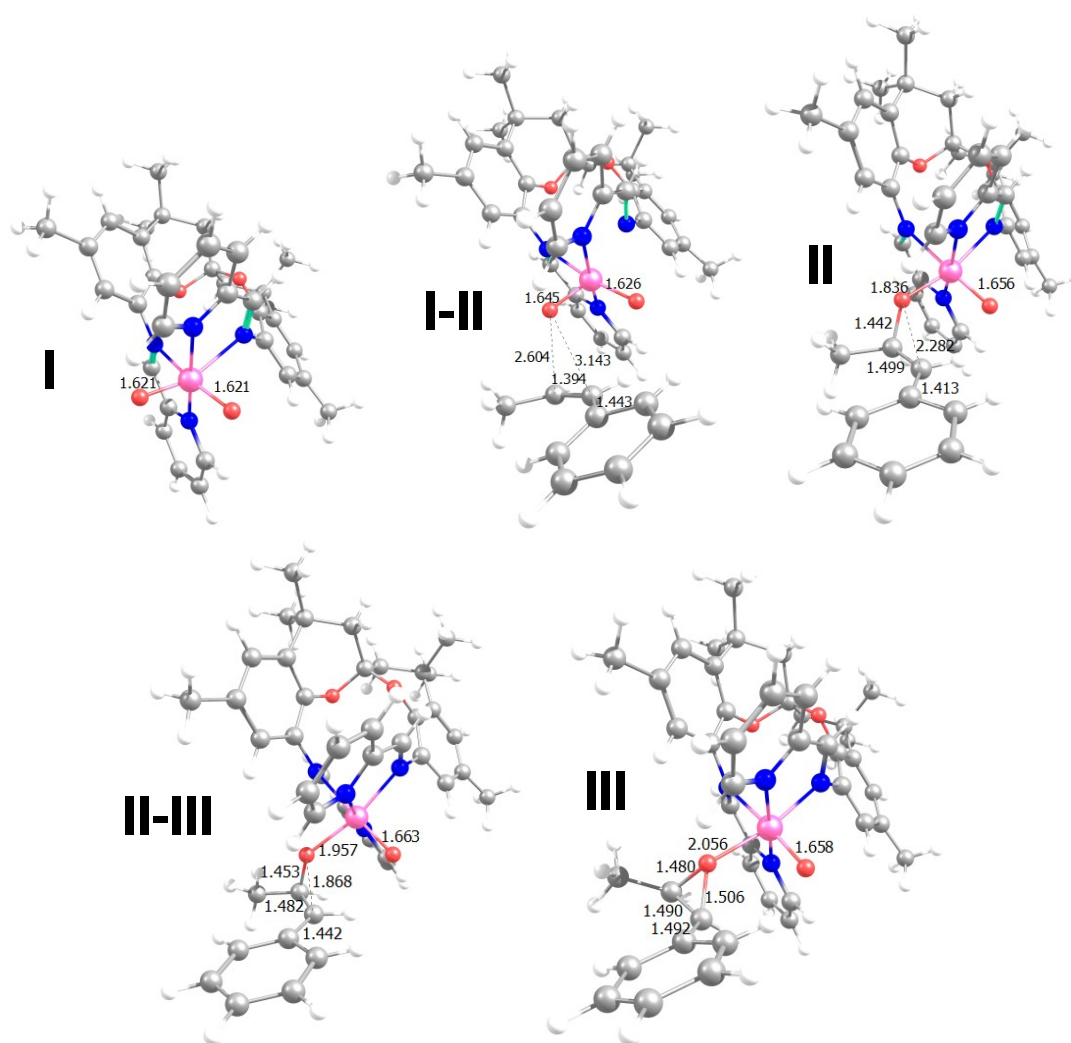|	**C1**·3CH$_3$CN	**C2**	**C6**	**C8**	**C14**·2THF
Empirical formula	C$_{41}$H$_{45}$Cl$_2$MnN$_7$O$_2$	C$_{37}$H$_{36}$F$_6$MnN$_4$O$_8$S$_2$	C$_{49}$H$_{56}$MnN$_6$O$_8$	C$_{51}$H$_{56}$F$_6$MnN$_4$O$_8$S$_2$	C$_{59}$H$_{72}$F$_6$MnN$_4$O$_{10}$S$_2$
Formula weight	793.68	897.76	911.94	1086.06	1230.27
Crystal system	Triclinic	Monoclinic	Tetragonal	Monoclinic	Triclinic
Space group	P-1	C2/c	P3(1)21	C2	P1
a [Å]	10.2524(11)	21.17(2)	17.259(2)	25.227(19)	11.2161(6)
b [Å]	11.8632(13)	14.467(17)	17.259(2)	14.097(11)	13.3318(7)
c [Å]	17.2000(18)	15.489(18)	62.091(18)	16.064(12)	20.5430(10)
α [º]	100.507(2)	90	90	90	100.225(3)
β [º]	93.612(2)	118.735(18)	120	117.332(13)	90.700(3)
γ [º]	93.001(2)	90	120	90	100.100(3)
Volume [Å^3]	2048.5(4)	4160(8)	16017(6)	5075(7)	2973.2(3)
Z	2	4	12	4	2
Calculated density [Mg/m^3]	1.287	1.434	1.134	1.421	1.374
Temperature, K	100(2)	300(2)	300(2)	300(2)	100(2)
Absorption coefficient [mm^{-1}]	0.496	0.498	0.299	0.422	0.371
Final R indices	R1 = 0.0658	0.0619	0.1070	0.0817	0.0756
[I>2 σ (I)]	wR2 = 0.1848	0.1663	0.2556	0.1131	0.2100
R indices	R1 = 0.0793	0.1850	0.3678	0.1861	0.0789
(all data)	wR2 = 0.1951	0.2235	0.3902	0.1465	0.2157

Table S 2. Selected bond lengths [Å] and angles [deg] for **C1**.

Mn(1)-N(4)	2.248(2)	Mn(1)-N(3)	2.378(2)
Mn(1)-N(1)	2.261(2)	Mn(1)-Cl(1)	2.4466(8)
Mn(1)-N(2)	2.359(2)	Mn(1)-Cl(2)	2.4571(8)
N(4)-Mn(1)-N(1)	160.25(9)	N(2)-Mn(1)-Cl(1)	162.83(6)
N(4)-Mn(1)-N(2)	91.91(8)	N(3)-Mn(1)-Cl(1)	93.85(6)
N(1)-Mn(1)-N(2)	71.99(8)	N(4)-Mn(1)-Cl(2)	96.77(7)
N(4)-Mn(1)-N(3)	71.58(9)	N(1)-Mn(1)-Cl(2)	94.77(7)
N(1)-Mn(1)-N(3)	92.88(9)	N(2)-Mn(1)-Cl(2)	90.43(6)
N(2)-Mn(1)-N(3)	75.68(8)	N(3)-Mn(1)-Cl(2)	161.22(6)
N(4)-Mn(1)-Cl(1)	97.70(6)	Cl(1)-Mn(1)-Cl(2)	102.46(3)
N(1)-Mn(1)-Cl(1)	95.38(6)		

Table S 3. Selected bond lengths [Å] and angles [deg] for **C2**.

Mn(1)-O(2)	2.115(4)	Mn(1)-N(1)#1	2.264(4)
Mn(1)-O(2)#1	2.115(4)	Mn(1)-N(2)#1	2.286(4)
Mn(1)-N(1)	2.264(4)	Mn(1)-N(2)	2.286(4)
O(2)-Mn(1)-O(2)#1	95.7(2)	N(1)-Mn(1)-N(2)#1	101.84(15)
O(2)-Mn(1)-N(1)	98.59(15)	N(1)#1-Mn(1)-N(2)#1	72.08(15)
O(2)#1-Mn(1)-N(1)	86.54(15)	O(2)-Mn(1)-N(2)	96.78(15)
O(2)-Mn(1)-N(1)#1	86.54(15)	O(2)#1-Mn(1)-N(2)	156.61(14)
O(2)#1-Mn(1)-N(1)#1	98.59(15)	N(1)-Mn(1)-N(2)	72.08(15)
N(1)-Mn(1)-N(1)#1	172.39(19)	N(1)#1-Mn(1)-N(2)	101.84(15)
O(2)-Mn(1)-N(2)#1	156.61(14)	N(2)#1-Mn(1)-N(2)	78.98(18)
O(2)#1-Mn(1)-N(2)#1	96.78(15)		

Table S 4. Selected bond lengths [Å] and angles [deg] for **C6** (average of the molecules present in the crystal).

Mn(1)-O(6)	2.205	Mn(1)-N(1)	2.305
Mn(1)-O(4)	2.228	Mn(1)-N(2)	2.370
Mn(1)-N(4)	2.302	Mn(1)-N(3)	2.372
O(6)-Mn(1)-O(4)	118.4	N(4)-Mn(1)-N(2)	92
O(6)-Mn(1)-N(4)	83.8	N(1)-Mn(1)-N(2)	70.1
O(4)-Mn(1)-N(4)	109.4	O(6)-Mn(1)-N(3)	149.0
O(6)-Mn(1)-N(1)	105.8	O(4)-Mn(1)-N(3)	86.6
O(4)-Mn(1)-N(1)	83.3	N(4)-Mn(1)-N(3)	70.1
N(4)-Mn(1)-N(1)	158.4	N(1)-Mn(1)-N(3)	94
O(6)-Mn(1)-N(2)	85.6	N(2)-Mn(1)-N(3)	79.4
O(4)-Mn(1)-N(2)	148.5		

Table S 5. Selected bond lengths [Å] and angles [deg] for **C8** (diastereoisomer C8(+)).

Mn(1)-O(2)	2.159(6)	Mn(1)-N(1)	2.234(5)
Mn(1)-O(2)#1	2.159(6)	Mn(1)-N(2)#1	2.288(6)
Mn(1)-N(1)#1	2.234(5)	Mn(1)-N(2)	2.288(6)
O(2)-Mn(1)-O(2)#1	99.8(3)	N(1)#1-Mn(1)-N(2)#1	73.9(2)
O(2)-Mn(1)-N(1)#1	102.5(2)	N(1)-Mn(1)-N(2)#1	99.1(2)
O(2)#1-Mn(1)-N(1)#1	83.2(2)	O(2)-Mn(1)-N(2)	91.1(2)
O(2)-Mn(1)-N(1)	83.2(2)	O(2)#1-Mn(1)-N(2)	168.1(2)
O(2)#1-Mn(1)-N(1)	102.5(2)	N(1)#1-Mn(1)-N(2)	99.1(2)
N(1)#1-Mn(1)-N(1)	171.3(3)	N(1)-Mn(1)-N(2)	73.9(2)
O(2)-Mn(1)-N(2)#1	168.1(2)	N(2)#1-Mn(1)-N(2)	78.5(3)
O(2)#1-Mn(1)-N(2)#1	91.1(2)		

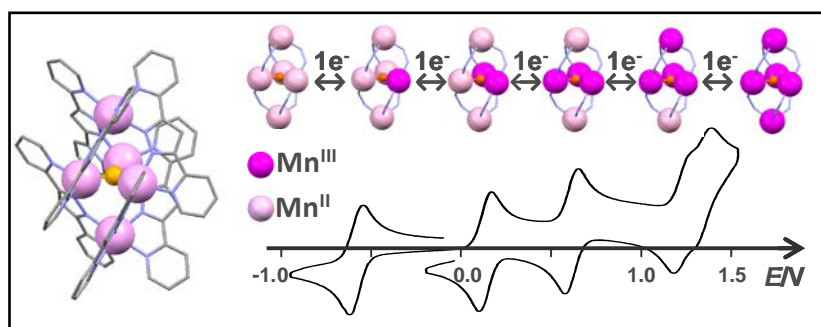**Table S 6.** Selected bond lengths [Å] and angles [deg] for **C8** (diastereoisomer C8(-)).

Mn(1A)-O(2A)	2.162(6)	Mn(1A)-N(1A)#2	2.252(6)
Mn(1A)-O(2A)#2	2.162(6)	Mn(1A)-N(2A)#2	2.281(7)
Mn(1A)-N(1A)	2.252(6)	Mn(1A)-N(2A)	2.281(7)
O(2A)-Mn(1A)-O(2A)#2	93.0(3)	N(1A)-Mn(1A)-N(2A)#2	95.6(2)
O(2A)-Mn(1A)-N(1A)	83.8(2)	N(1A)#2-Mn(1A)-N(2A)#2	73.2(2)
O(2A)#2-Mn(1A)-N(1A)	106.3(2)	O(2A)-Mn(1A)-N(2A)	93.0(2)
O(2A)-Mn(1A)-N(1A)#2	106.3(2)	O(2A)#2-Mn(1A)-N(2A)	173.9(2)
O(2A)#2-Mn(1A)-N(1A)#2	83.8(2)	N(1A)-Mn(1A)-N(2A)	73.2(2)
N(1A)-Mn(1A)-N(1A)#2	165.6(3)	N(1A)#2-Mn(1A)-N(2A)	95.6(2)
O(2A)-Mn(1A)-N(2A)#2	173.9(2)	N(2A)#2-Mn(1A)-N(2A)	81.1(3)
O(2A)#2-Mn(1A)-N(2A)#2	93.0(2)		

Table S 7. Selected bond lengths [Å] and angles [deg] for **C14** (average of the molecules present in the crystal).

Mn(1)-O(3)	2.148	Mn(1)-N(1)	2.2825
Mn(1)-O(6)	2.154	Mn(1)-N(2)	2.2765
Mn(1)-N(4)	2.282	Mn(1)-N(3)	2.293
O(3)-Mn(1)-O(6)	89.805	N(4)-Mn(1)-N(2)	96.75
O(3)-Mn(1)-N(4)	84.655	N(1)-Mn(1)-N(2)	74.93
O(6)-Mn(1)-N(4)	104.055	O(3)-Mn(1)-N(3)	94.775
O(3)-Mn(1)-N(1)	102.685	O(6)-Mn(1)-N(3)	174.70
O(6)-Mn(1)-N(1)	87.165	N(4)-Mn(1)-N(3)	74.30
N(4)-Mn(1)-N(1)	166.74	N(1)-Mn(1)-N(3)	93.915
O(3)-Mn(1)-N(2)	174.395	N(2)-Mn(1)-N(3)	80.515
O(6)-Mn(1)-N(2)	95.025		

Chapter 6

Multi-reversible redox processes in pentanuclear bis(triple-helical) manganese complexes featuring an oxo-centered triangular $\{Mn^{II}_2Mn^{III}(\mu_3\text{-}O)\}^{5+}$ or $\{Mn^{II}Mn^{III}_2(\mu_3\text{-}O)\}^{6+}$ core wrapped by two $\{Mn^{II}_2(bpp)_3\}^-$. Evaluation of the catalytic activity in oxidation reactions.

A new pentanuclear bis(triple-helical) manganese complex has been isolated and characterized by X-ray diffraction in two oxidation states. The structure consists of a central $\{Mn_3(\mu_3\text{-}O)\}$ core of $Mn^{II}_2Mn^{III}$ ($\mathbf{1}^{3+}$) or $Mn^{II}Mn^{II}_2$ ($\mathbf{1}^{4+}$) ions connected to two apical Mn^{II} ions through six bpp^- ligands. This complex exhibits a very rich redox behavior with five distinct and reversible one-electron processes and displays an unexpected and excellent stability of the pentanuclear structure in the following four oxidation states: Mn^{II}_5, $Mn^{II}_4Mn^{III}$, $Mn^{II}_3Mn^{III}_2$ and $Mn^{II}_2Mn^{III}_3$. The spectroscopic characteristics in solution of these four species as well as the solid state magnetic properties of $Mn^{II}_4Mn^{III}$ ($\mathbf{1}^{3+}$) and $Mn^{II}_3Mn^{III}_2$ ($\mathbf{1}^{4+}$) have been investigated. Furthermore, $Mn^{II}_4Mn^{III}$ has been tested as catalyst in epoxidation reactions.

TABLE OF CONTENTS

CHAPTER 6. Multi-reversible redox processes in pentanuclear bis(triple-helical) manganese complexes featuring an oxo-centered triangular {Mn$^{II}_2$Mn^{III}(μ_3-O)}$^{5+}$ or {Mn^{II}Mn$^{III}_2$(μ_3-O)}$^{6+}$ core wrapped by two {Mn$^{II}_2$(bpp)$_3$}$^-$. Evaluation of the catalytic activity in oxidation reactions.

6.1. Introduction

6.1.1. Mn clusters with pyrazole-based ligands

Polynuclear manganese complexes have attracted much attention because of their relevance to the active centers of biological systems as the oxygen-evolving complex of photosystem II,[1-5] and also for the design of single-molecule magnets owing to their remarkable magnetic properties which result from the exchange interaction between paramagnetic centers.[6-12] Hundreds of such complexes have been isolated in the last decades in various nuclearity, core topology and oxidation levels.[1,13-15] Their synthesis still relies on serendipitous self-assembly with appropriate ligands. While carboxylates, Schiff base derivatives, alkoxides and more recently oximes have been widely employed[16-25] as bridging ligands for the formation of these molecular manganese compounds, the use of pyrazole-based ligands is still limited (Figure 1).[26-32]
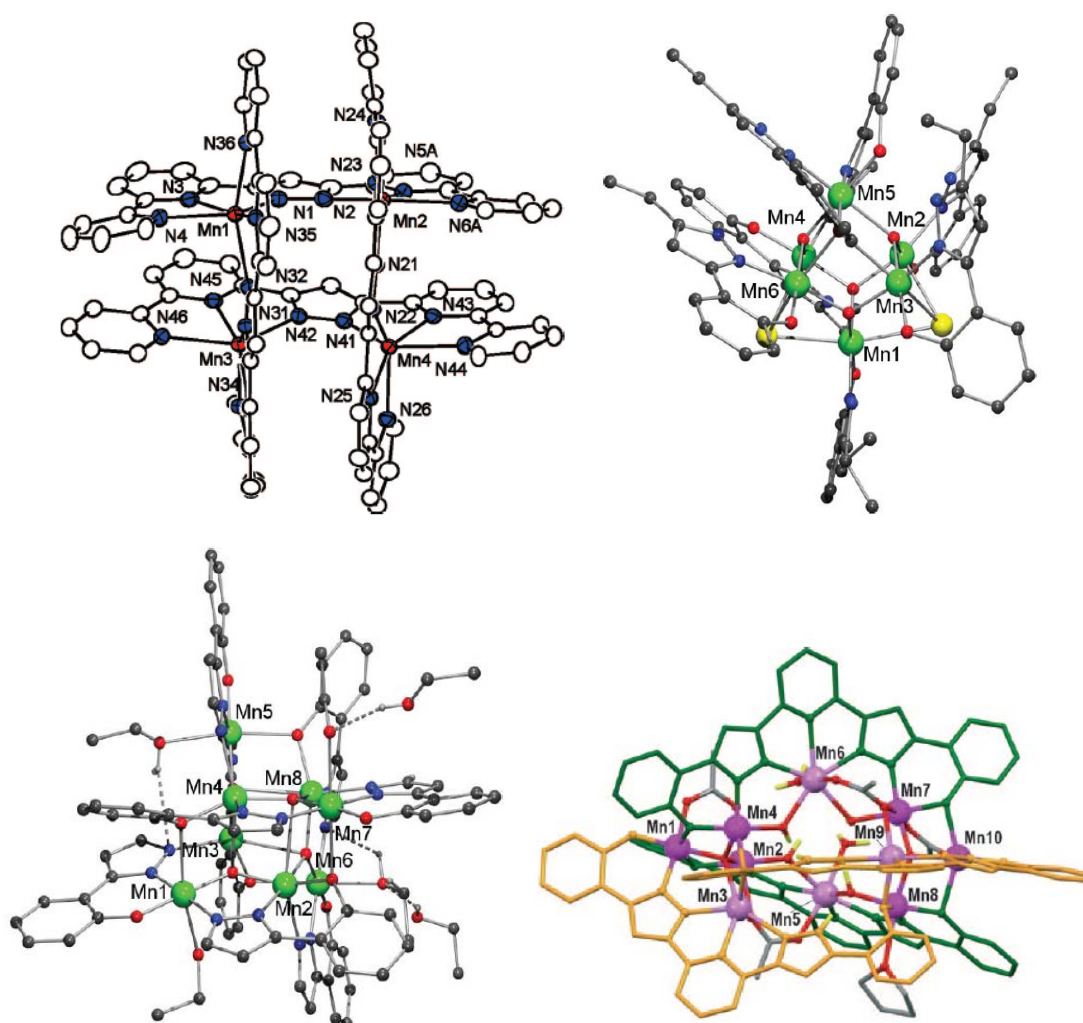

Figure 1. Some examples of Mn clusters with pyrazole-based ligands, with different nuclearity and core topology.

The 3,5-bis(pyridin-2-yl)-pyrazole ligand (Hbpp, Figure 2) is an attractive ligand of this family, which has lead to the isolation of several dinuclear complexes with ruthenium[33-35] and various first row transition metal ions (Ni^{2+}, Cu^{2+}, Fe^{2+}, Co^{2+}, Zn^{2+}), either homo-[27,36 -46] or hetero-bimetallic (Cr^{III}-$M^{II/III}$ with M = Fe^{2+}, Ln^{3+}, Mn^{2+} and Ni^{2+})).[47-50] Very recently, some larger complexes having intriguing triple-helical structure have been also obtained, namely $[Fe^{II}_5(\mu_3\text{-}O)(bpp)_6]^{2+}$ and $[M^{II}_5(\mu_3\text{-}OH)(bpp)_6]^{3+}$ (M = Ni^{2+}, Zn^{2+} or Cu^{2+}).[51-53] In these pentanuclear complexes, a central $\{M^{II}_3(\mu_3\text{-}O)\}^{4+}$ or $\{M^{II}_3(\mu_3\text{-}OH)\}^{5+}$ core is wrapped by two terminal $\{M^{II}(bpp)_3\}^-$ units, forming rare examples of helicates, in which metal cores define the helicate axis.[54 -62] Nevertheless, the use of the Hbpp ligand for the design of manganese compounds is restricted to the hetero-bimetallic dinuclear Cr^{III}-Mn^{II}.[50] In addition, the solution stability of the isolated $[M^{II}_5(\mu_3\text{-}O)(bpp)_6]^{2+}$ and $[M^{II}_5(\mu_3\text{-}OH)(bpp)_6]^{3+}$ compounds has been poorly investigated and limited to ESI-MS and ^1H NMR analyses[51,58] and their redox properties remain unexplored so far.

A $[M^{II}_5(\mu_3\text{-}O)(L)_6]^{2+}$ helicate structure has also been reported with two related L ligands, 3,5-bis(benzimidazol-2-yl)pyrazole (H_3bbp, with M = Zn^{2+} and Cd^{2+})[58] and 3,5-bis(pyridin-2-yl)-1,2,4-triazole (Hbpt, for M = Fe^{2+}) (Figure 2).[63]

Finally the study of the magnetic properties of this type of helicate complexes has been deeply investigated for $[Cu^{II}_5(\mu_3\text{-}OH)(bpp)_6]^{3+}$ and $[Fe^{II}_5(\mu_3\text{-}O)(bpt)_6]^{2+}$. It has been shown that the helicate arrangement introduces peculiar magnetic properties such as spin-frustation in the case of the copper complex,[53] while for the iron complex, the spin state of the two terminal iron(II) can be tuned by the nature of the counterion.[63]
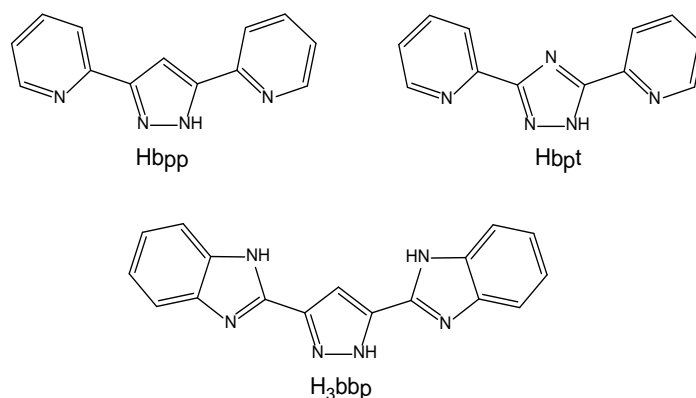

Figure 2. Pyrazole-based ligands.

6.1.2. Catalytic properties

Some small nuclearity Mn_x clusters (X≤4) containing Mn^{3+} and/or Mn^{4+} have been shown to function as homogeneous oxidation catalysts for reactions such as organic oxidation and water oxidation, using H_2O_2, organic peroxides, or other activated O-atom sources as oxidants.[64-70] Recently, Christou et al.[71] have studied the use of a new family of Mn_{12} and $CeMn_6$ clusters (Figure 3) as homogeneous catalysts for activation of molecular O_2 and its use in the selective oxidation of benzyl alcohol to benzaldehyde but this is one of the scarce works where high nuclearity Mn compounds have been studied as oxidation catalysts.
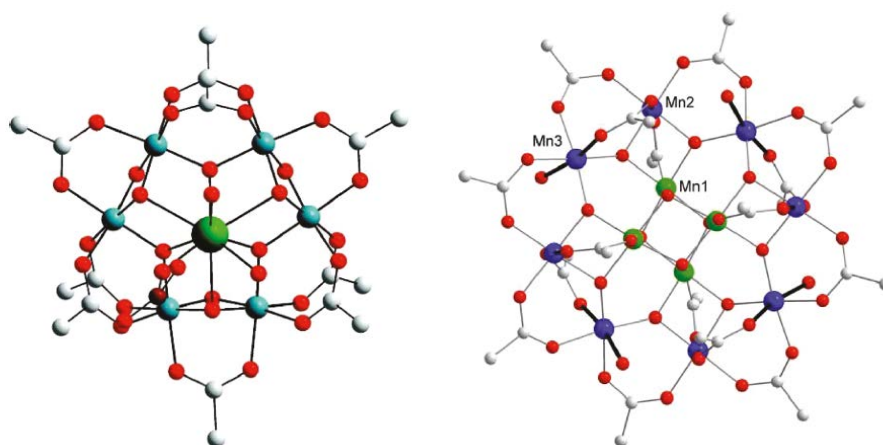
Figure 3. Clusters used in catalysis by Christou.

The understanding of the mechanism for O-O bond activation and the characterization of the reactive intermediates are crucial to design better catalysts for the oxygenation reactions. The exact nature of the oxygenating species and the mechanism of oxygen transfer to the substrate remain unclear, although the participation of multiple active oxidants has been proposed to account for the catalytic activity in most cases.[72-74]

6.2. Objectives

Our research group has extensively studied the coordination of ruthenium to the bridging ligand 3,5-bis(pyridin-2-yl)-pyrazole (Hbpp, Figure 2), as well as the catalytic activity of the complexes obtained towards water oxidation. With these precedents, the main objective of this chapter was to study the coordination of the Hbpp ligand to manganese ions.

We initially considered to synthesize and fully characterize the resulting complexes through structural, analytical, spectroscopic (EPR, UV-Vis, ESI-MS) and electrochemical (CV) techniques. The type of complex obtained led us to carry out a broader redox study together with a throughout magnetic characterization.

Finally, we were interested in the ability of the obtained polynuclear species towards the catalytic epoxidation of a series of substrates in homogeneous phase at room temperature, using commercial peracetic acid (32%) as the oxidant. This latest study allowed us to compare the degree of performance observed with that of related mononuclear manganese complexes previously synthesized.

6.3. Results and discussion

6.3.1. Synthesis and characterization

The pentanuclear complex $[\{Mn^{II}(\mu\text{-bpp})_3\}_2Mn^{II}_2Mn^{III}(\mu_3\text{-O})](ClO_4)_3$, $\mathbf{1}(ClO_4)_3$, was synthesized in ~ 50 % yield in a methanolic or acetonitrile medium under aerobic conditions, by stirring a reaction mixture consisting of $Mn(ClO_4)_2\cdot6H_2O$ and bpp$^-$ in a 5/6 molar ratio at reflux for few hours. The oxygen in air acts as an oxidant for the oxidation of one Mn^{II} ion of the complex into Mn^{III} leading to the isolation of the $Mn^{II}_4Mn^{III}$ ($\mathbf{1}^{3+}$) oxidation state. The corresponding $Mn^{II}_3Mn^{III}_2$ oxidation state ($\mathbf{1}^{4+}$) was obtained by an electrochemical oxidation of a solution of $\mathbf{1}^{3+}$ in acetonitrile and has also been isolated in the solid state (complex $[\{Mn^{II}(\mu\text{-bpp})_3\}_2Mn^{II}Mn^{III}_2(\mu_3\text{-O})](ClO_4)_4$, $\mathbf{1}(ClO_4)_4$, see Experimental section).

X-ray quality crystals of $\mathbf{1}^{3+}$ and $\mathbf{1}^{4+}$ were obtained by slow vapor diffusion of diethyl ether into solutions of the respective complex. Based on the charge of the cations, $\mathbf{1}^{3+}$ and $\mathbf{1}^{4+}$, and the presence of a μ_3-oxo bridge, the Mn oxidation states are given, as mentioned earlier, as $Mn^{II}_4Mn^{III}$ and $Mn^{II}_3Mn^{III}_2$ respectively. This mixed-valent description has been confirmed by a careful analysis of the X-ray structures, which evidenced the presence of Mn^{III} ion(s) in the central core (see below). The structures of $\mathbf{1}^{3+}$ and $\mathbf{1}^{4+}$ are shown in Figure 4 together with an ORTEP scheme of the central cores. Selected bond distances and angles are listed in Table 1 and Table 2, whereas main crystallographic data can be found in the supporting information (Table S 1).

The five Mn ions in $\mathbf{1}^{3+}$ and $\mathbf{1}^{4+}$ form a trigonal bipyramidal motif, in which the two Mn^{II} ions occupy the apical positions and the three Mn ions connected by a μ_3-O^{2-} ion are placed in the equatorial plane. The same topological motif was found in the single-molecule magnet $(NEt_4)_3[Mn_5O(salox)_3(N_3)_6Cl_2]$ (H_2salox = salicylaldoxime)[13,20,75] in which three Mn^{III} ions are located in the equatorial position. The central $\{Mn_3(\mu_3\text{-O})\}$ core of $Mn^{II}_2Mn^{III}$ ($\mathbf{1}^{3+}$) or $Mn^{II}Mn^{III}_2$ ions ($\mathbf{1}^{4+}$) is connected to the two apical Mn^{II} ions through six bpp$^-$ ligands. Both cations have a triple-stranded helicate configuration and a pair of enantiomers is present in each crystal as previously observed in related $[M^{II}_5(\mu_3\text{-O})(L)_6]^{2+}$ and $[M^{II}_5(\mu_3\text{-OH})(bpp)_6]^{3+}$ complexes.[51-53,58,63] In contrast to $\mathbf{1}^{3+}$, $\mathbf{1}^{4+}$ adopts a symmetric structure with a C_2 axis passing through the central Mn(3) and the μ_3-O ion that leads to the equivalence of the two remaining central manganese ions, Mn(1) and Mn(1)#, and also to the equivalence of the apical Mn(2) and Mn(2)#. In both compounds, the three Mn ions of the central core present a distorted N_4O trigonal

bipyramid environment. The oxo bridging ligand is located in the equatorial plane of each bipyramid, together with two N-pyridine atoms of two bpp$^-$ ligands. The axial positions are occupied by two N-pyrazole atoms of the latter bpp$^-$ ligands. The trigonal indices[76] for 1^{3+} are of τ = 0.83 (Mn(2)), 0.81 (Mn(4)) and 0.76 (Mn(5)), while for 1^{4+} they are of τ = 0.65 (Mn(1,1#)) and 0.82. (Mn(3)). The three Mn atoms of the {Mn$_3(\mu_3$-O)} central core form a nearly equilateral triangle with the oxygen in the center. For 1^{3+}, the central μ_3-O atom is slightly displaced from the Mn$_3$ triangular plane (0.033 Å) while for 1^{4+}, it lies on the C_2 axis and exactly in the plane of the Mn$_3$ triangle. All Mn···Mn distances in 1^{3+} are significantly longer than those in 1^{4+} (Mn$_{central}$···Mn$_{central}$: average, 3.492 Å for 1^{3+} and 3.279 Å for 1^{4+}; Mn$_{central}$···Mn$_{terminal}$: average, 4.403 Å for 1^{3+} and 4.281 Å for 1^{4+}).

The coordination geometry of the two apical Mn^{II} ions corresponds to a slightly distorted octahedron, consisting of six nitrogen atoms from three bridging bpp$^-$ ligands. Each tetradentate bpp$^-$ ligand bonds one apical and one equatorial Mn ion by one N-pyridine and one N-pyrazole. As usually observed in complexes with bpp$^-$ ligand,[27,33-46,51-53,77,78] the Mn-N$_{pyridine}$ distances are longer than the Mn-N$_{pyrazole}$ ones.

[Mn$_5(\mu_3$-O)(bpp)$_6$]$^{3+/4+}$ are the first manganese pentanuclear bis(triple-helical) complexes reported in which a {Mn$_3(\mu_3$-O)}$^{5+/6+}$ core is wrapped by two terminal {Mn^{II}(bpp)$_3$}$^-$ units. These manganese complexes are the first examples of such helicates that contain trivalent metal ion(s). Although many μ_3-O trinuclear complexes have been reported in the Mn^{II}Mn$^{III}_2$ and Mn$_3^{III}$ oxidation states,[1,12,19,21,24,31,79 -87] to the best of our knowledge, 1^{3+} contains the first example of an oxo-centered {Mn$^{II}_2$Mn$^{III}(\mu_3$-O)}$^{5+}$ trinuclear unit.

As expected for its lower oxidation state, the position of the Mn^{II} ions in the complexes can be assigned on the basis of the longer Mn-ligand bond distances compared to the Mn^{III} ions. In both systems, the two apical Mn ions are thus readily assigned to Mn^{II} centers since their Mn-N bond distances are (i) longer than those of the central core, and (ii) poorly affected by the change of the oxidation state of the complex (in 1^{3+}: average, 2.256 (0.062) Å for Mn(1) and 2.261 (0.060) Å for Mn(3); in 1^{4+}: average 2.244 (0.044) Å for Mn(2)). In addition, all Mn-ligand bond distances of the central core are significantly shorter in 1^{4+} than in 1^{3+}, in accordance with an additional Mn^{III} ion for 1^{4+}.
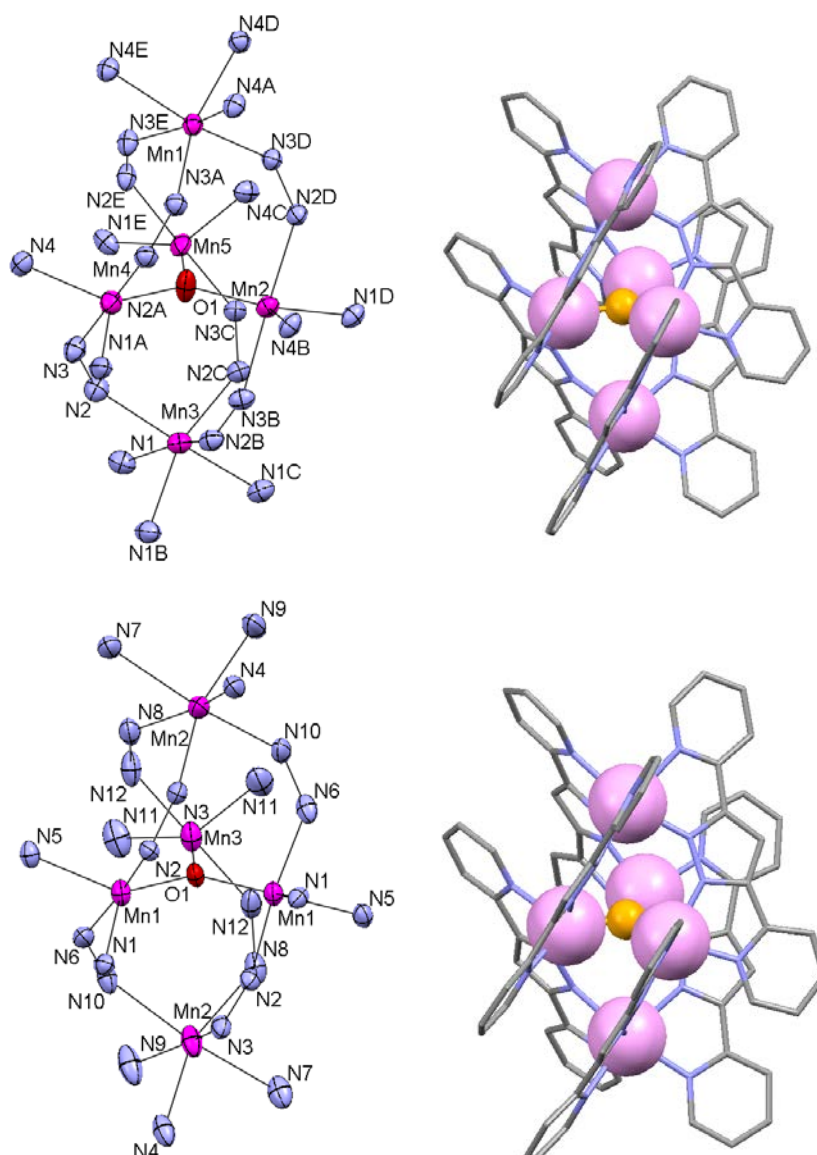
Figure 4. Structures of the $[\{Mn^{II}(\mu\text{-bpp})_3\}_2Mn^{II}_2Mn^{III}(\mu\text{-O})]^{3+}$ (1^{3+}) and $[\{Mn^{II}(\mu\text{-bpp})_3\}_2Mn^{II}Mn^{III}_2(\mu\text{-O})]^{4+}$ (1^{4+}) cations: left, ORTEP drawing (30 % probability thermal ellipsoids), noncoordinated atoms of the bpp⁻ ligands omitted for clarity; right, ball-and-stick representation; Mn ions in pink color and oxygen in orange.

Regarding the electron localization or delocalization in the central core, in 1^{4+}, the Mn(1,1#)-O(1) bond distances (1.870(3) Å) are notably shorter than the Mn(3)-O(1) bond distance (1.962(5) Å), and the Mn(1)···Mn(1)# bond distance (3.2384(16) Å) is shorter than the Mn(1,1#)···Mn(3) ones (3.319 Å). In fact, all bond distances to Mn(3) (average 2.053 (0.072) Å) are slightly longer than those for Mn(1,1#) (average 1.993 (0.112) Å). By comparison with the structural characteristics of the previously reported valence-trapped $\{Mn^{II}Mn^{III}_2(\mu_3\text{-O})\}^{6+}$ trinuclear complexes,[1,12,19,21,31,79-86] it can thus be

213

concluded that the central core in $\mathbf{1}^{4+}$ is not fully localized with, nevertheless, the Mn(3) site possessing a dominant +II oxidation state and Mn(1) and Mn(1#) having a dominant +III oxidation state.

Because, to our knowledge, the cation of $\mathbf{1}^{3+}$ contains the first example of an oxo-centered $\{Mn_2^{II}Mn^{III}(\mu_3\text{-O})\}^{5+}$ trinuclear unit, the crystallographic characteristics of this core can't be compared with literature data. One can however notice that the average of all bond distances around each Mn of the central core in $\mathbf{1}^{3+}$ (average, 2.154 (0.069) Å for Mn(2), 2.126 (0.070) Å for Mn(4) and 2.107 (0.087) Å for Mn(5)) are too long for a localized Mn^{III} ion (expected value $\leq$ 2.0 Å). This indicates that the trinuclear center core of $\mathbf{1}^{3+}$ is probably a fully electron delocalized spin system.

Table 1. Selected Bond Lengths (Å) and Angles (deg) for $\mathbf{1}(ClO_4)_3 \cdot 2.5CH_3CN \cdot C_4H_{10}O \; 0.5H_2O$.

Mn(1)-N(3A)[a]	2.1878(19)	Mn(3)-N(2B)[a]	2.193(2)		
Mn(1)-N(3D)[a]	2.1971(19)	Mn(3)-N(2C)[a]	2.2170(19)		
Mn(1)-N(3E)[a]	2.216(2)	Mn(3)-N(2)[a]	2.210(2)		
Mn(1)-N(4E)[b]	2.305(2)	Mn(3)-N(1B)[b]	2.316(2)		
Mn(1)-N(4D)[b]	2.3078(19)	Mn(3)-N(1C)[b]	2.318(2)		
Mn(1)-N(4A)[b]	2.323(2)	Mn(3)-N(1)[b]	2.314(2)		
Mn(2)-O(1)	2.0442(17)	Mn(4)-O(1)	2.0156(17)	Mn(5)-O(1)	1.9894(17)
Mn(2)-N(2D)[a]	2.1547(18)	Mn(4)-N(2A)[a]	2.121(2)	Mn(5)-N(2E)[a]	2.077(2)
Mn(2)-N(3B)[a]	2.1448(19)	Mn(4)-N(3)[a]	2.122(2)	Mn(5)-N(3C)[a]	2.084(2)
Mn(2)-N(1D)[b]	2.202(2)	Mn(4)-N(4)[b]	2.181(2)	Mn(5)-N(1E)[b]	2.195(2)
Mn(2)-N(4B)[b]	2.223(2)	Mn(4)-N(1A)[b]	2.192(2)	Mn(5)-N(4C)[b]	2.191(2)
Mn(2)-Mn(5)	3.509(5)	Mn(2)-Mn(4)	3.491(5)	Mn(4)-Mn(5)	3.476(5)
Mn(1)-Mn(2)	4.455(5)	Mn(1)-Mn(4)	4.377(5)	Mn(1)-Mn(5)	4.410(5)
Mn(3)-Mn(2)	4.377(5)	Mn(3)-Mn(4)	4.433(5)	Mn(3)-Mn(5)	4.368(5)
Mn(4)-O(1)-Mn(2) 119.59(8)		Mn(5)-O(1)-Mn(2) 119.88(8)		Mn(5)-O(1)-Mn(4) 120.45(9)	

[a]N-pyrazole. [b]N-pyridine.

Table 2. Selected Bond Lengths (Å) and Angles (deg) for **1**(ClO$_4$)$_4$·2CH$_3$CN·2C$_4$H$_{10}$O.

Mn(2)-N(8)^a	2.179(5)		
Mn(2)-N(3)^a	2.224(5)		
Mn(2)-N(10)^a	2.229(5)		
Mn(2)-N(9)^b	2.259(5)		
Mn(2)-N(4)^b	2.268(6)		
Mn(2)-N(7)^b	2.307(5)		
Mn(1)-O(1)^a	1.870(3)	Mn(3)-O(1)	1.962(5)
Mn(1)-N(2)^a	1.932(4)	Mn(3)-N(12)^a	2.024(5)
Mn(1)-N(6)^a	1.942(4)	Mn(3)-N(11)^b	2.127(6)
Mn(1)-N(5)^b	2.090(4)		
Mn(1)-N(1)^b	2.131(4)		
Mn(1)-Mn(1)#	3.238(2)	Mn(1)-Mn(3)	3.318(2)
Mn(2)-Mn(1)	4.266(1)	Mn(2)-Mn(1)#	4.268(1)
Mn(2)-Mn(3)	4.294(1)		
Mn(1)-O(1)-Mn(1)	120.0(3)	Mn(1)-O(1)-Mn(3)	120.02(13)

6.3.2. Electrochemistry

The cyclic voltammogram of **1**$^{3+}$ in CH$_3$CN (Figure 5A) displays one reversible reduction wave at $E_{1/2}$ = -0.58 V vs Ag$^+$/Ag (ΔEp = 70 mV) and four successive reversible oxidation waves at $E_{1/2}$ = +0.13 (ΔEp = 70 mV), +0.61 (ΔEp = 70 mV), +1.21 (ΔEp = 90 mV) and +1.33 V (ΔEp = 90 mV) at a scan rate of 100 mV·s^{-1}. Each of the five reversible redox processes corresponds to the exchange of one-electron per molecule of complex as evidenced by rotating disk electrode experiments (not shown). These waves are assigned to the Mn$^{II}_4$Mn^{III}/Mn$^{II}_5$, Mn$^{II}_3$Mn$^{III}_2$/Mn$^{II}_4$Mn^{III}, Mn$^{II}_2$Mn$^{III}_3$/Mn$^{II}_3$Mn$^{III}_2$, Mn^{II}Mn$^{III}_4$/Mn$^{II}_2$Mn$^{III}_3$, and Mn$^{III}_5$/Mn^{II}Mn$^{III}_4$ redox couples, respectively. The low value (-0.58 V *vs* Ag$^+$/Ag) found for the Mn$^{II}_4$Mn^{III}/Mn$^{II}_5$ redox couple is consistent with the obtaining of the one-electron oxidized complex straight from the synthesis as described above. Bulk electrolysis experiments confirm that the reduction process and the two first oxidation processes correspond to the exchange of one electron. The two oxidized species, Mn$^{II}_3$Mn$^{III}_2$ (**1**$^{4+}$) and Mn$^{II}_2$Mn$^{III}_3$ (**1**$^{5+}$), are quantitatively generated (Figure 5B and C) by two successive electrolyses at E = +0.35 and E = +0.90 V of a solution of **1**$^{3+}$. In contrast, the reduced Mn$^{II}_5$ species (**1**$^{2+}$) has

partially precipitated at the end of the electrolysis (E = -0.70 V) as an orange powder (Figure 5D). In all cases, back electrolyses restore quantitatively $\mathbf{1}^{3+}$, demonstrating the perfect reversibility of the different processes and the stability of the pentanuclear structure in four oxidation states, namely Mn^{II}_5 ($\mathbf{1}^{2+}$), $Mn^{II}_4Mn^{III}$ ($\mathbf{1}^{3+}$), $Mn^{II}_3Mn^{III}_2$ ($\mathbf{1}^{4+}$) and $Mn^{II}_2Mn^{III}_3$ ($\mathbf{1}^{5+}$). As verified by the X-ray diffraction analysis of crystals of $\mathbf{1}^{4+}$ (see above and experimental section), the two first oxidation processes located at +0.13 V and +0.60 V leading to $\mathbf{1}^{4+}$ and $\mathbf{1}^{5+}$, are related to the oxidation of the Mn^{II} ions of the central core.

The two last oxidation processes are thus related to the oxidation of the two apical Mn^{II} ions. The presence of two one-electron redox processes close in potential (+1.20 and +1.32 V) instead of a two-electron single wave is in accordance with the presence of two identical electroactive centres in the molecule that can electronically communicate.[88,89] This is the case of the two apical Mn^{II} sites that can interact through the conjugation of the bridging bpp$^-$ ligands and the central core. Attempts to electrogenerate the $Mn^{II}Mn^{III}_4$ ($\mathbf{1}^{6+}$) and Mn^{III}_5 ($\mathbf{1}^{7+}$) species have failed. Exhaustive electrolyses at E = +1.25 or +1.50 V involve a large excess of coulometry (5.5 additional electrons per molecule of complex are exchanged) and lead to the full decomposition of the pentanuclear structure attested by the disappearance of the five initial waves on the resulting cyclic voltammogram. Moreover, several new irreversible redox processes are observed (two weakly intense, quasi-reversible, at $E_{1/2}$= +1.12 and 1.02 V, and two more intense, irreversible, at E_{pc} = +0.38 and 0.0 V), which are not likely to correspond to a single species. Electrolyses performed at low temperature do not allow the stabilization of the $\mathbf{1}^{6+}$ and $\mathbf{1}^{7+}$ oxidation states.

The instability of $\mathbf{1}^{6+}$ and $\mathbf{1}^{7+}$ is probably due to the decoordination of some bpp$^-$ ligands of the apical Mn^{III}. Indeed, Mn^{III} complexes containing solely nitrogen based ligands are usually poorly stable and tend to form oxo-briged complexes by interaction with residual water in the solvent.[90-92] All electrogenerated solutions have also been analyzed by UV-visible and EPR spectroscopy (see below). The four stable oxidation states, from $\mathbf{1}^{2+}$ to $\mathbf{1}^{5+}$, have distinct UV-visible signatures (Figure 6). For each oxidation process, an increase of the absorbance in the visible region is observed consistent with the conversion of one Mn^{II} ion into Mn^{III}.[93,94]

The exceptional stability of the pentanuclear structure in four oxidation states ($\mathbf{1}^{2+}$ to $\mathbf{1}^{5+}$) is certainly due to its bis(triple-helical) structure that allows for maintaining the oxo-centered manganese trinuclear core at the $\{Mn^{II}_3(\mu_3\text{-O})\}^{4+}$, $\{Mn^{II}_2Mn^{III}(\mu_3\text{-O})\}^{5+}$, $\{Mn^{II}Mn^{III}_2(\mu_3\text{-O})\}^{6+}$ and $\{Mn^{III}_3(\mu_3\text{-O})\}^{7+}$ oxidation states. Indeed, although many oxo-centered trinuclear complexes have been reported in the $Mn^{II}Mn^{III}_2$ and Mn^{III}_3 oxidation states, to our knowledge, there is no example of multinuclear Mn complexes with either

a $\{Mn^{II}_3(\mu_3\text{-}O)\}^{4+}$ or a $\{Mn^{II}_2Mn^{III}(\mu_3\text{-}O)\}^{5+}$ unit as found in $\mathbf{1}^{2+}$ and in $\mathbf{1}^{3+}$. Divalent Mn ions are not able to stabilize O^{2-} ligands on their own and the unique example of such trinuclear structure contains a μ_3-OH bridged core, i.e., $[(py)_5Mn^{II}_3(OAc)_3(\mu_3\text{-}OH)(cat)]$.[95]
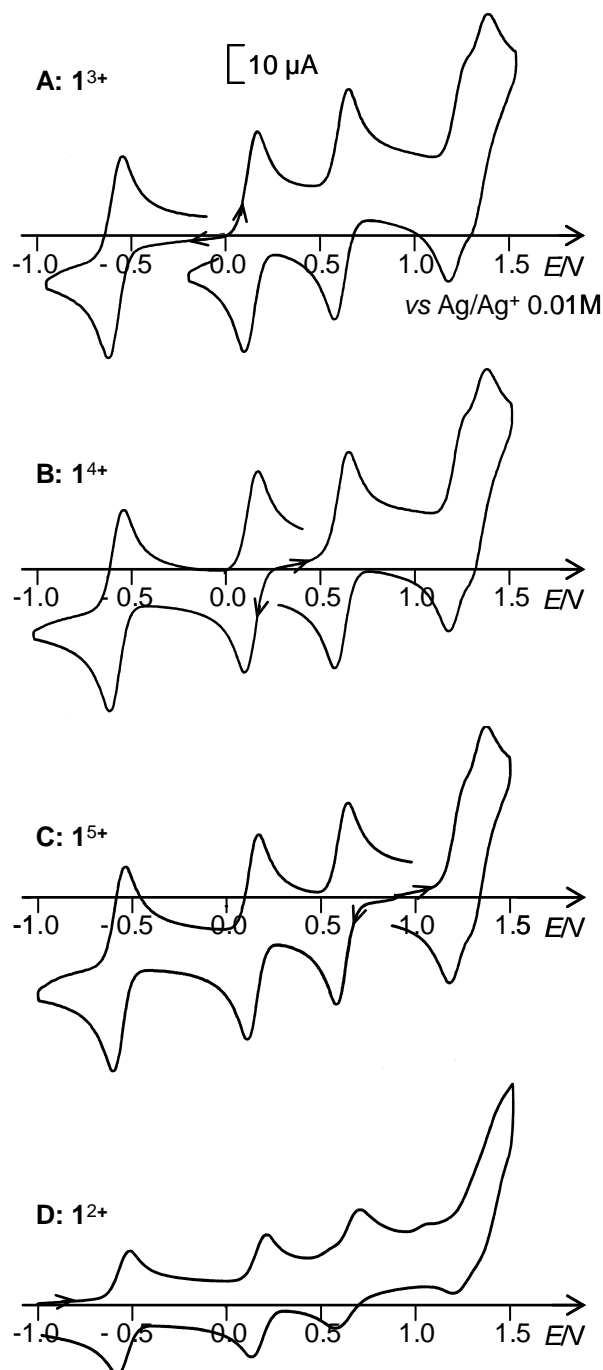
Figure 5. Cyclic voltammograms at a Pt electrode (diameter 5 mm) in CH_3CN, 0.1 M [Bu_4N]ClO_4 of: (A) a 0.70 mM solution of $\mathbf{1}^{3+}$, (B) after exhaustive oxidation at +0.35 V of the (A) solution (formation of $\mathbf{1}^{4+}$), (C) after exhaustive oxidation at +0.90 V of the (B) solution (formation of $\mathbf{1}^{5+}$), (D) after exhaustive reduction at -0.70 V of the (A) solution (formation of $\mathbf{1}^{2+}$); scan rate of 100 mV·s^{-1}.

Figure 6. Visible absorption spectra changes during electrolyses of a 0.70 mM solution of $\mathbf{1}^{3+}$ in CH$_3$CN, 0.1 M [Bu$_4$N]ClO$_4$: (a) initial solution; (b) after oxidation at +0.35 V of the (a) solution (formation of $\mathbf{1}^{4+}$); (c) after oxidation at +0.90 V of the (b) solution (forma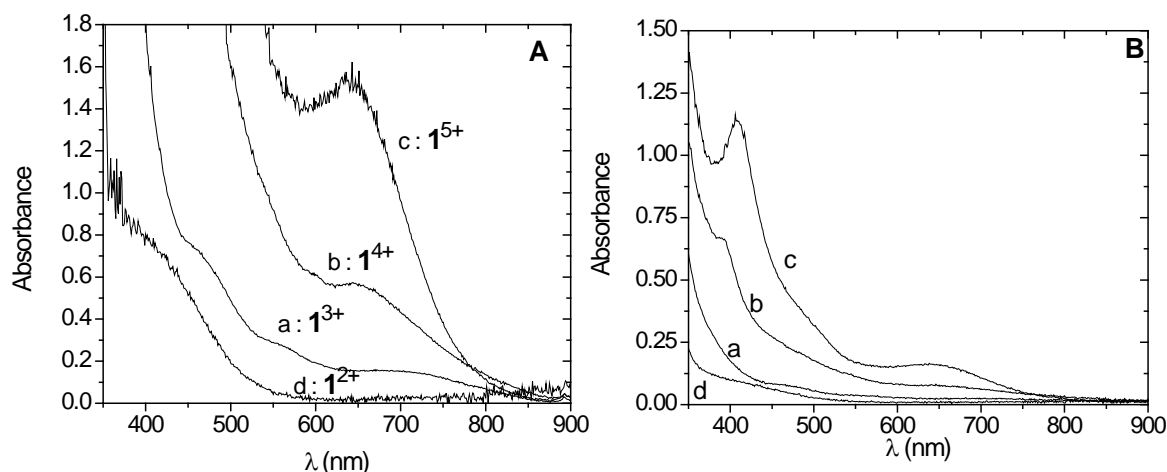tion of $\mathbf{1}^{5+}$); (d) after reduction at -0.70 V of the (a) solution (formation of $\mathbf{1}^{2+}$); (A) l = 1 cm, (B) l = 1 mm.

6.3.3. EPR spectroscopy

The powder X- and Q-band EPR spectra of complex $\mathbf{1}^{3+}$ have been recorded between 30 and 100 K (Figure 7 displays the spectra obtained at 30 K). In this range of temperatures, the total intensity of the spectra decreases when increasing the temperature. This temperature behavior and the shape of the spectra are consistent with an S = 5/2 spin species.[92,96-98] As determined by magnetism (*vide infra*), the {Mn$^{II}_2$Mn^{III}(μ_3-O)}$^{5+}$ trinuclear unit corresponds to an S = 2 spin state below 40 K. However, no EPR signal, even in parallel mode, corresponding to this species is observed at 30 K, certainly due to the large zero-field splitting expected for Mn^{III} ions. Based on these data, we can conclude that the S = 5/2 signal can be assigned to the two equivalent apical Mn^{II} ions.

With the aim of confirming this hypothesis, simulations of the EPR spectra have been performed using a full-matrix diagonalization procedure of the spin Hamiltonian displayed in Equation (1).

$$H = \mu_B \hat{H} \cdot [g] \cdot \hat{S} + D(\hat{S}_z^2 - 1/3\hat{S}^2) + E(\hat{S}_x^2 - \hat{S}_y^2) \qquad (1)$$

The first term represents the electronic Zeeman interaction with $\hat{H}$ being the magnetic field. The last two terms define the second-order (bilinear) *zfs* interaction with D and E representing the axial and rhombic parts, respectively. For neat powder EPR spectra, the ^{55}Mn hyperfine interaction is never resolved presumably because of the

intermolecular dipole-dipole interactions together with the *D*-strain that contribute to the broadening of the line. Therefore, they have been omitted in Equation (1). The good agreement obtained between the experimental and simulated spectra (Figure 7) confirms that these EPR spectra correspond to the signature of a unique Mn^{II} complex, implying that the two apical Mn^{II} units are equivalent. In addition, the |*D*| parameter of 0.071 cm^{-1} (0.102 K), issued from the Q-band EPR spectrum for which the high field limit conditions are reached (*D* << *hν*), is consistent with an N6 environment, when compared with the literature (0.010 < |D_{N6}| < 0.175 cm^{-1}).[98]
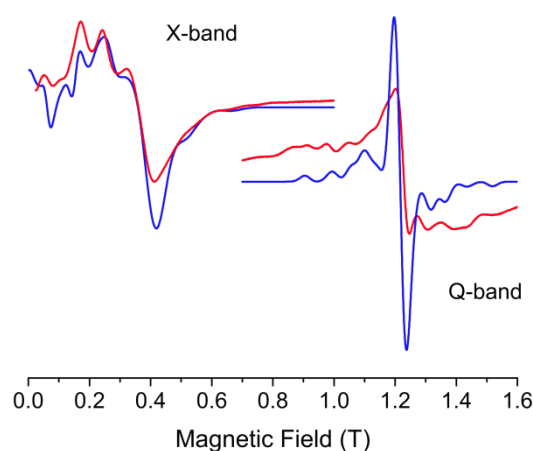

Figure 7. Experimental (red line) and simulated (blue line) powder X- and Q-band EPR spectra of **1**$^{3+}$ recorded at 30 K. Parameters used for the simulation: at X-band |*D*| = 0.073 cm^{-1}, |*E*| = 0.008 cm^{-1}, *E/D* = 0.110, $g_x=g_y=g_z$ = 2.0 and at Q-band |*D*| = 0.071 cm^{-1}, |*E*| = 0.009 cm^{-1}, *E/D* = 0.127, $g_x=g_y=g_z$ = 2.0.

The X-band EPR spectra in solution of **1**$^{3+}$ and of the electrogenerated solutions of **1**$^{4+}$, **1**$^{5+}$ and **1**$^{2+}$ have been recorded between 5 and 50 K (Figure 8 shows the EPR spectra at 30 K). In this range of temperatures, the global intensity of the spectra decreases with increasing temperatures for all the species, while the relative intensity and the broadening of the lines are not affected by the temperature. The EPR spectrum of **1**$^{3+}$ in solution is comparable to that recorded on powder (Figure 7), demonstrating that the structure of the complex is retained in solution, with the two magnetic-independent apical Mn(II) ions. The shape of the EPR spectrum of **1**$^{4+}$ drastically changes compared to **1**$^{3+}$ with a notable broadening of the resonance lines. This attests that in **1**$^{4+}$, the two apical {$Mn^{II}(bpp)_3$}$^-$ units are in magnetic interaction between each other, and/or more likely with the central core.

The EPR spectrum of $\mathbf{1}^{5+}$ is comparable to that $\mathbf{1}^{4+}$. Concerning $\mathbf{1}^{2+}$, the EPR spectrum is significantly modified with respect to $\mathbf{1}^{3+}$. A unique signal centered at $g = 2$ is observed that can tentatively be attributed to the sum of the spectra corresponding to five Mn^{II} ions. After full oxidation of the solution of the complex at $E = 1.50$ V, only a weak six-line EPR signal is observed (not shown), characteristic of Mn^{II}(CH$_3$CN)$_6$$^{2+}$,[99,100] that is formed in a very small amount.
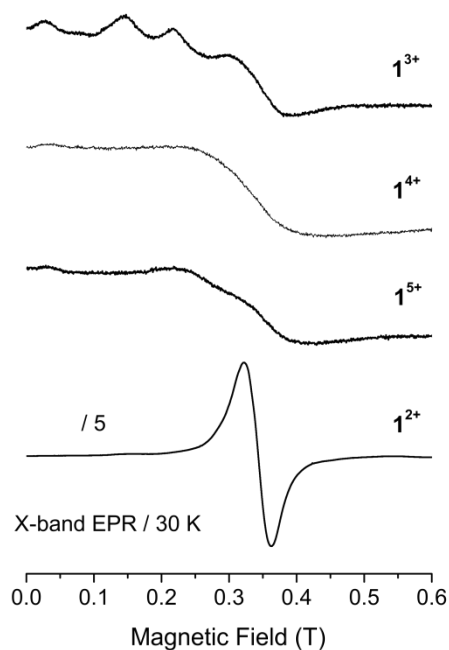

Figure 8. X-band EPR spectra at 30 K of 0.70 mM solution of $\mathbf{1}^{3+}$ in CH$_3$CN, 0.1 M [Bu$_4$N]ClO$_4$ and of the electrogenerated solutions of $\mathbf{1}^{4+}$, $\mathbf{1}^{5+}$ and $\mathbf{1}^{2+}$.

6.3.4. Magnetic properties

The magnetic properties of $\mathbf{1}^{3+}$ and $\mathbf{1}^{4+}$ have been studied on powder samples of $\mathbf{1}$(ClO$_4$)$_3$·2.5CH$_3$CN·C$_4$H$_{10}$O·0.5H$_2$O and $\mathbf{1}$(ClO$_4$)$_4$·2CH$_3$CN·2C$_4$H$_{10}$O. Between 300 and 40 K, the χT products decrease very slowly, from 13.3 and 16.3 cm^3 K mol^{-1} for $\mathbf{1}^{3+}$ and $\mathbf{1}^{4+}$ to a pseudoplateau (around 40 K) at 11.2 and 13.4 cm^3 K mol^{-1}, respectively (Figure 9). Below 40 K, the two compounds show different magnetic behaviors: the χT product is again decreasing for $\mathbf{1}^{3+}$ but in a more abrupt fashion to reach the value of 3.7 cm^3 K mol^{-1} at 1.8 K, while it is increasing for $\mathbf{1}^{4+}$ to reach the value of 16.5 cm^3 K mol^{-1} at 1.8 K. At room temperature, the χT products are low in comparison to the values of 20.5 and 19.125 cm^3 K mol^{-1} expected for high-spin Mn^{II} ($S = 5/2$, $g \approx 2$) and high-spin Mn^{III}

(S = 2, $g \approx$ 2) centers in 4:1 and 3:2 ratio in 1^{3+} and 1^{4+}, respectively. On the other hand, both χT values measured at 40 K are in very good agreement with two apical S = 5/2 $\{Mn^{II}(bpp)_3\}^-$ (C = 4.375 cm^3 K mol^{-1} with g = 2) and one S = 2 (C = 3 cm^3 K mol^{-1} with g = 2) non-interacting spins (11.75 cm^3 K mol^{-1}) for 1^{3+} and with three S = 5/2 non-interacting spins (13.125 cm^3 K mol^{-1}) for 1^{4+}. This result suggests that the $\{Mn^{II}_2Mn^{III}(\mu_3\text{-O})\}^{5+}$ and $\{Mn^{II}Mn^{III}_2(\mu_3\text{-O})\}^{6+}$ cores behave at low temperature like S = 2 and S = 5/2 spin centers, respectively.
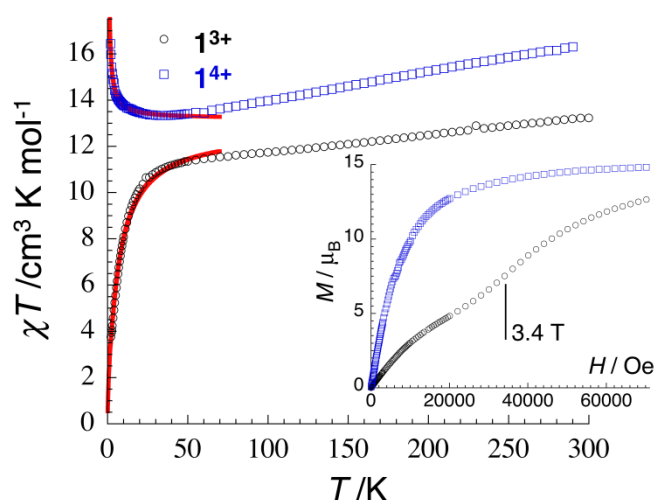

Figure 9. Temperature dependence of the χT products (where χ = M/H per [Mn$_5$] complex) measured at 0.1 T and inset: field dependence of the magnetization at 1.8 K for compound 1^{3+} (black open dots) and 1^{4+} (blue open squares). The solid red lines are the best fits to the Heisenberg model described in the text.

To explain the trinuclear core magnetic behavior above 40 K, two approaches can be envisioned. The first hypothesis is to consider electrons and thus spins localized on each manganese site. In this case, the magnetic data above 40 K should fit with simple Heisenberg triangular models with an S_i = 5/2; 5/2; 2 set of spins for 1^{3+} and an S_i = 5/2; 2; 2 set of spins for 1^{4+} with intra-core antiferromagnetic interactions. Unfortunately, we have been unable to reproduce, even qualitatively, the temperature dependence of the susceptibility above 40 K using this approach. Therefore the observed thermal behavior has to be explained in the frame of a delocalized model in which each trinuclear core is considered as an "entity" with a given spin. This approach is indeed in good agreement with the structural analysis described above. As mentioned previously, the magnetic data suggest that the ground state of the $\{Mn^{II}_2Mn^{III}(\mu_3\text{-O})\}^{5+}$ and $\{Mn^{II}Mn^{III}_2(\mu_3\text{-O})\}^{6+}$ cores are, respectively, S = 2 and S = 5/2.

Then the increase of the χT product above 40 K is simply the signature of the thermal population of the low-lying excited spin states of the trinuclear core as it is observed for spin-crossover complexes.

Below 40 K, the trinuclear core of the complex can be considered as a single localized spin (S = 2 and S = 5/2 for $\mathbf{1}^{3+}$ and $\mathbf{1}^{4+}$, respectively) and therefore taking into account the two apical S = 5/2 {Mn^{II}(bpp)$_3$}$^-$ motifs, the magnetic properties of the complexes can be modelled using the following Heisenberg spin Hamiltonian:

$$H = -2JS_C(S_{Mn1} + S_{Mn2}) \qquad (2)$$

with S_C and S_{Mni} being the spins of the central trinuclear core and the apical Mn(II) metal ions, respectively. For $\mathbf{1}^{4+}$, the increase of the χT product below 40 K is clearly indicative of intra-complex ferromagnetic interactions between S = 5/2 spins. These magnetic exchange is well estimated at +0.05(1) K (g = 2.0(1)) from the fit of the experimental data to the analytical theoretical susceptibility (see Equation S 1 in the supporting information) in the low field approximation (red line on the blue squares, Figure 9) deduced from Equation (2) and the application of the van Vleck equation.[101,102] The field dependence of the magnetization for $\mathbf{1}^{4+}$ at 1.8 K, shown inset of Figure 9, confirms the presence of ferromagnetic interactions with a rapid increase of the magnetization at low field. Indeed, antiferromagnetic interactions would lead to an "S" shape curve. It is worth further mentioning that the magnetization reaches 14.9 μ_B in very good agreement with the presence of three S = 5/2 spins (note that the M vs H data at 1.8 K are well fitted to a sum of three S = 5/2 Brillouin functions with g = 2.0, consistent with the occurrence of very weak interactions) and thus an S_T = 15/2 ground state for this complex induced by the intra-complex ferromagnetic couplings.

The analysis of the magnetic behavior for $\mathbf{1}^{3+}$ below 40 K is not so straightforward. The decrease of the χT product below 40 K highlights the presence of intra-complex antiferromagnetic interactions between apical S = 5/2 spins and the central trinuclear core considered as an effective S = 2 spin at these temperatures. The presence of this antiferromagnetic interaction is further supported by the M vs H plot at 1.8 K (inset Figure 9) that displays a clear inflection point around 3.4 T. Considering that this field, H^*, corresponds to the energy necessary to overcome the intra-complex antiferromagnetic interactions (i.e., to have all the spins aligned in the applied dc field), the following relation: $8JS_{Mni}S_C = -2g\mu_B HS_C$ is obtained from Equation (2) and thus the equality between the exchange and the Zeeman energies. Therefore the intra-complex antiferromagnetic interaction between apical S = 5/2 spins and the central trinuclear spin is estimated at -0.45 K (with g = 2). At high field, the magnetization increases

without clear saturation and reaches 12.7 μ_B at 7 T (inset Figure 9) in agreement with the field alignment of two $S = 5/2$ and one $S = 2$ spins (expected saturation value at 14 μ_B). In parallel, the χT vs T data (Figure 9) below 40 K have been modelled using the same analytical approach as for $\mathbf{1}^{4+}$ (Equation (2) and Equation S 2 in the supporting information) but this time, the experimental data could be reproduced only introducing additional inter-complex magnetic interactions in the frame of the mean field approximation.[103] The comparison between the crystal packing of $\mathbf{1}^{3+}$ and $\mathbf{1}^{4+}$ reveals that the Mn...Mn distances between the closest ions are significantly longer in $\mathbf{1}^{4+}$, consistent with stronger inter-molecular interactions in $\mathbf{1}^{3+}$. The best fit shown in solid red line in Figure 9 (on the open black dots) corresponds to $J/k_B = -0.40(5)$ K, $zJ'/k_B = -0.19(3)$ K and $g = 2.0(1)$. It is worth noting that the intra-complex interactions deduced from the M vs H and the χT vs T data are perfectly consistent around -0.4 K and thus induce an $S_T = 3$ ground state for $\mathbf{1}^{3+}$ but that the inter-complex interactions, zJ', are certainly overestimated by this modelling approach as their value also contains phenomenologically the effects of the magnetic anisotropy brought by the Mn^{III} metal ion. Attempts to simulate numerically the experimental data (M vs H and χT vs T) for $\mathbf{1}^{3+}$ including both effects failed and lead to multiple solutions and thus overparametrization of the simulation.

Finally, the magnetic measurements demonstrate that the controlled oxidation of $\mathbf{1}^{3+}$ in $\mathbf{1}^{4+}$ induces a change of effective spin state of the delocalized {Mn$_3$(μ_3-O)} core from $S = 2$ to $S = 5/2$ and convert an $S_T = 3$ [Mn$_5$] complex into an $S_T = 15/2$ system.

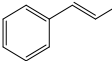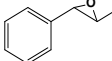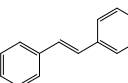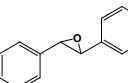## 6.3.5. Catalytic epoxidation of alkenes

As a consequence of the perfect stability of four oxidation states ($\mathbf{1}^{2+}$ to $\mathbf{1}^{5+}$), this kind of polynuclear oxo-bridged manganese systems might represent interesting potential catalysts for the oxidation of organic compounds, as recently demonstrated by Christou et al.[71] for the well-known Mn$_{12}$ family of complexes, [Mn$_{12}$O$_{12}$(OCR)$_{16}$(H$_2$O)$_4$] (R = Et, Ph, etc.), which also display multiple one-electron reversible processes. However, only a few reports have appeared in the literature dealing with the capacity of some Mn cluster complexes to carry out epoxidation reactions in a catalytic manner with relatively good conversion and/or yields.[68,69]

The pentanuclear complex $\mathbf{1}^{3+}$ has been tested in epoxidation catalysis using commercial peracetic acid (32%) as the oxidant. Reaction with olefins in presence of the complex resulted predominantly in the formation of epoxides as main products

though minor amounts of the corresponding aldehydes are also formed. Table 3 reports the conversion and selectivity values for the epoxide product derivatives together with the TOF values for substrate consumption. No epoxidation occurred in the absence of catalyst.

Table 3. Catalytic oxidation of different alkenes by the pentanuclear Mn complex $\mathbf{1}^{3+}$, using CH_3CO_3H as the oxidant.[a]

Entry	Substrate	Product	Conversion (%)	Selectivity (%)	TOF, min^{-1}
1^{b}			100	75	50
2			100	92	20
3^{c}			100	59	20
4			100	50	20
5			95	71	19
6^{d}			98	62	19.6

[a] **Conditions**: catalyst (2 µmol), substrate (200 µmol), CH_3CN (1 mL). Peracetic acid 32% (400 µmol) is added within 1 minute at 0ºC, then the reaction is left to reach R.T along 5 minutes.
[b] Reaction time: 2 minutes.
[c] 88% *cis*, 12% *trans*
[d] 100% 4-vinyl-1-cyclohexene 1,2 epoxide

Oxygen transfer reactions catalyzed by $\mathbf{1}^{3+}$ occurred in less than 5 minutes after the addition of peracetic acid. A complete conversion of the corresponding substrate was achieved with aromatic alkenes whereas aliphatic olefins were almost completely oxidized. It is particularly remarkable the epoxidation of styrene, where total consumption of 100 equivalents of substrate took place within two minutes with a TOF value of 50 min^{-1} and a selectivity for the epoxide product of 75%.

The epoxidation of the rest of the olefins tested took place at somewhat lower rate values, with TOF values between 19 and 20 min^{-1}. *Trans*-β-methylstyrene was epoxidized with good conversion and selectivity whereas in the case of *trans*-stilbene only a moderate selectivity was observed, with formation of 50% of benzaldehyde by-product.

Cis-β-methylstyrene was oxidized rapidly under the reaction conditions, giving 88% of *cis*-epoxide as major product and 12% of isomerized *trans*-epoxide. This fact, together

with the oxidation experiments described previously for $\mathbf{1}^{3+}$, would indicate that a Mn^{III}-OOC(O)R peroxyl radical species might be involved in the epoxidation pathway.[104] On the other hand, mechanistic studies of the olefin epoxidation reaction promoted by tetranuclear chalcocyanide cluster compounds have provided evidence that multiple active oxidant species operate simultaneously in the epoxidation process.[69] This could also be the case for complex $\mathbf{1}^{3+}$, thus explaining the moderate chemoselectivity found for some of the substrates tested.

In order to get deeper insight into the nature of the reactive species, the chemical oxidation of complex $\mathbf{1}^{3+}$ upon addition of peracetic acid was followed by UV-vis spectroscopy (Figure 10). The addition of two equivalents of peracetic acid leads, after 1 minute, to an UV-vis spectrum similar to the one obtained electrochemically for $\mathbf{1}^{4+}$, instead of the two-electron oxidized product $\mathbf{1}^{5+}$. This partial oxidation is certainly due to kinetic factors since the addition of an excess of oxidant leads to an hypsochromic displacement of the maximum wavelength up to around 645 nm, presumably resulting in the formation of the two-electron oxidized species $\mathbf{1}^{5+}$.
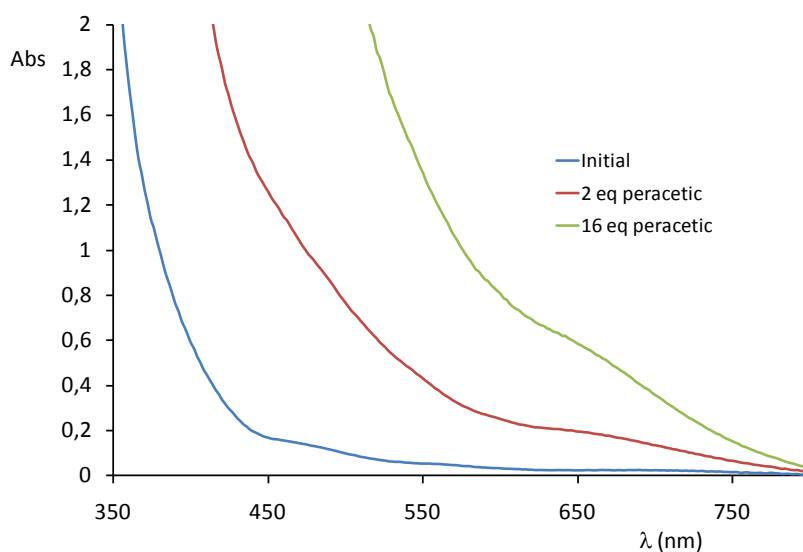
Figure 10. Evolution of UV-vis spectrum of complex $\mathbf{1}^{3+}$ in CH_3CN at room temperature ($0.67 \cdot 10^{-3}$ M solution), upon addition of 2 and 16 eq. of peracetic acid.

A global look at Table 3 reveals that the aromatic olefins are in general epoxidized at a faster rate than the aliphatic ones, thus indicating the influence of electronic factors on the catalytic performance. However, the role of geometrical parameters is also manifested since the epoxidation of the terminal olefin styrene (entry 1) is completed at a considerably faster pace than the substituted ones (entries 2-4). It is also noticeable that 1-octene, a terminal aliphatic alkene which usually tends to be one of the less

reactive olefins in metal catalyzed epoxidations,[105] is readily epoxidized with peracetic acid and the pentanuclear complex as catalyst, presenting good conversion and selectivity values comparable to those presented by other cluster complexes described in the literature.[106]

Finally, for 4-vinycyclohexene, complex **1**[3+] leads to almost quantitative conversion and moderate chemoselectivity, though with regiospecificity for oxidation of the substrate at the alkene ring position. To the best of our knowledge, the epoxidation of 4-vinylcyclohexene with polynuclear manganese complexes has been only scarcely studied and the results indicate that a mixture of the two possible regioisomers is formed.[106]

An overall comparison between the reactivity of the pentanuclear compound and some mononuclear Mn-N_4 compounds described previously (chapters 4 and 5)[107] indicates that epoxidation of olefins with peracetic acid occurs with unequal reactivity and selectivity values, probably indicating the different nature of the reactive species responsible for the epoxidation step. The polynuclear nature of catalyst **1**[3+] could also favor the simultaneous occurrence of diverse active species within the catalyst itself and further mechanistic studies are being developed to clarify this point.

6.4. Experimental section

6.4.1. Materials

The electrolytes tetra-*n*-butylammonium perchlorate, [Bu$_4$N]ClO$_4$, tetra-*n*-butylammonium tetrafluoroborate, [Bu$_4$N]BF$_4$, and acetonitrile (CH$_3$CN, Rathburn, HPLC grade) were used as received and stored under an argon atmosphere in a glove box. The tetra-*n*-butylammonium hydroxide ([Bu$_4$N]OH, 40 % in water, Fluka) and the ligand 3,5-bis(pyridin-2-yl)-pyrazole (Hbpp) (98 %, TCI) were used as received.

6.4.2. Preparations

CAUTION! *Perchlorate salts of compounds containing organic ligands are potentially explosive. Although we have encountered no such problems, only small quantities of these compounds should be prepared and handled with care.*

Synthesis of [{Mn^{II}(μ-bpp)$_3$}$_2$Mn^{II}$_2$Mn^{III}(μ-O)](ClO$_4$)$_3$, 1(ClO$_4$)$_3$.

Method A. A solution of Mn(ClO$_4$)$_2$·6H$_2$O (120 mg, 0.33 mmol) in methanol (30 mL) was added to a stirred solution of Hbpp (106 mg, 0.47 mmol) and NaOH (19 mg, 0.47 mmol) in methanol (120 mL). The reaction mixture was refluxed for 2 hours under air. To the resulting brown solution was added a saturated aqueous solution of NaClO$_4$. The precipitate formed was then filtered, redissolved in dichloromethane and washed with water. The organic phase was then dried over Na$_2$SO$_4$ and the solvent was evaporated to dryness. The brown-black powder obtained was reprecipitated in CH$_3$CN/diethyl ether. Black single crystals of **1**(ClO$_4$)$_3$·2.5CH$_3$CN·C$_4$H$_{10}$O·0.5H$_2$O were obtained by slow vapor diffusion of diethyl ether into an acetonitrile solution of the complex (Yield: 80 mg, 61%). Elemental analysis calcd (%) for C$_{78}$H$_{54}$Mn$_5$O$_{13}$N$_{24}$Cl$_3$·3.5H$_2$O (1979.52 g mol^{-1}): C, 47.32; H, 3.10; N, 16.98. Found: C, 47.47; H, 2.96; N, 16.61. ESI-MS: *m/z* (%) 1187.1 (2) [{Mn^{II}(μ-bpp)$_3$}$_2$Mn^{II}$_2$Mn^{III}(μ-O)(ClO$_4$)$_2$]$^+$, 858.1 (25) [{Mn^{II}(μ-bpp)$_3$}$_2$Mn^{II}$_2$Mn^{III}(μ-O)(ClO$_4$)]$^{2+}$, 539.0 (100) [{Mn^{II}(μ-bpp)$_3$}$_2$Mn^{II}$_2$Mn^{III}(μ-O)]$^{3+}$.

Method B. A solution of Mn(ClO$_4$)$_2$·6H$_2$O (135 mg, 0.37 mmol) in acetonitrile (10 mL) was added to a stirred solution of Hbpp (100 mg, 0.45 mmol) and Bu$_4$NOH (0.4 mL, 0.54 mmol) in acetonitrile (15 mL). The reaction mixture was refluxed for 4 hours under air which led to the complete dissolution of the white precipitate formed initially. The resulting brown solution was then cooled to room temperature and filtered. Slow vapor

diffusion of diethyl ether into this solution afforded black crystals of $1(ClO_4)_3$. To obtain a pure sample of the complex, this recrystallization procedure was repeated several times (Yield: 70 mg, 47%).

Electrochemical synthesis of [{Mn^{II}(μ-bpp)$_3$}$_2$Mn^{II}Mn^{III}$_2$(μ-O)](ClO$_4$)$_4$, 1(ClO$_4$)$_4$.

A solution of $1(ClO_4)_3$ (50 mg) in acetonitrile (10 mL) containing 0.1 M of [Bu$_4$N]ClO$_4$ was oxidized at 0.35 V on a platinum plate under an argon atmosphere. Addition of diethyl ether to the solution after complete electrolysis (one electron exchanged per molecule of initial complex) led to the precipitation of $1(ClO_4)_4$ which was filtered off and dried under air (Yield: 36 mg, 70%). Elemental analysis calcd (%) for $C_{78}H_{54}Mn_5O_{17}N_{24}Cl_4 \cdot 3.5H_2O$ (2078.97 g mol^{-1}): C, 45.06; H, 2.96; N, 16.17. Found: C, 45.08; H, 3.25; N, 16.22. Brown-black crystals of $1(ClO_4)_4 \cdot 2CH_3CN \cdot 2C_4H_{10}O$ were obtained by slow vapor diffusion of diethyl ether into the electrolyzed solution.

6.4.3. X-Ray structure determination

Data collection for 1^{3+} was made on a Bruker-Nonius diffractometer equipped with an APPEX 2 4K CCD area detector, a FR591 rotating anode with Mo Kα radiation, Montel mirrors as monochromator and a Kryoflex low temperature device (T = -173 °C). Full-sphere data collection was used with ω and φ scans. Programs used included data collection APEX-2,[108] data reduction Bruker Saint[109] V/.60A and absorption correction SADABS.[110] For structure solution and refinement SHELXTL was used.[111] Diffraction data for 1^{4+} were collected on a Bruker Smart Apex CCD diffractometer using graphite-monochromated Mo Kα radiation (λ = 0.71073 Å) from an X-Ray tube. Programs were for data collection, Smart V. 5.631 (Bruker AXS 1997-02); data reduction, Saint+ Version 6.36A (Bruker AXS 2001); absorption correction, SADABS version 2.10 (Bruker AXS 2001) and structure solution and refinement, SHELXTL Version 6.14 (Bruker AXS 2000-2003). Crystallographic data in CIF format can be found in the electronic supporting information or in CCDC: 818591 (1^{3+}) and 818592 (1^{4+}).

6.4.4. Electrochemistry

All electrochemical measurements were made under an argon atmosphere in a dry-glove box at room temperature. Cyclic voltammetry and controlled potential electrolysis experiments were performed by using an EG&G model 173 potentiostat/galvanostat

equipped with a PAR model universal programmer and a PAR model 179 digital coulometer. A standard three-electrode electrochemical cell was used. Potentials were referred to an Ag/0.01 M AgNO$_3$ reference electrode in CH$_3$CN + 0.1 M [Bu$_4$N]ClO$_4$. Potentials referred to that system can be converted to the ferrocene/ferricinium couple by subtracting 87 mV, to SCE by adding 298 mV or to NHE reference electrode by adding 0.548 V. The working electrodes for cyclic voltammetry were a platinum disk (5 mm in diameter) or a vitreous carbon disk (3 mm in diameter) polished with 2 μm diamond paste (Mecaprex Presi). Exhaustive electrolyses were carried out on reticulated vitreous carbon electrode 45 PPI (the electrosynthesis Co. Inc.; 1 cm^3) or on a platinum plate (5 cm^3). The auxiliary electrode was a Pt wire in CH$_3$CN + 0.1 M [Bu$_4$N]ClO$_4$.

6.4.5. Spectroscopy

X- and Q-band EPR spectra were recorded with a Bruker EMX. For the X-band 100 K experiments, it was equipped with an ER-4192 ST Bruker cavity and an ER-4131 VT. For the 4.5 K experiments, an Oxford Instruments ESR-900 continuous-flow helium cryostat was used with an ER-4116 DM Bruker cavity for the X-band and an ER-5106 QTW Bruker cavity for the Q-band. For electrochemical experiments, electronic absorption spectra were recorded on a Varian Cary 50 or 100 absorption spectrophotometer. Initial and electrolyzed solutions were transferred to conventional quartz cells with 0.1 or 1 cm path length in the glove box. ESI-MS experiments were performed on a Navigator LC/MS chromatograph from Thermo Quest Finigan, using acetonitrile as a mobile phase. The simulation of the powder EPR spectra of **1**$^{3+}$ was performed with the SIM program written by Weihe and co-workers.[112] The parameters given in the text are issued from the best-simulated spectra obtained for each frequency.

6.4.6. Magnetic susceptibility measurements

The magnetic susceptibility measurements were obtained with the use of MPMS-XL Quantum Design SQUID magnetometer. This magnetometer works between 1.8 and 400 K for dc applied fields ranging from -7 to 7 T. Measurements were performed on polycrystalline samples of 18.73 and 13.00 mg for **1**$^{3+}$ and **1**$^{4+}$ respectively, introduced in a polyethylene bag (3 × 0.5 × 0.02 cm). The ac susceptibility measurements were

measured with an oscillating ac field of 3 Oe with frequency between 1 to 1500 Hz. It is worth noting that no out-of-phase ac susceptibility signal has been detected above 1.8 K. The magnetic data were corrected for the sample holder (plastic bag) and the diamagnetic contribution.

6.4.7. Catalytic epoxidation experiments

An CH_3CN (1 ml) solution of alkene (200 μmol), catalyst (2 μmol) and biphenyl (200 μmol, internal standard) was prepared in a 10 ml flask and cooled in an ice bath. Afterwards, 32% peracetic acid (400 μmol) was added via syringe over 1 min under stirring. The reaction vessel was then taken out of the ice bath and allowed to progressively warm to RT. Each aliquot of the reaction taken for analysis was filtered through a basic alumina plug and was analyzed in a Shimadzu GC-2010 gas chromatography apparatus equipped with an Astec CHIRALDEX G-TA column and a FID detector. Quantification was achieved from calibration curves. GC conditions: injection temperature 250 ºC, detector temperature 250 ºC, carrier gas He at 25 mL/min. Selectivity for the epoxide is calculated as (Yield/Conversion)x100.

6.5. Conclusions

A new pentanuclear manganese complex, namely $[\{Mn^{II}(\mu\text{-bpp})_3\}_2Mn^{II}_2Mn^{III}(\mu_3\text{-O})]^{3+}$ ($\mathbf{1}^{3+}$), has been isolated and structurally characterized by reacting Mn^{2+} ions and the rigid tetradentate bis(pyridyl)-pyrazolate ligand. Its electrogenerated one-electron oxidized form, $[\{Mn^{II}(\mu\text{-bpp})_3\}_2Mn^{II}Mn^{III}_2(\mu_3\text{-O})]^{4+}$ ($\mathbf{1}^{4+}$), has also been isolated and characterized. These complexes join the small family of bis(triple-helical) pentanuclear complexes featuring a triangular oxo-centered $\{M^{II}_3(\mu_3\text{-O})\}^{4+}$ (M = Fe^{2+} or Cd^{2+}) or $\{M^{II}_3(\mu_3\text{-OH})\}^{5+}$ (M = Ni^{2+}, Zn^{2+} or Cu^{2+}) connected to two apical $\{M^{II}(L)_3\}^-$ units (L = bpp⁻ or bpt⁻). In contrast to all these previously reported helicate compounds, which contain only divalent metallic ions, the aerobic conditions used for the synthesis of $\mathbf{1}^{3+}$ has led to its isolation in a mixed divalent and trivalent oxidation states.

Complexes $\mathbf{1}^{3+}$ and $\mathbf{1}^{4+}$ have been characterized by X-ray diffraction and the structures consist of five Mn ions connected through six bpp⁻ ligands. The five Mn ions form a trigonal bipyramidal motif in which two Mn^{II} ions occupy the apical positions and the three Mn ions connected by a $\mu_3\text{-O}^{2-}$ ion are placed in the equatorial plane. In both complexes, the three Mn ions of the central core present a distorted N_4O trigonal bipyramid environment, whereas the coordination geometry of the two apical Mn ions corresponds to a slightly distorted octahedron. In contrast to $\mathbf{1}^{3+}$, $\mathbf{1}^{4+}$ adopts a symmetric C_2 axis.

Complex $\mathbf{1}^{3+}$ exhibits very rich redox behavior with five distinct and reversible one-electron processes located between -1.0 and +1.5 V. In addition, bulk electrolyses have evidenced the exceptional stability of the complex in four oxidation states. Indeed, the oxidation states of the oxo-centered trinuclear core can switch between $\{Mn^{II}_3(\mu_3\text{-O})\}^{4+}$, $\{Mn^{II}_2Mn^{III}(\mu_3\text{-O})\}^{5+}$, $\{Mn^{II}Mn^{III}_2(\mu_3\text{-O})\}^{6+}$ and $\{Mn^{III}_3(\mu_3\text{-O})\}^{7+}$, while the two Mn apical ions remain at the +II oxidation state. The peculiar bis(triple-helical) structure certainly allows for the unusual stability of the $\{Mn^{II}_3(\mu_3\text{-O})\}^{4+}$ and $\{Mn^{II}_2Mn^{III}(\mu_3\text{-O})\}^{5+}$ oxidation levels since, to our knowledge, there is no example of trinuclear or larger multinuclear Mn complexes presenting such motif at these low oxidation states.

Regarding the electron delocalization we can conclude that the trinuclear central core of $\mathbf{1}^{3+}$ ($Mn^{II}_2Mn^{III}$) is probably a fully electron delocalized spin system, while for $\mathbf{1}^{4+}$ ($Mn^{II}Mn^{III}_2$) the system is not fully localized although two of the Mn ions have a

dominant +III oxidation state and the last Mn ion possesses a dominant +II oxidation state.

The powder X- and Q-band EPR signature of $\mathbf{1}^{3+}$ at low temperature indicate an $S = 5/2$ spin state for this species, characterized by a small zero-field splitting parameter ($|D| = 0.071$ cm^{-1}). This D value is consistent with an N6 environment and is attributed to the two apical Mn^{II} ions, which are in this case equivalent and magnetically independent. In contrast, in $\mathbf{1}^{4+}$ the two apical units present a magnetic interaction with each other and also likely with the central core. The experimental spectra have been confirmed with mathematical simulations with good agreement.

The magnetic susceptibility measurements at 40 K are consistent with two apical $S = 5/2$ {Mn^{II}(bpp)$_3$}$^{-}$ and one $S = 2$ non-interacting spins (11.75 cm^3 K mol^{-1}) for $\mathbf{1}^{3+}$, whereas three $S = 5/2$ non-interacting spins (13.125 cm^3 K mol^{-1}) are found for $\mathbf{1}^{4+}$. This indicates that the {Mn^{II}$_2$Mn^{III}(μ_3-O)}$^{5+}$ and {Mn^{II}Mn^{III}$_2$(μ_3-O)}$^{6+}$ cores behave at low temperature like $S = 2$ and $S = 5/2$ spin centers, respectively. The thermal behavior below 40 K highlights the presence of intra-complex magnetic interactions between the two apical spins and the central core in both $\mathbf{1}^{3+}$ and $\mathbf{1}^{4+}$ that are antiferromagnetic for $\mathbf{1}^{3+}$ (leading to an $S_T = 3$) and ferromagnetic for $\mathbf{1}^{4+}$ (giving thus an $S_T = 15/2$ ground state). Above 40 K, the increase of the χT product with temperature is associated exclusively to the interactions taking place within the trinuclear central core.

$\mathbf{1}^{3+}$ has been tested in the catalytic epoxidation of alkenes, showing very fast conversion with good selectivities for the epoxide products, either for aromatic or aliphatic alkenes. This complex has also revealed regiospecificity for the ring alkene in the epoxidation of 4-vinylcyclohexene. The partial isomerisation of *cis*-β-methylstyrene to the *trans*-epoxide could indicate the presence of a radical species in the epoxidation pathway. However, the polynuclear nature of the catalyst allows for the occurrence of multiple active species.

6.6. References

[1] Mukhopadhyay, S.; Mandal, S.K.; Bhaduri, S.; Armstrong, W.H. *Chem. Rev.* **2004**, *104*, 3981-4026.

[2] Weatherburn, D.C.; Mandal, S.; Mukhopadhyay, S.; Bahduri, S.; Lindoy, L.F. *Manganese,* in *Comprehensive Coordination Chemistry II*, Eds. McCleverty, J.A.; Meyer, T.J.; Elsevier Pergamon: Oxford, **2004**, Vol. 5, p. 1.

[3] Wu, A.J.; Penner-Hahn, J.E.; Pecoraro, V.L. *Chem. Rev.* **2004**, *104*, 903-938.

[4] Mullins, C.S.; Pecoraro, V.L. *Coord. Chem. Rev.* **2008,** *252*, 416-443.

[5] Collomb, M.-N.; Deronzier, A. *Eur. J. Inorg. Chem.* **2009**, 2025-2046.

[6] Gatteschi, D.; Sessoli, R. *Angew. Chem. Int. Ed.* **2003,** *42*, 268-297.

[7] Bagai, R.; Christou, G. *Chem. Soc. Rev.* **2009**, *38*, 1011-1026.

[8] Roubeau, O.; Clérac, R. *Eur. J. Inorg. Chem.* **2008**, 4325-4342.

[9] Hill, S.; Datta, S.; Liu, J.; Inglis, R.; Milios, C.J.; Feng, P.L.; Henderson, J.J.; del Barco, E.; Brechin, E.K.; Hendrickson, D.N. *Dalton Trans.* **2010**, *39*, 4693-4707.

[10] Milios, C.J.; Vinslava, A.; Wernsdorfer, W.; Moggach, S.; Parsons, S.; Perlepes, S.P.; Christou, G.; Brechin, E.K. *J. Am. Chem. Soc.* **2007**, *129*, 2754-2755.

[11] Milios, C.J.; Inglis, R.; Vinslava, A.; Bagai, R.; Wernsdorfer, W.; Parsons, S.; Perlepes, S.P.; Christou, G.; Brechin, E.K. *J. Am. Chem. Soc.* **2007**, *129*, 12505-12511.

[12] Stamatatos, T.C.; Foguet-Albiol, D.; Lee, S.C.; Stoumpos, C.C.; Raptopoulou, C.P.; Terzis, A.; Wernsdorfer, W.; Hill, S.O.; Perlepes, S.P.; Christou, G. *J. Am. Chem. Soc.* **2007**, *129*, 9484-9499.

[13] Kostakis, G.E.; Ako, A.M.; Powell, A.K. *Chem. Soc. Rev.* **2010**, *39,* 2238-2271.

[14] Chen, H.Y.; Collomb, M.-N.; Duboc, C.; Blondin, G.; Riviere, E.; Faller, J.W.; Crabtree, R.H.; Brudvig, G.W. *Inorg. Chem.* **2005**, *44*, 9567-9573.

[15] Baffert, C.; Orio, M.; Pantazis, D.A.; Duboc, C.; Blackman, A.G.; Blondin, G.; Neese, F.; Deronzier, A.; Collomb, M.-N. *Inorg. Chem.* **2009**, *48*, 10281-10288.

[16] Nayak, S.; Evangelisti, M.; Powell, A.K.; Reedijk, J. *Chem. Eur. J.* **2010**, *16*, 12865-12872.

[17] Milios, C.J.; Stamatatos, T.C.; Perlepes, S.P. *Polyhedron* **2006**, *25*, 134-194.

[18] Afrati, T.; Dendrinou-Samara, C.; Raptopoulou, C.R.; Terzis, A.; Tangoulis, V.; Kessissoglou, D.P. *Angew. Chem. Int. Ed.* **2002**, *41*, 2148-2150.

[19] Sreerama, S.G.; Pal, S. *Inorg. Chem.* **2002**, *41*, 4843-4845.

[20] Yang, C.I.; Wernsdorfer, W.; Lee, G.H.; Tsai, H.L. *J. Am. Chem. Soc.* **2007**, *129*, 456-457.

[21] Yang, C.I.; Wernsdorfer, W.; Cheng, K.H.; Nakano, M.; Lee, G.H.; Tsai, H.L. *Inorg. Chem.* **2008**, *47*, 10184-10186.

[22] Pathmalingam, T.; Gorelsky, S.I.; Burchell, T.J.; Bedard, A.C.; Beauchemin, A.M.; Clérac, R.; Murugesu, M. *Chem. Commun.* **2008**, 2782-2784.

[23] Inglis, R.; Jones, L.F.; Milios, C.J.; Datta, S.; Collins, A.; Parsons, S.; Wernsdorfer, W.; Hill, S.; Perlepes, S.P.; Piligkos, S.; Brechin, E.K. *Dalton Trans.* **2009**, 3403-3412.

[24] Manolopoulou, E.; Stoumpos, C.C.; Siczek, M.; Lis, T.; Brechin, E.K.; Milios, C.J. *Eur. J. Inorg. Chem.* **2010**, 483-489.

[25] Inglis, R.; Stoumpos, C.C.; Prescimone, A.; Siczek, M.; Lis, T.; Wernsdorfer, W.; Brechin, E.K.; Milios, C.J. *Dalton Trans.* **2010**, *39*, 4777-4785.

[26] van der Vlugt, J.I.; Demeshko, S.; Dechert, S.; Meyer, F. *Inorg. Chem.* **2008**, *47*, 1576-1585.

[27] Klingele, J.; Dechert, S.; Meyer, F. *Coord. Chem. Rev.* **2009**, *253*, 2698-2741.

[28] Penkova, L.; Demeshko, S.; Pavlenko, V.A.; Dechert, S.; Meyer, F.; Fritsky, I.O. *Inorg. Chim. Acta* **2010**, *363*, 3036-3040.

[29] Viciano-Chumillas, M.; Tanase, S.; de Jongh, L.J.; Reedijk, J. *Eur. J. Inorg. Chem.* **2010**, 3403-3418.

[30] Viciano-Chumillas, M.; de Ruiter, G.; Tanase, S.; Smits, J.M.M.; de Gelder, R.; Mutikainen, I.; Turpeinen, U.; de Jongh, L.J.; Reedijk, J. *Dalton Trans.* **2010**, *39*, 4991-4998.

[31] Viciano-Chumillas, M.; Tanase, S.; Roubeau, O.; Teat, S.J.; de Jongh, L.J.; Reedijk, J. *Eur. J. Inorg. Chem.* **2010**, 947-951.

[32] Costa, J.S.; Craig, G.A.; Barrios, L.A.; Roubeau, O.; Ruiz, E.; Gómez-Coca, S.; Teat, S.J.; Aromí, G. *Chem. Eur. J.* **2011**, *17*, 4960-4963.

[33] Sens, C.; Romero, I.; Rodríguez, M.; Llobet, A.; Parella, T.; Benet-Buchholz, J. *J. Am. Chem. Soc.* **2004**, *126*, 7798-7799.

[34] Bozoglian, F.; Romain, S.; Ertem, M.Z.; Todorova, T.K.; Sens, C.; Mola, J.; Rodríguez, M.; Romero, I.; Benet-Buchholz, J.; Fontrodona, X.; Cramer, C.J.; Gagliardi, L.; Llobet, A. *J. Am. Chem. Soc.* **2009**, *131*, 15176-15187.

[35] Planas, N.; Christian, G.J.; Mas-Marzá, E.; Sala, X.; Fontrodona, X.; Maseras, F.; Llobet, A. *Chem. Eur. J.* **2010**, *16*, 7965-7968.

[36] Casabó, J.; Pons, J.; Siddiqi, K.S.; Teixidor, F.; Molins, E.; Miravitlles, C. *J. Chem. Soc., Dalton Trans.* **1989**, 1401-1403.

[37] Pons, J.; López, X.; Benet, E.; Casabó, J.; Teixidor, F.; Sánchez, F.J. *Polyhedron* **1990**, *9*, 2839-2845.

[38] Pons, J.; López, X.; Casabó, J.; Teixidor, F.; Caubet, A.; Rius, J.; Miravitlles, C. *Inorg. Chim. Acta* **1992**, *195*, 61-66.

[39] Pons, J.; Sánchez, F.J.; Labarta, A.; Casabó, J.; Teixidor, F.; Caubet, A. *Inorg. Chim. Acta* **1993**, *208*, 167-171.

[40] Munakata, M.; Wu, L.P.; Yamamoto, M.; Kuroda-Sowa, T.; Maekawa, M.; Kawata, S.; Kitagawa, S. *J. Chem. Soc., Dalton Trans.* **1995**, 4099-4106.

[41] Nakano, K.; Suemura, N.; Kawata, S.; Fuyuhiro, A.; Yagi, T.; Nasu, S.; Morimoto, S.; Kaizaki, S. *Dalton Trans.* **2004**, 982-988.

[42] Nakano, K.; Kawata, S.; Yoneda, K.; Fuyuhiro, A.; Yagi, T.; Nasu, S.; Morimoto, S.; Kaizaki, S. *Chem. Commun.* **2004**, 2892-2893.

[43] Yoneda, K.; Nakano, K.; Fujioka, J.; Yamada, K.; Suzuki, T.; Fuyuhiro, A.; Kawata, S.; Kaizaki, S. *Polyhedron* **2005**, *24*, 2437-2442.

[44] Du, M.; Chen, S.T.; Guo, Y.M.; Bu, X.H.; Ribas, J. *J. Mol. Struct.* **2005**, *737*, 17-21.

[45] Yoneda, K.; Adachi, K.; Hayami, S.; Maeda, Y.; Katada, M.; Fuyuhiro, A.; Kawata, S.; Kaizaki, S. *Chem. Commun.* **2006**, 45-47.

[46] Ishikawa, R.; Fuyuhiro, A.; Hayami, S.; Inoue, K.; Kawata, S. *J. Mol. Struct.* **2008**, *892*, 220-224.

[47] Ni-iya, K.; Fuyuhiro, A.; Yagi, T.; Nasu, S.; Kuzushita, K.; Morimoto, S.; Kaizaki, S. *Bull. Chem. Soc. Jpn.* **2001**, *74*, 1891-1897.

[48] Kawahata, R.; Tsukuda, T.; Yagi, T.; Subhan, A.; Nakata, H.; Fuyuhiro, A.; Kaizaki, S. *Chem. Lett.* **2003**, *32*, 1084-1085.

[49] Kawahata, R.; Tsukuda, T.; Yagi, T.; Fuyuhiro, A.; Kaizaki, S. *J. Alloys Compd.* **2006**, *408*, 976-980.

[50] Morioka-Yonezawa, A.; Sakagami-Yoshida, N.; Fuyuhiro, A.; Kaizaki, S. *Inorg. Chim. Acta* **2008**, *361*, 3623-3630.

[51] Yoneda, K.; Adachi, K.; Nishio, K.; Yamasaki, M.; Fuyuhiro, A.; Katada, M.; Kaizaki, S.; Kawata, S. *Angew. Chem. Int. Ed.* **2006**, *45*, 5459-5461.

[52] Hou, J.Z.; Li, M.; Li, Z.; Zhan, S.Z.; Huang, X.C.; Li, D. *Angew. Chem. Int. Ed.* **2008**, *47*, 1711-1714.

[53] Ishikawa, R.; Nakano, M.; Fuyuhiro, A.; Takeuchi, T.; Kimura, S.; Kashiwagi, T.; Hagiwara, M.; Kindo, K.; Kaizaki, S.; Kawata, S. *Chem. Eur. J.* **2010**, *16*, 11139-11144.

[54] Bera, M.; Aromi, G.; Wong, W.T.; Ray, D. *Chem. Commun.* **2006**, 671-673.

[55] Bermejo, M.R.; González-Noya, A.M.; Pedrido, R.M.; Romero, M.J.; Vázquez, M. *Angew. Chem. Int. Ed.* **2005**, *44*, 4182-4187.

[56] Vázquez, M.; Bermejo, M.R.; Licchelli, M.; González-Noya, A.M.; Pedrido, R.M.; Sangregorio, C.; Sorace, L.; García-Deibe, A.M.; Satunartin, J. *Eur. J. Inorg. Chem.* **2005**, 3479-3490.

[57] Bermejo, M.R.; González-Noya, A.M.; Martínez-Calvo, M.; Pedrido, R.; Romero, M.J.; Vázquez López, M. *Eur. J. Inorg. Chem.* **2008**, 3852-3863.

[58] Zhu, A.X.; Zhang, J.P.; Lin, Y.Y.; Chen, X.M. *Inorg. Chem.* **2008**, *47*, 7389-7395.

[59] Zhan, S.Z.; Li, M.; Hou, J.Z.; Ni, J.; Li, D.; Huang, X.C. *Chem. Eur. J.* **2008**, *14*, 8916-8921.

[60] Saalfrank, R.W.; Low, N.; Trummer, S.; Sheldrick, G.M.; Teichert, M.; Stalke, D. *Eur. J. Inorg. Chem.* **1998**, 559-563.

[61] Baxter, P.N.W.; Lehn, J.M.; Baum, G.; Fenske, D. *Chem. Eur. J.* **2000**, *6*, 4510-4517.

[62] Pedrido, R.; Vázquez López, M.; Sorace, L.; González-Noya, A. M.; Cwiklinska, M.; Suárez-Gómez, V.; Zaragoza, G.; Bermejo, M. R. *Chem. Commun.* **2010**, *46*, 4797-4799.

[63] Bao, X.; Leng, J.D.; Meng, Z.S.; Lin, Z.J.; Tong, M.L.; Nihei, M.; Oshio, H. *Chem. Eur. J.* **2010**, *16*, 6169-6174.

[64] Fish, R.H.; Fong, R.H.; Vincent, J.B.; Christou, G. *J. Chem. Soc., Chem. Commun.* **1988**, 1505-1506.

[65] Sarneski, J.E.; Michos, D.; Thorp, H.H.; Didiuk, M.; Poon, T.; Blewitt, J.; Brudvig, G.W.; Crabtree, R.H. *Tetrahedron Lett.* **1991**, *32*, 1153-1156.

[66] Matsushita, T.; Sawyer, D.T.; Sobkowiak, A. *J. Mol. Catal. A: Chem.* **1999**, *137*, 127-133.

[67] Shul'pin, G. B.; Süss-Fink, G.; Shul'pina, L. S. *J. Mol. Catal. A: Chem.* **2001**, *170*, 17-34.

[68] Carrell, T.G.; Cohen, S.; Dismukes, G.C. *J. Mol. Catal. A: Chem.* **2002**, *187*, 3-15.

[69] Lee, S. H.; Xu, L.; Park, B.K.; Mironov, Y.V.; Kim, S.H.; Song, Y.J.; Kim, C.; Kim, Y.; Kim, S.-J. *Chem. Eur. J.* **2010**, *16*, 4678-4685.

[70] Winkler, R.; Zocher, G.; Richter, I.; Friedrich, T.; Schulz, G.E.; Hertweck, C. *Angew. Chem. Int. Ed.* **2007**, *46*, 8605-8608.

[71] Maayan, G.; Christou, G. *Inorg. Chem.* **2011**, *50*, 7015-7021.

[72] Collman, J.P.; Zeng, L.; Brauman, J.I. *Inorg. Chem.* **2001**, *43*, 2672-2679.

[73] Collman, J.P.; Zeng, L.; Decreau, R.A. *Chem. Commun.* **2003**, 2974-2975.

[74] Bryliakov, K.P.; Babushkin, D.E.; Talsi, E.P. *J. Mol. Catal. A: Chem.* **2000**, *158*, 19-35.

[75] Kostakis, G.E.; Powell, A.K. *Coord. Chem. Rev.* **2009,** *253*, 2686-2697.

[76] Addison, A.W.; Rao, T.N.; Reedijk, J.; Rijn, J.V.; Verschoor, G.C. *J. Chem. Soc., Dalton Trans.* **1984**, 1349-1356.

[77] Sens, C.; Rodriguez, M.; Romero, I.; Llobet, A.; Parella, T.; Benet-Buchholz, J. *Inorg. Chem.* **2003,** *42*, 8385-8394.

[78] Sens, C.; Rodriguez, M.; Romero, I.; Llobet, A.; Parella, T.; Sullivan, B.P.; Benet-Buchholz, J. *Inorg. Chem.* **2003,** *42*, 2040-2048.

[79] Kessissoglou, D.P. *Coord. Chem. Rev.* **1999**, *185-6*, 837-858.

[80] Baca, S.G.; Stoeckli-Evans, H.; Ambrus, C.; Malinovskii, S.T.; Malaestean, I.; Gerbeleu, N.; Decurtins, S. *Polyhedron* **2006**, *25*, 3617-3627.

[81] Bhula, R.; Gainsford, G.J.; Weatherburn, D.C. *J. Am. Chem. Soc.* **1988**, *110*, 7550-7552.

[82] Ribas, J.; Albela, B.; Stoeckli-Evans, H.; Christou, G. *Inorg. Chem.* **1997**, *36*, 2352-2360.

[83] Kim, J.; Jin, M. L.; Dom, Y., *Eur. J. Inorg. Chem.* **2003**, 2563-2566.

[84] Viciano-Chumillas, M.; Giménez-Marqués, M.; Tanase, S.; Evangelisti, M.; Mutikainen, I.; Turpeinen, U.; Smits, J.M.M.; de Gelder, R.; de Jongh, L.J.; Reedijk, J. *J. Phys. Chem. C* **2008**, *112*, 20525-20534.

[85] Cano, J.; Cauchy, T.; Ruiz, E.; Milios, C.J.; Stoumpos, C.C.; Stamatatos, T.C.; Perlepes, S.P.; Christou, G.; Brechin, E.K. *Dalton Trans.* **2008**, 234-240.

[86] Lampropoulos, C.; Abboud, K.A.; Stamatatos, T.C.; Christou, G. *Inorg. Chem.* **2009**, *48*, 813-815.

[87] Viciano-Chumillas, M.; Tanase, S.; Mutikainen, I.; Turpeinen, U.; de Jongh, L.J.; Reedijk, J. *Inorg. Chem.* **2008**, *47*, 5919-5929.

[88] Bard, A.J. *Pure Appl. Chem.* **1971**, *25*, 379-394.

[89] Ammar, F.; Saveant, J.M. *J. Electroanal. Chem.* **1973**, *47*, 115-125.

[90] Dunand-Sauthier, M.-N.C.; Deronzier, A.; Pradon, X.; Ménage, S.; Philouze, C. *J. Am. Chem. Soc.* **1997**, *119*, 3173-3174.

[91] Romain, S.; Duboc, C.; Neese, F.; Rivière, E.; Hanton, L.R.; Blackman, A.G.; Philouze, C.; Leprêtre, J.-C.; Deronzier, A.; Collomb, M.-N. *Chem. Eur. J.* **2009**, *15*, 980-988.

[92] Romain, S.; Baffert, C.; Duboc, C.; Lepretre, J.C.; Deronzier, A.; Collomb, M.-N. *Inorg. Chem.* **2009**, *48*, 3125-3131.

[93] Vincent, J.B.; Chang, H.R.; Folting, K.; Huffman, J.C.; Christou, G.; Hendrickson, D.N. *J. Am. Chem. Soc.* **1987**, *109*, 5703-5711.

[94] Brunold, T.C.; Gamelin, D.R.; Stemmler, T.L.; Mandal, S.K.; Armstrong, W.H.; Penner-Hahn, J.E.; Solomon, E.I. *J. Am. Chem. Soc.* **1998**, *120*, 8724-8738.

[95] Reynolds, R.A.; Yu, W.O.; Dunham, W.R.; Coucouvanis, D. *Inorg. Chem.* **1996**, *35*, 2721-2722.

[96] Duboc, C.; Collomb, M.-N.; Pécaut, J.; Deronzier, A.; Neese, F. *Chem. Eur. J.* **2008**, *14*, 6498-6509.

[97] Rich, J.; Castillo, C.E.; Romero, I.; Rodriguez, M.; Duboc, C.; Collomb, M.-N. *Eur. J. Inorg. Chem.* **2010**, 3658-3665.

[98] Duboc, C.; Collomb, M.-N.; Neese, F. *Appl. Magn. Reson.* **2010**, *37*, 229-245.

[99] Baffert, C.; Dumas, S.; Chauvin, J.; Leprêtre, J.-C.; Collomb, M.-N.; Deronzier, A. *Phys. Chem. Chem. Phys.* **2005**, *7*, 202-210.

[100] Romain, S.; Baffert, C.; Dumas, S.; Chauvin, J.; Leprêtre, J.-C.; Daveloose, D.; Deronzier, A.; Collomb, M.-N. *Dalton Trans.* **2006**, 5691-5702.

[101] van Vleck, J.H. *The Theory of Electric and Magnetic Susceptibility*; Oxford University Press: New-York: 1932.

[102] Kambe, K. *J. Phys. Soc. Jpn.* **1950,** *5*, 48-51.

[103] In order to take into account the interactions between complexes, the following definition of the susceptibility has been used:

$$\chi = \frac{\chi_{complex}}{1 - \frac{2zJ'}{Ng^2\mu_B^2}\chi_{complex}}$$

see for example: (a) Myers, B.E.; Berger, L.; Friedberg, S. *J. Appl. Phys.* **1969**, *40*, 1149-1151. (b) O'Connor, C.J. *Prog. Inorg. Chem.* **1982**, *29*, 203-283

[104] Battioni, P.; Renaud, J.P.; Bartola, J.F.; Reina-Artiles, M.; Fort, M.; Mansuy, D. *J. Am. Chem. Soc.* **1988**, *110*, 8462-8470.

[105] Ho, K.P.; Wong, W.L.; Lam, K.M.; Lai, C.P.; Chan, T.H.; Wong, K.Y. *Chem. Eur. J.* **2008**, *14*, 7988-7996.

[106] Kang, B.; Kim, M.; Lee, J.; Do, Y.; Chang, S. *J. Org. Chem.* **2006**, *71*, 6721-6727.

[107] Rich, J.; Rodríguez, M.; Romero, I.; Vaquer, L.; Sala, X.; Llobet, A.; Corbella, M.; Collomb, M.-N.; Fontrodona, X. *Dalton Trans.* **2009**, 8117-8126.

[108] Data collection with APEX II v2009.1-02; Bruker AXS Inc.: Madison, Wisconsin, USA, 2007.

[109] Data reduction with Bruker SAINT V7.60A; Bruker AXS Inc.: Madison, Wisconsin, USA, 2007.

[110] SADABS: V2008/1; Bruker AXS Inc.: Madison, Wisconsin, USA, 2001; Blessing, *Acta Crystallogr.* **1995**, A51, 33-38.

[111] Sheldrick, G.M. *Acta Crystallogr.* **2008**, A64, 112-122. SHELXTL V6.14.

[112] Glerup, J.; Goodson, P.A.; Hodgson, D.J.; Michelsen, K.; Nielsen, K.M.; Wiehe, H. *Inorg. Chem.* **1992**, *31*, 4611-4616.

5.7. Supporting information

Table S 1. Crystal data and structure refinement for $\mathbf{1}(ClO_4)_3 \cdot 2.5CH_3CN \cdot C_4H_{10}O \cdot 0.5H_2O$ and $\mathbf{1}(ClO_4)_4 \cdot 2CH_3CN \cdot 2C_4H_{10}O$.

	$\mathbf{1}(ClO_4)_3 \cdot 2.5CH_3CN \cdot C_4H_{10}O \cdot 0.5H_2O$	$\mathbf{1}(ClO_4)_4 \cdot 2CH_3CN \cdot 2C_4H_{10}O$
Chemical formula	$C_{87}H_{72.50}Cl_3Mn_5N_{26.50}O_{14.50}$	$C_{90}H_{80}Cl_4Mn_5N_{26}O_{19}$
Formula weight	2102.26	2246.30
T/K	100	100
λ/Å	0.71073	0.71073
Crystal system	monoclinic	monoclinic
Space group	P2(1)/n	C2/c
a/Å	15.4109(7)	25.843(5)
b/Å	22.5910(10)	28.270(5)
c/Å	26.9272(11)	14.482(3)
α/°	90.00	90.00
β/°	101.9130(10)	93.709(3)
γ/°	90.00	90.00
Volume/Å^3	9172.7(7)	10559(3)
Z	4	4
Density/mg m^{-3}	1.522	1.413
μ/mm^{-1}	0.836	0.759
F(000)	4288	4588
Reflections collected	35236	12962
R1[a]	0.0537	0.0848
wR2[b]	0.1253	0.1927

[a] $R1 = \Sigma||Fo| - |Fc||/\Sigma|Fo|$. [b] $wR2 = [(\Sigma w(|Fo| - |Fc|)^2/\Sigma wFo^2)]^{1/2}$

Equation S 1. Analytical expression of the magnetic susceptibility for an S = 5/2 - 5/2 - 5/2 magnetic trimer in the low field analytical expression of the magnetic susceptibility:

$$\chi_{Mn3}T = \frac{N\mu_B^2 g_{av}^2}{4k_B}\left[\begin{array}{l} \dfrac{680e^{55\frac{J}{k_BT}} + 455\left(e^{40\frac{J}{k_BT}} + e^{50\frac{J}{k_BT}}\right) + 286\left(e^{27\frac{J}{k_BT}} + e^{37\frac{J}{k_BT}} + e^{45\frac{J}{k_BT}}\right) +}{8e^{55\frac{J}{k_BT}} + 7\left(e^{40\frac{J}{k_BT}} + e^{50\frac{J}{k_BT}}\right) + 6\left(e^{27\frac{J}{k_BT}} + e^{37\frac{J}{k_BT}} + e^{45\frac{J}{k_BT}}\right) +} \\[3ex] \dfrac{165\left(e^{16\frac{J}{k_BT}} + e^{26\frac{J}{k_BT}} + e^{34\frac{J}{k_BT}} + e^{40\frac{J}{k_BT}}\right) + 84\left(e^{7\frac{J}{k_BT}} + e^{17\frac{J}{k_BT}} + e^{25\frac{J}{k_BT}} + e^{31\frac{J}{k_BT}} + e^{35\frac{J}{k_BT}}\right) +}{5\left(e^{16\frac{J}{k_BT}} + e^{26\frac{J}{k_BT}} + e^{34\frac{J}{k_BT}} + e^{40\frac{J}{k_BT}}\right) + 4\left(e^{7\frac{J}{k_BT}} + e^{17\frac{J}{k_BT}} + e^{25\frac{J}{k_BT}} + e^{31\frac{J}{k_BT}} + e^{35\frac{J}{k_BT}}\right)} \\[3ex] \dfrac{35\left(e^{10\frac{J}{k_BT}} + e^{18\frac{J}{k_BT}} + e^{24\frac{J}{k_BT}} + e^{28\frac{J}{k_BT}} + e^{30\frac{J}{k_BT}}\right) +}{3\left(e^{10\frac{J}{k_BT}} + e^{18\frac{J}{k_BT}} + e^{24\frac{J}{k_BT}} + e^{28\frac{J}{k_BT}} + e^{30\frac{J}{k_BT}}\right) +} \\[3ex] \dfrac{10\left(e^{5\frac{J}{k_BT}} + e^{13\frac{J}{k_BT}} + e^{19\frac{J}{k_BT}} + e^{23\frac{J}{k_BT}}\right) + e^{10\frac{J}{k_BT}} + e^{16\frac{J}{k_BT}} + 35}{2\left(e^{5\frac{J}{k_BT}} + e^{13\frac{J}{k_BT}} + e^{19\frac{J}{k_BT}} + e^{23\frac{J}{k_BT}}\right) + e^{10\frac{J}{k_BT}} + e^{16\frac{J}{k_BT}} + 3} \end{array} \right]$$

Equation S 2. Analytical expression of the magnetic susceptibility for an S = 5/2 - 2 - 5/2 magnetic trimer in the low field analytical expression of the magnetic susceptibility:

$$\chi_{Mn3}T = \frac{N\mu_B^2 g_{av}^2}{3k_B}\left[\begin{array}{l} \dfrac{840e^{44\frac{J}{k_BT}} + 546\left(e^{30\frac{J}{k_BT}} + e^{40\frac{J}{k_BT}}\right) + 330\left(e^{18\frac{J}{k_BT}} + e^{28\frac{J}{k_BT}} + e^{36\frac{J}{k_BT}}\right) +}{15e^{44\frac{J}{k_BT}} + 13\left(e^{30\frac{J}{k_BT}} + e^{40\frac{J}{k_BT}}\right) + 11\left(e^{18\frac{J}{k_BT}} + e^{28\frac{J}{k_BT}} + e^{36\frac{J}{k_BT}}\right) +} \\[3ex] \dfrac{180\left(e^{8\frac{J}{k_BT}} + e^{18\frac{J}{k_BT}} + e^{26\frac{J}{k_BT}} + e^{32\frac{J}{k_BT}}\right) + 84\left(1 + e^{10\frac{J}{k_BT}} + e^{18\frac{J}{k_BT}} + e^{24\frac{J}{k_BT}} + e^{28\frac{J}{k_BT}}\right) +}{9\left(e^{8\frac{J}{k_BT}} + e^{18\frac{J}{k_BT}} + e^{26\frac{J}{k_BT}} + e^{32\frac{J}{k_BT}}\right) + 7\left(1 + e^{10\frac{J}{k_BT}} + e^{18\frac{J}{k_BT}} + e^{24\frac{J}{k_BT}} + e^{28\frac{J}{k_BT}}\right) +} \\[3ex] \dfrac{30\left(e^{4\frac{J}{k_BT}} + e^{12\frac{J}{k_BT}} + e^{18\frac{J}{k_BT}} + e^{22\frac{J}{k_BT}} + e^{24\frac{J}{k_BT}}\right) + 6\left(e^{8\frac{J}{k_BT}} + e^{14\frac{J}{k_BT}} + e^{18\frac{J}{k_BT}}\right)}{5\left(e^{4\frac{J}{k_BT}} + e^{12\frac{J}{k_BT}} + e^{18\frac{J}{k_BT}} + e^{22\frac{J}{k_BT}} + e^{24\frac{J}{k_BT}}\right) + 3\left(e^{8\frac{J}{k_BT}} + e^{14\frac{J}{k_BT}} + e^{18\frac{J}{k_BT}}\right) + e^{12\frac{J}{k_BT}}} \end{array} \right]$$

Chapter 7

General Conclusions

7. General conclusions

1- Six new manganese complexes containing the chiral ligand (–)pinene[5,6]bipyridine ((–)-**L**) have been synthesized and thoroughly characterized: [{Mn((–)-**L**)Cl}$_2$(μ-Cl)$_2$] (**C1**), [{Mn((–)-**L**)}$_2$(μ-OAc)$_3$](PF$_6$) (**C2**), [Mn((–)-**L**)Cl$_2$(H$_2$O)] (**C3**), [Mn((–)-**L**)$_2$Cl$_2$] (**C4**), [Mn((–)-**L**)$_2$(CF$_3$SO$_3$)$_2$] (**C5**) and [Mn((–)-**L**)$_2$)(NO$_3$)(H$_2$O)](NO$_3$) (**C6**).

The mononuclear complexes containing two pinene-bipyridine ligands and two monodentate (Cl, CF$_3$SO$_3$ or NO$_3$) ligands (**C4**-**C6**) display hexacoordination and are obtained as a sole isomer, *trans,trans*, which seems to be energetically favoured thanks to H-bonding interactions involving pyridyl groups and monodentate ligands.

The magnetic studies show that the two dinuclear complexes (**C1** and **C2**) present weak antiferromagnetic interactions. By means of EPR studies the ZFS of a series of mononuclear Mn^{II} complexes has been investigated and the experimental *D* values all fall within a small magnitude range of 0.035–0.086 cm^{-1}, which prevents the establishment of magnetostructural correlations with the coordination number of the Mn^{II} ion (6 vs. 7) or with the N/O ratio of their coordination sphere.

The chlorocomplexes **C1** and **C4** exhibit reversible electrochemical redox processes whereas for **C2**, **C3**, **C5** and **C6** the cyclic voltammograms show irreversible processes. The bulk electrolyses of **C1** and **C4** lead to a similar mononuclear Mn^{III} species.

All the complexes synthesized have been tested in styrene epoxidation and present moderate performance, being the chloro complexes **C1** and **C4** the ones exhibiting the highest conversions. These chloro complexes have also been shown to catalyze epoxidation of other olefinic substrates with good efficiency and revealed to be specific for the *cis* epoxide when using *cis*-β-methylstyrene as substrate, in the absence of additives. Moreover, the epoxidation activity of these chloro complexes is strongly dependent on the steric encumbrance of the substrates employed. Complexes **C1** and **C4** constitute the first examples of Mn chloro complexes with simple N-pyridyl ligands successfully applied in epoxidation catalysis.

The presence of additives (imidazole or NaHCO$_3$) in the catalytic media in epoxidation of alkenes with the chloro complexes **C1** and **C4** and peracetic acid as oxidant has proved to increase enormously the conversion and selectivity values, especially in the

case of the more basic $NaHCO_3$. The main role of the additives seems to be the control of the pH into the catalytic media because their basic nature can partially neutralize the acidity of the peracid added in large excess in the solution.

The Mn(II) chloro complexes **C1** and **C4** display a remarkable effectiveness and selectivity in epoxidation catalysis carried out in ionic liquid:solvent media ([bmim]PF_6:CH_3CN), with better results when compared to the use of acetonitrile as sole solvent. This system constitutes the first example of polypyridyl Mn(II) complexes tested under these conditions. Both catalysts also show excellent reusability employing different substrates (for **C4**, up to 7-9 runs with overall turnover numbers of 298 for styrene, 271 for *cis*-β-methylstyrene, 596 for *trans*-β-methylstyrene and 168 for 1-octene).

The active intermediate formed in situ at low temperature is proposed to be an oxo-bridged binuclear Mn_2(IV,IV) species for the chloro complexes **C1** and **C4**, whereas a mixed-valent Mn_2(III,IV) species is found for the triflate compound **C5**. This study revealed the crucial role of the monodentate ligands (chloro or triflate) attached to the metal center in the formation of the active intermediate species. This seems to be in accordance with the different performance observed for the two types of catalysts (**C4** shows higher conversion and selectivity values than those of **C5** with regard to the epoxidation of some alkenes under the same conditions, in spite of their structural similarity). This study also revealed that similar species are observed in the presence of additives.

2- Five new tetradentate N-donor ligands containing the spiro-2,2'-bi(chroman) backbone (SPANimine) have been synthesized and fully characterized. With these ligands a family of new racemic and chiral Mn(II) complexes, with the general formula MnLCl_2, MnL(CF_3SO_3)$_2$ or MnL(NO_3)$_2$ where L = SPANrac, SPANrac-pinene[5,6], SPAN(+)-pinene[4,5], SPAN(+)-pinene[5,6] or SPAN(-)-pinene[5,6], has been prepared and thoroughly characterized.

The X-Ray structures of the complexes when determined show a Mn ion coordinated by four nitrogen atoms of the SPANimine ligand and two labile anions. These two anions are in *cis* position and the SPANimine ligand folds around the metal ion using a *cis*-α conformation. These ligands are flexible and have small bite angles (75-81º).

All the complexes synthesized have been tested in the catalytic epoxidation of styrene, with only moderate performances when carrying out the catalytic experiments in acetonitrile without the use of additives. In all the cases benzaldehyde was detected as side product of the oxidation reaction. The chloro complexes exhibit better conversion and selectivity values than the analogous triflate or nitrate compounds when the catalytic essays are performed in absence of additives.

The complexes bearing the span ligands with the bulky 5,6-pinene groups in close proximity to the labile sites display considerably lower conversion rates than the analogous complexes containing the 4,5-pinene groups or the pyridyl analogues. A similar degree of performance is observed when comparing sets of related complexes containing a central (+) or (-) spiro building block. Unfortunately, low values of enantiomeric excess were obtained.

The use of additives such as imidazole or $NaHCO_3$ remarkably increases the conversion and the selectivity for the epoxide product. The significant increase in the selectivity indicates that the mechanistic pathway leading to the epoxide should be favoured with regard to alternative non-desired routes and thus the additives might have an active role in the choice of the preferred mechanistic path.

One of the chloro complexes has been tested in the epoxidation of *cis*-β-methylstyrene and the catalyst has proved to be selective and stereospecific for the formation of the *cis* epoxide. Computational calculations give a lower barrier for the closure of the ring (0.1 kcal/mol) with respect to the C-C bond rotation leading to *cis-trans* isomerization (4.1 kcal/mol). This supports the absence of the thermodynamically more stable *trans* epoxide in experimental epoxidation.

3- A new bis(triple-helical) pentanuclear manganese complex, [{Mn^{II}(μ-bpp)$_3$}$_2$ $Mn^{II}_2Mn^{III}$(μ_3-O)]$^{3+}$ ($\mathbf{1}^{3+}$), has been isolated and structurally characterized by reacting Mn^{2+} ions and the bridging ligand bis(pyridyl)-pyrazolate. Its electrogenerated one-electron oxidized form, [{Mn^{II}(μ-bpp)$_3$}$_2Mn^{II}Mn^{III}_2$(μ_3-O)]$^{4+}$ ($\mathbf{1}^{4+}$), has also been isolated and characterized.

Complexes $\mathbf{1}^{3+}$ and $\mathbf{1}^{4+}$ have been characterized by X-ray diffraction and their structures consist of five Mn ions connected through six bpp$^-$ ligands, in which two Mn^{II}

245

ions occupy the apical positions and the three remaining Mn ions, connected by a μ_3-O^{2-} ion, are placed in the equatorial plane.

Complex $\mathbf{1}^{3+}$ exhibits very rich redox behavior with five distinct and reversible one-electron processes located between -1.0 and +1.5 V. In addition, bulk electrolyses have evidenced the exceptional stability of the complex in four oxidation states. Indeed, the oxidation states of the oxo-centered trinuclear core can switch between $\{Mn^{II}_3(\mu_3\text{-}O)\}^{4+}$, $\{Mn^{II}_2Mn^{III}(\mu_3\text{-}O)\}^{5+}$, $\{Mn^{II}Mn^{III}_2(\mu_3\text{-}O)\}^{6+}$ and $\{Mn^{III}_3(\mu_3\text{-}O)\}^{7+}$, while the two Mn apical ions remain at the +II oxidation state and their oxidation involves the breaking of the pentanuclear structure.

The two apical Mn^{II} ions are equivalent and magnetically independent in $\mathbf{1}^{3+}$, whereas in $\mathbf{1}^{4+}$ the two apical units present a magnetic interaction with each other and also likely with the central core.

The magnetic susceptibility measurements at 40 K are consistent with two apical $S = 5/2$ $\{Mn^{II}(bpp)_3\}^{-}$ and one $S = 2$ non-interacting spins for $\mathbf{1}^{3+}$, whereas three $S = 5/2$ non-interacting spins are found for $\mathbf{1}^{4+}$. This indicates that the $\{Mn^{II}_2Mn^{III}(\mu_3\text{-}O)\}^{5+}$ and $\{Mn^{II}Mn^{III}_2(\mu_3\text{-}O)\}^{6+}$ cores behave at low temperature like $S = 2$ and $S = 5/2$ spin centers, respectively. The thermal behavior below 40 K highlights the presence of intra-complex magnetic interactions between the two apical spins and the central core in both $\mathbf{1}^{3+}$ and $\mathbf{1}^{4+}$ that are antiferromagnetic for $\mathbf{1}^{3+}$ (leading to an $S_T = 3$) and ferromagnetic for $\mathbf{1}^{4+}$ (giving thus an $S_T = 15/2$ ground state).

$\mathbf{1}^{3+}$ has been tested in the catalytic epoxidation of alkenes, showing very fast conversion with good selectivities for the epoxide products, either for aromatic or aliphatic alkenes. This complex has also revealed regiospecificity for the ring alkene site in the epoxidation of 4-vinylcyclohexene. The partial isomerisation of cis-β-methylstyrene to the trans-epoxide could indicate the presence of a radical species in the epoxidation pathway. However, the polynuclear nature of the catalyst probably allows for the occurrence of multiple active species.

4- In the particular case of the ligands used in this thesis:

- Complexes with two bidentate bpy ligands present a better performance when compared to analogous complexes with tetradentate SPAN ligands.

- Ligands with pinene groups fused to pyridine rings do not induce enantioselectivity in the epoxidation of alkenes with the corresponding manganese catalysts.

In general, this work has demonstrated that:

- The chloro complexes present higher conversion and selectivity values in the epoxidation of alkenes when compared to triflate and nitrate analogues. Indeed, the monodentate ligands attached to the metal center have a crucial role in the formation of the active intermediate species.

- The presence of additives in the catalytic media significantly increases the conversion and selectivity values in the epoxidation of alkenes with peracetic acid as oxidant. The ionic liquids also improve their performance and allow the reusability of the catalysts.

- The pentanuclear compound displays the best performance in the epoxidation of alkenes probably due to the occurrence of multiple active species.